UNIVERSITY OF
BIRMINGHAM

IMPREGNATION OF ACTIVATED CARBONS FOR PRE- AND POST-COMBUSTION CO_2 CAPTURE IN A FIXED BED PRESSURE SWING ADSORPTION REACTOR: A MODELLING AND EXPERIMENTAL COMPARISON

By

DOUGLAS SOARES DOS SANTOS

Primary supervisor: Prof. Joe Wood

Secondary supervisor: Dr. Andrew Ingram

A thesis submitted to the University of Birmingham for the degree of

DOCTOR OF PHILOSOPHY

Reaction and Catalysis Engineering Group

School of Chemical Engineering

College of Engineering and Physical Sciences

The University of Birmingham

March 2019

ABSTRACT

The mitigation of greenhouse gases, such as carbon dioxide, is of timely concern in the energy sector, requiring new techniques and process options to treat acidic gases and develop solutions for capture and reuse. Solid adsorbents are potentially viable for application as the next generation carbon capture technology. Activated Carbon Norit® RB1 and Cabot Norit® R2030 were selected for this study, owing to their potentially high adsorption rates and affinity with carbon dioxide molecules. The purpose of thesis was to modify the adsorbent using chemical and amine solutions via an impregnation process to provide high adsorption capacity and performance, focusing on surface area modification and attachment of primary amine groups to improve the solid/gas interaction. Diverse characterisation techniques were used to examine and explore the essential properties and parameters of the modified adsorbents developed. Specifically, scanning electron microscopy (SEM) was used to investigate the surface morphology, thermogravimetric analysis (TGA) was applied to test the adsorption capacity with a pure CO_2 flow, a high-pressure volumetric analyser (HPVA) was used to measure the gas volume adsorbed at the pre-combustion condition, producing adsorption-desorption isotherms under nitrogen and carbon dioxide binary mixtures, and the textural properties were determined by Brunauer-Emmett-Teller (BET) analysis, allowing comparison of the pore size and the volume adsorbed per sample.

The dynamic adsorption behaviour of the activated carbons (ACs) was studied in a fixed bed reactor using a carbon dioxide concentration range of 10–50% combined with a nitrogen flow. The original and modified adsorbents were tested under pre and post-combustion conditions, with the highest uptake of carbon dioxide found to be for MEA+MDEA+AMP Norit® RB1 AC

under pre-combutions and MEA (20%) Norit® RB1 AC under post-combustion conditions. The introduction of amine groups into the sample lead to the enhancement of chemisorption, while the treatment with KOH modified the surface area of the adsorbents, thereby improving uptake behaviour.

Additionally, a Pressure Swing Adsorption (PSA) model using a fixed bed reactor was developed for carbon dioxide capture at pre-combustion conditions (25ºC and 25 bar) using gPROMS® ModelBuilder software [version 4.1; developed by Process System Enterprise, PSE]. A parameter estimation was executed using similar conditions as applied in the fixed bed reactor rig at the laboratory scale. Nitrogen and carbon dioxide were applied to this model taking into account the physical behaviour of the PSA unit. The estimations demonstrated an excellent approximation to the experimental breakthrough curve for both adsorbents, which also validated the model supported by the sum of squared residuals (SSR) values. Furthermore, the parameter estimation confirmed the novelty of the two amine modified adsorbents for pre-combustion carbon dioxide adsorption, due to their high potential to capture the desired gas in a binary mixture in the PSA fixed bed reactor process.

DEDICATION

To God, my wife and my mother.

ACKNOWLEDGEMENTS

First of all, I would like to thank my supervisors Prof Dr Joseph Wood and Dr Andrew Ingram for all their encouragement, advice, and highly-valued contributions during the development of this project. I have learnt a lot during these years working in cooperation with both of you. Additionally, I would also like to thank Lee Stevens and Colin Snape for their collaboration for HPVA and BET tests processed at the Energy Technologies Building (School of Chemical, Environmental and Mining Engineering) at the University of Nottingham.

I want to express my gratitude to the Brazilian National Council for Scientific and Technological Development (CNPq, Brazil) for their financial support from the Science without Borders (SwB) programme.

This project would not be possible without the vital support of my wife, family and friends, especially my wife, who followed me without hesitation and faced this precious challenge daily by my side in a foreign country; thanks for your patience, comprehension during these years. In parallel, I would like to thank my mother and my father for understanding the importance of this dream to me and my career, supporting me during these years.

Lastly, special thanks to my friends who supported me during this period: Manoel V. Avancini, Dr. Lais Speranza, Rebeca A. Solares, Dr. Mostapha Ariane, Gianluca Ferraro, Ravenna Lessa, Ane Borges, Dr. Carolina Musse. Thanks for making these years unforgettable!

PAPERS AND CONFERENCES

From the development of the work described in this thesis, the following papers have been submitted:

- **Solares, R. A. A.**, **Santos, D. S. D.**, Wood, J. Modelling and parameter estimation of breakthrough curves for amine modified activated carbons under pre-combustion carbon capture conditions. Fuel 253: 1130–1139, in press.

- **Santos, D. S. D.**, Majewski, A., Stevens, L. Snape, C. Wood, J. Novel modified activated carbons via amine solutions for post-combustion CO_2 adsorption. In preparation.

The research findings were disseminated at the following conferences:

- **Santos, D. S. D.**, Ingram, A., Wood, J. Carbon capture process via adsorption technology. Oral presentation at the 8th ABEP-UK (Brazilian Association of Post-graduate Students and Researchers in the United Kingdom) Conference, London, United Kingdom, 14 May 2016.

- **Santos, D. S. D.**, Ingram, A., Wood, J. Activated carbon impregnation method via chemical solutions for pre and post-combustion CO_2 adsorption technology in a fixed bed reactor process. Oral presentation at the Catalysis and Reaction Engineering Symposium, University of Sheffield, Sheffield, United Kingdom, 31 May 2017.

- **Santos, D. S. D.**, Ingram, A., Wood, J. Adsorbent modification procedure for pre and post-combustion via chemical solutions to CO_2 adsorption technology. Oral presentation at the 9th ABEP-UK (Brazilian Association of Post-graduate Students and Researchers in the United Kingdom) Conference, London, United Kingdom, 10 June 2017.

- **Santos, D. S. D.**, Ingram, A., Wood, J. Activated carbon impregnation method via chemical solutions for pre and post-combustion CO_2 adsorption technology in a fixed bed reactor process. Oral presentation at the 2nd International Conference on Catalysis and Chemical Engineering, Paris, France. 19–21 February 2018.

TABLE OF CONTENTS

LIST OF ILLUSTRATIONS

LIST OF TABLES

GLOSSARY OF TERMS AND ABBREVIATIONS

AC	Activated Carbon
ADS	Adsorption
AMP	2-Amino-2-Methyl-1-Propanol
B10	Biodiesel with 10% of ethanol in the diesel
B15	Biodiesel with 15% of ethanol in the diesel
B100	Pure biodiesel
BEIS	Department for Business, Energy and Industrial Strategy
BET	Brunauer-Emmett-Teller technique
BFDM	Backward Finite Difference Method
BT	Breakthrough curve
CAC	Commercial Activated Carbon
CCS	Carbon Capture and Storage
CCUS	Carbon Capture, Utilisation and Storage
CO	Carbon Monoxide
CO_2	Carbon Dioxide
COP21	21st Conference of the Parties

DEA	Diethanolamine
DECC	Department for Energy and Climate Change
DFT	Density Functional Theory method
ECMMS	Extended Cooperative Multimolecular Sorption
EU	European Union
EOR	Enhanced Oil Recovery
FBR	Fixed Bed Reactor
FDM	Finite Difference Method
FFDM	Forward Finite Difference Method
FTIR	Fourier Transform Infrared Spectroscopy
GHG	Greenhouse Gas
GWP	Global Warming Potential
H_2	Hydrogen
H_3PO_4	Phosphoric Acid
HCl	Hydrochloric Acid
HPVA	High-Pressure Volumetric Analyser
H-K	Horvath-Kawazoe method
IAS	Ideal Adsorbed Solution

IGCC	Integrated Gasification Combined Cycle
IPCC	Intergovernmental Panel on Climate Change
IR	Infrared
IUPAC	International Union of Pure and Applied Chemistry
KOH	Potassium Hydroxide
LDF	Linear Driving Force
MDEA	Methyl-diethanolamine
MEA	Monoethanolamine
MMscfd	Million standard cubic feet per day
MOF	Metal-Organic Framework
N_2	Nitrogen
nm	Nanometer
Non-OECD	non-Organization for Economic Cooperation and Development
O&G	Oil and Gas sector
^oC	Celsius degree
P/Po	Partial pressure of the gas at the equilibrium
ppm	Parts per million
PADEs	Partial Algebraic Differential Equations
PCC	Post-combustion Capture

PSA	Pressure Swing Adsorption
PSE	Process Simulation Enterprise
PSD	Pore Size Distribution
R&D	Research and Development
SEM	Scanning Electronic Microscopy
SSR	Sum of Squared Residuals
STP	Standard Temperature and Pressure
TEA	Triethanolamine
TEPA	Tetraethylenepentamine
TGA	Thermogravimetric Analyser
TSA	Thermal Swing Adsorption
UDF	User Defined Function
UNFCC	United Nations Framework Convention on Climate Change
VOC	Volatile Organic Compounds
VSA	Vacuum Swing Adsorption
VTSA	Vacuum & Temperature Swing Adsorption
XRD	X-ray Diffraction
$ZnCl_2$	Zinc Chloride

LIST OF SYMBOLS

b_i	Langmuir isotherm coefficients for i component (1/Pa)
C_i	Concentration of i component in the gas phase (mol/m^3)
C^i_{pg}	Specific heat for i component in the gas phase (J/mol. K)
C_e	Adsorbate initial concentration (-)
C_{ps}	Sorbent specific heat (J/kg. K)
D_{AB}	Diffusion coefficient (m^2/s)
D_x	Dispersion coefficient (m^2/s)
D_p	Sorbent particle diameter (m)
e	Electronic charge (C)
$\mathcal{E}_b$	Bed void fraction (-)
e_s	Sorbent density (kg/m^3)
$\mathcal{E}_t$	Total void fraction (-)
F_i	Molar flowrate of i component (mol/s)
h	Planck's constant (J/s)
h_i	Effective heat transfer coefficient (J/m^3.s.K)
ΔH_i^{ads}	Heat of adsorption of i component (J/mol)
K_i	Effective mass transfer coefficient for i component (1/s)
K_f	Freundlich isotherm constant (mmol/g)
L	Bed height (m)

m	Electron mass (kg)
m_{ads},	Mass of adsorbent in the bed (g)
n	Freundlich isotherm temperature-dependant constant (-)
n_f	Freundlich isotherm constant related to adsorption intensity (-)
M^i_w	Molecular weight of i component (kg/mol)
P	Pressure (bar)
P_{feed}	Pressure of feed stream (-)
q_e	Equilibrium adsorption capacity (mmol/g)
$q_{mi,}$	Langmuir isotherm coefficients for i component (mol/kg)
Q^*_i	Sorbent loading for i component in equilibrium (mol/kg)
q_{mi}	Maximum sorbent loading for i component (mol/kg)
Q_i	Sorbent loading of i component (mol/kg)
R	Ideal gas constant (J/mol. K)
t	Time (s)
T	Temperature (K)
T_w	Wall temperature (K)
v	Gas velocity (m/s)
V	Accelerating voltage (V)
V_b	Fixed bed reactor volume (m^3)

GREEK SYMBOLS

λ	Wavelength of an electron (nm)
λ^{l}	Axial heat dispersion coefficient (J/s. m. K)
μ_g	Viscosity of the gas phase (Pa. s)
θ	Theta (-)

CHAPTER 1: INTRODUCTION

1.1. Background

Separation processes have been used extensively throughout world history, being applied to extract more than one product from the same raw material or the same product in different ways. Indeed, separation techniques have been implemented since early civilisations, for instance, to obtain salt from the sea water by evaporation (Rufford et al., 2012), extract essential essences from flowers (Arami-Niya, Daud & Mjalli, 2010), as well as petrol distillation to obtain countless products and sub-products (British Petroleum, 2018) among other examples (Henley, 2011; Rufford et al., 2012; Carpenter & Long, 2017; Siqueira et al., 2017; Hao et al., 2018).

Currently, the carbon dioxide (CO_2)concentration in the atmosphere (411 ppm) is much higher than the pre-industrial period (300 ppm) (NASA, 2019). Consequently, to encourage countries to develop long-term goals to achieve low-emissions development strategies and mitigate global warming, the Paris Agreement established the global temperature limit lower than 2ºC, restricting it to 1.5ºC (The UN Environment, 2017).

Owing to rising industrial activity and energy consumption, the conversion of fossil fuels contributed actively to the rise in greenhouse gas emissions. The mitigation of these gases has been discussed, and targets have been established by different countries and global companies to achieve the policy regulations. Development and implementation of strategies are necessary to develop solutions for climate change mitigation since this problem is potentially damaging, as reported by the Intergovernmental Panel on Climate Change (IPCC, 2018). A task that is predicted to become even more challenging is the creation of strategies to control the global energy demand (Rao & Rubin, 2002).

Europe is committed to reducing 80% of greenhouse gases emissions by 2050, with defined emission reduction targets and promises to comply with these goals on a global scale (Stern,

2006). Regarding electricity production, technologies to reduce the use of carbon have been investigated, primarily aiming to accomplish a reduction in the utilisation of fossil fuels on a large scale, particularly the use of coal and gas (UNFCC, 2011).

Various technologies are available to capture acidic CO_2 from a mixture of gases (for instance, natural gas), as shown in Figure 1.1 (Rao & Rubin, 2002). Such CO_2 capture technologies include chemical absorption (Rochelle, 2009), adsorption (Wiheeb et al., 2016a) and physical (Dortmundt & Doshi, 1999) (e.g., membranes and cryogenic processes) or hybrid methods (Liu et al., 2014). The challenge to choose a suitable CO_2 capture process depends on the product composition, conditions of the CO_2 source (e.g., concentration), temperature, pressure and storage method required in reservoir conditions (Kohl & Nielsen, 1997).

Modern conversion fuel systems have received more attention in the oil and gas energy mix. In the pre-combustion processes, CO_2 is captured from the fuel before it is burnt, producing an exhaust gas containing CO and H_2, followed by reaction with water to convert CO into CO_2, as shown in Equation 1.1 (Casas et al., 2012).

$$CO + H_2O \leftrightarrow H_2 + CO_2 \qquad \text{Eq. (1.1)}$$

By contrast, in the post-combustion industrial processes, CO_2 is extracted (mainly from nitrogen) from the exhaust gases by adsorption, absorption, cryogenic and membrane permeation techniques (Rashidi & Yusup, 2016). In oxyfuel processes, the fuel is burnt with high oxygen rates rather than air, and the obtained, entirely pure CO_2, is recovered as exhaust gas (Thambimuthu et al., 2005; Henley, 2011; Carpenter & Long, 2017). After capture, CO_2 must be compressed and transported to the injection area in a geologically appropriate place, mainly by "carboducts" or ships (Valencia, 2007).

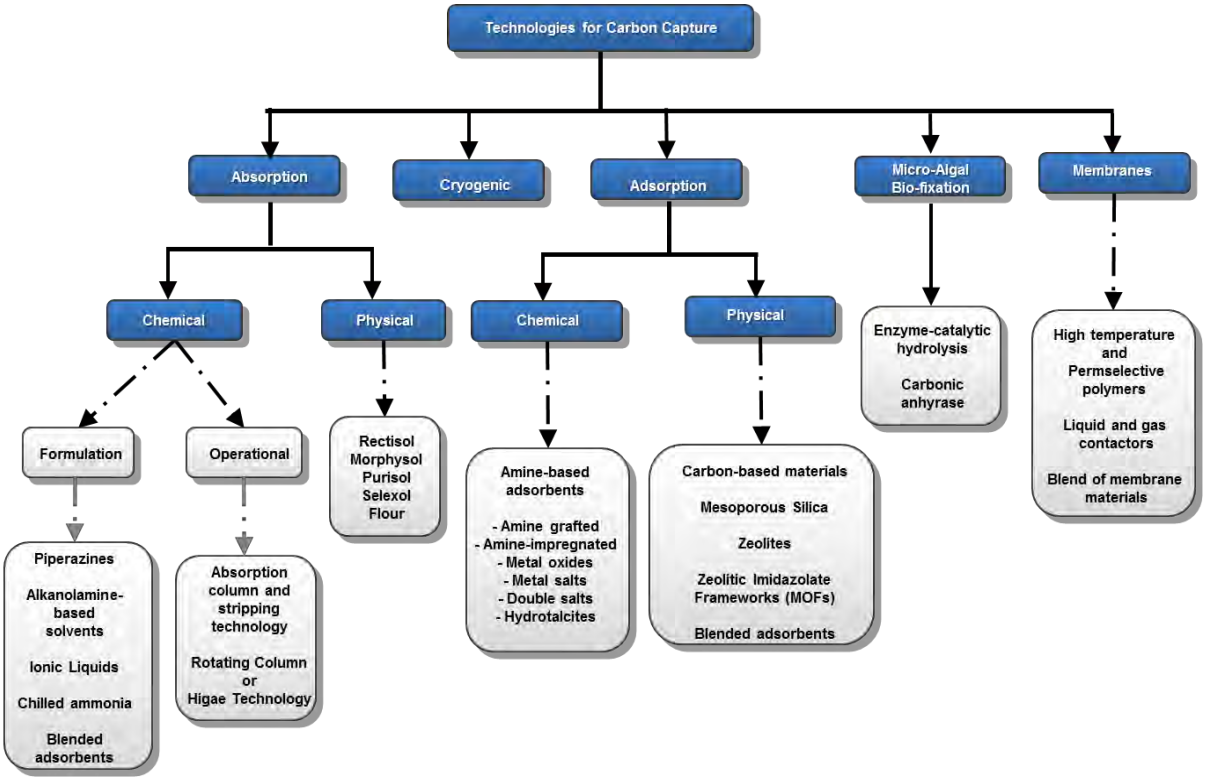

Figure 1.1. Summary of carbon capture technologies available for off/onshore (Ben-Mansour et al., 2016; Dortmundt & Doshi, 1999)

In primary offshore processing, membrane permeation is an alternative to chemical absorption due to its smaller spatial footprint (Dortmundt & Doshi, 1999). However, it is limited by the high cost of membrane material and its selectivity.

Absorption processes have traditionally been used in off and onshore scenarios by chemical or physical solvents, exhibiting a large amount of carbon capture for acidic gases extracted from several reservoirs around the world. This process mostly operates with alkanolamine aqueous solutions, which are predicted to be the most suitable technology until 2030 (Rochelle, 2009). However, this solvent demonstrates higher corrosion potential and requires large absorber volumes (Riboldi & Bolland, 2017). Additionally, the gas compression and the high energy

consumption for solvent regeneration makes chemical absorption less cost-effective. The main disadvantages of liquid amine absorption processes are the considerable space required for the plant installation, high thermal/electric energy demand, and high-cost investment for the solvent (Zhao et al., 2018).

Adsorption has been regarded as a promising technology to mitigate the emissions of CO_2 (Figueroa et al., 2008). Researchers are continually developing materials which confer fast kinetics, thermal stability, superior mechanical properties, high adsorption capacity and selectivity (Sayari, Belmabkhout & Serna-Guerrero, 2011). The use of adsorbents have several advantages over amine liquids (applied in absorption technologies), such as they are more natural to regenerate, have lower energy penalty and high capacity to minimise the amount of sorbent. Additionally, they have desirable kinetics and transport properties for rapid sorption, and there is no tendency to promote undesirable chemical reactions, reducing operational cost (Abanades et al., 2015; Zhao et al., 2018).

Activated carbons require surface modifications to obtain high adsorption rates, improve their capacity, selectivity and performance, such as changing the surface via a chemical process, where the porous modification increases the solid/gas interaction and improves their adsorption capacity for better adsorption (Khalil, Aroua & Daud, 2012). According to Marsh and Rodríguez-Reinoso (2006), impregnation of AC can be used to enhance adsorption properties. Moreover, impregnation and grafting are the most applied methods for various amines supports, such as MCM41 (Zeleňák et al., 2008), MCM48 (Huang et al., 2003), SBA15 (Hiyoshi, Yogo & Yashima, 2005), carbon nanotubes (Su, Lu & Chen, 2011), membranes (Cota & Fernandez Martinez, 2017), and zeolites (Su et al., 2011; Nik, Nohair & Kaliaguine, 2011). Recently, amine modified supports have been regarded as potential materials to minimise the cost of CO_2

capture, improving the adsorbent capacity and reducing the amount of adsorbent required for the PSA process (Gray et al., 2008).

Activated carbons exhibit a large capacity and versatility to adsorb specific materials in liquid and gaseous phases, but they also have several limitations. For instance, the adsorption of toxic gases with low molecular mass, low boiling point and notable polarity is not possible using conventional ACs, where the adsorbate retention is insufficient (Marsh & Rodríguez-Reinoso, 2006). Consequently, surface and pore modifications for higher interactions are necessary for ACs, increasing their capacity for carbon dioxide capture for adsorption processes. Surface modifications and treatments are applied to enhance adsorption rates and adsorption capacity, with chemical solvents employed to modify pore structure and improve the solid/gas interaction for a high adsorption capacity (Khalil et al., 2012).

1.2. Study Aims

Activated carbons (ACs), Norit® RB1 and Cabot R2030, were investigated for their potential for carbon capture, aiming to provide stable adsorbents for use in high adsorption temperature processes, such as pre- and post-combustion conditions. For this purpose, the study objectives were to:

- Achieve surface and pore modification via impregnation procedures adapted from Wang and Guo (2016) and Khalil et al., (2012) based on chemical and amine solutions to improve the adsorption capacity and affinity for CO_2 molecules when exposed to a gas binary mixture.

- Obtain high adsorption capacities and selectivity, focusing on the surface area and pore modifications, and improvement of solid/gas chemical affinity for carbon dioxide adsorption under pre- and post-combustion conditions.
- Optimise the conditions and loading of surface modification treatments to maximise the adsorbent behaviour for the uptake of CO_2.
- Characterise the modified and unmodified ACs potential for CO_2 adsorption via:
    - high pressure volumetric analyser (HPVA), Brunauer-Emmett-Teller (BET), thermogravimetric analyser (TGA), X-ray diffraction (XRD), Fourier transform infrared spectroscopy (FTIR) and scanning electron microscopy (SEM).
- Test the unmodified and modified ACs according to an adaptation of the methodology described by Sun et al. (2015) and Caldwell et al. (2015) for FBR-PSA experiments under pre (25ºC/25 bar) and post-combustion (70ºC/10 bar) conditions. Evaluate the adsorbents in a laboratory scale fixed bed reactor (FBR) process via PSA methodology, generating breakthrough curves experimentally measured for novel adsorbents developed in this study.
- Compare experimental data to the computational FBR-PSA process, including prediction of parameters required for Carbon Capture and Storage (CCS) models, by fitting a gPROMS® fixed bed axial dispersion model to data for conditions such as dispersion and mass transfer coefficients.

Additionally, the novelty of this work arises from the use of blended amine solutions for post- and pre-combustion adsorption process. In the post-combustion scenario, among fifteen treated

adsorbents with amine solutions, seven modified ACs provided higher capacity and selectivity towards carbon dioxide compared to their unmodified versions. In parallel, from twenty-two modified samples, four impregnated ACs showed high affinity and capacity for carbon dioxide molecules at pre-combustion adsorption conditions.

1.3. Thesis Outline

This thesis comprises seven chapters. Chapter one provides the study background and primary aim. Chapter two reviews the literature regarding carbon dioxide capture technologies used worldwide, outlining the current energy trends for countries with consolidated carbon capture and storage rules as well as strategies for pre- and post-combustion scenarios in the oil and gas field. Integrated gasification combined cycle (IGCC) power plants and developing technologies are also explored, followed by adsorbent materials and typical properties for PSA processes.

Chapter three details the experimental methodology used, describing the modified AC impregnation method via amine and chemical solutions, as well as introducing the characterisation techniques employed, for instance, BET, HPVA, Fourier transform infrared spectroscopy (FTIR), SEM, thermogravimetric analyser (TGA), XRD, and the PSA process applied in a FBR.

Chapter four describes the post-combustion experiments, critically dicussing the methodology and the pertinent results for unmodified and modified carbons experiments from the characterisation techniques mentioned in chapter three. The results of the pre-combustion experiments are presented in chapter five and compared to predicted capacities from HPVA studies.

Chapter six reports the mathematical modelling of PSA developed in gPROMS® Model Builder v4.1.0 software [created by Process System Enterprise (PSE), London-UK]. Parameter estimation studies were conducted by fitting the model to the data obtained from PSA experiments, estimating the breakthrough curve of the unmodified and modified carbons by fitting different parameters in the model, such as axial dispersion, mass transfer and particle size. PhD student Rebeca Azpiri Solares provided the model codes used for the process simulations, while Douglas Soares provided the experimental data used to run the parameter estimation fitting. This work was performed in collaboration.

The conclusions of the experimental and modelling evaluation are provided in chapter seven, with suggestions and proposals for further work.

CHAPTER 2: LITERATURE REVIEW

2.1. Introduction

Despite recent advances in alternative technologies, such as wind, batteries and solar power, greenhouse gas mitigation is still a problem faced by many countries around the world. It is supported by the elevated amount of CO_2 emitted by industrial activities and the limited investments to develop technologies to reduce this problem. Moreover, the solution is likely to require cooperative international effort. Carbon dioxide is the main greenhouse gas, due to its high potential to accelerate global warming and the massive amount emitted into the atmosphere, being concentrated in levels above than 411 ppm according to the Global Climate Change programme of the National Aeronautics and Space Administration (NASA, 2019). Biofuels and alternative ways to produce clean energy have been developed and are starting to be applied in many countries, gaining a larger market share in some parts of the world. Relative to the annual biofuels production, Brazil produced 4.3 million cubic metres converted from sugar cane biomass, equivalent to 56.2% of the overall capacity of biofuel (B100) plants (Ministry of Mines & Energy of Brazil, 2017). In contrast, biofuel implementation in the UK is rather limited, with two of Europe's largest biofuels plants (Vivergo and Ensus) located in the UK (Financial Times, 2015) being closed. Vivergo was the largest biofuel plant in the UK, owing to a production capacity of up to 420 million litres. The production of biofuel has been not widely implemented due to political concerns, delaying the application of E10 in the UK energy mix (Biofuels Digest, 2018).

Wind and solar energy (total world production: 1122.7 and 442.6 Terawatt-hours, respectively) are an attractive expansion in comparison with the total world production of biofuels (84 Mt oil equivalent) referred to the world fuel production scenario in 2017. Moreover, hydropower remains the most abundant source, but is losing ground to wind and solar energy production

(European Commission, 2018; Eurostat, 2018; British Petroleum, 2018). Life cycle programmes, such as the EU Action Plan, encourage the application of methods to solve the problems of waste and greenhouse gas emissions by re-utilisation of products, assisting the environment and the economy. Furthermore, this programme impacts on the low carbon economy, providing sources of employment, improving competitiveness as well as efficiency. Greenhouse gas levels in the EU are below those of other developed countries, such as United States, Canada and Australia. Developing countries, such as Brazil and China, have committed to contributing to greenhouse gas (GHG) reduction targets, following the Paris Agreement proposal (China National Renewable Energy Centre & Energy Reform Institute, 2018). In parallel, energy policies have been implemented to achieve the proposed targets as well as reducing energy consumption. On the large scale, the only country which decreased their dependency and use of primary energy more than EU countries was Japan, whose consumption was 16% less in 2015 compared with 2005 (Eurostat, 2018; China National Renewable Energy Centre & Energy Reform Institute, 2018).

World CO_2 emissions are predicted to increase from 32.2 billion metric tonnes in 2012 to 35.6 billion metric tonnes in 2020, and probably 43.2 billion metric tonnes in 2040, according to an IE02016 study case (U.S. Energy Information Administration (EIA), 2016). Most of these emissions are from the non-Organization for Economic Cooperation and Development (non-OECD) nations, for instance, Brazil and China, due to their strong dependency on fossil fuels. The EU is the largest investor in global warming mitigation (British Petroleum, 2018), with most EU countries willing to respect the targets proposed. As a corrective action, the EU Council determined in October 2009 to achieve a 80–95% reduction in global warming by 2050, reaching similar levels to 1990s (European Commission, 2016; China National Renewable Energy Centre & Energy Reform Institute, 2018). Denmark is considered as a pioneer in clean

energy generation, the transition impacting on electricity and heating methods (China National Renewable Energy Centre & Energy Reform Institute, 2018), with Germany being the highest investor in renewable energy in Europe. The German status of annual renewable energy production is solar: 39.9 Terawatt-hours; wind: 106 Terawatt-hours; and biofuels: 3293 thousand tonnes oil equivalent, demonstrating their massive investment in research for climate change mitigation (British Petroleum, 2018). The German low carbon energy transition plan is supported by the targets of GHG reduction, reaching a reduction of 27.6% by 2017 and aiming to achieve -40% in 2020, -55% in 2030, -70% in 2040 and up to 80–90% until 2050 (Hedberg, 2017).

Recently, efforts to develop technology in carbon dioxide emissions reduction were applied in the UK to mitigate their contribution to the acceleration of global warming. Renewable sources have been incorporated in the UK energy mix, substituting coal-fired electric production with clean sources. Additionally, low carbon generation technologies have been introduced, including CCS fitted to fossil fuel power plants. Three different scenarios has been proposed in the UK to achieve the COP21 target by 2030 [Concentrated: 2 projects for gas conducted to CCS at Southern North Sea (SNS) storage; and Enhanced Oil Recovery (EOR)]. Recent studies demonstrated that the carbon emissions in the UK have fallen for the sixth consecutive year (based on the Department of Business, Energy and Industrial Strategy's report), wherein the amount emitted in 2018 was estimated at 361 million tonnes ($MtCO_2$), providing a reduction of 1.5% (Climate Action, 2019). However, efforts still need to be applied to achieve future GHG mitigation targets as shown in Table 2.1.

Table 2.1. Energy production overview by countries with profiles corresponding to the largest producers

Countries	CO_2 reduction target[1]	Period	Clean Energy Amount Produced (until December 2017)				References
			Wind (TWh)	Hydropower (TWh)	Biofuels	Solar	
Brazil	30%	2030	42.7	410.24	18465	0.7	(Carbon Brief, 2015; Barros et al., 2018; British Petroleum, 2018; Climate Action Tracker, 2018; International Hydropower Association, 2017)
Canada	30%	2030	32.5	379.63	1239	3.2	
China	20%[2]	2030	286.1	1,180.70	2147	108.2	
Germany	80-90%	2050	106.6	21,50	3293	39.9	
UK	80%	2050	49.6	4,53	617	11.5	
EU	40%	2030	383.4	595	14167	124.1	
	80-95%	2050					
USA	26-28%[2]	2025	256.8	266.39	36936	77.9	

[1]Quantity of carbon dioxide proposed to be captured to achieve and be compared with 1990 levels.

[2]Quantity of carbon dioxide to be captured and compared to the 2005 levels.

Brazil has the third-largest electricity sector in the Americas, competing only with the United States and Canada, respectively (U.S. Energy Information Administration (EIA), 2016; Coballasi et al., 2018). Large scale studies of renewable fuels have been conducted in Brazil to reduce the dependence on hydropower and fossil fuel generation, as well as the impact on the energetic mix. Solar and wind power generation are advantageous for Brazil due to its climate and land area. Moreover, biofuels projects, such as the production of ethanol from sugarcane bagasse and biogas from biomass, have been widely exploited to reduce the reliance on fossil fuels and hydropower, aiming to substitute the new fuels to supply transport with biodiesel from B10 (10% of ethanol in the diesel) to achieve B15 levels until 2020. Additionally, the industrial energy supply of ethanol from sugarcane bagasse conversion has also been considered (Román,

2014). By contrast, investments in the oil and gas sector have been made to promote Brazil as one of the largest oil producers in the world by 2021.

Carbon capture and storage has received considerable attention in Brazil. Projects for greenhouse gas mitigation, from the total 0.1 Mt/year CO_2 emitted, have been implemented to meet targets proposed in COP21 (Ketzer et al., 2014; Global CCS Institute, 2018). However, these investments have been on a small scale, with most carbon dioxide emissions from oil and coal utilisation (1.07 and 0.92 kg $CO_{2equivalent}$/kWh). Nevertheless, hydropower generation occupies the position as the primary renewable source to generate energy, providing 0.08 kg $CO_{2equivalent}$/kWh to the global warming potential (GWP) (Barros et al., 2018).

Most of the CO_2 captured (providing an estimated capacity of 950 $MtCO_2$) is transported to a reservoir for reinjection via Enhanced Oil Recovery (EOR) application in the Campos basin of the Pre-salt region (Rockett et al., 2013). EOR techniques increase the quantity of oil that can be extracted from the reservoir, up to 30–60%, whereby the reinjection of CO_2 raises the pressure and extends their lifetime by forcing more oil out of the rock matrix than would otherwise occur (Jansen et al., 2015).

Bioenergy and Carbon Capture and Storage (BECCS) is as an alternative to greenhouse gas mitigation in Brazil. The sugar cane bagasse process provides negative emissions destined for ethanol and electricity generation (Moreira et al., 2016). The main idea proposed is bioenergy generation combined with carbon capture and storage. However, this process involves a lot of criteria that reduces its motivation, such as the demand for bioenergy from the vehicles and competition with food production (Anderson & Peters, 2016).

China's economy has been growing significantly year by year, and this fact is reflected in clean energy production investments. China is trying to catch up with the biggest countries in the

fight against climate change, promoting energy transition cooperation projects and developing long-term energy process scenarios involving low carbon emissions with Brazil and India. The 'Made in China 2025' plan consists of clean technology (renewable energy) applied to diverse sectors, for instance, electric vehicles, and advanced power programs (China National Renewable Energy Centre and Energy Reform Institute, 2018; U.S. Energy Information Administration (EIA), 2016). Solar energy has been added to the Chinese energy mix, with investments increasing from 16% to 26% from 2005 to 2016 to improve air quality, minimise fossil fuel dependency and reduce greenhouse gas emissions.

Greenhouse gas mitigation is the primary target against climate change by many companies and countries around the world, respecting the Paris Agreement (COP21) established in 2015 and updated in 2018 at the 24th Conference of the Parties (COP24) (Global CCS Institute, 2017; UNFCC, 2018). The main agreement was concerned with "holding the increase in the global average temperature to well below 2^{o}C above pre-industrial levels and pursuing efforts to limit the temperature increase to 1.5^{o}C above pre-industrial levels". Many countries around the world have already published their targets, purposing to participate in GHG mitigation to help achieve the global target (40 Gt CO_2) (Anderson & Peters, 2016). However, due to the rigorous COP21 target compared to emissions and the stage reached by many countries, it is anticipated that this mission may be unsuccessful.

Recently, new technologies and materials (such as adsorbents with high potential for CC application) have been introduced to help mitigate global warming. Researchers around the globe are attempting to develop processes to try to meet the targets proposed. Furthermore, the only technology which has reached a mature stage for utilisation is chemical absorption with alkanolamine solvents (da Silva & Svendsen, 2004; Gabrielsen et al., 2005; Lin & Park, 2011;

Yu, Huang & Tan, 2012; Spigarelli & Kawatra, 2013). However, physical absorption using propylene carbonate as the main solvent, membrane permeation, cryogenic and adsorption remain at an early stage of development (Ruthven, 1984; Thambimuthu et al., 2005; Plaza et al., 2017).

Moreover, the most promising technology for adsorption on a solid is the PSA process due to its facility for adsorbent regeneration and lower energy penalty compared with regenerating liquid absorbents. Hoever, adsorption technology is limited by the need to develop a novel adsorbent with high CO_2 affinity and capacity for the gas separation process (Yang, 1987; Wang et al., 2015; Siqueira et al., 2017; Dowson et al., 2016).

2.2. Carbon dioxide capture strategies and respective technologies commonly applied to greenhouse gas mitigation

In practical terms, CO_2 capture processes are most readily applied at sources which present high acidic gas concentration levels, for instance, fossil fuel power and processing plants. Strategies for CO_2 capture from industrial process streams were created more than 80 years ago based on the chemical absorption process. However, they were not widely applied due to the lack of political and economic motivation for carbon dioxide mitigation (Kohl & Nielsen, 1997). Adsorption technology is a promising future carbon capture system due to the numerous advantages when compared with the developed absorption process (Thambimuthu et al., 2005; Siqueira et al., 2017). The chemical absorption process has been widely used for carbon dioxide sequestration, but is associated with several disadvantages including:

- the solvent cost (Bonalumi et al., 2017).

- stripper columns, which require a massive amount of energy to regenerate the solvent (Liu et al., 2014; Yu et al., 2012), 60% of the overall energy required for the plant operation (Rochelle, 2009; Wiheeb et al., 2016b).
- high corrosion levels promoted by the aqueous amines solutions, which reduce the lifetime plant utilisation due to the tubes and equipment (Sutar et al., 2012; Hasib-ur-Rahman, Siaj & Larachi, 2012).
- high volatility potential for the amine solvents, where a small amount of the solution might be exhaled and emitted to the stripper column along with flue gas (Rochelle, 2009; Wiheeb et al., 2016a).
- high energy consumption, which is required for the cooling stage of the solvent and the flue gas when products leave the stripper column and are transferred for regeneration. The product from the stripper column is detached from the solvent in a flash vase and also needs to be cooled, then compressed. In offshore conditions, the natural cold water from the sea is used for cooling, but onshore, heat exchange is required to achieve the recommended temperature.
- CO_2 gas compression requires high energy consumption to achieve the desired final conditions for the product absorbed.

Another fact that needs to be considered is the oxidative/thermal degradation of the solvent during regeneration, which impacts on the overall amount of amine solution in the stripper column, resulting in a low potential for absorption and reactivity. To avoid this problem, fresh absorbent injection needs to be carried out periodically, elevating the operating cost (Dutcher, Fan & Russell, 2015). The gas composition may present some differences from various

reservoirs around the world, which must be considered when selecting the most suitable carbon capture technology to purify the gas, particularly taking into account the acidity levels. Solid adsorbents are ranked as the most suitable materials for CO_2 capture due to their considerably solid/gas affinity, adsorption capacity, selectivity and high-pressure resistance, avoiding loss in performance when submitted to repeated adsorption-desorption cycles at pre-combustion conditions. Two different forces (physical and chemical) occur for CO_2 adsorption at the surfaces of the adsorbents in an adsorption process, known as physisorption or chemisorption interactions (Veneman, Kamphuis & Brilman, 2013).

Adsorption processes have many advantages compared to chemical/physical absorption processes because there is no necessity to apply energy for solvent regeneration. Other important reasons need to be considered, for instance, a faster and simpler process to regenerate the adsorbent with low cost, adsorbents generally have high capacity, fast kinetics, and long-term working capacity (Satyapal et al., 2001; Kapdi et al., 2005; Eze & Agbo, 2010; Wiheeb et al., 2016a). The reduction in the total energy consumption of the regeneration process makes this process more attractive, which significantly reduces the overall cost. Two types of regeneration strategy are considered in CO_2 capture from a gas mixture in the adsorption process (Grande, 2012):

- PSA in which the CO_2 adsorbed is removed from the adsorbent surface/pores, and the adsorbent can be reused through the operational pressure reduction
- Thermal Swing Adsorption (TSA), where the regeneration of the adsorbent is applied through the operating temperature variation

The typical sources of CO_2 suited for capture arise from point sources, namely, coal thermoelectric, refineries and industries. The principal modes for operation of carbon capture

technology are pre- and post-combustion, although oxyfuel is another technique gaining attention. The aim of pre-combustion is to first gasify the fuel and convert it via reforming to a mixture of CO_2 and hydrogen. The hydrogen produced can be burnt to generate electricity or used to power cars and homes, while the CO_2 needs to be separated for sequestration or utilisation. Pre-combustion power plants have to be designed as an integrated unit connected with the separation step. However, it has the advantage that the CO_2 is captured from a concentrated stream. Post-combustion involves fitting a capture process to the flue of conventional power plants, which facilitates separation of gaseous streams of CO_2 from nitrogen. In post-combustion conditions, the adsorption is conducted at low pressure (at atmospheric conditions, 1 bar) and higher temperature (typical temperature for a flue gas: 50–150^oC) conditions (Chen et al., 2013).

According to Figure 2.1, relative to post-combustion and industrial processes, CO_2 is extracted from mainly nitrogen in the exhaust gases by adsorption, absorption, cryogenic and membrane permeation techniques. In the pre-combustion processes, the carbon dioxide is extracted from the fuel before they are burnt, producing a binary mixture of hydrogen and carbon monoxide (CO), then the gas reacts with water to convert CO into CO_2.

In oxyfuel processes, the fuel is burnt with high oxygen rates rather than air, and the obtained CO_2, being entirely pure, is recovered as exhaust gas. After capture, CO_2 needs to be compressed and transported to the injection area in a geologically appropriate place. CO_2 transport is mainly accomplished by “carboducts” or by ships, which is the most economical (Valencia, 2007).

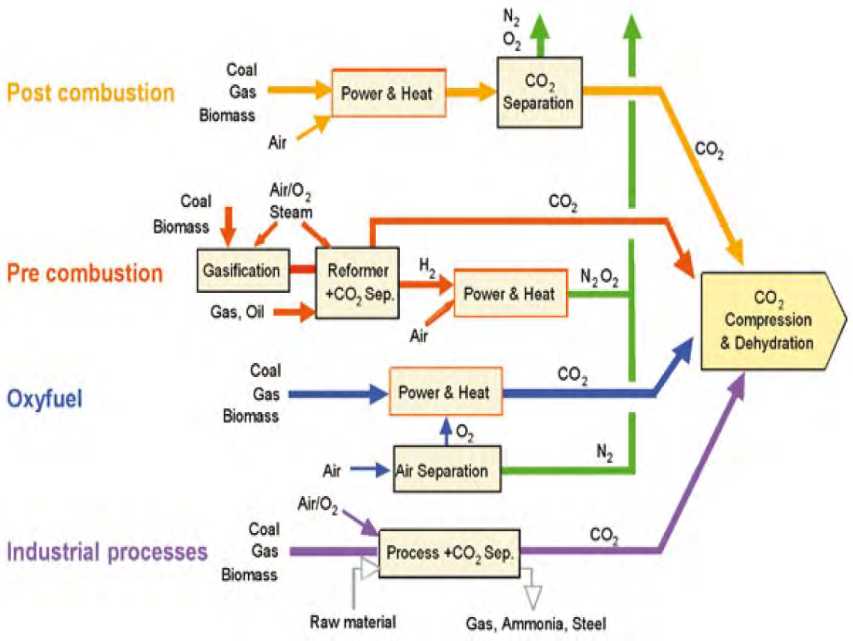

Figure 2.1. Four main processes for carbon capture applied to adsorption technology (Global CCS Institute, 2018)

Adsorbent physical properties must be carefully designed to achieve elevated amounts of CO_2 separation, so that the materials exhibit high mechanical strength and are stable in multi-cycle adsorption-desorption (Spigarelli & Kawatra, 2013; Li and Hitch, 2015). Physisorbent materials, for instance, AC and zeolites, are potential candidates due to their low cost to the manufacturers (Dantas, Rodrigues & Moreira, 2012).

The application of adsorbents impregnated by amine solvents have been studied by various research groups due to the lower heat capacity provided by these modified adsorbents when submitted to adsorption stages (Hahn et al., 2015). Yu and Chuang (2016) investigated the nature and structure of adsorbed CO_2 on immobilised amine sorbent tested in the presence and absence of water vapour via infrared spectroscopy. It was observed that the reaction between the CO_2 and amines molecules occurred in two stages. In the primary amine, a reaction occurred

to generate ammonium carbamate, and the secondary amine to generate the carbamic acid. The adsorption capacity and the accessibility of amine sites on the immobilised adsorbent increased in the presence of water vapour at the secondary amine stage, the binding strength, the adsorbed species interaction onto the immobilised adsorbents and the CO_2 molecules.

Quang et al. (2016) investigated the thermal stability of amino-functionalised adsorbents for CO_2 capture. The mesoporous silica adsorbent was impregnated using 3-aminoproprytriethoxysilane (APTES), wherein amino functional groups were chemically bonded to the adsorbent surface. The amine impregnation provided high stability and CO_2 adsorption capacity when tested at 205^oC (89.3 mg CO_2/g, constantly) compared to other modified mesoporous silica impregnated with polyethylenimine (160^oC) when tested at seven adsorption-desorption cycles. The constant CO_2 loading by the impregnated APTES mesoporous silica make the adsorbent suitable for carbon dioxide capture utilisation.

Hahn et al. (2016) investigated the mechanism of CO_2 adsorption on primary, secondary and bibasic aminosilanes synthetically functionalised in porous SiO_2 via FTIR, TGA and quantum mechanical modelling. The principle for amine and CO_2 interaction followed a similar mechanism reported by Yu and Chuang (2016). The high base strength of secondary amines enables the stabilisation of carbamic acid due to their association with Si-OH groups (either protonation or hydrogen bonding). It was concluded that the steric hindrance of the formation of intermolecular ammonium carbamates leads to higher uptake capacities for secondary amines functionalised on the SiO_2 surface and pores at higher amine densities.

Santiago et al. (2019) reported the success of the amine impregnated on mesoporous silica using 3-aminoproprytriethoxysilane (APTES), as investigated by Quang et al. (2016). The modified adsorbent was tested in a FBR under CO_2-N_2 adsorption TSA (adsorption temperature: 90^oC)

conditions. High values of adsorption enthalpy (100 $kJ.mol^{-1}$) demonstrated the occurrence of chemisorption related to the CO_2 with the amines impregnated. The breakthrough curves generated by pure carbon dioxide, nitrogen and the CO_2-N_2 mixture (15/75% v/v) indicated good agreement with the uptake amount of CO_2 when compared to the curves generated by tests under individual gases. The material showed very stable behaviour after twenty sucessive cycles, so was considered suitable for adsorption cyclic processes application.

Zhao et al. (2019) enhanced the CO_2 adsorption capacity by the impregnation of tetraethylenepentamine (TEPA) onto an amine-tethered sorbent. The adsorbent tested at 60ºC and 15% CO_2 in a flowrate of 1200 $ml.min^{-1}$ achieved high CO_2 uptake capacity 1.19 mmol CO_2/g. Additionally, the amine-tethered modified adsorbent demonstrated stable adsorption capacity during the five repeated cycles. Goeppert et al. (2019) also reported the impregnation of TEPA on propylene oxide (PO) surface to enhance their CO_2 adsorption capacity, concluding that the modified adsorbent provided high resistance and stability, specially under oxidative conditions, when compared to the virgin conditions. The amine modification also impacted positively on the CO_2 adsorption capacity, wherein the adsorbent was able to capture more CO_2 molecules from different sources, including ambient air and indoor air containing CO_2 (400–1000 ppm).

These studies on the development and insertion of amine functional groups onto adsorbent surfaces significantly contributed to the creation of novel adsorbents for carbon dioxide capture in the adsorption process. However, ACs are considered as the most potent material for CO_2 sequestration in adsorption processes, owing to their high hydrophobicity. This behaviour means that the adsorbents are not too adversely affected by moisture in the flue gas, improving relevant aspects such as adsorption capacity and selectivity for the acidic gas), as well as their

highly inter-connected porosity network, which helps the gas to diffuse into the interior of the adsorbent (Rashidi & Yusup, 2016).

Post-combustion is the most employed route for industrial carbon sequestration, which promotes the removal of exhaust gas from fossil fuel combustion. A highlighted advantage, related with acceptance for this process, is the ease of retrofitting the implemented power plant process with no need to change the combustion system (Leung, Caramanna & Maroto-Valer, 2014; Singh, Anil Kumar & Kumar, 2015; Hammond & Spargo, 2014). Furthermore, the power plant can continue operation even if problems occur in the capture system (Songolzadeh et al., 2014).

The application of adsorbents in post-combustion conditions has been most frequently investigated, for instance, submission to high adsorption temperatures and CO_2 concentrations. This method can reduce efficiency penalties when compared to absorption processes (Montagnaro et al., 2015; Rashidi & Yusup, 2016; Cormos, 2015). A FBR allows investigation of adsorption and desorption procedures providing operational cycles. The main challenge for post-combustion conditions in PSA is to develop a low-cost material which provides elevated capacity potential, high affinity for CO_2, chemical and mechanical stability when applied to an extensive operational cycle.

Relative to pre-combustion processes, new concepts have been included as a powerful technology to capture CO_2 and improve the efficiency of the process, for instance, IGCC (DOE/NETL, 2009, 2013). This process is integrated with pre-combustion conditions and allows capturing the CO_2 emitted from a power plant which uses fossil fuel, such as coal, as raw material. The fuel is gasified by steam and oxygen, obtaining CO and hydrogen. Then, the CO is converted to CO_2, via a water-gas-shift reaction, obtaining the final products of CO_2 and

water, as well as a certain quantity of hydrogen. The outlet product stream is found at elevated pressures (35 bar), is composed of CO_2 (0.4) and hydrogen (0.6). Consequently, the CO_2 needs to be separated from the gas mixture. However, the proportion of the CO_2 extracted is not higher when compared to the final product after the water-gas-shift reaction, where the composition is found at low pressures (1 bar) and 3–15% of the CO_2 volume (Casas et al., 2012). For this reason, the PSA process is the most effective for CO_2 capture owing to the high capture rates and purity.

2.3. Adsorption: concepts and definitions

Adsorption is a physicochemical phenomenon defined by transportation of components from gaseous and liquid phases to solid surfaces considering the enrichment of components in the surface of a determined material. The components adsorbed in this stage are denominated as adsorbates, and the solid phase which promotes adsorbate retention is defined as adsorbent (Masel, 1996; Gregg & Sing, 1982).

Adsorption efficiency depends on the surface area that is exposed to a gas (Von Saussure, 1814). When adsorbents are exposed in contact with a gas concentration at a certain pressure, the adsorption process starts. The adsorbent weight increases with increasing pressure of the gas as equilibrium is achieved, as represented in Figure 2.2 (Gregg & Sing, 1982; Delgado et al., 2006). Consequently, the pressure of the system stabilises and the mass of the adsorbent does not further increase. Adsorption isotherms are produced by the measurements at constant temperature and at a determined pressure. The relationship or plot of the adsorbed gas as a function of pressure provides an adsorption isotherm (Gregg & Sing, 1982).

Adsorption occurs due to the forces between the adsorbent and the gas molecules. During weak interactions, such as Van der Waals forces, physisorption occurs in the system, but when chemical bonds attach to the adsorbent, chemisorption is promoted (Campbell, 1988), otherwise, desorption has the opposite function. This process is defined as the disconnection of weak/chemical interactions, promoting the expulsion of the gas adsorbed from the surface via a reduction in the pressure (PSA) of the system, or also when submitted to temperature (TSA) higher than that used in the adsorption stage (Campbell, 1988; Gregg & Sing, 1982). Nowadays, the process most used is based on PSA conditions combined with TSA at the desorption stage. It is motivated by the number of heating cycles required for a complete CO_2 desorption in the bed packed with adsorbents. The adsorbent is surrounded by particles in a fixed bed through which the fluid phase flows continuously until there is no mass transfer when the bed becomes saturated.

Adsorption has been used for CO_2 capture via the synthesis gas for hydrogen production. However, this process has not been used on a commercial scale due to the limitations concerned with the development of powerful adsorbents more selective for CO_2 molecules (Thambimuthu et al., 2005; Zhao et al., 2018). CO_2 can be captured from the post or pre-combustion gas streams, where several elements need to be respected (Valencia, 2007):

- A pre-treatment for the flue gas flow needs to be applied, reducing the impurities (e.g., NO_x, SO_x, and H_2O) present in the stream
- CO_2 molecules compete with the components previously mentioned for the adsorption sites, where the CO_2 adsorption capacity tends to be sharply reduced
- The flue gas needs to be subjected to a drying stage before the adsorption

2.3.1. Adsorption materials

Adsorbents have the ability to selectively adsorb one or more gases from a simple flow or a gas mixture. A variety of solid adsorbent materials for adsorption of gases and liquids are defined by their selectivity and capacity, qualifying as potential candidates for commercial adsorbents application (Henley, 2011). However, there are limitations, motivated by the lack of effective adsorbents, which encourages researchers to focus on the design and synthesis of advanced CO_2 adsorbents (Zhao et al., 2018). Figure 2.2 represents the adsorbent properties and how the adsorbed molecules are allocated on their surface, respective of molecule sizes.

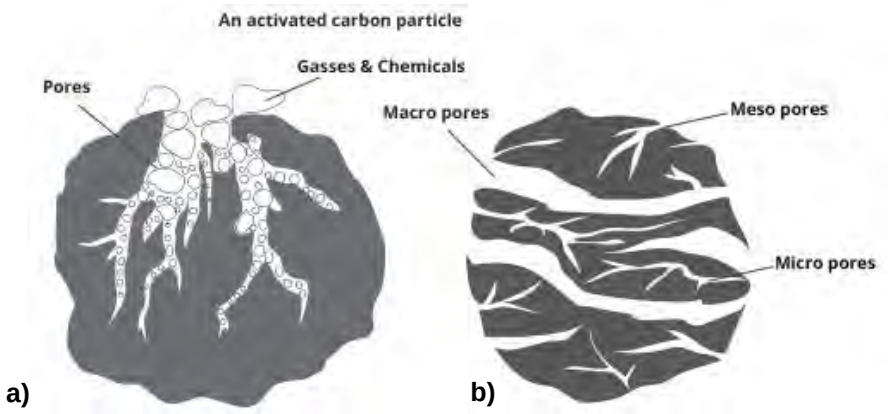

Figure 2.2. Schematic representation of adsorption on the adsorbent surface and how the gas molecules are arranged inside the pores (AquaCache, 2018): A) gaseous molecules adsorption mechanism; and B) pore diameter classifications for AC materials.

As shown in Figure 2.2, sizes are classified by their diameter and defined in three categories (Campbell, 1988; Gregg & Sing, 1982):

- Microporosity: pores smaller than 2 nm
- Mesoporosity: intermediate diameter range between 2 nm to 50 nm

- Macroporosity: pore diameter greater than 50 nm

It is necessary to further investigate the type of adsorbent most suited to treat the fluid applied. Details about adsorbent properties, their typical application and conditions are briefly described in Table 2.2, including a list of the most commonly used absorbents.

Table 2.2. Adsorbents and their main operational settings for adsorption (Zhao et al., 2018; Rufford et al., 2012)

Adsorbent	Type	CO_2 capacity (mol/kg)	CH_4 capacity (mol/kg)	CO_2/CH_4 equilibrium selectivity	CO_2/CH_4 kinetic selectivity	Adsorption temperature (ºC)	Pressure (kPa)	Ref
Pyrazole	Organic compound	8.0	Not mentioned			25	100	(Abdelmoaty et al., 2017)
Hexamethoxymethylmelamine	Resin	3.0				30	100	(Tiwari et al., 2016)
Palm Shell	Biomass	5.3				40	40	(Kongnoo et al., 2016)
Olive stones	Biomass	2.8				40	100	(Plaza et al., 2009)
Mg-MOF-74	MOF	8.50	1.00	8.50	3.8	25	100	(Bao et al., 2011b)
5A (Sinopec)	Zeolite	4.55	0.88	5.19	3.6	25	100	(Saha et al., 2010)
PCB, Calgon Corp	AC	2.41	0.73	3.29		23	100	(Ritter and Yang, 1987)

Adsorbent	Type	CO_2 capacity (mol/kg)	CH_4 capacity (mol/kg)	CO_2/CH_4 equilibrium selectivity	CO_2/CH_4 kinetic selectivity	Adsorption temperature (ºC)	Pressure (kPa)	Ref
Norit RB1 extra	AC	2.20	1.10	2.00		25	100	(Dreisbach, Staudt and Keller, 1999)
PET-DC-0	AC/CMS	2.08	0.02	100.0	100.0	25	100	(Cansado et al., 2010)
Cu-MOF	MOF	0.65	0.35	1.86	9.7	25	100	(Bao et al., 2011a) (Bae et al., 2011)
Maxsorb	AC	13.00	6.00	2.17		25		(Himeno, Komatsu and Fujita, 2005)
Sutcliffe Speakman carbon	AC	8.01	3.69	2.17		25	1000	(Esteves et al., 2008)
Norit RB1 extra	AC	7.60	4.00	1.90		25	1000	(Dreisbach et al., 1999)
PCB, Calgon Corp	AC	7.20	3.90	1.85		23	1000	(Ritter and Yang, 1987)
13X	Zeolite	6.40	2.90	2.21		25	1000	(Cavenati, Grande and Rodrigues, 2004)
1C'-Li	MOF	5.30	2.40	2.21		25	1000	(Mason et al., 2015)
MSC-3k-161	CMS	4.03	2.73	1.48		25	1000	(Watson et al., 2009)

Zeolites have been applied as an adsorbent for CO_2 sequestration. This material has high competitive adsorption of carbon dioxide and water (humidity) for post-combustion studies, which reduces the adsorbent working capacity and stability to deficient levels (Yang, Kim & Ahn, 2010; Yang et al., 2013; You et al., 2013). Their high affinity for water molecules reduces the adsorbent working capacity, so AC application is the most convenient material for the adsorption process under pre- or post-combustion adsorption conditions.

MOFs exhibit high porosity, and the surface has a predisposition for chemical treatment, as shown by gas adsorption studies (Furukawa et al., 2013; Kitagawa, 2017). MOFs present unlocked metal sites which provide high affinity and interaction towards CO_2 molecules, assuring a moderate adsorption capacity (Yaumi, Abu Bakar & Hameed, 2017; Yu et al., 2017). Nevertheless, potential risks to material stability occur, so it is necessary to improve their thermal and structural stability to achieve requirements for operational application on a large scale (Belmabkhout, Guillerm & Eddaoudi, 2016). In contrast, carbon-based materials are an alternative adsorbent of relevance to CCS technology, owing to their high affinity and selectivity for carbon dioxide adsorption in a binary gas mixture. There are many ways to obtain carbon-based adsorbents, including the conversion of biomass, for example, lignin (Saha et al., 2017; Hao et al., 2017), rice husk (Kalderis et al., 2008; Zeng et al., 2016), palm shell (Kongnoo et al., 2016), waste Coca Cola® bottles (Boyjoo et al., 2017), pine cones (Zhu, Shang & Guo, 2016), coconut shell (Guo et al., 2016), cotton stalk (Zhang et al., 2014), chitosan (Fan et al., 2013), and others.

Furthermore, porous AC (carbon-based material) can be obtained from coal, providing low-cost production and aggregating high value for coal utilisation (Olivares-Marín & Maroto-Valer, 2012). For such ACs, a pre-oxidation treatment is incorporated into the carbonisation

procedure to upgrade the pore volume and surface area of the adsorbent. The extension of AC pores is determined by the circumstances in which the material is produced, for instance, carbonisation temperature and the type of precursor selected (Campbell, 1988; Zhao et al., 2018). Oxidation during the AC preparation creates additional crosslinks, which strengthen the stability and structure of the material and decreases their propensity for softening when exposed to high temperatures. With the conclusion of this treatment, these materials have a surface area higher than 1000 m^2/g and are potentially more stable than the original microporous materials (Sun et al., 1997).

There have been many recent studies of AC, regarding adaptability for operational conditions post- and pre-combustion due to the favourable pre-disposal of such materials for CO_2 capture (Zhao et al., 2018; Riboldi & Bolland, 2017). Adsorption occurs at the surface and into the pores of the material, which have the favourable property of a large surface area. Modifications to the AC surface area and pores can be implemented to improve the working capacity, resulting in basic sites over the material surface to increase the interaction for acidic CO_2 capture (Zhao et al., 2018).

2.3.2. Adsorbent treatments: an overview of the impacts of this technique

Activated carbon is applied as commercial adsorbent for diverse treatments besides carbon capture, for instance, water treatment, since it provides a considerable surface area and easiness for their raw material conversion (Khalil et al., 2012). The AC manufacturing process is comprised of four steps: the preparation of the raw material (e.g., wood, coal, petroleum coke and coconut shell), pelletising, low temperature carbonisation process, and lastly, activation (Yang, 1987). The activation process is carried out in a range of 400 to 500^{o}C to remove the

volatiles, then partial gasification at 800–1000ºC. These controlled conditions govern the mechanical properties and the pore structure (porosity and surface area) of the adsorbent (Gregg & Sing, 1982; Zhao et al., 2018).

Regarding surface modifications, AC provides a structure that is amenable to chemical and physiochemical changes by solvents via impregnation. This technique can potentially increase the affinity of the surface for the adsorption of CO_2, leading to enhanced capacity. However, the pore blockage effect by the amines may reduce their capacity to adsorb CO_2, depending upon the conditions of the tests (pre- or post-combustion conditions). For AC, the energy penalty for the adsorbent regeneration is potentially lower than other adsorbents (AC: 3 kJ/mole (25ºC); zeolites: 30 kJ/mole), which offers an economic advantage (Wahby et al., 2010; Montagnaro et al., 2015; Deng et al., 2015; Radosz et al., 2008). However, the activation of the adsorbent during their production does not confer high adsorption affinity during the adsorption stage for particular applications, such as post-combustion conditions (Park & Yang, 2005). Activated carbon presents a limited working capacity when exposed to high adsorption temperatures, due to their pore structure and surface chemistry (Siriwardane et al., 2001). Due to this problem, the relevance of the impregnation treatment to the adsorbent surface increases, aiming to elevate their resistance and capacity for CO_2 capture at high temperature. Many studies for application of adsorbents have concentrated upon post-combustion conditions from coal flue gas, due to the challenge in heat transfer control in large-scale solid systems to achieve high CO_2 capture amounts (Lockwood, 2017).

Impregnation influences the adsorption for CO_2 capture. However, this does not necessarily mean that the adsorbent will achieve high adsorption levels due to the possibility of decreasing the textural features (surface area), which sometimes reduces interaction relative to the insertion

of external groups. This is dependent on the type of solvent selected for the chemical impregnation owing to their reactivity rate over the adsorbent surface and pores.

Figure 2.3. shows the chemical structures corresponding to the amine solvents selected for the AC impregnation in this thesis. Fundamental factors, such as the amine reactivity and the affinity for capturing CO_2 molecules, determined the selection. The selected amine solvents were inspired by the most reported type of amines for absorption processes, and due to their potential capacity to increase the adsorption of CO_2 molecules. Tetraethylenepentamine (TEPA) has the highest potential for carbon dioxide affinity, followed by monoethanolamine (MEA) and methyldiethanolamine (MDEA). TEPA also allows the regeneration of the adsorbent under less intense conditions, for instance, lower temperature and pressure than other alkanolamines (Bonenfant, Mimeault & Hausler, 2003). MDEA and 2-amino-2-methyl-1-propanol (AMP) also work as a co-solvent in MEA solutions to increase the overall capture efficiency of CO_2 (Lin & Park, 2011; Huang, Li & Tsai, 2017). DEA provides a lower vapour pressure when compared with MEA, and this solvent is less favourable to volatilisation (Treese, Pujadó & Jones, 2015).

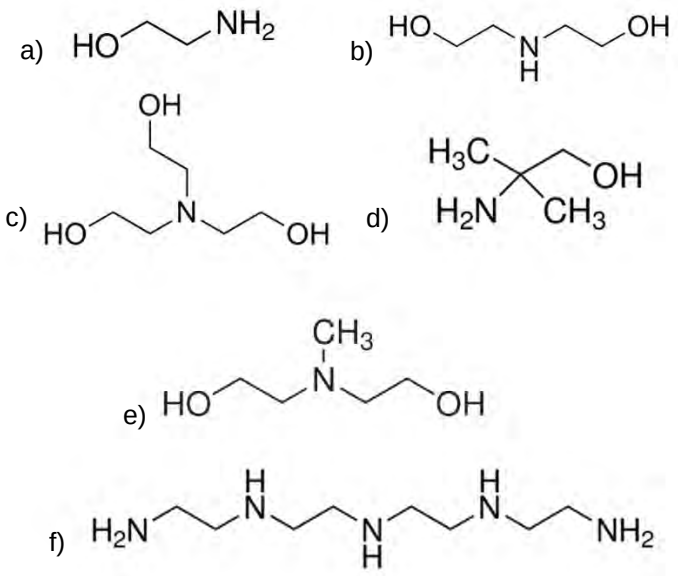

Figure 2.3. Alkanolamine structures applied to post-combustion AC impregnation: A) monoethanolamine (MEA); B) diethanolamine (DEA); C) triethanolamine (TEA); D) 2-amino-2-methyl-1-propanol (AMP); E) methyldiethanolamine (MDEA); and F) tetraethylenepentamine (TEPA)

As the primary objective of this treatment, chemical bonds are created in the material impregnated, improving the gas-solid interactions for CO_2 capture and potentially increasing the time that the adsorbed gas spends on the solid surface (Khalil et al., 2012; Hedin et al., 2013; Lockwood, 2017). Diverse chemicals have been impregnated based on chemical solvents such as potassium hydroxide (KOH), zinc chloride ($ZnCl_2$) and phosphoric acidic (H_3PO_4) for pre-combustion processes. Researchers are also trying to develop adsorbents for chemisorption using MEA as the base solvent. The list of developed adsorbents includes zeolites, MOFs, mesoporous silicas and ACs (Sumida et al., 2012; Bezerra et al., 2011; Chatti et al., 2009; Dantas et al., 2009).

Primary and secondary amines insertion onto the AC surface by impregnation has been considered as a promising technique to reduce costs (Hahn et al., 2015; Grande et al., 2017;

Zhao et al., 2018; Rashidi & Yusup, 2016; Ohs, Krödel & Wessling, 2018; Gholidoust, Atkinson & Hashisho, 2017). Carbon dioxide adsorption on AC typically occurs by the carbamate mechanism, wherein there is a possibility to generate carbamic acid, as represented in nucleophilic attack which generates the chemical mechanism between monoethanolamine (MEA; also applied to other alkanolamines) and carbon dioxide molecules. The active alkanolamine groups attack the partially positive carbon atom relative to CO_2, generating the zwitterionic (ZW) intermediate, then attracting CO_2 molecules from the flue gas to the AC surface, as demonstrated in the following equations (Huang et al., 2017; Das & Meikap, 2018).

$$CO_2 + R_1R_2NH \leftrightarrow R_1R_2NCOOH^- \quad \text{Eq. (2.1)}$$

$$R_1R_2NCOOH + R_1R_2NH \leftrightarrow R_1R_2NCOO^- + R_1R_2NH_2^+ \quad \text{Eq. (2.2)}$$

Zwitterion Mechanism:

$$CO_2 + R_1R_2NH \leftrightarrow R_1R_2NH^+COO^- \quad \text{Eq. (2.3)}$$

$$R_1R_2NH^+COO^- + B \leftrightarrow R_1R_2NCOO^- + BH^+ \quad \text{Eq. (2.4)}$$

Where, R1 and R2 represent alkyl groups.

In parallel, when the reaction occurs in an enviroment that contains water, the primary amine will react as demonstrated in the following equations:

$$CO_2 + OH\text{-}CH_2\text{-}CH_2\text{-}NH_2 \leftrightarrow OH\text{-}CH_2\text{-}CH_2\text{-}NH_2^+\text{-}COO^- \quad \text{(Carbamate) Eq. (2.5)}$$

$$OH\text{-}CH_2\text{-}CH_2\text{-}NH_2^+\text{-}COO^- + OH^- \leftrightarrow OH\text{-}CH_2\text{-}CH_2\text{-}NH_2\text{-}COO^- + H_2O \quad \text{Eq. (2.6)}$$

The MEA reaction mechanisms towards carbon dioxide are described in Eq. 2.1-2.6. The reaction forming carbamate is very fast and the tendency to attract CO_2 is higher than MEA molecules, as the primary amine is more stable than other amines due to their lower viscosity compared to other amine solvents, which affects the CO_2 to a greater extent (Das & Meikap, 2018). MEA provides a higher inductive effect of the only alcohol molecule in the structure, whereas the two alcohol groups present in DEA act as an electron repellent to the N+ ion in the

Zwitterions (Gholidoust et al., 2017). For this reason, the DEA is more unstability for CO_2 capture compared to MEA on the AC surface. Consequently, the MEA modified adsorbents will tend to provide higher adsorption capacities as long the impregnation ratio increases in the amine impregnation (Huang et al., 2017; Das & Meikap, 2018; Rashidi & Yusup, 2016; Grande et al., 2017).

Therefore, the purpose of amine molecules impregnation onto ACs properties was concentrated in the lack of suitable materials for application in post-combustion adsorption conditions. The treatment aims to attach amine groups on the AC surface and pores, which can be activated at higher adsorption temperatures compared to pre-combustion conditions. The basicity level of the adsorbent obtained by alkanolamine impregnation contributes to the improved adsorbent capacity for acid gas adsorption, for instance, carbon dioxide (Lee et al., 2013; Gholidoust et al., 2017).

The amine solvents can cause a reduction in the surface area and pore size due to the pore filling promoted by the attached molecules. This influence tends to impact on the adsorption capacity and selectivity for CO_2, leading to a trade off between enhanced capacity due to chemisorption versus reduced capacity due to loss of surface area (Bezerra et al., 2014). The particular improvement or impairment depends on the material and conditions. Studies on a grafting technique using amine groups have shown that after treatment, the AC CO_2 adsorption capacity was reduced when exposed to high temperatures (Dantas et al., 2009). Researchers are trying to study the insertion of solvents on the AC surface via different techniques, such as impregnation, immobilised amines, oxidation, sulphonation and bromination, aiming to optimise the adsorbent properties (Gholidoust et al., 2017; Khalil et al., 2012).

Studies on immobilised amines have also been conducted. The principle of this adsorbent is quite similar to chemisorption processes. Consequently, it may present high CO_2 uptake levels in post-combustion conditions, with capture on the amine groups supported by adsorbent materials, such as MCM-41 and silica (Franchi, Harlick & Sayari, 2005; Sayari & Belmabkhout, 2010; Serna-Guerrero, Belmabkhout & Sayari, 2010; Hicks et al., 2008; Drese et al., 2009). Although, a disadvantage for this adsorbent is the concern regarding the desorption stage, owing to the limited regeneration and the possibility to modify the amines (Sayari & Belmabkhout, 2010; Choi et al., 2016; Jung et al., 2017; Darunte et al., 2016).

2.3.3. Adsorption equilibrium and isotherms

The adsorbent performance is measured from the adsorption equilibrium data, wherein the information of gas uptake is extracted by the solid surface at equilibrium. It is also essential to understand the role of heat and mass transfer between the gas and adsorbent (Valencia, 2007).

In simple systems, only one curve represents the adsorbate concentration on the solid surface, where the abscissa shows the pressure relative to the saturation vapour pressure, and the ordinate the quantity adsorbed per mass of adsorbent. Each curve is obtained for a given temperature, thus is called an isotherm (Figure 2.4).

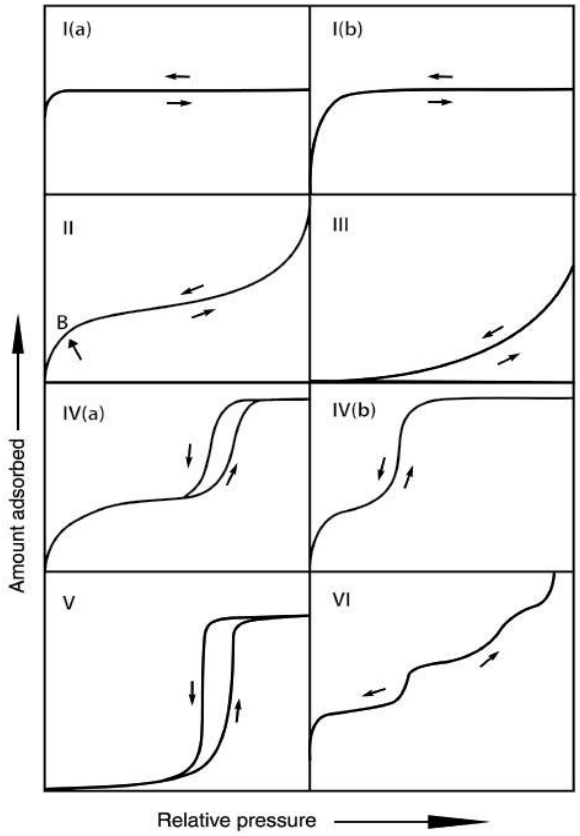

Figure 2.4. The five types of adsorption isotherms (I to V) obtained by BET classification, and the type VI relative to the stepped isotherm. An up-to-date format, relative to the new characteristic isotherms recognised and corresponding to particular pore structures discovered recently, was implemented in the physisorption isotherm classification previously published by IUPAC (Thommes et al., 2015; Gregg & Sing, 1982)

The isotherm results are classified in five different groups (from type I to V) as originally suggested by BET, or just Brunauer classification (Brunauer, Emmett & Teller, 1938; Brunauer, 1944). Type I refers to the properties of a microporous solid material with limited external surfaces (e.g., AC is included in this classification due to its textural properties). The typical curve relative to type I physisorption isotherm shows concave behaviour, plotted by P/P_o axis vs the amount adsorbed. Type I(a) isotherm is obtained from microporous materials which present primary narrow micropores (with a width smaller than 1 nm). Type I(b) is related to

micropore adsorbents which have pore size distributions (PSD) with a wider spread diameter reaching the lowest mesopores limit range of mesopores (lower than 2.5 nm).

Type II isotherm is when an adsorbent has macroporosity. The presence of an unrestricted monolayer or multilayer adsorption when the material is submitted to high pressure gives the shape as shown in Figure 2.4. Point B refers to the formation of a complete monolayer, pressures after this point indicate the possibility of multilayer adsorption (Gregg & Sing, 1982; Thommes et al., 2015).

Type III physisorption isotherm is the most suitable among macroporous materials. Different from type II, there is no point B and no monolayer formation due to the adsorbent-adsorbate weak interactions. Type IV physisorption isotherm is linked with mesoporous materials (such as industrial adsorbents and mesoporous molecular sieves), determined by the absorbent-adsorptive interactions and via the molecule interactions (when in condensate state). The final saturation stage is considered as a typical characteristic of type IV isotherm. Type V isotherm presents a shape similar to type III in low pressure owing to the low adsorbent-adsorbate interactions. When studies are conducted at high pressure, a molecular grouping happens after the pore filling, as observed in mesoporous materials hydrophobic and mesoporous adsorbents applied for water adsorption. The type VI physisorption isotherm is attributed to materials which exhibit adsorption onto the highly uniform nonporous surface (Gregg & Sing, 1982; Thommes et al., 2015).

Hysteresis is defined when the adsorption is not reversible along the same curve of volume adsorbed at specific ranges of P/Po, and its shape and extension are correlated to the operational temperature (Gregg & Sing, 1982; Sing & Williams, 2004), as presented in Figure 2.5. This phenomenon is found in physisorption isotherms obtained from materials with multilayers, and

is connected to the capillary condensation (Thommes et al., 2015). Six different hysteresis types are included in Figure 2.5, where four types (H1, H2(a), H3 and H4) correspond to the first IUPAC classification (1985) (Sing & Williams, 2004; Thommes et al., 2015). However, extensions were applied to the previous classification due to the recently discovered hysteresis types.

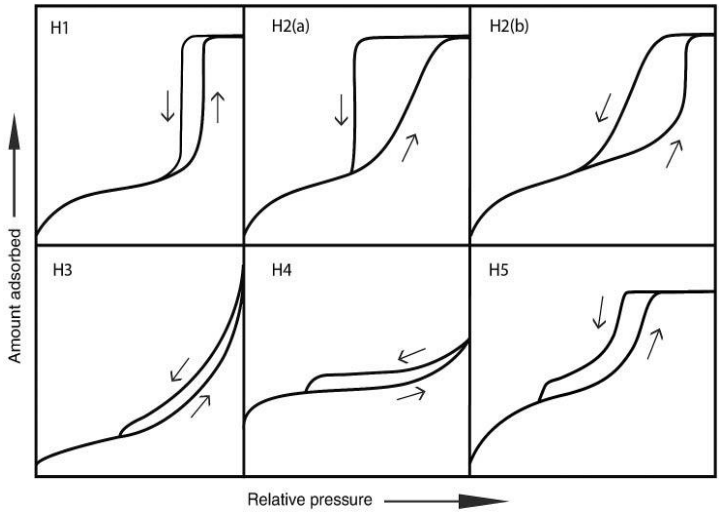

Figure 2.5. Types of hysteresis relative to results from high-pressure studies, HPVA and BET techniques, extended to AC data observed from isotherms generated. Adapted from Thommes et al. (2015).

Types H1 and H2(a) are found by materials with a narrow range of mesopores, such as SBA-15, MCM-41 and MCM-48 as shown in Table 2.2. Hysteresis loops of Type H1 have been found in agglomerates or spherical uniform particles, indicating a high PSD uniformity and contribute to the pore connectivity. Type H2 is obtained in materials with more complicated pore structures influenced by the network effect. Type H2(a) is relative to the pore interruptions or blockages in a short range of the pore structure. Type H2(b) also refers to pore blocking. However, the width size distribution is higher, as shown by silica and other mesoporous adsorbents (Gregg & Sing, 1982; Sing & Williams, 2004; Thommes et al., 2015).

Type H3 is derived by the adsorption of non-polar gases into the mesoporous material, also presenting a feature of desorption shoulders and lower locked points. Type H4 hysteresis loops are associated with the filling of microporous materials and capillary condensation, typically exhibited by AC adsorbents and nanoporous adsorbents. Type H5 is a rare phenomenon derived from materials with determined pore structures that contain open and partially blocked mesopores (Sing & Williams, 2004; Thommes et al., 2015). Isotherms and hysteresis data are typically obtained from HPVA and BET studies. These techniques were ranked to compose the adsorbent characterisation stage, presented by a deep evaluation and discussion in chapter 4 and 5. The most applied isotherms are included in sections 2.3.4 and 2.3.5, which describe the adsorption isotherm equilibrium as an essential requisite to extract information to evaluate a carbon dioxide separation process.

2.3.4. Langmuir isotherm

The Langmuir adsorption isotherm was suggested by Irving Langmuir in 1916, where a variance of adsorption occurred relative to the pressure application (Langmuir, 1916). This equation correlates the number of active sites on the adsorbent surface submitted to the adsorption stage and the pressure. There are five premises involved in the Langmuir adsorption isotherm, which are considered as the main characteristics for this equation application, as shown below (Langmuir, 1917; Huang & Shih, 2016; Bolster & Hornberger, 2008; Langmuir, 1916):

- The number of active sites on the adsorbent surface is not variable

- On the adsorbent surface, these active sites present similar pores shapes and formats

- Relative to the active site, only one gas molecule adsorbs per site, and a determined heat energy amount is released during this process; these sites have equivalent energy, and the adsorbed molecules do not interact among them

- A relation between the gas molecules amount adsorbed versus the gas amount which was not adsorbed will provide the dynamic equilibrium in the system

- The adsorption will occur in adsorbents which present a monolayer or homogenous surface

Among the many existing models of isotherms, the Langmuir isotherm is the most common to represent the monolayer adsorption. In the equilibrium stage, the equation is shown as:

$$\theta = \frac{KP}{1+KP} \qquad \text{Eq. (2.7)}$$

where $\boldsymbol{K}=k_a/k_d$ is the adsorption equilibrium constant, **P** is the pressure of the system, and:

$$\theta = \frac{q}{q_m} \qquad \text{Eq. (2.8)}$$

where $\boldsymbol{q_m}$ is the maximum loading referent to the surface covering, and $\boldsymbol{q}$ is the equilibrium adsorption capacity (mmol/g). Thus, the Langmuir adsorption isotherm is restricted to a monomolecular layer. Combining these equations, their result may be expressed as the *Langmuir isotherm*:

$$q = \frac{Kq_mP}{1+kp} \qquad \text{Eq. (2.9)}$$

The Langmuir isotherm was developed considering: (i) a limited number of approachable adsorption sites, providing similar energy (ii) reversible adsorption. When the rate of adsorption of the molecules on a surface is equal to the desorption rate, it can be condsidered that equilibrium is achieved (Tchobanoglous, 2014). This methodology is widely applied in HPVA studies, where the adsorbent surface is exposed to a gas under high pressure to predict the maximum adsorption capacity and simulate the adsorbent performance. This model was fitted to the HPVA data to describe adsorption behaviours via linear regression, giving the best fit to the isotherms generated and the sorption details obtained. From the fit, the kinetic parameters, such as maximum adsorption capacity and the adsorption equilibrium constant can be derived.

2.3.5. Freundlich isotherm

The empirical isotherm model proposed by Freundlich (1909) summarises the relationship between the material quantity adsorbed and the material concentration in the system (McKay, 1995; Chen, 2015). This model is typically applied to heterogeneous surfaces and used for multilayer adsorption, considered as a non-ideal system. Freundlich isotherm considers that a heterogeneous solid is referred to an exponential distribution to distinguish diverse adsorption active sites types, showing a variety of energy related to the adsorptive stage (Febrianto et al., 2009). This isotherm defines an exponential distribution of heat adsorption and is commonly used to describe a heterogeneous surface controlled by the following equation:

$$q = kp^{1/n} \qquad \text{Eq. (2.10)}$$

Where $\boldsymbol{n}$ and $\boldsymbol{k}$ are temperature-dependent constants for an adsorbent; $\boldsymbol{p}$ is pressure (bar); $\boldsymbol{q}$ represents the amount of gas adsorbed. This fact promotes an unbalanced adsorbent surface due

to the different energies that are given to the active sites, where some active sites might be considered as having highly energetic power (resulting in strong bonds to the gas used) and others as lower energetic power, consequently, impacting on the solid/gas interaction (Cooney, 1999).

To consider the adsorption as favourable, the value for *n* tends to be in the range 1 to 10. Relative to strong adsorbate/adsorbent interactions, the value for *n* needs to be elevated (lower than 1/n). When the value of 1/n is equal to 1, it indicates that the adsorption is linear, and the energy is constant to all active sites involved in the adsorption stage. However, when the value of 1/n is higher than *n*, a higher affinity among the adsorbent and gas is shown, impacting on the promotion of strong intermolecular interactions (Delle Site, 2001). Lastly, this equation is unable to predict adsorption equilibrium data when the gas is submitted to elevated concentrations (Cooney, 1999).

2.3.6. Fixed Bed Reactor (FBR) for breakthrough curve generation in Pressure Swing Adsorption (PSA) process

Adsorption via FBRs has been applied in the PSA process. This process is operated cyclically, to readily achieve high adsorption performance, where the gas is fed at high pressure for adsorption stage and low pressure for desorption step (Ruthven, 1984).

Focusing on high CO_2 adsorption capacity achievement (>99.99% carbon dioxide purity), a variety of PSA processes have been developed to implement an adsorbent with high potential for pre-combustion conditions. At the same time, the typical conditions for CO_2 capture process

may be defined as 95% for gas purity and 90% for capture rate by the utilisation of the most effective commercial adsorbent (Casas et al., 2012; Knox et al., 2016).

Generally, laboratory research consists of two parts. Firstly, tests to determine isotherms to demonstrate the technological viability of treatment with AC, which can be determined from HPVA and the material textural properties from BET studies. Secondly, tests conducted in the column to obtain data which will be used in the large scale project (Walther, 1980). Breakthrough curves are derived from a FBR adsorption process and provide crucial adsorbent information for better understanding relative to their capture capacity. However, there are five different factors affecting this dynamic process which might disrupt the breakthrough curves and the solid/gas interaction performance during the adsorption process, as presented below:

- **Adsorption capacity:** confers a massive outcome in the breakthrough curve impacting on the expansion of the breakthrough time, and empowers the adsorbent to capture more molecules during the process (Bastos-neto et al., 2011; Möller et al., 2017; Montagnaro et al., 2015);

- **Kinetics effect:** responsible for modifying the breakthrough (BT) curve profile, for instance, when the rate of kinetics is faster, the mass transfer area will be reduced. Otherwise, when the mass transfer velocity from the gas into active sites is faster, a reduction in the time required to reach equilibrium occurs (Ruthven, 1984; Bastos-neto et al., 2011; Brunauer, 1944);

- **Mass transfer:** corresponds to the diffusion of gas across a boundary film surrounding the particles and into the pores, providing growth in the adsorbent

mass (Farooq & Ruthven, 1990a; Siqueira et al., 2017; Möller et al., 2017; Ling et al., 2015);

- **Release of heat:** this effect might contribute to the mass transfer phenomenon over the adsorption stage when higher temperature occurs as a result of the heat of adsorption. Such temperature gradients tend to improve the mass transfer level (Farooq & Ruthven, 1990a, 1990b; Raganati, Ammendola & Chirone, 2016; Campbell, 1998; Xiao et al., 2016);

- **Axial dispersion:** occurs when the gas becomes mixed along the length of the bed due to local phenomena, such that the residence time distribution spreads out from the sharp pulse that would be expected if a purely plug flow occurred. The purpose of this effect is to reduce the concentration of gas adsorbed in the FBR. An initial factor to contribute to this effect is when the adsorbent is not well packed in the reactor (Gunn, 1987; Carberry & Bretton, 1958; Delgado, 2006). Another mechanism that also impacts in the breakthrough curve is the turbulence and wall effects, which influences axial dispersion (Knox et al., 2016).

The term breakthrough curve (BT; presented as the primary result obtained from PSA studies) refers to the gas concentration amount at the outlet of a fixed bed, related to the mass transfer zone for the captured gas. Firstly, pure nitrogen flow through the bed such that initial desorption (at 150^{o}C; temperature depends on the methodology applied) occurs to prepare the sample, removing residual gas components from the system. With the conclusion of this stage, the experiment starts by switching to the flow of a gas mixture (volume flow rate of 0.6/0.4, N_2 and CO_2, respectively). The amount of CO_2 adsorbed on the AC surface and pores is calculated from the BT curves by the application of a mass balance equation (2.11) for the bed, as follows:

$$q_{CO_2} = \frac{1}{m_{adsorbent}} \left[\int_0^{t_s} \left(F_{CO_2,in-} F_{CO_2,out} \right) \, dt - \frac{y_{CO_2,feed} \cdot P \cdot V_b}{RT} \right] \quad \text{Eq. (2.11)}$$

where, $\boldsymbol{q_{CO_2}}$ corresponds to the specific carbon dioxide adsorption capacity for the tested adsorbent, $\boldsymbol{m_{adsorbent}}$ refers to the amount of adsorbent (mass) in the packed bed, $\boldsymbol{F_{CO_2,in}}$ and $\boldsymbol{F_{CO_2,out}}$ corresponds to the inlet and outlet molar flowrate of CO_2 in the packed bed, respectively, $\boldsymbol{t_s}$ is the time dedicated by the adsorbent until to achieve the saturation, $\boldsymbol{y_{CO_2,feed}}$ is the carbon dioxide molar fraction added to the system, $\boldsymbol{T}$ and $\boldsymbol{P}$ refers to temperature (°C) and pressure (bar) bed during the equilibrium stage, $\boldsymbol{V_b}$ is the volume of the bed and $\boldsymbol{R}$ corresponds to the universal gas constant.

Points of CO_2 concentration in the flow are obtained in function of time, obtained from the adsorption phenomenon. Figure 2.6 shows four different stages, which compose the breakthrough curve for the adsorption process. Chemically modified AC particles were used for an adsorption test to represent a typical BT curve behaviour. The adsorption process is plotted by the CO_2 mole fraction in the gas exit flow versus time (seconds).

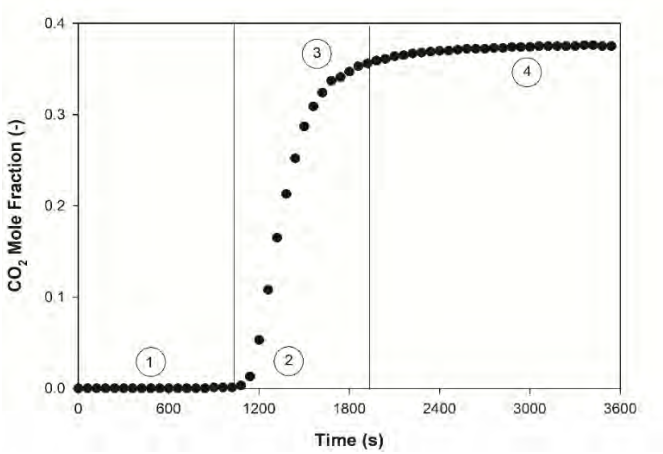

Figure 2.6. A breakthrough curve example extracted from an adsorption test with the FBR packed with a chemically modified AC

Point number 1 on Figure 2.6 refers to the adsorption saturation stage, where the adsorbent adsorbs the carbon dioxide immediately after contact with the binary mixture stream with high efficiency when the concentration of the acidic gas is zero. In this period, the CO_2 adsorption takes place in different zones of the FBR (from the inlet to outlet of the bed) until complete adsorption in the pores of the overall adsorbent amount packed in the bed. The point highlighted number 2 represents the breakpoint when the adsorbent is practically saturated, and the zones of the bed are almost saturated by the CO_2 adsorption. The CO_2 outlet concentration increases rapidly when the adsorbent is completely saturated in the bed, and there is no adsorption inside of the bed. Number 3 represents the zone where the mass transfer (lower mass transfer resistance has the power to provide high adsorption capacity) and dispersion effects will be shown in the breakthrough curve. Point number 4 is the total saturation of the adsorbent, giving a stable line corresponding to the total CO_2 quantity fed leaving the reactor with no interaction with the adsorbent.

2.3.7. Adsorption by PSA models using a FBR process: a parameter estimation evaluation

Process simulation has been developed to represent the flow, the mass/heat transfer and adsorption processes occurring in fixed beds, helping to simulate dynamic capture techniques, such as pressure and temperature swing adsorption. It can be used to predict bed performance indicators such as breakthrough time and purity of CO_2 captured. Process optimisation has been introduced to reduce the costs of plant utilisation for carbon capture adsorption, testing different material properties and alternative conditions explored by dynamic modelling studies. To compose a fixed bed adsorption model, mass and energy balance equations and boundary conditions are formulated. Adsorption isotherms are also included in the model, due to the

capacity to insert experimental data to establish comparisons and approaches with the model simulated.

Many adsorption models have been developed and published for adsorption dedicated to FBR application recently. Mulgundmath et al. (2012) developed a model using a fixed bed adsorption and a binary gas mixture (CO_2 and N_2; 10/90% gas feed composition, respectively), which predicted heat and mass transfer parameter correlations compared with the data obtained from breakthrough curves generated from a dynamic adsorption pilot plant unit.

A mathematical adsorption model using post-combustion conditions for carbon dioxide capture was proposed by Plaza et al. (2017), with the aim to develop a process of decreased environmental impact. In parallel, they provide a high reduction impact on energy consumption and total cost. A critical comparison of three different scenarios was conducted using absorption, membranes and adsorption (where a FBR model was described). This model was compared with the data obtained from a fixed bed adsorption plant in laboratory scale, adopting the Vacuum & Temperature Swing Adsorption (VTSA) methodology to promote cycles to the adsorption process. A gaseous mixture of water vapour, nitrogen and carbon dioxide was fed (in a dry and humid gaseous mixture) into the system at post-combustions conditions to test the hydrophobicity potential for microporous biochar (converted from olive stones) adsorbent. As previously mentioned in this chapter, CO_2 adsorption capacity is reduced when the gaseous mixture (0.84/0.14/0.02 for nitrogen, CO_2 and water, respectively) is not on a dry basis (as long as the amount of water loading increases, reduced the adsorbent capacity), where it is disturbed by the water molecules present in the flue gas fed at post-combustion (ads. time: 30 minutes; ads. temperature: 50ºC; pressure: 1.4 bar; feed flow rate (controlled by MFC): 143 $cm^3.min^{-1}$(STP)) conditions.

In contrast, in the study of Plaza et al. (2017), the water saturated the adsorbent first, but the CO_2 capture was not blocked, and the adsorbent could continue to adsorb the acidic gas molecules. However, the presence of water in the gaseous mixture promoted a reduction in the adsorbent working capacity, reaching 15% CO_2 and 28% water captured. Even in the presence of water, the adsorbent continued to work, although this component reduces its selectivity for CO_2 molecules.

Plaza et al. (2017) simulated a FBR adsorption simulation in a dynamic model in Aspen Adsorption V8.8 based on the non-isothermal non-adiabatic model to authenticate the VTSA experimental data. Assumptions were adopted in the model, such as the linear driving force (Equation 2.12) (LDF) to report the mass transfer effect and Ideal Adsorbed Solution (IAS) to describe the competitive adsorption. The Toth equation (Eq. 2.13) was used to report carbon dioxide and nitrogen adsorption, and the extended cooperative multimolecular sorption (ECMMS) (Eq. 2.14) theory was applied to describe the amount of water adsorbed relative to the proportion added in the wet gaseous mixture. Mass balance, kinetic and initial boundary conditions were also included in the simulation. The model generated a fair correlation to the physical process, owing to the estimated CO_2 and water composition in the outlet. Additionally, the adsorbent working capacity given by the modelling was very similar to the value obtained in the FBR via VTSA methodology:

$$f(t) = 1 - e^{-k_l t} \qquad \text{Eq. (2.12)}$$

$$q_i = q_{s,i} \frac{b_i P}{[1+(b_i P)^t]^{1/t}} \qquad \text{Eq. (2.13)}$$

$$n_{H_2O} = \frac{n_L b_L P_{H_2O}}{1+ b_L P_{H_2O}} + \frac{n_{sat} K_0 P_{H_2O}}{K_0 P_{H_2O} + \left\{\frac{1}{2}\left[1- K_1 P_{H_2O} + \sqrt{(1- K_1 P_{H_2O})^2 + 4K_0 P_{H_2O}}\right]\right\}^2} \qquad \text{Eq. (2.14)}$$

where, $\boldsymbol{q_i}$ corresponds to a specific amount adsorbed of component i in the adsorbent (mol/kg); $\boldsymbol{P}$ is pressure (kPa); $\boldsymbol{f(t)}$ is the fractional uptake at time $\boldsymbol{t}$; $\boldsymbol{k_l}$ corresponds to the mass transfer coefficient for LDF model; $\boldsymbol{n_L}$ correspond to the maximum adsorption capacity on the surface functional groups; $\boldsymbol{n_{H_2O}}$ is the overall amount of water adsorbed by the carbon; $\boldsymbol{b_L}$ refers to the Langmuir affinity constant for the interaction of water with the surface functional groups; $\boldsymbol{P_{H_2O}}$ is the partial pressure of water; $\boldsymbol{n_{sat}}$ is the saturation capacity for the adsorption of water in the micropores; $\boldsymbol{K_0}$ corresponds to the equilibrium constant for the adsorption on the primary site.

Dynamic adsorption simulations using typical volatile organic compounds (VOCs, presented as five different flows with different compounds) were carried out to promote adsorption of these compounds. Activated carbon (commercial type, CAC) surface via a FBR process (with an overall flow rate fed was of 0.02 m/s) was simulated by Zhang et al. (2018). The AC (surface area: 1099.74 $m^2.g^{-1}$) was tested with five different compounds ranked as VOCs pollutants: acetone, ethyl acetate, propyl acetate, and isopropanol. The VOCs inlet flow rate was invariably defined to 0.021 m/s and 10 L/min for nitrogen at the desorption stage. The Banham equation was found to be the best fit to the adsorption uptake models, due to the elevated value to R^2 (<0.99) and the shorter difference among the physical FBR process and the simulation relative to the uptake amount of the VOCs.

The laboratory data were used to validate the process model by two dynamic adsorption/desorption simulations to describe the breakthrough curves, including models of Boltzmann (Eq. 2.15) and Yoon-Nelson (Eq. 2.16). Four kinetic models to describe the dynamic adsorption behaviours: pseudo-first-order (Eq. 2.17), pseudo-second-order (Eq. 2.18), Elovich (Eq. 2.19) and Banham adsorption rate equation (Eq. 2.20) were incorporated, as demonstrated below:

$$y = \frac{A_1 - A_2}{1 + e^{(x-x_o)/d_x}} + A_2 \qquad \text{Eq. (2.15)}$$

$$t = \tau + \frac{1}{K'} \ln\left(\frac{1}{K'}\right) \qquad \text{Eq. (2.16)}$$

$$q_t = q_e \left[1 - \exp(-k_1 t)\right] \qquad \text{Eq. (2.17)}$$

$$q_t = \frac{k_2 q_{e\,t}^2}{1 + k_2 q_e t} \qquad \text{Eq. (2.18)}$$

$$q_t = \frac{1}{\beta_E} \ln \frac{1}{\beta_E} + \frac{1}{\beta_E} \ln t \qquad \text{Eq. (2.19)}$$

$$q_t = q_e \left[1 - \exp^{(-kt^z)}\right] \qquad \text{Eq. (2.20)}$$

where, $1/d_x$ refers to half concentration point for the slope (C/C_0 = 0.5); A_1 and A_2 correspond to the starting and ending points of the curve; t is the time; τ is the time of the half breakthrough point; x_0 is the time of the half concentration point; K' corresponds to the adsorption rate constant; C and C_0 are VOC gas inlet and outlet, respectively; k_1 and k_2 are the adsorption rate constants of pseudo-first-order and pseudo-second-order models, respectively; β_E is the desorption rate constant, z is a constant; k is a constant (min^{-z}).

The model formulated by Zhang et al. (2018) was presented as a tool to evaluate the overall uptake capacity of the selected adsorbent. Relative to the dynamic adsorption-desorption model, Boltzmann was introduced as the best model, owing to the fitting accuracy with the experimental data and the lower mass transfer effect of the compounds, which showed enhanced performance in the fixed bed studies. Through a modified Langmuir kinetic application, CO_2 adsorption modelling using an amine-functionalised adsorbent was also evaluated by Jung et al. (2018). The equation presented was modified by including the temperature, and the amount of CO_2 adsorbed as a dependent exponential term. Isotherms were estimated in MATLAB®

2016b, fitting the data obtained from HPVA studies, establishing a parameter estimation for this data. This adsorbent was presented as a competitive material to AC, due to the ability to dampen the mass transfer effect by connecting carbon dioxide-neutral surfactant at the adsorbent surface. A comparison was made with a FBR at the lab scale and a process model. The adsorbent used was PEI-functionalised silica (0.37EB-PEI; exhibiting a working capacity of 2.2 $mmol.g^{-1}$), where this adsorbent presents a large pore volume and fast adsorption rate by repeated stability for adsorption/desorption tests when compared to different adsorbents, such as MCM-41 and SBA-15. The adsorbent was tested under different conditions for breakthrough curve generation in the temperature range from 313 to 393 K and CO_2 concentration (from 2.5 to 15%) using an Autochem apparatus (a FBR process in a small scale). The Langmuir equation was perfectly fitted to the data obtained from HPVA and the FBR due to the control in the mass transfer effect in the breakthrough curves. However, this adsorbent did not show any competitive capacity to AC or modified AC, due to the low amount of CO_2 adsorbed compared with different types of AC. This methodology looks promising, but it is still not more attractive than the AC samples for CO_2 adsorption.

A critical evaluation relative to the mass transfer effect conducted in the FBR was conducted by Abdullah and Qasim, (2016). An adsorption evaluation using nanoporous AC for a binary mixture composed by CH_4/CO_2 was conducted in a fixed bed and simulations were executed in ANSYS FLUENT® 14. Adsorption properties inserted in the model were defined by the AC evaluation via HPVA studies, with analysis conducted via 50 cm^3/min of CO_2/CH_4 (0.2/0.8, respectively). Corresponding to the modelling, a dynamic adsorption modelling was projected relative to the FBR (based on an isothermal ambient correlative to the short length of the HPVA bed), aiming to reduce the mass transfer effect [guided by the LDF model; however, the mass transfer rate was defined by the User Defined Function (UDF)]. The gas feed was modified

according to the physical natural gas purification, from 50 cm^3/min to 250 cm^3/min along the bed. Carbon dioxide capture efficiency was reduced as long as the gas feed velocity reached higher values, also impacting on the gas residence time in the bed. In order words, the modelling predicted that the high CO_2 gas concentration (from 10% to 50%) impacted on the adsorbed amount (from 47.8% to 15.9%, respectively), providing high capture efficiency for low CO_2 concentrations.

PSA modelling process has been developed by many researchers. However, there is a limited number of high pressure CO_2 adsorption models at pre-combustion conditions in development. For this reason, the difficulty in studying this process at pre- and post-combustion prevents comprehensive understanding of the PSA process, where it is complicated to identify the stages which disturb the higher adsorption capacity by the adsorbent due to the effects involved in the process.

CHAPTER 3: ACTIVATED CARBON IMPREGNATION TREATMENT AND CHARACTERISATION TECHNIQUES

3.1. Introduction

Adsorbent textural and sorption capacity properties were investigated at the Catalysis and Reaction Engineering Laboratory in the School of Chemical Engineering at the University of Birmingham. Adsorbents were submitted to a sequence of chemical impregnation treatments to optimise the CO_2 adsorption capacity under pre- (25ºC/25 bar) and post-combustion (70ºC/10 bar) conditions. The main purpose was to evaluate the performance of the modified ACs in a FBR via PSA. In addition, various techniques were utilised to investigate the adsorption capacity of the modified ACs, observing their behaviour under different thermal and pressure exposure via BET, HPVA and TGA.

High Pressure Volumetric Analyser (HPVA; Micromeritics HPVA 100) and Brunauer-Emmet-Teller (BET; Micromeritics ASAP 2420) experiments were performed at the Energy Technologies Building (School of Chemical, Environmental and Mining Engineering) at the University of Nottingham. Two different types of adsorbents were selected for analysis, Activated Carbon Norit® RB1 (Supplier: Sigma-Aldrich®) and Activated Carbon Norit® Cabot R2030 (Supplier: Cabot® Corporation). These materials were submitted to a sequence of experiments, including a variety of characterisation techniques, to observe the evolution of applied treatments, the influence of the morphology improvements, and the impact on the CO_2 uptake stage (calculated by breakthrough curves generated).

Additional adsorption parameters were calculated and fitted against the datasets for novel adsorbents, such as modified ACs. Breakthrough curves of carbon dioxide/nitrogen were also recorded in a laboratory scale FBR for novel adsorbents, wherein the modification procedure is described further in this chapter. These breakthrough curves were represented by a fixed bed axial dispersion model developed using gPROMS® software in collaboration with Rebeca

Azpiri Solares (Eng. D. Student in Chemical Engineering at the University of Birmingham-UK), who provided the model codes. The model was fitted to experimental data (recorded by D Soares) using parameter estimation software, which was used to determine parameters such as the dispersion (glass bead experiments) and mass transfer coefficients (AC breakthrough curves) and compared with values from the literature.

3.1.1. Procedure for activated carbon modification

The two selected ACs were subjected to a set of treatments to improve their properties as an adsorbent of CO_2 molecules (Figure 3.1). In particular, chemical treatments were designed to modify the pore size or volume using KOH (99.9% purity; Supplier: Fluka), $ZnCl_2$ (99.9% purity; Supplier: Sigma-Aldrich) and H_3PO_4 (99.9% purity; Supplier: Sigma-Aldrich). The impregnation of basic amine groups was designed to increase the selectivity of the adsorbent surface for CO_2 molecules. The AC treatment with chemical solutions was conducted by impregnation as shown in Figure 3.1 and described below:

- KOH, $ZnCl_2$ and H_3PO_4 solutions: these solutions were destined for pre-combustion studies to modify the pore, surface, and the volume uptake improvements at high pressure and low temperature for the adsorption stage;
- Amine solutions (99.9% purity; Sigma-Aldrich): these solutions were applied with the intention to improve the surface and CO_2 interaction in pre- and post-combustion conditions by the insertion of reactive groups onto the AC to promote chemical bonding during adsorption. These solvents covered the AC surface to fill the pores of the adsorbent, providing higher working capacity and affinity for CO_2 molecules during the adsorption stage via the basicity level generated after treatment.

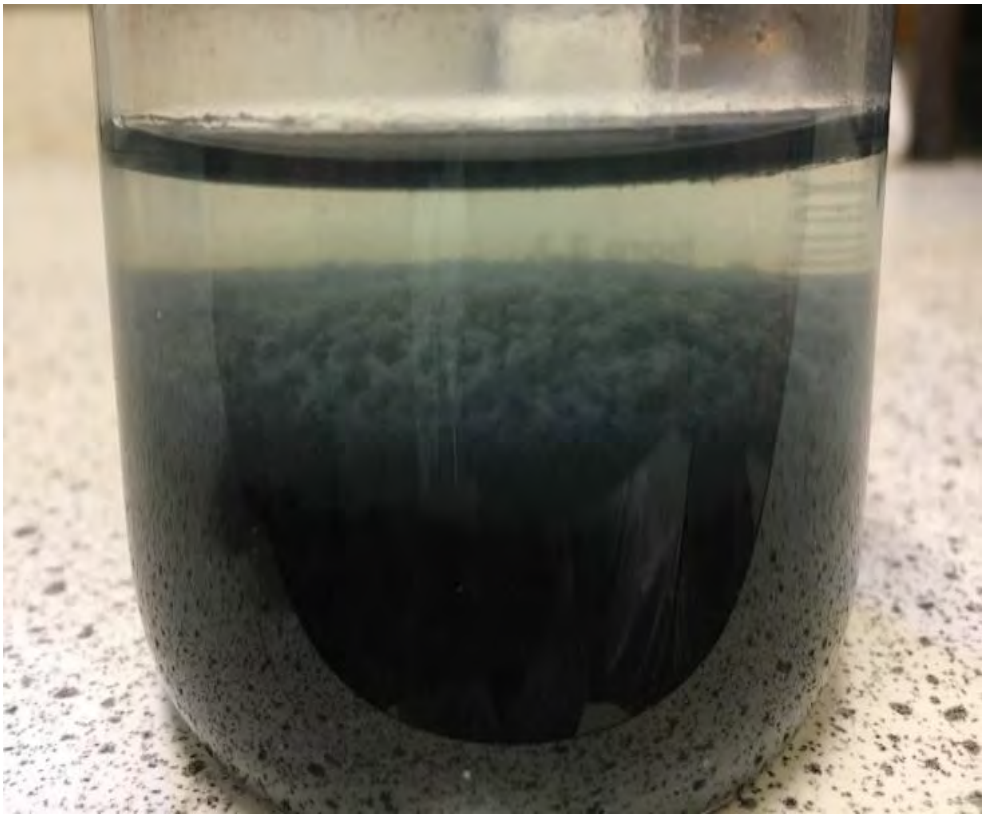

Figure 3.1. Laboratory solvent impregnation onto the AC surface

AC samples were modified to improve the chemical solid/gas interaction through the physical structure of the micropores by increasing the potential for CO_2 capture throught solvent contact with the adsorbent surface as listed in Table 3.1.

Table 3.1. Supplementary information regarding the ACs and solvents selected for impregnation

	Materials	Solution number	Ratio	Concentration (solvent/water)	Form	Application
Pre-combustion application	Potassium hydroxide (KOH)	1	1:1	0.2/0.8, 0.6/0.4 and 0.7/0.3	Aqueous solution	Impregnation
	Zinc chloride ($ZnCl_2$)	2	1:1	0.2/0.8		
	Phosphoric acid (H_3PO_4)	3	1:1			
Pre- and Post-combustion application	Monoethanolamine (MEA) combined with 2-amino-2-methyl-1-propanol (AMP)	4	1:0.6	0.2 – 0.6/0.4		
	Diethanolamine (DEA) combined with 2-amino-2-methyl-1-propanol (AMP)	5	1:0.6	0.2/0.8		
	Triethanolamine (TEA) combined with 2-amino-2-methyl-1-propanol (AMP)	6	1:0.6	0.2/0.8		
	Monoethanolamine (MEA) combined with methyldiethanolamine (MDEA) and 2-amino-2-methyl-1-propanol (AMP)	7	1:0.6	0.6/0.4		
	Diethanolamine (DEA) combined with methyldiethanolamine (MDEA) and 2-amino-2-methyl-1-propanol (AMP)	8	1:0.6	0.6/0.4	Aqueous solution	Impregnation
	Triethanolamine (TEA) combined with methyldiethanolamine (MDEA) and 2-amino-2-methyl-1-propanol (AMP)	9	1:0.6	0.6/0.4		
	Monoethanolamine (MEA)	10	1:0.6	0.2-0.6/0.4		
	Tetraethylenepentamine (TEPA) combined with anhydrous ethanol	11	1:0.6	0.2/0.8 and 0.3/0.7		
	Hydrochloric acid (HCl)	12	-	Purity of 99%		pH equilibrium
Adsorbents	Activated Carbon Norit® RB1	-	-	-	Pellets	Raw material
	Activated Carbon Norit® R2030 Cabot	-	-	-		

As described in Table 3.1, a variety of impregnation solutions were produced to conduct the modification of the AC surface. The list of chemicals was organised into the two different application groups for the adsorption experiments. These chemical modifications were performed using the proposed solvents at selected concentrations according to Table 3.1.

In the early stages, 20 g of AC (no pre-treatment needed) was held with a solution of KOH (150 ml) in a beaker at room temperature for three hours of soaking time. This stage was important to confer adhesion of the active groups onto the AC surface and pores. Excess solvent was removed using a pipette and samples were transferred to a ceramic crucible within a quartz tube in a furnace, as shown in Figure 3.2. The ACs were then dried under a flow of N_2 (100 Nml.min^{-1}) at 700ºC (heating rate of 10ºC/min) and holding time of 24 h. Afterwards, the AC samples were cooled to room temperature under N_2 flow, with a cooling time of 8 hours. The MEA impregnation procedure was initiated using 20 g of AC in a beaker, then 45 ml of MEA and 45 ml of AMP were separately added to the beaker with 60 ml of deionised water to facilitate the amine impregnation process. Relative to the amine modified ACs which contain MDEA in the solution (solutions 7–9 in Table 3.1), the solution preparation procedure was conducted by the addition of 30 ml of each solvent (MEA, AMP and MDEA, respectively) to 60 ml of deionised water. This solution was magnetically stirred at 500 rpm for 30 s before transfer to a beaker with AC. The mixture was stirred at 500 rpm for 3 h at ambient temperature to enhance the interaction of the solvent and promote chemical bonding to the AC surface. The excess solution was removed from the beaker with a pipette, then the adsorbent was transferred to a crucible boat and dried in an oven at 150ºC (constant temperature) under a N_2 flow for 24 h.

This procedure was repeated for the remaining solvents listed in this work, DEA, TEA and blends with MDEA. The amine treatment for the TEPA modified ACs was conducted as described in the MEA+MDEA+AMP solution impregnation treatment, but 150 ml of TEPA

(45 ml of TEPA combined with 45 ml anhydrous ethanol in 60 ml deionised water) solution was applied to the sorbent surface instead.

For solutions 4–9, the AMP (2-amino-2-methyl-1-propanol) solvent was added to improve the amine reactivity in contact with the AC and enhance the treatment results. Moreover, this material has high viscosity, so it might block pores and reduce the adsorbent capacity under the pre-combustion condition (low temperature). For this reason, analysis of these samples was conducted under post-combustion conditions due to the higher adsorption temperatures, which could help to improve the chemical bonds for CO_2 at post-combustion adsorption temperatures due to mobility promoted to the reactive groups on the AC surface. Accordingly, the resistance effects could be potentially reduced, and the adsorption improved.

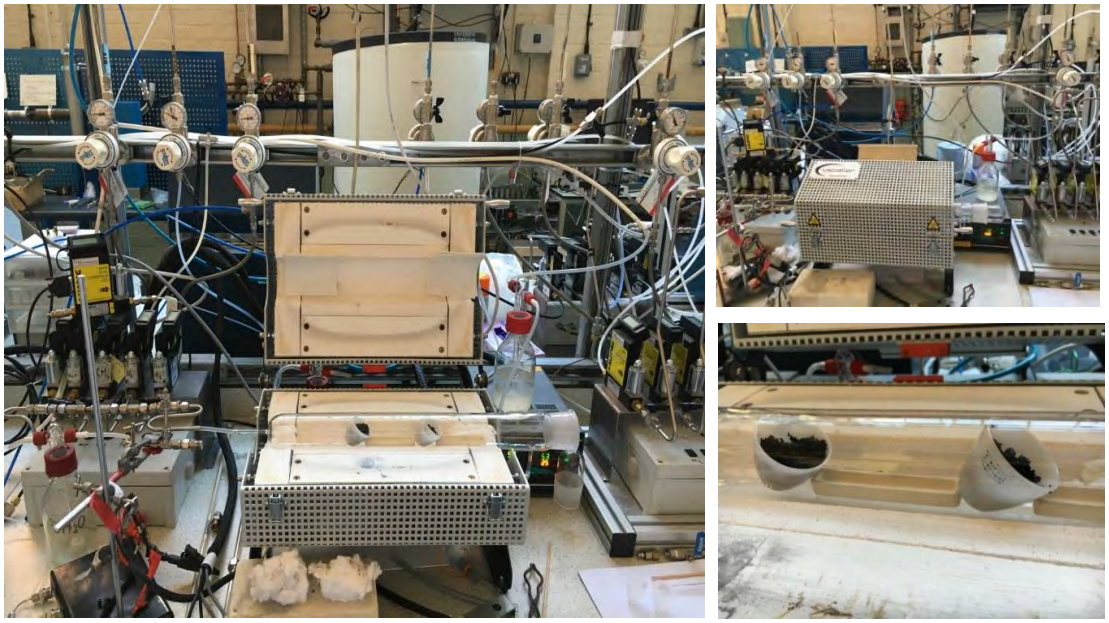

Figure 3.2. Drying system for the AC samples in the Fuel Cell Laboratory at the University of Birmingham

Modified ACs with the different primary amines (solution 10) and without any AMP were produced to test the pore blockage potential due to the high solvent viscosity in ambient conditions. It was tested in post-combustion conditions to evaluate the AC adsorption capacity

via PSA studies. The solvent composition for a modified AC (60%) was based on the amount of 90 ml of pure MEA in 60 ml deionised water.

The chemically modified ACs removed from the furnace (Figure 3.2) were submitted to the second stage of the treatment. The AC samples were transferred from the ceramic crucible to a beaker immersed in the 5M HCl solution, and pH tapes were used to verify the basicity (pH ~12–13) during this stage. The pH was adjusted by 5M HCl. The second soaking was completed after 3 h at ambient conditions in the fume cupboard. Subsequently, the ACs were rinsed with distilled water until the carbons were considered free of chloride ions and pH strips were used to control the neutrality (~7.0–7.5) of the sample. Lastly, the samples were dried at 700ºC for 24 h for pre-combustion samples (KOH, $ZnCl_2$ and H_3PO_4). The lower temperature for the amine samples is justified by the maximum temperature exposure limit for the solvent degradation (170ºC), according to the solvent safety data sheet.

Relative to the alkanolamine modifications, solution 11 was treated in a similar way using 20 and 30% TEPA solution. TEPA solvent (45 ml)was blended with 30 ml of anhydrous ethanol and diluted in 75 ml of deionised water to achieve 30% loading of TEPA solvent. This solution was sonicated for 30 min to ensure that the solvent was fully dissolute. Then, 20 g of unmodified AC was transferred to the beaker and placed in the ultrasonic equipment (Mujigae - Technique Ultrasonic) for an extended period (180 min). Lastly, the solvent excess was removed with a pipette, and the AC was transferred to the ceramic crucible and dried at 150ºC for 24 h under N_2 flow (100 $Nml.min^{-1}$).

3.1.2. Thermogravimetric analysis (TGA)

TGA was applied to test the thermal influence on the adsorption capacity under pure CO_2 flow. Adsorbents were tested using pre- (25ºC/0.5 bar) and post-combustion (70ºC/0.5 bar) temperatures in the thermogravimetric analyser (NETZSCH TG 209 F1 Libra). The direction of the flow was concentrated from the top to the bottom of the equipment, passing through the TGA balance to improve the sample weight accuracy, as shown in Figure 3.3. The flow outlet was located on the right of the TGA.

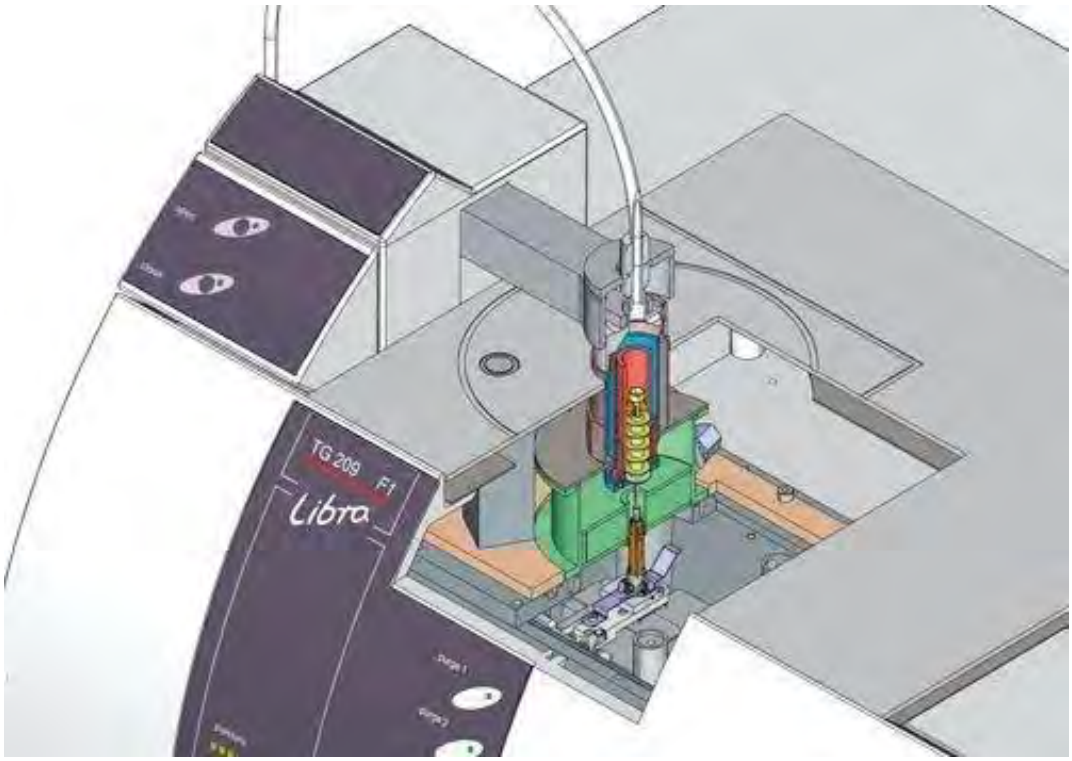

Figure 3.3. Representation of the TGA internal mechanism for sample allocation and gas contact with the AC (NETZSCH, 2019)

The TGA studies presented a limitation in the gas inlet pressure due to the maximum range (0.5 bar) supported by the equipment. For this reason, the same pressure was applied for pre- and post-combustion studies. Comparison of the CO_2 uptake measured by TGA also allowed the prediction of the most suitable treatment to modify the ACs. Moreover, this technique was

selected to evaluate the stability of the adsorbents and test the adsorption capacity of each sample using 50 ml/min of CO_2. Chemisorption bonds between CO_2 and amine impregnated groups were evaluated for the modified ACs, as the main solvent modification proposed was concentrated in these interaction improvements.

Firstly, a correction file (supported by newest the TGA calibration) was created containing all settings corresponding to the adsorption conditions previously stipulated. Different features were proposed for the adsorbent analysis, including pre and post-combustion temperatures during a unique stage. Relative to pre and post-combustion studies, the ACs were submitted to a sequence of steps, programmed in the NETZSCH easurement software (NETZSCH-Geraetebau GmbH, version 4.8.4, 30/08/2007) as mentioned below:

- **Stage 1 Pre-treatment:** the sample was held for 60 min at a transfer temperature set from 25 to 150^{o}C (heating rate of 5K/min) under a N_2 flow (50 ml/min) to remove any residual moisture or gas previously adsorbed by the sample before further analysis in the TGA system. The TGA required 1 h and 42 min to achieve the required temperature. Additionally, when the sample was submitted to elevated temperatures, physisorption forces may be overcome and physisorbed molecules removed from the surface, so the adsorbent cannot increase their weight as long as the adsorption stage is not reached; this was confirmed by a mass loss observed in the thermal curve.
- **Stage 2 Cooling process:** in this stage, the sample was cooled under a pure N_2 flow (50 ml/min) to the analysis temperature (25 and 70^{o}C for pre- and post-combustion temperatures, respectively) at a cooling rate of 5K/min. The entire duration of this stage was 2 h and 8 min for pre-combustion studies, and 1 h and

34 min for post-combustion experiments. The mass of the adsorbent was stable (or zeroed) without variation until the beginning of the next stage.

- **Stage 3 Adsorption stage:** when the system achieved the desired temperature for pre- or post-combustion experiments, the adsorption stage was started automatically and held for 60 min. The N_2 flow was manually switched to a pure CO_2 flow (50 ml/min). The adsorption curve shows a rise in the amount adsorbed, which increases sharply when a breakthrough point occurs.
- **Stage 4 Desorption stage:** another desorption stage was added to remove the gas previously adsorbed. The gas flow was switched back to pure N_2 (50 ml/min). The system was heated to 150ºC again (heating rate of 5K/min), and the adsorbent was held for 10 min to ensure that the sample was free from any adsorbate and the end of the experiment.

To test repeatability, the TGA process was performed in five continuous adsorption-desorption cycles at pre- and post-combustion temperatures to test the overall adsorbent capacity and its resistance (regarding stabilisation of the amount adsorbed) under a sequence of thermal variation intervals. The stability of the bonding of the amine groups on the surface of the ACs was also evaluated by multiple cycles to determine if they could retain the sample adsorption behaviour of the freshly modified sample.

Relative to the sample preparation, the NETZSCH measurement software was started, and the system status was checked (relative to their normalisation) to tare the empty balance. Secondly, an empty ceramic crucible (Al_2O_3) was added to the TGA balance under CO_2 flow, and the equipment was then closed. The balance was tared (zeroed) again, and the equipment required up 1 min to stabilise the zeroed weight.

Firstly, it was necessary to create a temperature ramp, programming all of the experimental steps for stages 1–4. Details of the material of the empty ceramic crucible were inserted, and the temperature ramp test was started. When the calibration curve test finished, it was possible to start the experiment, loading the measurement created and adding information relative to the sample inserted. The procedure followed the initial recomendations described in stages 1–4.

In sequence, the balance was zeroed and two min were necessary to achieve balance stabilisation. The TGA was then opened, and the crucible was removed from the balance. The TGA was closed to check if the negative difference in the balance was reached. A small amount of AC was added to the crucible, and it was placed back on the TGA balance. The adsorbent mass within the range of 10–25 mg was recorded. Consequently, the sample weight was recorded, then, the experiment was started. The total time for pre-combustion experiments was 13 h 23 min and 10 h 36 min for post-combustion studies.

Some limitations of this equipment were observed due to the use of manual flowmeters which disturb the gas flow on switching from N_2 to CO_2, impacting the curve, with some undesirable peaks occurring in the trace corresponding to the cooling and adsorption processes. However, these peaks did not influence the adsorption measurements. The experimental adsorption data was considered after these peaks, which occurred in the final stage of the cooling process.

The calculation of the ACs CO_2 adsorption capacities was conducted based on the conversion of the mass of the adsorbent in the thermal-adsorption period (stage 3). Firstly, the overall AC mass inserted was subtracted by the mass loss during the pre-treatment, defining the exact amount in the early stage of the adsorption step. Then, the amount of CO_2 adsorbed (mg/g AC) was calculated as a function of time (s) of the entire stage. Lastly, the adsorbed amount was

divided by the mmol of CO_2 that entered the TGA during the adsorption stage, providing the AC adsorption capacity (mmol/g).

3.1.3. Scanning Electron Microscopy (SEM)

The SEM (Philips XL-30 (LaB6) with Link Isis EDS) was used to explore the surface morphology of the activated carbons, allowing comparisons of the size of the crevices, open-wide mouths, cracks and other possible surface features before and after treatment. This equipment was located in the Centre for Electron Microscopy of the University of Birmingham.

A metallic sample holder (aluminium) was used due to its ability to conduct the electric current. The metallic sample holder, or stub, supported up to six different samples at the same time. ACs were placed over the double-sided carbon tape (triangular tapes over the aluminium sample holder), which is also an electric conductor. Each sample was numbered close to the tape for further identification, then the metallic holders were transferred to a sputter to coat the AC surface.

In SEM studies, the sample needs to conduct electricity, and for this reason, they were submitted to metallisation overnight in a low vacuum sputter and carbon thread coater, where the surface of the sample was covered with a light conductive layer. Furthermore, the sample was placed in the SEM, and a vacuum was applied to start the experiment. The samples were numbered in the Philips' GSR NT Microscopy Control software (version 3.2), recording their initial localisation for image capture. The ACs were enumerated in the software by their respective image position and number written in the stub by the sample side to facilitate the analysis and to confer more accuracy to the experiment.

The particle beam of electrons was used by the microscope to illuminate the sample and generate a magnified image. The potential of resolution for light microscopy is given by the visible photon wavelength used. SEM can provide greater image definition and magnification (2 million times) when compared with optical microscopes. This affirmation is supported by the smaller wavelength of the electron than the visible photons usually applied in optical microscopes. When smaller wavelengths and higher acceleration voltage (***V***) are obtained, the SEM produces images with high resolution, as demonstrated in De Broglie equation below:

$$\lambda = \frac{h}{\sqrt{2meV}} \qquad \text{Eq. (3.1)}$$

where, $\boldsymbol{\lambda}$ corresponds to the electron wavelenghts; ***m*** represents the electron mass (9.11×10^{-31} kg); ***h*** is related to the Planck's constant (6.63×10^{-34} J/s); ***e*** is the electronic charge (1.60×10^{-19} C); ***V*** represents the accelerating voltage ($0.5 - 3 \times 10^{4}$ V). Electrostatic and electromagnetic lenses are commonly used in SEM studies to generate the image, regulating the electron beam to focus at the sample situated over the stub plane surface. Image colour balance was carried out to adjust the light of the microscope to the quality of the magnified image generated, providing photographs with excellent resolution (Viswanathan, Kannan & Deka, 2010). Consequently, high resolution photos were produced in a range from 500 to 10 μm for each sample tested, allowing to observe the textural properties of the adsorbent.

3.1.4. Fourier Transform Infrared Spectroscopy (FTIR)

The primary purpose of this experiment was to identify the surface functional groups on the AC adsorbents. The BRUKER TENSOR 27 FTIR spectrometer (Bruker AXS, Inc., Madison, WI, USA) was set to generate spectra (transmittance) with an optical resolution of 4 cm^{-1} in a range

from 4000 to 400 cm^{-1}, controlled by OPUS software [version 4.0, build: 4.0.24 (20020320)]. The detector was cooled by liquid nitrogen (77 K) for 20 min. A signal calibration test was conducted to evaluate the quality of the signal produced before running the samples. In this stage, potassium bromide (KBr) was pulverised in a porcelain crucible and transferred to a sample holder to evaluate the equipment signal. Through the background scan, it was possible to confirm that there was no external interference during the scan. This procedure was repeated three times to ensure that the equipment could identify the adsorbent molecular groups.

Subsequently, AC samples were weighed and mixed with potassium bromide (KBr) in the proportion of 1:100 (AC and KBr, respectively). Then, the weighed materials were placed in the porcelain crucible, pulverised to a powder, and transferred to the sample holder. Three scans were conducted for spectra generation with an optical resolution of 4 cm^{-1} in a range from 4000 to 400 cm^{-1} (including the time for a complete scan of 4 minutes, each) for each adsorbent to compare the spectra and to certify the accuracy of the FTIR signal. Relative to the absence of an updated chemical library in the FTIR software, the data evaluation to match the compounds represented in the spectra was based on the literature.

3.1.5. High-Pressure Volumetric Analyser (HPVA)

Carbon dioxide adsorption studies under high pressure (99.9% purity; Supplier: BOC), maximum pressure range (0–200 bar), and maximum temperature (500ºC) system were carried out via the HPVA equipment (HPVA 100, Supplier: Micromeritrics), which provides equilibrium adsorption-desorption isotherms utilising gases such as N_2, methane (CH_4), H_2 and CO_2. HPVA was used to measure equilibrium adsorption isotherms at high pressure, whereas TGA and fixed bed measurements are conducted under a dynamic flow of gas. Furthermore,

the amount of CO_2 uptake can be evaluated using a chiller/heater bath during the experiments, providing stable temperatures to calculate heat as adsorption. However, the adsorption isotherms are generated under ambient temperatures and at 50 barg (maximum), owing to the CO_2 condensation when submitted to higher pressures.

From a volumetric gaseous dose, the AC sample was evaluated when in contact with the adsorptive gas. The final pressure is registered when the complete equilibrium is reached by the sample and the gas applied. The amount of adsorbed gas is calculated by manipulation from the equilibrium data. Adsorption-desorption cycles were repeated to achieve the maximum pressure selected, when the pressure is reduced, the desorption isotherm is then generated.

The volume adsorbed and equilibrium pressure registered relative to the equilibrium stage was used to plot the isotherm graphs. Initially, the sample (0.5–1 g) was placed in a cell (stainless steel tube with 2 ml of capacity), and N_2 (pressure: 1.2 bar) was used to start the degassing procedure at 120ºC to purge all residual components from the sample for 24 h.

After the conclusion of this stage, the sealed tube was placed in the HPVA 100 and the analysis was started at 25ºC, with a range of pressures from 1 to 40 bar for adsorption and 40 to 1 bar for desorption. The final result was recorded when the sample reached complete equilibrium. The adsorption capacity was calculated using the Langmuir adsorption equation (3.2), and the linear Langmuir isotherm equation (3.3), as follows:

$$q = \frac{kq_m P}{1 + k_p} \qquad \text{Eq. (3.2)}$$

$$\left(\frac{C_e}{q_e}\right) = \left(a_L — k_l\right) C_e + \frac{1}{k_l} \qquad \text{Eq. (3.3)}$$

where $\boldsymbol{q}$ is the amount of adsorbate in the adsorbent at equilibrium (mmol/g); $\boldsymbol{C_e}$ is the adsorbate initial concentration (mmol/g); $\boldsymbol{k}$ is an empirical constant; $\boldsymbol{q_m}$ is the maximum monolayer coverage capacities (mmol/g); the $\boldsymbol{a_L}$ and $\boldsymbol{k_l}$ represents constants extracted from the slope and intercept values obtained from the straight line graphs, respectively.

The adsorbents were also tested in parallel via the Freundlich linearised equation to establish a base comparison with the Langmuir linearised plots. The Freundlich linearised equation is given as follows:

$$\ln\ (q_e) = \ln K_F + \frac{1}{n_F} \ln P \qquad \text{Eq. (3.4)}$$

where, $\boldsymbol{q_e}$ (mmol/g) = equilibrium adsorption capacity; $\boldsymbol{K_F}$ (mmol/g) = Freundlich isotherm constant related to adsorption capacity; $\boldsymbol{n_F}$ = Freundlich isotherm constant related to adsortion intensity; and $\boldsymbol{P}$ (bar) = Pressure.

3.1.6. Surface Area Analysis: Brunauer-Emmett-Teller (BET)

The AC samples were submitted to physisorption tests to obtain the textural and surface area properties of the adsorbents analysed using BET nitrogen (77 K) adsorption-desorption studies. Additional parameters, such as pore size and the volume of gas adsorbed per sample were also obtained. The Barrett, Joyner and Halenda (BJH) procedure was applied to measure the pore volume and pore area distributions for mesopore samples. Micropore distribution was determined by the application of the total micropore volume and MP method plotted by the t-plot method. Density functional theory (DFT) determines the micro and mesoporosity from an isotherm experiment, given by the continuous distribution of pore volume considering the AC pore size. The Horvath-Kawazoe (H-K) method was applied to determine the pore size

distribution in the AC particles used in this work. Hysteresis loops (H4 type) was also observed by this technique, relative to the capillary condensation.

The Micromeritics ASAP 2020 BET equipment was used to generate the AC adsorption data (sample mass: 0.1 g) for liquid nitrogen (77 K) and the relevant parameters for (un)modified samples derived from data in the adsorption-desorption stages. This equipment comprised two programmable stations for degassing, a vacuum cold trap, an isothermal jacket and long-duration Dewar, when combined, they can prolong the life of the equipment, guaranteeing a constant thermal profile during the experiment for the saturation pressure (P_o) and the sample. There were six analysis gas inlets dedicated for physisorption studies, with the most used gases being N_2, Ar, Kr, CO, CO_2, H_2 and He.

Initially, the degassing procedure (under vacuum and heating) was conducted to thoroughly remove water and other possible components physically adsorbed for more accurate data accquisition. The vacuum and heating rates respected the material properties, maintaining the original adsorbent conditions. If the degassing procedure is not carried out correctly, it may affect the overall specific surface area result due to the presence of undesirable molecules covering the adsorbent surface area. Consequently, this step is critical for conferring higher precision and accuracy for specific surface area studies.

Samples were placed in a glass cell (12 mm, size recommended for pellets/granulate samples), then a glass rod was inserted to reduce the amount of space free in the glass cell. The cell was then placed in heating blankets and connected to the vacuum system to start the degassing procedure. Subsequently, the cell was moved to the analyse module and partially submerged in liquid nitrogen to cool the sample and keep the low temperature in the adsorbent. The contact of the adsorbent with nitrogen promotes stronger gas molecule interactions during the

adsorption stage. To calibrate the sample and the dead volume inside the cell, helium gas was used due to its zero potential for adsorption in the sample surface. After calibration, N_2 was injected into the cell to start the adsorption-desorption studies.

3.1.7. X-ray Diffraction and Elemental Analysis (XRD)

Diffraction is based on the interaction of X-rays with the sample, allowing identification of organisation of the molecules on the adsorbent structure. When the X-ray begins contact with the sample, it provides a geometric position according to the distance between the atoms. The wavelengths (λ) used in this equipment have a range of 0.5 to 2.5 Å and are produced at the moment when electrons of sufficient kinetic energy rapidly decelerate through an impact on a target. The wavelength intensity is linked to the tube voltage. In most XRD equipment, there is an anode (kept at ground potential; positive) and cathode (high negative potential) which works in a range from 30 kV to 50 kV. When the tube voltage increases, it impacts on the rise in wavelength intensity and reduction in their position to shorter wavelengths. The angle of reflection of the diffracted beam is represented as theta (θ). This is a powerful method to characterise the arrangement of the adsorbent molecules, supported by the diffraction phenomenon, wherein the incidence of the X-rays occurs in all directions to form a diffracted beam.

In contrast with other techniques, no special pre-treatment is required prior to sample for the XRD equipment, but all sample preparation instruments should be cleaned with acetone to remove any previous impurities. AC virgin samples were used for XRD analysis one week after the conclusion of the impregnation treatment. A specific amount of AC was placed in the porcelain crucible and reduced to powder for better XRD. Then, the adsorbent was transferred

to a stainless steel sample holder (named as powder specimen holder). A glass blade was used to remove the excess and balance the height of the sample, creating a uniform layer. The limit of the powder specimen holder was respected, and it was used as a reference to fill the sample over the holder. Then, the samples were placed in the sample support inside the equipment and the analysis was performed using the following settings:

- type of scan: Coupled Two θ/θ
- scan mode: continuous PSD fast
- θ diffraction range
- wavelength (λ): 1.789 Å
- the time (s) to rotate the sample, then modifying the sample angle position
- the angle position was another essential parameter. The x-ray range limit needed to be respected, delimiting this value up to 5º due to the ideal extension around the sample area
- the rotation speed:15 l/min
- the analysis interval in 2θ was comprehended between 5–120º

Experiments were conducted in ambient conditions and continuous PSD fast scan at 0.02º/min, taking 30 min for each sample. The data was analysed in the DIFFRAC.EVA software (version 3.1a, 2012), which contains a library of chemical compounds and matches for the XRD data evaluation.

3.1.8. Fixed Bed Reactor process via Pressure Swing Adsorption (PSA)

The dynamic adsorption behaviour of the ACs was studied in a FBR (raw material: stainless steel; mass: 552.14 g; diameter: 2.5 cm; length: 6.9 cm; height: 2 cm; with an adsorbent located at 0.2 cm from the bottom and 6.3 cm for the section packed with the adsorbent into the reactor), as schematised in Figure 3.4. Mass flow controllers (BROOKS 5850EM series; MFC, numbers 1 and 2) of N_2 (maximum flow rate: 400 $Nml.min^{-1}$) and CO_2 (maximum flow rate: 100 $Nml.min^{-1}$) were used to keep a constant gas flow rate from the gas cylinders (both 99.9% purity) to the inlet of the bed, controlled by IGI systems (Brooks Instrument) – Smart Interface tool (version 1.0.3.1, 2016).

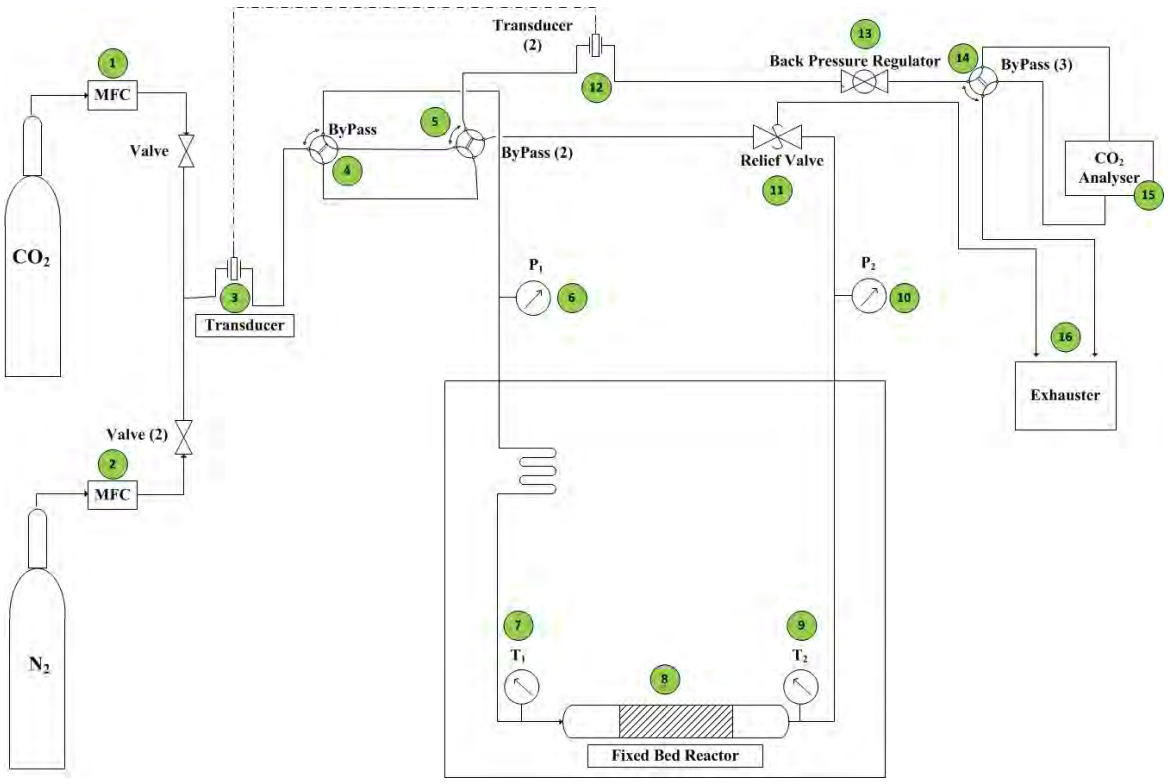

Figure 3.4. FBR process for CO_2 capture via PSA technology.

The temperature of the adsorbent was continuously monitored by two K-type thermocouples (7 and 9) allocated in the inlet and outlet of the bed. These thermocouples were connected to a thermocouple data logger (model: PICO thermocouples USB TC-08) and controlled by the

PicoLog Recorder software (Pico Technology Ltd, version 5.20.09 (1997-2009). Transducers (Swagelok S; pressure range: 1–600 psig; numbers 3 and 12) worked as pressure sensors, which displayed the inlet and outlet pressure in a panel placed next to the rig.

Numbers 4, 5 and 14 in Figure 3.4 show the bypass (Swagelok Stainless Steel Tee-Type Particulate Filter, 1/4 in), which works as a gas flow pathway to the reactor or directly to the exhaust (16). A relief valve (Swagelok 316, pressure range: 24.1–51.7 bar) was used to secure safety operation, and a back pressure regulator (Swagelok 316 Stainless Steel PR Regulator, pressure range: 1–500 psig) (13) controlled the FBR pressure. These valves prevented any disturbances that might be generated while the experiment was in operation.

A CO_2 analyser (SERVOFLEX MiniMP 5200) (15) measured the CO_2 concentration in the outlet of the reactor, controlled by Microsoft® HyperTerminal (version 5.1, 2001). The gas was conducted directly to the vent/exhaust (16). This equipment was calibrated for low range (0%) with pure N_2 (200 Nml/min) and high range (100%) with pure CO_2 flow (100 Nml/min). The silica gel (regenerated overnight heating at 140ºC, then placed in the tube in the CO_2 analyser inlet) was used to remove moisture from the inlet gas to calibrate the CO_2 analyser accurately.

Figure 3.5. A) Oven used to heat the reactor and provide a stable temperature for PSA tests, and B) FBR inside the oven with the two thermocouples inserted at the gas flow inlet and outlet

Initially, a bed regeneration procedure was applied with pure N_2 flow and the oven (Figure 3.5) heated to 150ºC for 60 min at a rate of 10ºC/min. After this step, when the reactor temperature reached the conditions predicted for pre (25 bar/25ºC) and post-combustion (10 bar/70ºC), the pressure was increased to the pre-defined value for 5 min. Then, the quantity of N_2 was reduced to 120 Nml.min^{-1}, and simultaneously, 80 Nml.min^{-1} CO_2 flow was introduced to the reactor for a 60/40% gas mixture (N_2/CO_2, respectively). The amount of gas that left the bed was recorded during the adsorption procedure (3600 seconds) until the total bed saturation was achieved, generating a breakthrough curve.

Finally, the bed was submitted to the regeneration process, where the system was exposed to high temperature (150ºC) and low pressure (1 bar) for both conditions for AC regeneration for 1 h under pure N_2 flow. The primary goal of this procedure was to remove the CO_2 adsorbed from the AC pores and surface, regenerating the adsorbent for a new adsorption cycle.

3.1.8.1. Pre and Post-combustion studies

The ACs were submitted to dynamic adsorption-desorption tests via two different conditions for PSA studies using a CO_2 concentration range 10–50% (CO_2 flowmeter maximum capacity) combined with N_2. The overall flow rate was 200 Nml.min^{-1} during all stages involved. Pre- (25ºC/25 bar) and post-combustion (70ºC/10 bar) conditions were applied. Pre-combustion conditions have been commonly used for chemical absorption processes, where the acidic gas is removed before it is burnt. The conversion of fossil fuel to syngas in power plants is achieved by the reaction with oxygen or air, generating a flue gas containing H_2 and CO_2, with the captured CO_2 separated from H_2 in a catalytic reactor, typically conducted under high pressure and low temperatures (generally, ambient temperature). In this work, the PSA pre-combustion

experiments were initially fed with pure N_2 at 1 bar to conduct the fixed bed desorption stage. Then, the reactor was heated from 25 to 150ºC at a rate of 10ºC/min, and the temperature was held for 3600 seconds. The desorption performance was controlled using the CO_2 analyser, which was responsible for confirming the absolute absence of CO_2 in the bed during the proposed time. Then, after satisfactory conclusion of the desorption procedure, the bed was automatically conducted to the ambient temperature (25ºC) under a flow of pure N_2. At the same time, the bed pressure was manually increased from 1 to 25 bar using the back pressure regulator. When the bed achieves the high-pressure stage, 300 seconds were dedicated for the bed equalisation to acclimatise the adsorbents and check for any possible leaks in the system under high pressure. Then, the flow of N_2 was reduced and CO_2 increased, generating a binary gas mixture to initiate adsorption, and the whole process continued for 3600 seconds. In post-combustion processes, the CO_2 capture occurs from flue gas arising from the combustion of biomass or fossil fuel. This procedure aims to sequestrate the CO_2 passing through separation equipment, reducing its emission to the atmosphere, operating under high temperature (50–80ºC) and low pressure (typically, at 1 bar). The captured CO_2 is reinjected following the EOR requirements or designated to energy conversion.

CHAPTER 4: CARBON DIOXIDE ADSORPTION IN POST-COMBUSTION STUDIES

4.1. Introduction

Post-combustion CO_2 capture technology is a process with substantial thermodynamic conflicts, and its operational conditions usually have to deal with flue gases that have low pressures and low CO_2 concentration (Zhao et al., 2018; Spigarelli & Kawatra, 2013). This method requires an adsorbent that can achieve high adsorption capacities and selectivity for capturing CO_2 over N_2 at low pressures. Meanwhile, these materials might adsorb SO_x and NO_x irreversibly, leading to degradation or poisoning of the adsorbent (Zhao et al., 2018).

The unmodified AC is considered a non-polar adsorbent, which tends to demonstrate selectivity towards CO_2 in pre-combustion adsorption conditions (Ruthven, 1984). However, the amount of CO_2 adsorbed by non-polar adsorbents IN post-combustion adsorption conditions is relatively low, wherein unrealistic sizes of the process plants are required to achieve high purity and recovery in the final product (Abanades et al., 2015). To overcome this problem and achieve good adsorption capacity and selectivity, enhancement of the CO_2 affinity for the adsorbents is preferred. The proposed solution modifies the weak adsorption sites doping the adsorbent by impregnation of the amine solutions, which improves the interaction with CO_2, giving better adsorption site capacities (Choi et al., 2016; Jung et al., 2017). The textural properties of porous materials can also be modified to improve the adsorbent adsorption capacity. The adsorption of CO_2 and the material performance can be modified by the insertion of external functionalities, with the inclusion of amine groups onto the AC surface promoting strong chemical bonds with CO_2 (Abanades et al., 2015).

Some adsorbents considered as candidates for post-combustion capture (PCC) are immobilised MOFs and amine modified ACs (considered as the most appropriated material for PCC processes). However, the costs involved for AC production are much lower in comparison with

MOFs, attracting more attention as carbon adsorbents. Activated carbons also present advantages for post-combustion, summarised as fast adsorption/desorption kinetics, high cyclic stability, hydrophilic behaviour and low regeneration costs. In contrast, the adsorption capacity and selectivity improvements for CO_2 are the major issues for carbon materials in post-combustion processes, which need to be controlled by the adsorbent porous structure and surface chemistry (Zhao et al., 2018). The CO_2 separation from N_2 is an important step in power plants, taking the flue gas, which typically contains 3–15% CO_2 and more than 70% N_2, as the steam requiring purification (Zhao, Liu & Han, 2015). PSA studies (as described in Figure 3.4) were carried out in this work, operating at 10 bar and 70ºC for the adsorption stage, and 1 bar and 150ºC for the desorption (heating rate of 10ºC/min). In this work, the adsorbent modification consisted of treatment with the most reactive amine solutions commonly used for chemical absorption processes, for instance, MEA (primary amine) and secondary and tertiary amines (industrially namely DEA and TEA, respectively) also blended with MDEA, also including TEPA solution. The motivation for choosing these solvents was the high reactivity and affinity for CO_2 offered by MEA and TEPA (being four times more reactive than MEA). The modification procedure is described in section 3.1.1, and amine modified adsorbents are highlighted as the novelty of this work, due to their potentially high impact on CO_2 affinity and solid/gas interaction improvements for Activated Carbon Norit® RB1 and R2030 samples.

4.2. Results and Discussion

The ACs were submitted to six techniques for characterisation to evaluate their characteristics and performance for CO_2 capture. Thermal resistance, morphological and physicochemical

investigations were conducted to expand the knowledge and the impact of the chemical impregnation treatment over the modified adsorbents.

4.2.1. Morphological investigation of the AC surface by SEM

Morphology analysis was performed on the modified and unmodified samples, observing the impact of the treatment on the adsorbent surface and pores. Since the scale bar on the SEM is 500 μm, it was not possible to observe individual pores of the order of nm, rather this analysis focused on the surface changes that occur on the ACs after treatment. Figure 4.1.a illustrates magnified SEM photographs at 500 μm relative to the unmodified AC.

The comparison of unmodified and modified ACs indicated that chemical impregnation promotes morphological modification of the adsorbents, creating crevices over the AC surface corresponding to the amine modified adsorbents (for instance, Figures 4.1.b-f). The cracks and erosions were promoted by the amine solutions during the impregnation procedure, as described in section 3.1.1. The modification is expected to lead to an increase in the number of active sites, owing to the wider opening of the mouth of the crevices, in turn, access to the active sites within the pores after treatment with the amine solutions.

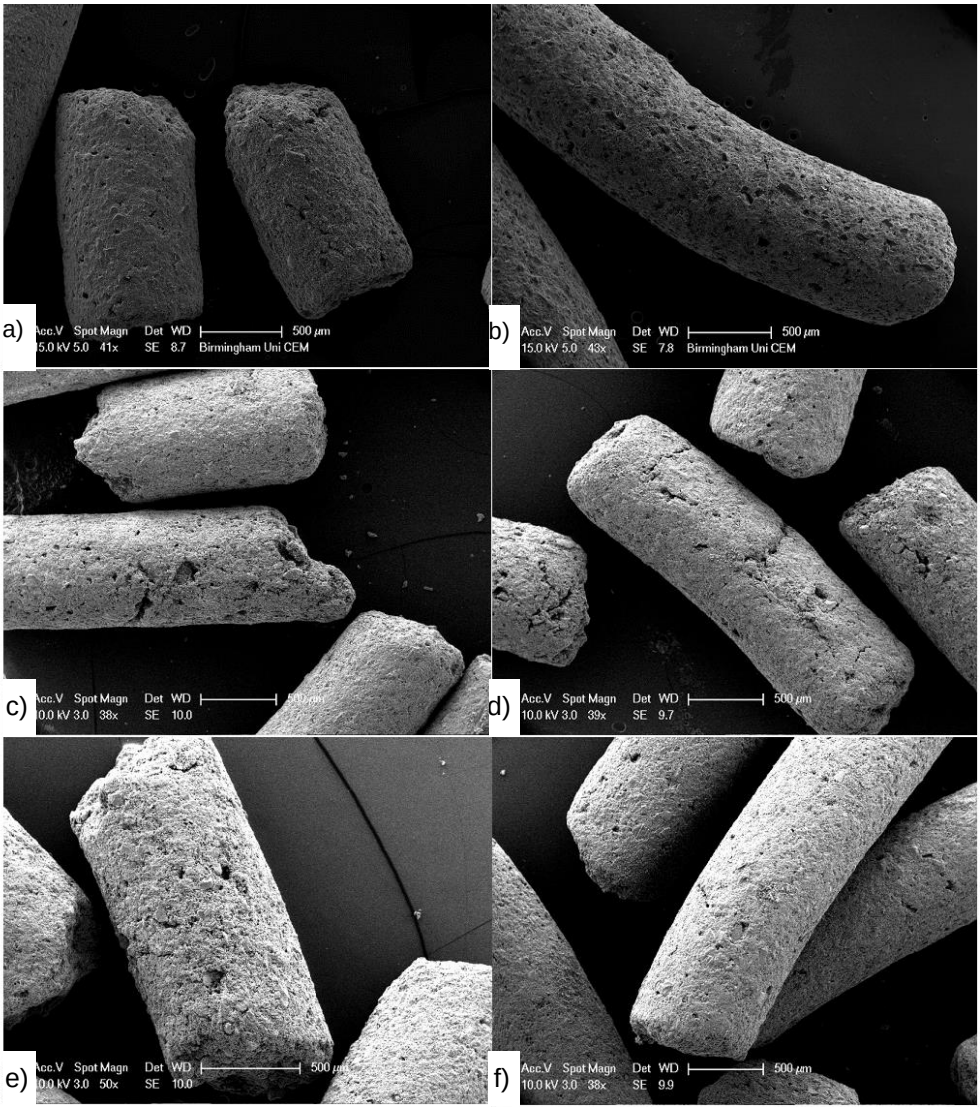

Figure 4.1. SEM images: A) unmodified Norit RB1, 41x magnification; B) TEPA 20%, 43x magnification; C) DEA+MDEA+AMP, 38x magnification; D) TEA+MDEA+MDEA, 39x magnification; E) MEA 20%, 50x magnification; and F) MEA+MDEA, 38x magnification; scale bar = 500 µm

Textural changes were also observed in the untreated pellets of the amine modified ACs. The TEPA 20%, TEA+MDEA+AMP and MEA 20% modified RB1 AC surfaces (Figures 4.1.b,d and e, respectively) became smooth after the material was impregnated in comparison to the rough surface area of the unmodified RB1 AC.

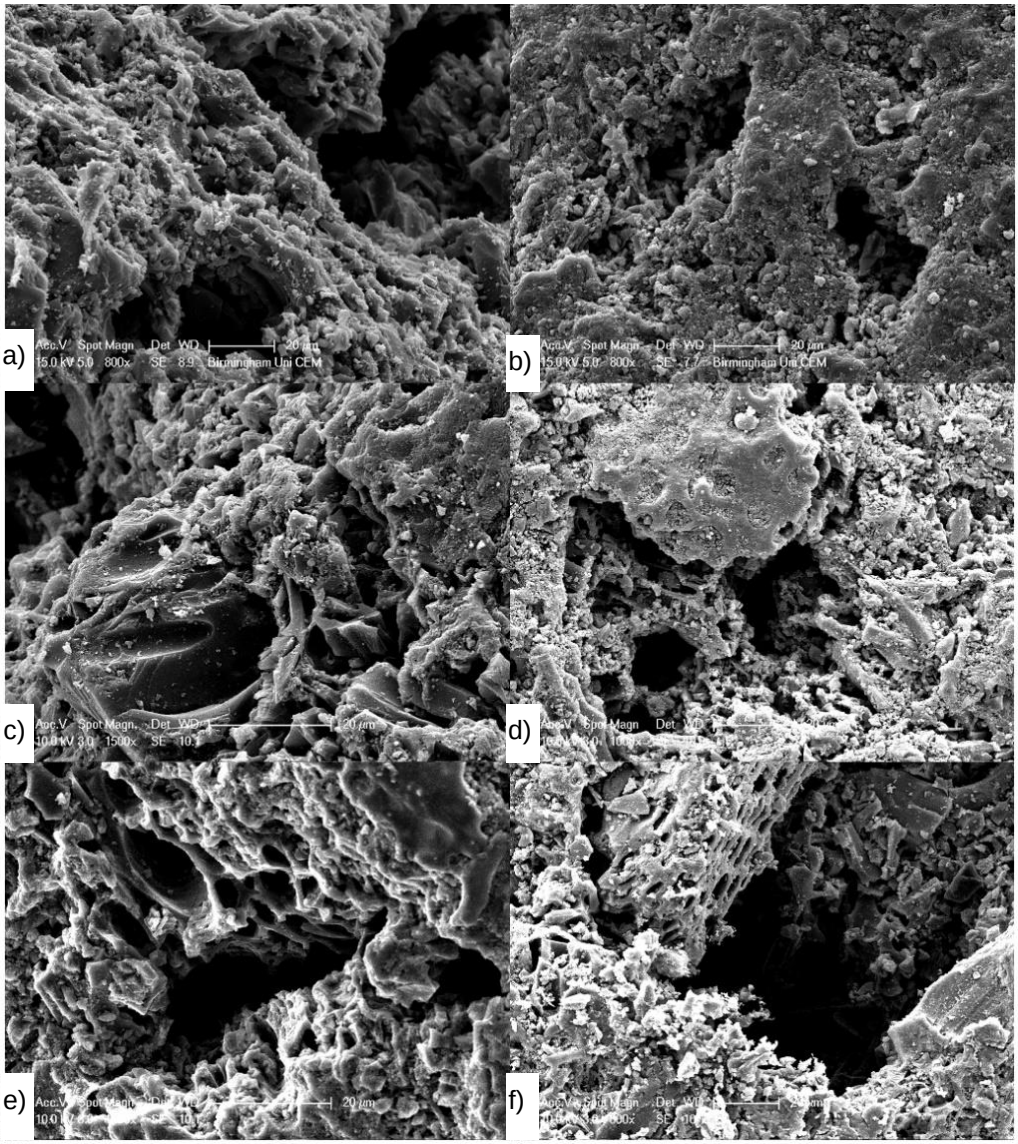

Figure 4.2. SEM images: A) unmodified Norit® RB1 AC, 800x magnification; B) TEPA (20%) modified Norit® RB1 AC, 800x magnification; C) TEA+AMP, 1500x magnification; D) TEA+MDEA+AMP blend modified Norit® RB1 AC, 1000x magnification; E) DEA+AMP blend modified Norit® RB1 AC, 1000x magnification; and F) MEA (20%) modified Norit® RB1 AC, 800x magnification; scale bar = 20 μm

The microphotographs of the AC material showed that the dark areas (Figure 4.2.a-c) indicated pores. The grey areas of the carbon matrix showed the rough surface of the adsorbent, which provided a large surface area for adsorption. Moreover, the AC unmodified impurities were removed with the chemical impregnation, observed as micro white particles on the adsorbent

surface as shown in Figure 4.2.a. These impurities were removed by the reaction between the solvent and the AC surface during impregnation, which promoted oxidation on the hydrocarbon structure and other compounds presented in the AC, thereby eroding the AC surface, as observed in Figure 4.3 (Rampe & Tiwow, 2018).

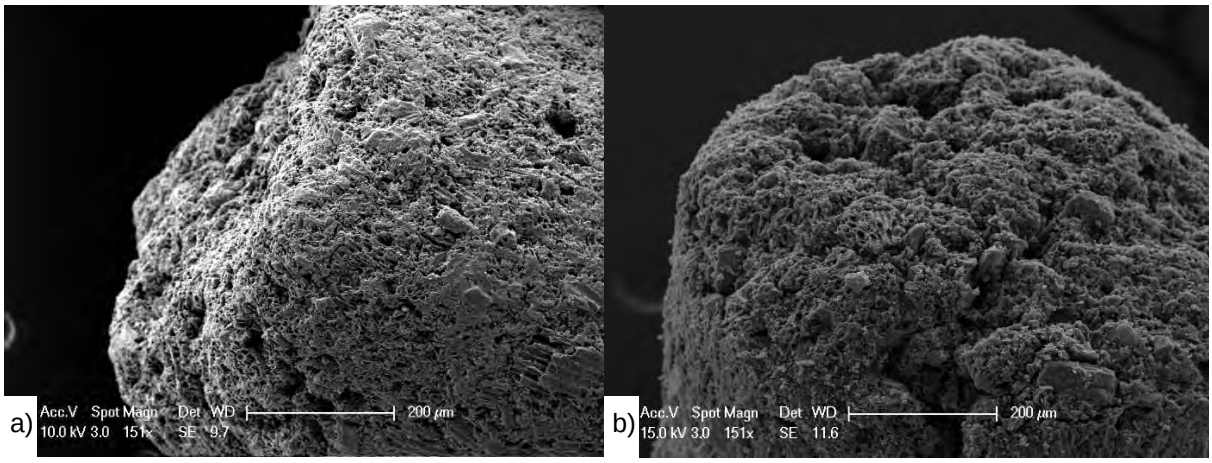

Figure 4.3. SEM images: a) unmodified Norit® R2030 Cabot AC 151x magnification; b) MEA (50%) modified AC Norit® R2030 Cabot, 151x magnification; scale bar = 200 µm

The unmodified R2030 Cabot and modified version are shown in Figure 4.3. From a visual analysis, this unmodified adsorbent exhibited a higher number of cracks and crevices on the surface than the unmodified RB1. However, significant differences in surface morphology were not observed for the Cabot samples treated by chemical impregnation. After the treatment with amine solutions (Figures 4.1-4.3), these cracks were filled by the amines, covering the gaps, potentially leading to reduced pore connectivity for CO_2 diffusion into the active sites (Khalil et al., 2012). Additionally, the reduction of impurities was also observed after amine impregnation of the unmodified R2030 and MEA (50%) modified R2030 AC comparison (Figures 4.3.a-b) (Gangupomu, Sattler & Ramirez, 2016). The overall changes on the modified ACs were provided using the BET technique, as reported in the following section.

4.2.2. Adsorption-Desorption Isotherms studies using BET

The study of pore characteristic represents a crucial point for the adsorbent application, supported by the evaluation of the adsorption capacity. Nitrogen adsorption isotherms were obtained and the respective adsorbed amount derived from BET analysis. The isotherms provide additional information about the pore characteristics by the shape of the curve, according to the IUPAC classification (as demonstrated in Figure 2.4).

Surface area studies also contribute to understanding how the adsorbent reacts in the presence of other gases. Physisorption isotherms (type I.b, according to Figure 2.4) were generated from BET studies with N_2 at 77 K, as shown in Figures 4.4-4.8. Hysteresis loops could also be observed from Figure 4.4-4.8, where the most suitable classification is the type H4 loops (given by many activated carbons and some other nanoporous adsorbents), which is associated with type I isotherms, also indicative of microporosity (Gregg & Sing, 1982; Sing & Williams, 2004). Figures 4.4.a and b provide the N_2 (77 K) adsorption isotherms relative to the unmodified and MEA (50%) modified R2030 Cabot ACs. The volume of gas adsorbed by the amine modified R2030 AC sample was considerably lower (0.06911 m^2/g) than the amount adsorbed (0.13269 m^2/g) by the unmodified AC, as shown in Table 4.1. This may be explained by the amine molecules filling the entrance of the pores, blocking the access to the internal pores, and limiting the contact with the gas inserted during the experiment. The TEA+MDEA+AMP modified AC did not provide higher adsorption capacity as predicted when compared to the TEA+AMP modified AC, as observed in Figures 4.4.c and d.

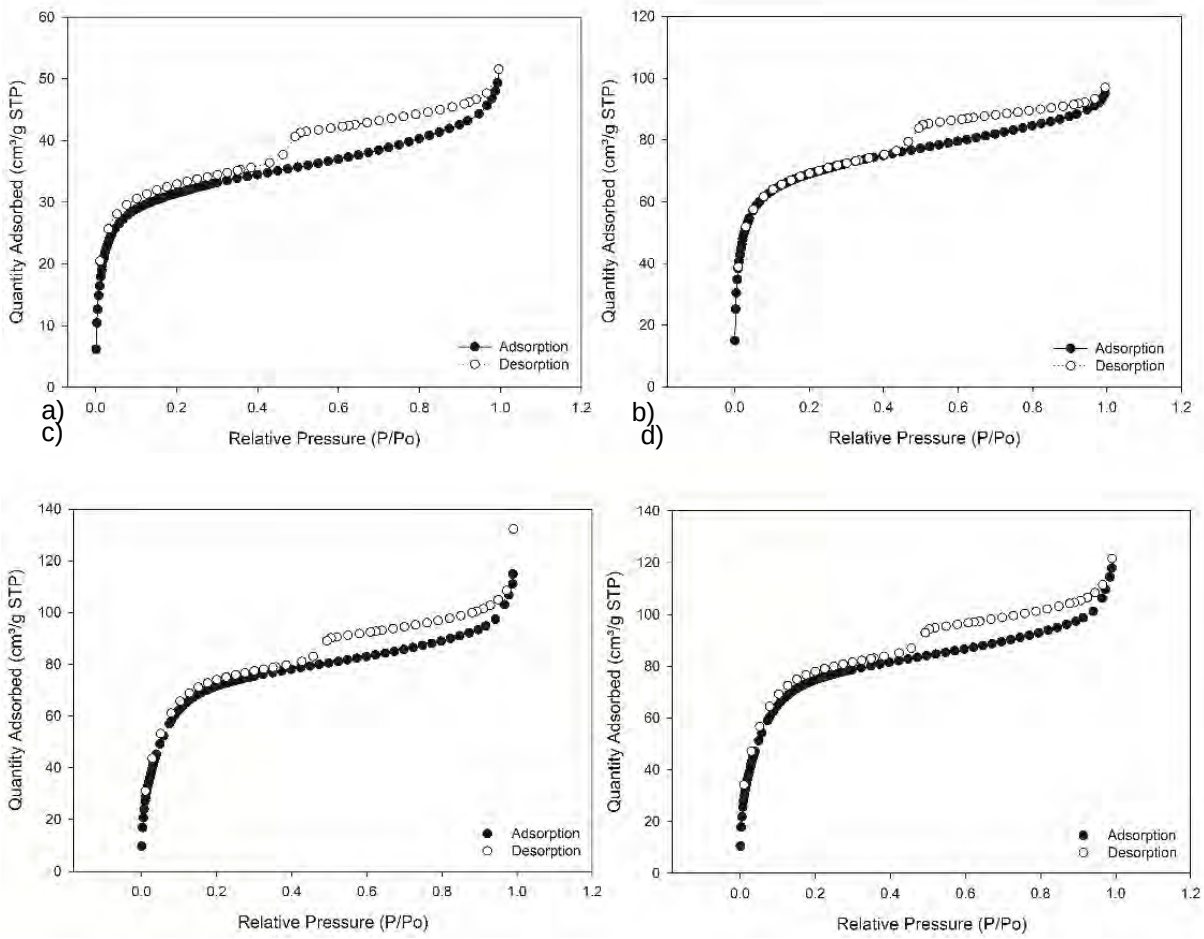

Figure 4.4. Physisorption isotherms generated from BET analysis with N_2 at 77 K for: a) MEA (50%) modified R2030 AC; b) unmodified R2030 AC; c) TEA+MDEA+AMP modified RB1 AC; and d) TEA+AMP modified RB1 AC

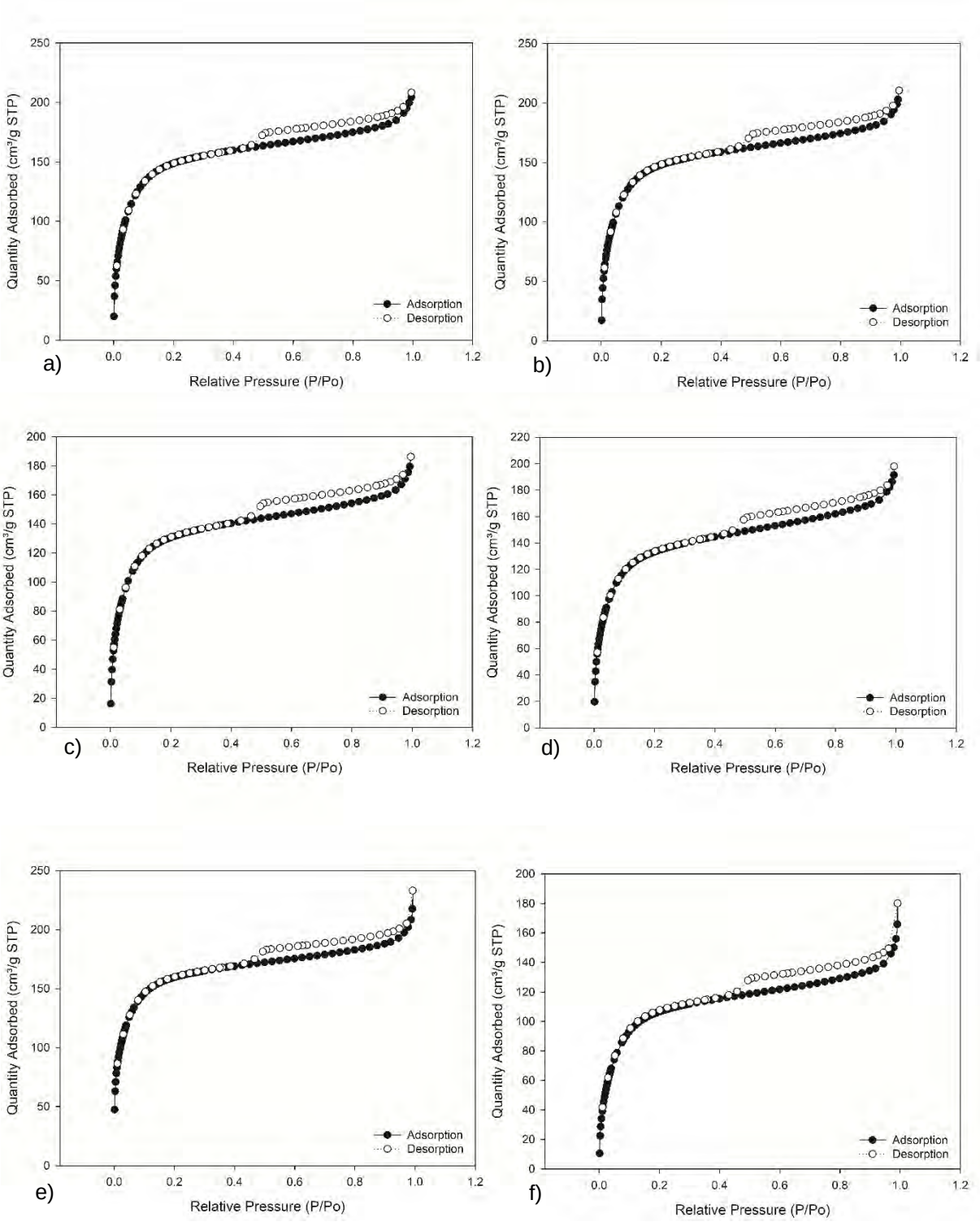

Figure 4.5. Physisorption isotherms generated from BET analysis with N_2 at 77 K for: a) MEA (20%) modified RB1 AC; b) MEA (30%) modified RB1 AC; c) MEA (40%) modified RB1 AC; d) MEA (50%) modified RB1 AC; e) MEA (60%) modified RB1 AC; and f) MEA+MDEA+AMP modified RB1 AC

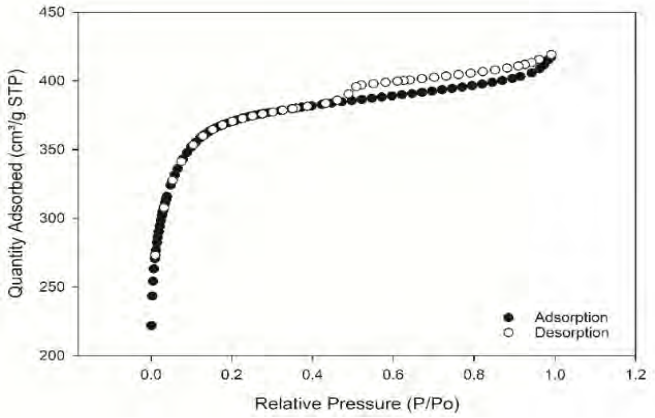

Figure 4.6. Physisorption isotherm generated from BET analysis with N_2 at 77 K for the unmodified RB1 AC

From the isotherms generated, it was possible to observe the amount of N_2 adsorbed per sample, with the unmodified sample demonstrating the best capacity (410 cm^3/g STP), as shown in Figure 4.6. However, the hysteresis was slightly impacted in the amine modified adsorbents (especially the TEA+AMP and TEA+MDEA+AMP modified AC, Figures 4.4.c and d.), due to the occurrence of mesoporosity (Figure 4.7 and 4.8) indicated by the fact that the adsorption isotherm does not reveal a truly horizontal plateau at relative pressures > 0.1. The BET surface area for the modified AC samples was compared with the unmodified AC and the overall data obtained regarding the textural proerties are shown in Table 4.1. A variety of adsorbents, for example, TEPA (30%), DEA (20%), DEA+MDEA+AMP and TEA+MDEA+AMP modified RB1 ACs) suffered reductions in their surface area as observed by BET, due to the solvent coverage of the surface and possible blockage of the smaller pores.

Table 4.1. Textural properties of the modified and unmodified samples

	Surface Area (m^2/g)		DFT Pore Size (nm)		Horvath-Kawazoe	
Samples	S_A (m^2/g)	S_{BET} (cm^3/g)	V_{total} (m^2/g)	A_{Total} (nm)	V_{Max} (cm^3/g)	W_{median} (nm)
Unmodified Norit® R2030 Cabot AC	248.66	268.73	0.13	21.58	0.15	1.72
MEA (50%) modified Norit® R2030 Cabot AC	113.10	119.74	0.07	11.43	0.08	2.08
Unmodified Norit® RB1 AC	1,378.76	1,437.31	0.58	42.45	0.65	1.05
MEA+MDEA+AMP blend modified Norit® RB1 AC	364.63	443.90	0.23	55.19	0.28	2.52
MEA (20%) modified Norit® RB1 AC	518.02	606.92	0.29	61.11	0.32	2.01
MEA (30%) modified Norit® RB1 AC	513.86	605.50	0.29	63.30	0.33	2.06
MEA (40%) modified Norit® RB1 AC	456.07	534.28	0.25	54.29	0.29	2.05
MEA (50%) modified Norit® RB1 AC	463.93	539.52	0.27	58.38	0.31	2.12
MEA (60%) modified Norit® RB1 AC	570.86	632.95	0.30	43.34	0.36	1.92
TEPA (20%) modified Norit® RB1 AC	921.90	888.01	0.26	49.68	0.29	1.97
TEPA (30%) modified Norit® RB1 AC	490.50	575.14	0.27	57.98	0.31	2.05
DEA+AMP blend modified Norit® RB1 AC	54.41	140.08	0.01	0.75	0.03	1.23
DEA+MDEA+AMP blend modified Norit® RB1 AC	422.83	505.72	0.15	12.91	0.08	0.78
TEA+AMP blend modified Norit® RB1 AC	253.11	292.14	0.17	41.31	0.19	2.44
TEA+MDEA+AMP blend modified Norit® RB1 AC	243.59	282.56	0.17	39.19	0.21	2.92

S_A = Single point surface area at P/Po = 0.099458015; S_{BET} = BET Surface Area; V_{total} = Volume in Pores (<1.857 nm); A_{Total} = Total Area in Pores (>= 1.857 nm); V_{Max} = Maximum pore volume (cm3/g) at P/Po = 0.994989778; W_{median} = Median pore width (nm).

From Table 4.1, the amine modified RB1 samples presented a surface area reduction with different amine loadings, ranging from 606.92 to 539.52 cm^3/g for a 20 to 50% amine loading, respectively. However, among the amine samples, 60% amine loading increased the surface area to 632.96 cm^3/g and provided an expansion in the pores measured by the H-K method, as shown in Table 4.1. In contrast, all amine samples suffered a significant reduction when compared to the unmodified RB1 original surface area (1,437.30 cm^3/g), where the most affected sample was DEA+AMP (140.08 cm^3/g).

The volume of adsorbed gas was used to derive the surface area, wherein the unmodified R2030 AC provided a surface area of 268.73 cm^3/g and amine covered R2030 AC had a reduced surface area of 119.74 cm^3/g. The Horvath-Kawazoe (H-K) method was applied to define the micropore volume along the experimental isotherm. The maximum volume measured for the unmodified R2030 AC (0.15 cm^3/g) was almost twice the modified AC (0.08 cm^3/g), which suggests that solvent coverage could lead to blockage of some micropores. The MEA R2030 AC adsorption isotherm showed a hysteresis loop during the desorption stage, which is associated with a pore network effect in which blocked pores are only able to empty during depressurisation at lower pressures when surrounding pores have also desorbed the condensed gas they contain (Sing, 1985; Chiang & Juang, 2016).

The BET surface area for the modified sample treated with DEA+AMP modified RB1 AC shows a remarkable reduction of 95% compared with the untreated sample, with the pore volume (A_{total} given by DFT pore size calculation) decreasing by 80%, as presented in Table 4.1. The pore size (Horvath-Kawazoe) of the DEA+AMP modified RB1 AC decreased 70% over the untreated sample. These results suggest that the DEA+AMP modifiers block some of the microporosity of the sample, a relatively small fraction of the pore volume but a larger

fraction of the surface area. Additionally, the DEA+MDEA+AMP, TEA+AMP and TEA+MDEA+AMP samples also suffered substantial reduction in BET surface area of 90%, accompanied with an increase in pore volume of 110% and an increase of 15% in pore size. This anomalous result suggests that there is a pore-blockage effect. The adsorbing N_2 interacts differently with DEA+AMP, DEA+MDEA and TEA+AMP modified surface, leading to a misleading high value of the pore volume which does not correspond to the reduction observed in the surface area (Rashidi & Yusup, 2016; Gholidoust et al., 2017; Kongnoo et al., 2016; Su et al., 2011; Khalil et al., 2012; Samanta et al., 2012).

Adsorbents with high surface area (m^2/g) were also tested in BET studies reported by Yu et al., (2012) and Rashidi et al., (2016). Thirteen adsorbents were listed and presented similar pore size (nm) compared with the variety of adsorbents used in this work, as shown in Table 4.2. The thirteen adsorbents in Table 4.2 presents an average volume in the range 0.67–1.44 cm^3/g and the pore size ranged from 2.7 to 40.5 nm. When compared with the amine modified ACs pore dimensions in Table 4.1, it was observed that their pore size provided uppermost values, for instance, MEA+MDEA+AMP, TEPA (30%) and TEA+MDEA+AMP modified RB1 ACs, owing to the absence of the amine pore blockage effect. However, it does not necessarily mean that the solid/gas interaction is higher than the unmodified ACs.

Table 4.2. Comparison of surface area and pore volume with published data for N_2 adsorption and desorption studies (Yu et al., 2012; Rashidi, Yusup & Borhan, 2016)

	Surface area (m^2/g)	**Pore size (nm)**	**Pore volume (cm^3/g)**	**References**
Unmodified Norit® RB1 AC	1,378.76	21.58	0.15	
MEA+MDEA+AMP blend modified Norit® RB1 AC	364.63	0.23	0.28	
Activated Carbon Unmodified	1762	Not mentioned	Not mentioned	(Plaza et al., 2008)
MCM-41	1229	2.7	1.15	(Xu et al., 2002)
SBA-15	950	6.6	1.31	(Ma, Wang & Song, 2009)
KIT-6	895	6.0	1.22	(Son, Choi & Ahn, 2008)
HMS	561	9.8	1.44	(Chen et al., 2010)
Meso-Al_2O_3	271	Not mentioned	Not mentioned	(Plaza et al., 2008)
Norit® SX2	660.73	40.5	0.67	(Rashidi et al., 2016)
Activated Carbon unmodified	838	Not mentioned	0.68	(Khalil et al., 2012)
Activated Carbon impregnated with MEA	65	Not mentioned	0.08	
Activated Carbon impregnated with AMP	102	Not mentioned	0.04	
Activated Carbon unmodified	1727	Not mentioned	1.204	(Bezerra et al., 2014)
Activated Carbon Impregnated with MEA+Methanol (10%)	749	Not mentioned	0.468	
Activated Carbon Impregnated with MEA+Methanol (20%)	237	Not mentioned	0.175	

The success of the chemical treatment is dependent upon the reactivity of the amine group attached to the AC surface, owing to the possibility of enhancement of the functionality of the

active sites by the presence of these chemical groups (Khalil et al., 2012; Grande et al., 2017). The N_2 adsorption of the amine modified ACs showed an improvement of 50% over the samples analysed in the studies reported by Yu et al., (2012) and Rashidi et al., (2016). This fact contributed to the success of the amine treatment on the activated carbon surface, demonstrating high potential to be considered as a novel and successful technique. In the study by Khalil et al., (2012), the modified adsorbents provided a reduction of 90% in their surface area (AC unmodified: 838 m^2/g; AC impregnated with AMP: 102 m^2/g; and AC impregnated with MEA: 65 m^2/g). The AC surface area reduction was also observed by Bezerra et al. (2014), wherein the AC surface suffered a drastic reduction after the chemical treatment (unmodified AC: 1727 m^2/g; AC with 10% amine loading: 749 m^2/g; and AC with 20% amine loading: 237 m^2/g). The pore filling effect also affects these samples to achieve high adsorption capacity towards CO_2 capture at relatively low temperatures.

As shown in the DFT pore size section in Table 4.1, the total pore area of the modified ACs demonstrated a pore blockage effect, related to the substantial pore size reduction as exhibited by DEA+AMP (0.75 nm), DEA+MDEA+AMP (12.91 nm), TEA+AMP (41.31 nm), and TEA+MDEA+AMP (39.2 nm) when compared with the unmodified adsorbent (42.45 nm). In this analysis, the solvent filled the AC micropores, and an increase was observed in the volume of the mesopores and macropores. Relative to the adsorbent physical properties, AC presents micro- and mesoporous structures. The PSD obtained by the BET studies improves the understanding of the AC performance during the adsorption stage. The unmodified AC demonstrates microporosity behaviour (as demonstrated in Figure 4.7.a), and when subjected to amine treatment, the microporosity reduces accompanied by an increase in mesoporosity. Figure 4.7 and 4.8 presents the PSD for unmodified and modified samples. A comparison

between the unmodified R2030 and the monoethanolamine (50% loading) modified R2030 shown in Figure 4.7.b and c illustrates the effect of the treatment on adsorbent pore size.

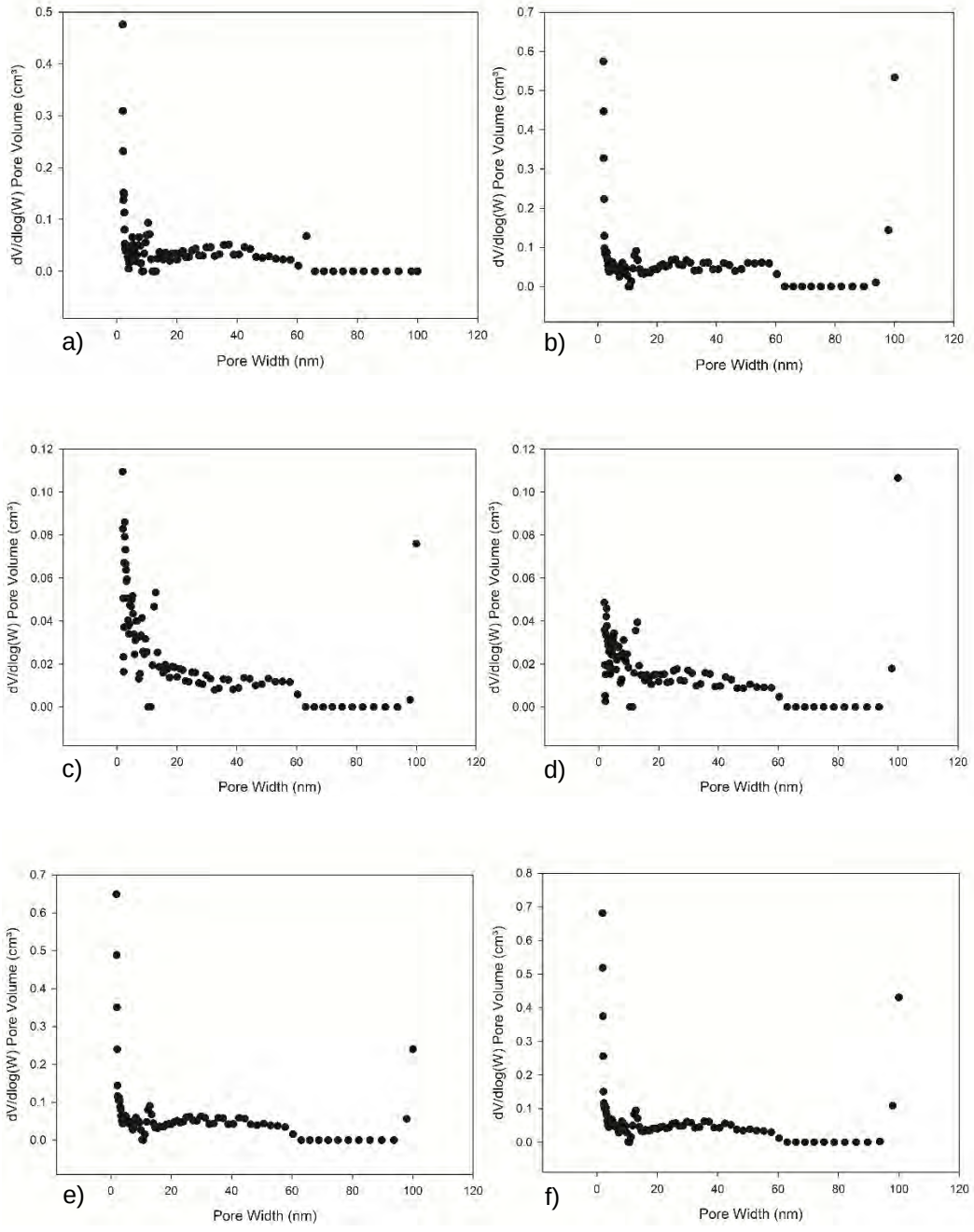

Figure 4.7. PSD comparison for: a) unmodified RB1 AC; b) MEA+MDEA+AMP modified RB1 AC; c) Unmodified R2030 AC; d) MEA (50%) modified R2030 AC; e) MEA (20%) modified RB1 AC; and f) MEA (30%) modified RB1 AC

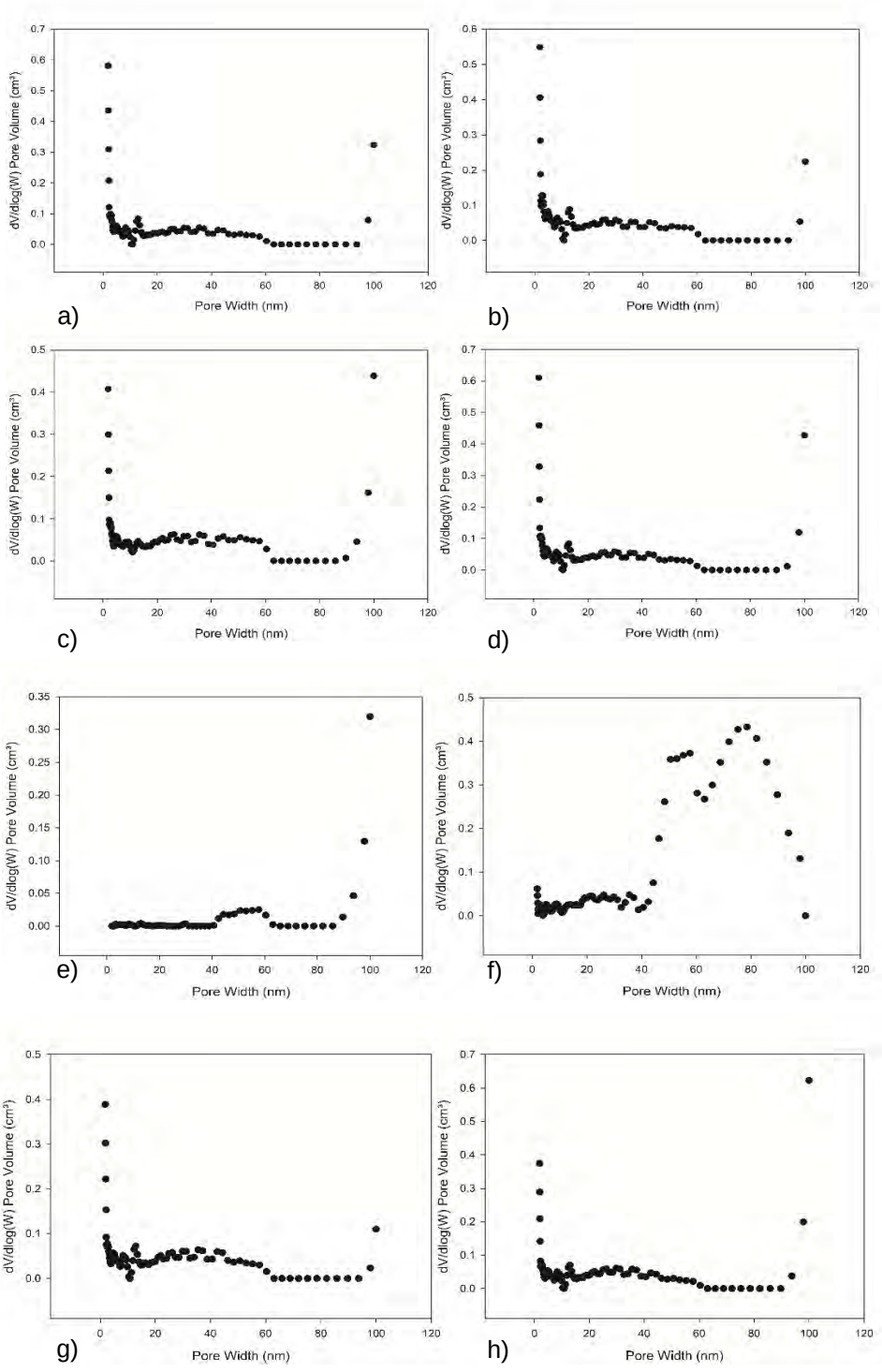

Figure 4.8. PSD comparison for: a) MEA (40%) modified RB1 AC; b) MEA (50%) modified AC; c) MEA (60%) modified RB1 AC; d) TEPA (30%) modified RB1 AC; e) DEA+AMP modified RB1 AC; f) DEA+MDEA+AMP modified RB1 AC; g) TEA+AMP modified RB1 AC; and h) TEA+MDEA+AMP modified RB1 AC

The amine ACs isotherms demonstrated lower N_2 adsorption capacity when compared to the unmodified plot. This fact is supported by the consideration that BET N_2 adsorption isotherms are typically associated with physisorption forces, which reduces the amines affinity towards the adsorptive gas on the AC surface compared with the unmodified AC, as confirmed by TGA and PSA experiments. Additionally, chemisorption might occur in parallel with the physisorption forces. However, the power of the chemisorption forces could be absolutely low, due to the required adsorption temperature (35–80^{o}C) to activate the amine groups on the AC (Thambimuthu et al., 2005; Zhao et al., 2018; Grande et al., 2017). In most of the AC amine samples, relative to the adsorption uptake values tested in TGA and PSA studies, weak interactions (physisorption) are removed by the introduction of a high-temperature difference during the initial adsorbent preparation/desorption. Site activation occurs, favouring the occurrence of chemisorption by the energy given to the molecules in the pores, attaching the chemical bonds to the surface (Campbell, 1988). Alternatively, the heat treatment applied in the modification method may have burnt away some of the support, leading to larger pore size and volume but lower surface area.

Pore volume and pore width comparison has been shown in Figure 4.8.e-g, where it was possible to evaluate the PSD of the materials using the non-linear DFT method obtained from N_2 isotherms generated at 77 K.

The mesopore distribution was more well-connected after the amine treatment, as shown in Figures 4.7.c-e and 4.8.b-g. As mentioned in section 2.3.1, the amine impregnation solvent promotes crosslinks during oxidation (Buczek, 2016; Chen et al., 2013; Fan et al., 2013). Increased crosslinks may lead to an increase in the adsorbent capacity for CO_2 capture if pores connections become opened to allow the adsorbing molecule to access possible additional sites.

The mesoporous region of the amine modified ACs showed an simultaneous increase with loss of micropore range (Bezerra et al., 2014)**,** which may be explained by the pores becoming filled with solvent and affected by the heating during impregnation, thereby increasing the mesopore region (Hesas et al., 2013). The widening of the mesoporous range (2–50 nm) was observed where the PSD ranged from meso- through macroporous range 40 to 100 nm for DEA+AMP, from 20 nm to 100 nm for TEA+MDEA+AMP and from 20 to 100 nm for DEA+MDEA+AMP modified RB1 ACs, as shown in Figures 4.7.a-f and 4.8.

A similar effect was observed in Figure 4.7.b, where the MEA+MDEA+AMP modified AC PSD had a considerable reduction in the microporous range, increasing the mesopore range distribution. It was also observed with the PSD for primary amine modified samples with different loadings (especially in Figure 4.8.c) and for the DEA+MDEA+AMP, TEA+AMP and TEA+MDEA+AMP (Figure 4.8.f, g and h, respectively), where the mesoporosity range showed higher distribution when compared with the unmodified RB1 AC.

From Figure 4.8.a-h, it was possible to observe and compare the effect of different amine loadings on the modified AC surface. The monoethanolamine solvent loading in contact with the unmodified adsorbent reduced its micropores to 20%, and the mesopores increased up to 10%, as shown in Figure 4.7.e. The monoethanolamine (0.3 and 0.6) modified adsorbent showed a higher distribution for the presence of macropores on the adsorbent surface, increasing 10% compared with the other amine modified ACs. Another sample worthy of note is the DEA+MDEA+AMP modified AC, which presented a considerable increase in the volume of macropores, as confirmed by Figure 4.8.f. In contrast with the MEA modified ACs, the adsorbent modified with TEPA solution presented a reduction of 5% for the pore volume in the micropore range. The micropore range was sharply reduced in the MEA modified ACs

compared to the unmodified RB1, as shown in Figure 4.7. Mesoporous adsorbents tend to present higher gas diffusion than microporous adsorbents. Additionally, this aspect might decrease the limitations related to the mass transfer into micropores during the adsorption (Hedin et al., 2013).

4.2.3. Physicochemical and structural analysis for the ACs characterisation via XRD studies

Materials with their structure predominantly based on carbons present high tendency to exhibit amorphous behaviour (Girgis et al., 2007). XRD was used to characterise and observe the original chemical structure ordering and the impact after exposure of the ACs to chemical impregnation.

The modified AC diffraction patterns were crucial to observe the chemical treatment effectiveness and the insertion of reactive elements into their physical structure. Additionally, a qualitative investigation of the effect of the chemicals impregnated on the adsorbent surface was made. In parallel, the impact of the chemical treatment temperature was considered, observing possible alterations into the structure order. As reported by Girgis et al. (2007), these structures have the degree of order closely related to the thermal treatment applied to the AC.

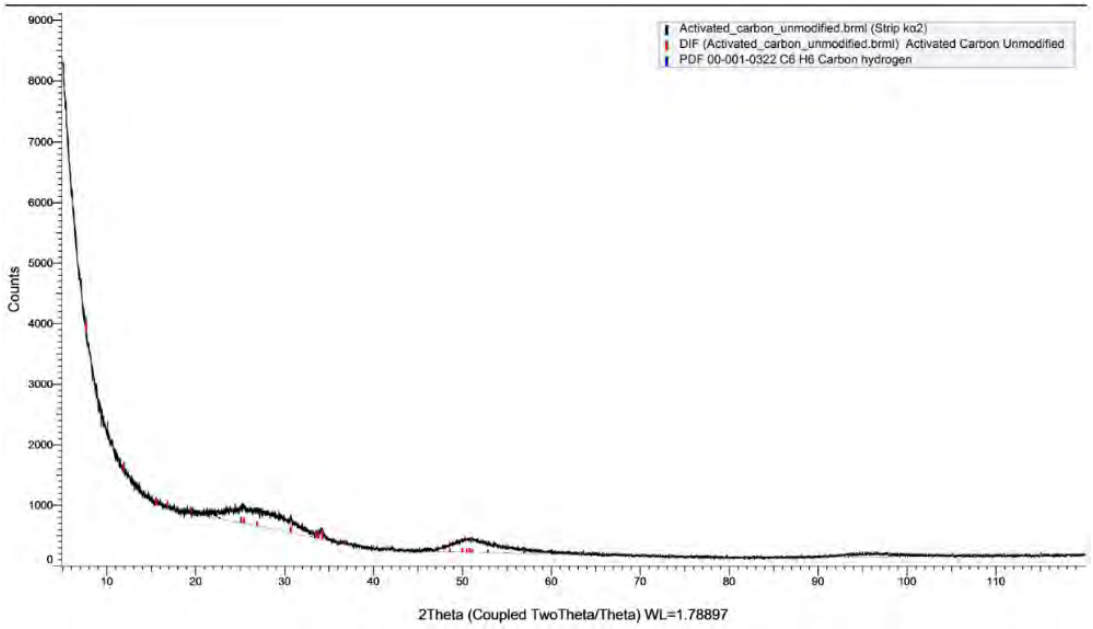

Figure 4.9. Unmodified Norit® RB1 AC XRD pattern analysed from 5 to 120º 2θ

The unmodified RB1 AC diffraction pattern is shown in Figure 4.9. Four low intensity (represented by counts in the graph) peaks were observed at 2θ = 26º, 2θ = 34º, 2θ = 42º and 2θ = 51º in the spectrum, which correspond to carbon bonds relative to the AC fundamental structure (in particular, the 2θ = 26º which corresponds to the 002 graphite structure), where the pattern that best fitted the data was matched by the chemical library in the XRD software. The absence of an accentuated peak and the broad diffraction background reveals the amorphous adsorbent structure (Omri & Benzina, 2012; Kennedy et al., 2007; Kumar & Gupta, 1994; Das, Samal & BC, 2015). However, considering the impregnation of the amine groups onto the AC surface, the amine treated AC XRD graphs showed extra peaks compared to the original RB1 AC, which correspond to the low crystallinity provided by the molecules added to the AC surface (as shown in Figure 4.10). The amine groups were observed in Figure 4.10.a and 4.10.b relative to the monoethanolamine with AMP blend. The primary amine pattern shown peaks broadly extended at 2θ = 26º, 2θ = 52º, 2θ = 77º and 2θ = 98º.

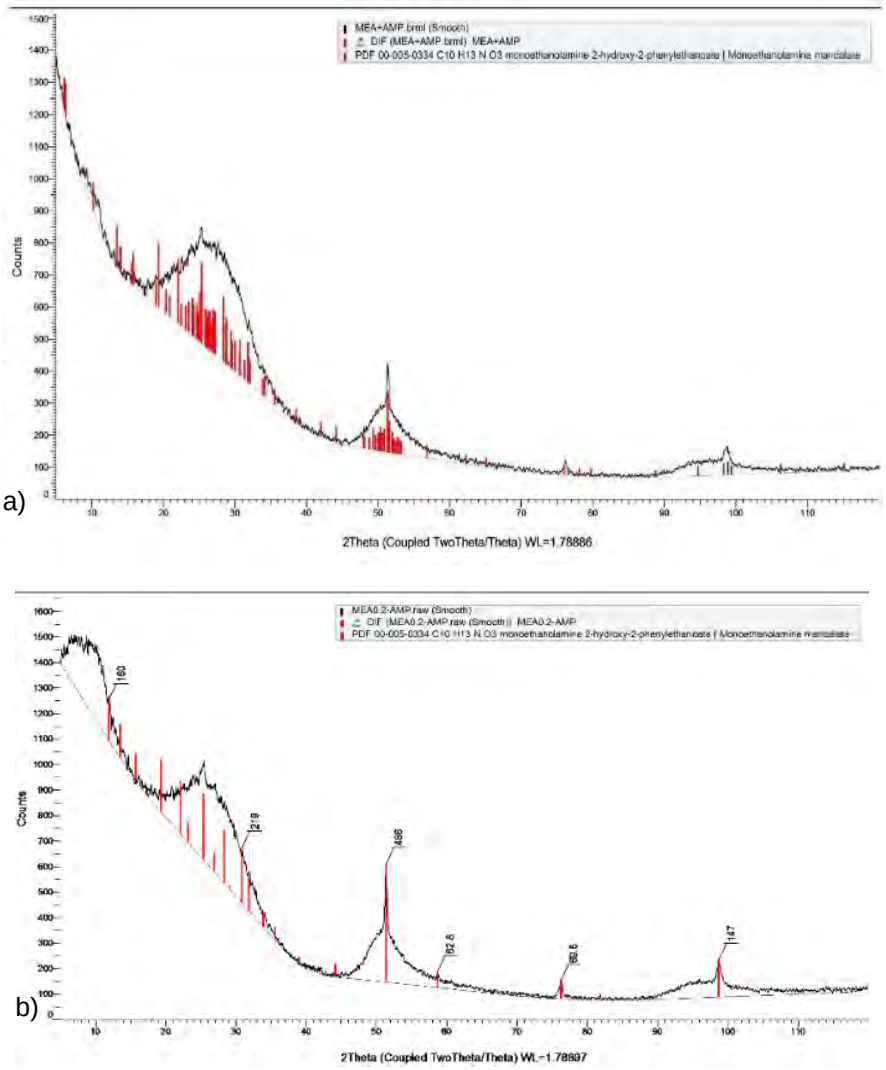

Figure 4.10. MEA+AMP blend modified Norit® RB1 AC (a) and (b) MEA (20%) modified Norit® RB1 AC XRD pattern analysed from 5 to 120º 2θ

The monoethanolamine groups were found along the spectra, supporting the amine covering the AC impregnated surface. The intensity of the amine groups on the AC powder was observed and marked in red. It can be concluded that the amine groups were distributed and identified in different ranges of the AC. The amine distribution along the spectra was intensified with the insertion of the primary amine without the AMP solvent, which was applied as a co-solvent for amine reactivity improvement towards CO_2 capture. However, the co-solvent reduced the amine intensity over the AC powder in the XRD pattern, as shown in Figure 4.10.a. In contrast,

Figure 4.10.b displays the MEA (20%) pattern which includes a higher distribution of the primary amines, represented by six strong spectral bands (2θ = 9º, 2θ = 27º, 2θ = 52º (highest peak), 2θ = 59º, 2θ = 76º, 2θ = 99º). A comparative diffraction pattern is exhibited in Figure 4.11.a-d, relative to the amine modified AC including different loadings, wherein the MEA (60%) modified AC displayed the highest peaks compared to the unmodified AC XRD pattern, as shown in Figure 4.11.c. The intensity of these peaks was reduced to 55% with the increase in solvent loading.

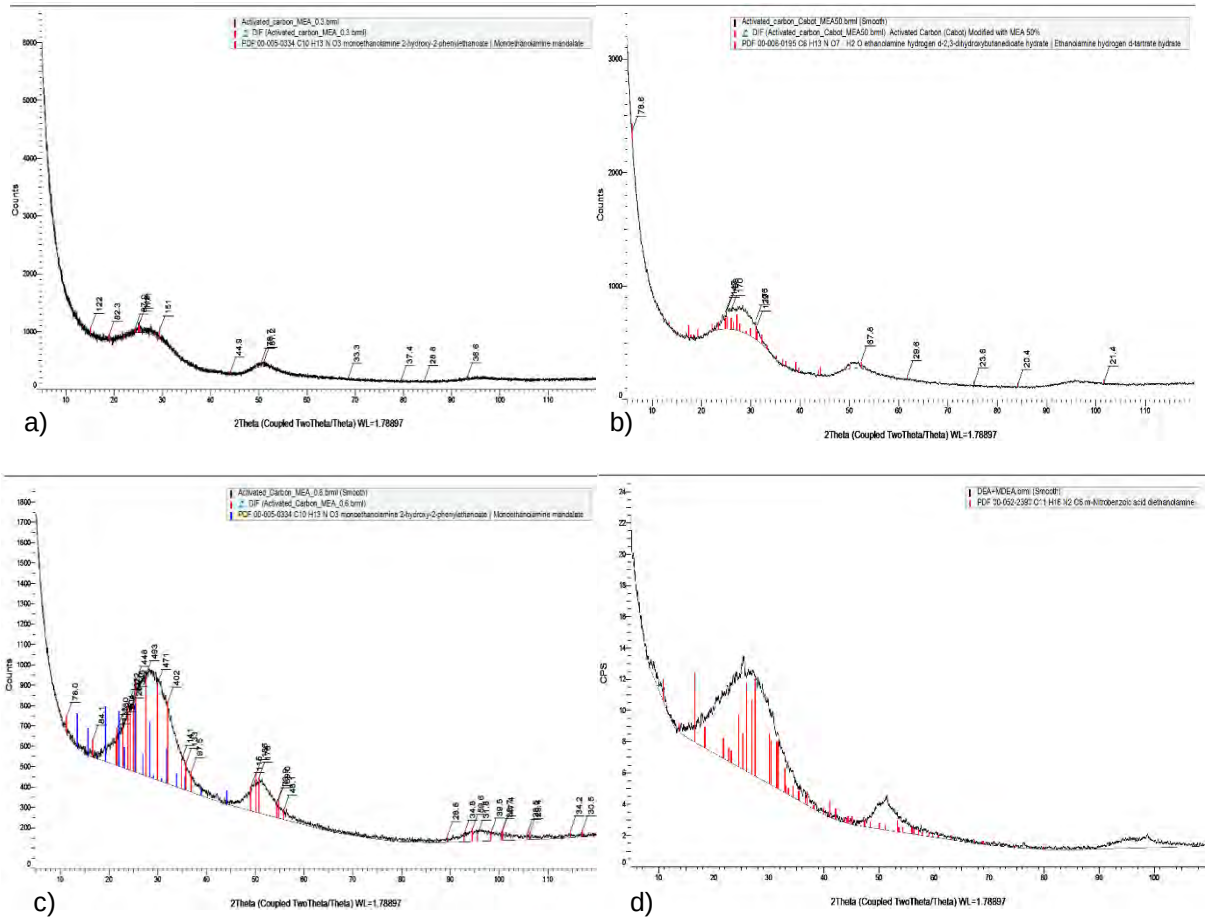

Figure 4.11. XRD patterns for: a) MEA (30%) blend modified Norit® RB1 AC; b) MEA (50%) blend modified Norit® RB1 AC; c) MEA (60%) blend modified Norit® RB1 AC; and d) DEA+MDEA+AMP blend modified Norit® RB1 AC analysed from 5 to 120º (2θ)

Figure 4.11.d shows the XRD spectra for the DEA+MDEA+AMP modified RB1 AC. However, no matches for MDEA solvent were found in the chemical library. The amine chemical groups matches were limited due to the low chemical library database in the XRD software, which only covers primary and secondary amines, so the base comparison was restricted for these two solvents. Consequently, TEPA, TEA and AMP solvents were also limited to matching the XRD patterns. For this reason, the investigation of the chemical groups on the AC properties (for instance, TEA+AMP, TEA+MDEA+AMP and TEPA modified RB1 AC) from their respective XRD patterns could not be chemically completed.

The low intensity peaks can also be related to the mesopore formation, as predicted by PSD in BET studies. This fact is supported by the appearance of a large sharp peak followed by small peaks along the MEA (50%), MEA (60%) and DEA+MDEA+AMP modified XRD patterns (Figure 4.11.b-d) (Rampe & Tiwow, 2018). These amines modified ACs showed the creation of mesopores along the AC structure as proven in section 4.2.2, which were verified by the PSD measurements (Figures 4.8.c).

The temperature of the AC amine treatment was considered as the main factor affecting intensity reduction observed in the XRD patterns of the amine modified AC. In these patterns, this effect contributed to improving the understanding of the AC structure, where originally a short-range layered structure of carbon atoms was found in arrangements (Girgis et al., 2007; Schettino Jr et al., 2007). The impregnation of amine molecules onto the AC surface increased crystallinity, due to the generation of microstructures in the solid phase of these adsorbents, as observed in their respective XRD graphs (Figures 4.10-4.12) (Liu et al., 2014; Lendzion-Bieluń et al., 2018; Tiwari et al., 2016; Ben-Mansour et al., 2016; Rampe & Tiwow, 2018). This effect

implies the reduction of the microporosity level of the AC by the action of these microstructures (Kumar & Gupta, 1994; Girgis et al., 2007; Shamsuddin, Yusoff & Sulaiman, 2016).

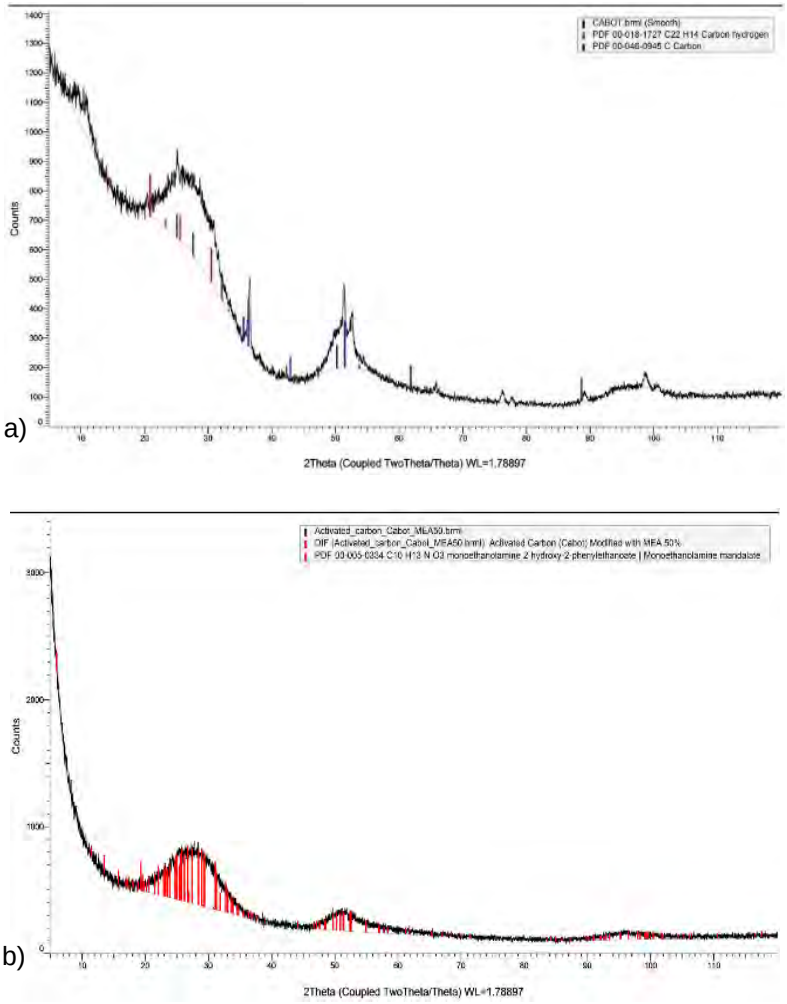

Figure 4.12. XRD patterns for: a) unmodified Norit® R2030 Cabot AC; and b) MEA (50%) modified Norit® R2030 AC analysed from 5 to 120º (2θ)

Figure 4.12 displays the XRD pattern for the unmodified R2030 AC analysed from 5 to 120º (2θ), where a lower intensity (1300) was provided compared with the unmodified RB1 AC (8000). The main peaks were presented at 12º, 24º, 37º, 52º, 54º, 76º, 78º, 89º, 99º and 101º in 2θ range. These peaks were identified and matched with the carbon and carbon-hydrogen groups from the chemical library, due to the compatibility presented. As demonstrated in Figure

4.12.b, relative to the amine modified R2030 XRD pattern, it was possible to observe an increase in the initial spectra intensity that occurred after the chemical treatment in the 5–10º in 2θ range. This resulted in a reduction in the degree of order relative to the unmodified AC structure, promoted by the creation of microstructures within the adsorbent which originated from the impregnation of amine groups.

4.2.4. Carbon dioxide adsorption in TGA experiments

The ability and capacity of the ACs for carbon capture under post-combustion temperature conditions was initially assessed by TGA with an adsorption stage at 70ºC. This temperature was selected as typical of flue gas temperatures encountered in PCC. However, it is known that the capacity of adsorbents decreases with temperature, particularly over 50°C, also their selectivity changes so that they become sensitive to the choice of operating conditions when utilised in a high-temperature process (Yu et al., 2012; Plaza et al., 2010). The decision of the chemical impregnation method was intended to reduce this limitation and make the adsorbents more suitable for use at high temperatures in post-combustion adsorption conditions.

In post-combustion CO_2 capture processes, gases containing mainly CO_2 and N_2 are obtained from the combustion at a relatively high temperature of 70ºC (temperature used for the adsorption stage) and the separation is carried out at low pressure. The methodology was described in section 3.1.2. The TGA presented limitations, wherein only one gas flow was used to obtain a desired steady state, due to the disturbance created when the ACs were tested under a combined flow of mixed gases or manually switched between gases. For this reason, the thermal adsorption stage was conducted under a rate of 50 ml/min of pure CO_2 flow.

A pre-treatment stage (150ºC for 60 min) was applied to remove residual moisture, as well as to promote higher surface adsorption energy and molecular diffusion to help remove residual CO_2 (Maroto-Valer, Tang & Zhang, 2005). The pre-treatment step broke the physisorption forces, due to the thermal difference.

After the pre-treatment, an improvement in the chemisorption energy was expected due to the pore activation. However, the temperature difference did not promote an elevation in the chemical bond energy effect and reduced the amine reactivity, as shown by the reduced CO_2 uptake in Figures 4.13 and 4.14. This phenomenon was most likely caused by pore blockage due to solvent filling. Another factor that should be considered is the low pressure used in these studies, which may not help the site activation and achieve high CO_2 uptake capacity.

CO_2 uptake capacities were calculated by the conversion of the mass loss to mmol of CO_2/g, considering only the adsorption time to this calculation, as described in section 3.1.2. The active sites of the AC improved their affinity for CO_2 capture due to the impregnation treatment applied.

Figure 4.13 shows the only competitive and promising amine modified AC for post-combustion in thermal-adsorption studies. TEPA (20%) modified RB1 provided high CO_2 uptake capacity (0.9 mmol/g), owing to the highest group reactivity towards CO_2 when compared with MEA groups, due to the activation of the molecules allocated inside the pores. TEPA molecules present high reactivity towards CO_2 (3.2 mmol/g) compared to the groups of amines selected to the impregnation treatment (Fauth et al., 2007).

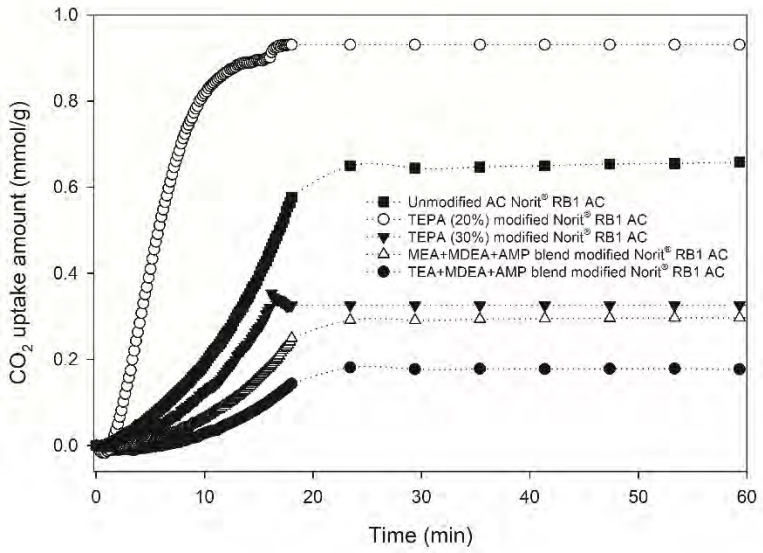

Figure 4.13. Adsorbents TEA+MDEA+AMP blend (black circles), TEPA (20%) modified AC (white circles), TEPA (30%) modified AC (black triangles) and MEA+MDEA+AMP modified AC (white triangles) tested under chemisorption studies to measure CO_2 uptake potential and compare with the unmodified AC

The presence of multiple amine groups on the AC surface originating from the TEPA chemical structure (as shown in Figure 2.3.f), confers high reactivity for CO_2 capture (Bonenfant et al., 2003). In contrast, the TEPA impregnation treatment provided pore blockage and surface area reduction in comparison with the unmodified sample in BET studies (Table 4.1), suggesting that the amine solvent created a hard cover over the AC after impregnation. Moreover, the adsorption temperature applied to post-combustion conditions improved the adsorbent surface and gas interaction due to the thermal activation of amine molecules.

The adsorbent modified with the secondary (DEA and DEA+MDEA+AMP blend) and tertiary amine (TEA) did not interact with the CO_2 molecules during the thermo-adsorption experiments, providing no generation of gas uptake curve. These solvents do not have the same reactivity and affinity towards CO_2 as the primary amine (MEA, 0.33–0.40 mol CO_2/mol amine), where two groups from the primary amine structure react with one CO_2 molecule (Hedin et al., 2013; Rufford et al., 2012). Relative to the secondary (DEA) and the co-amine

(MDEA), according to the literature, the potential for acid gas molecules sequestration is between 0.21–0.81 and 0.20–0.81 mol CO_2/mol amine, respectively (Rufford et al., 2012). However, the TEA+MDEA+AMP blend improved the tertiary amine affinity for CO_2, and a gas uptake curve was generated under post-combustion conditions. By contrast, as presented in Figure 4.13, the amount adsorbed by TEA+MDEA+AMP sample (0.2 mmol/g) was less compared to the unmodified AC (0.7 mmol/g) analysed in the same conditions presented in Table 4.3. The amine modified Cabot R2030 AC thermo-adsorption performance was compared with their unmodified version in Figure 4.14. Thermo-adsorption studies provided the performance of these ACs under a low-pressure system. As represented in Figure 4.15, a reduction in the adsorption capacity affected the amine modified AC performance under chemisorption, where the amine adsorbent demonstrated a CO_2 uptake of 0.35 mmol/g lower than the unmodified AC. A possible explanation for the reduced performance of R2030 AC may be due to the loss of microporosity and increased mesoporosity relative to the unmodified AC (Figures 4.7.c-d), leading to lower surface area available for adsorption to occur. Surface area and the volume adsorbed by these samples during the BET tests confirmed this behaviour for the amine modified AC.

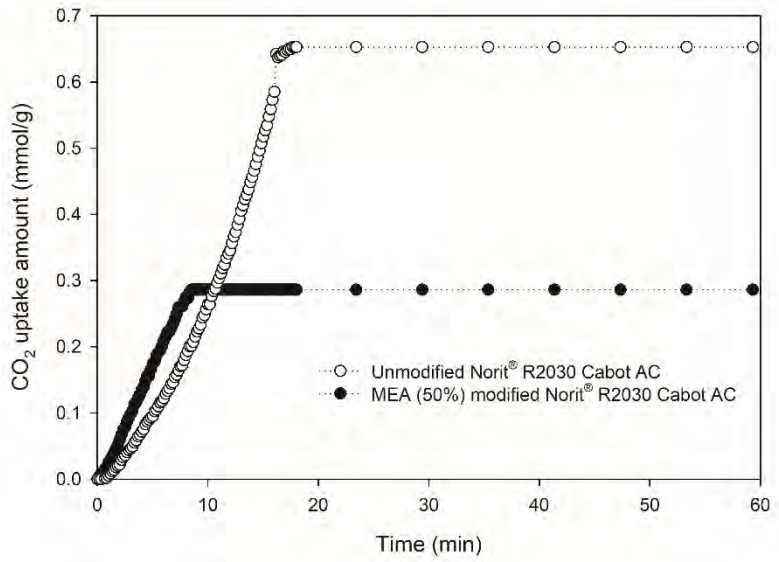

Figure 4.14. Chemisorption studies comparing the quantify of CO_2 uptake by unmodified and the MEA modified R2030 Cabot AC

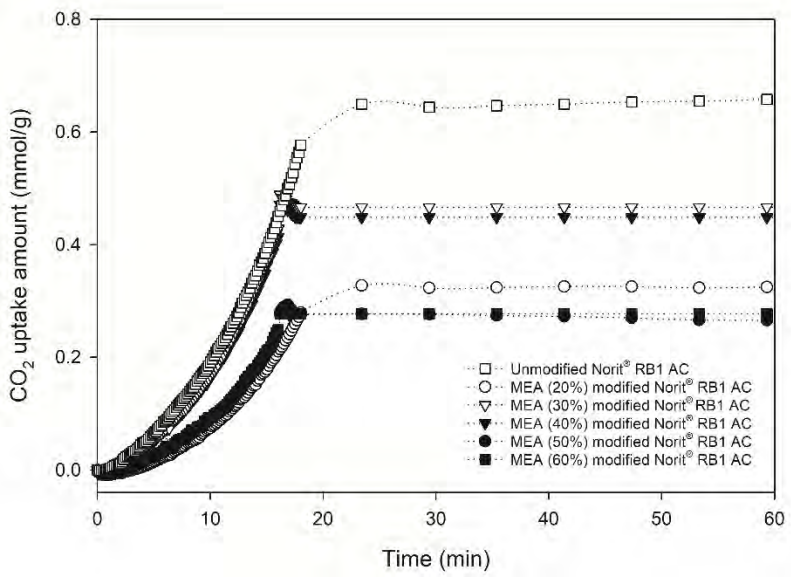

Figure 4.15. TGA curves for the amines ACs: MEA (20%) modified AC (white circles), MEA (30%) modified AC (white triangles), MEA (40%) modified AC (black triangles), MEA (50%) modified AC (black circles) and MEA (60%) modified AC (black squares) and the unmodified RB1 AC (white squares), establishing an adsorption capacity comparison

Studies including the different amine loaded ACs were compared with the unmodified RB1 AC in Figures 4.13 and 4.15, showing the adsorption uptake (cooling/adsorption process) of these samples as a function of time. A similar behaviour to the amine modified Cabot AC was observed for the amine modified RB1 ACs, where the different loadings of amines were not enough to increase the adsorbent affinity for CO_2 relative to the unmodified sample. Although the primary amine provides the highest reactivity level to capture CO_2, it did not improve the AC capacity as expected. Rather the excess of impregnated solvent excess may disturb the activation of adsorption sites, as represented by the loading of 50 and 60% amine curves in Figure 4.15, where these materials reached only 0.3 mmol/g of CO_2 during the adsorption studies compared to 0.65 mmol/g recorded for the unmodified RB1 material. The CO_2 adsorption results obtained for all analysed samples are shown in Table 4.3.

Table 4.3. Thermal adsorption results for the ACs tested under pure CO_2 flow at 70ºC

Samples	CO_2 uptake amount (mmol/g)
Unmodified AC Norit® RB1 AC	0.7
MEA+AMP blend modified Norit® RB1 AC	0.4
MEA+MDEA+AMP blend modified Norit® RB1 AC	0.3
DEA+AMP blend modified Norit® RB1 AC	No BT generation
DEA+MDEA+AMP blend modified Norit® RB1 AC	
TEA+AMP blend modified Norit® RB1 AC	
TEA+MDEA+AMP blend modified Norit® RB1 AC	0.2
TEPA (20%) modified Norit® RB1 AC	0.9
TEPA (30%) modified Norit® RB1 AC	0.4
MEA (20%) modified Norit® RB1 AC	0.4
MEA (30%) modified Norit® RB1 AC	0.5
MEA (40%) modified Norit® RB1 AC	0.5
MEA (50%) modified Norit® RB1 AC	0.3
MEA (60%) modified Norit® RB1 AC	0.3
Unmodified AC Norit® R2030 Cabot	0.7
MEA (50%) modified AC Norit® R2030 Cabot	0.3

From Table 4.3, it was concluded that the MEA modification reduced CO_2 adsorption capacity compared to the unmodified RB1 AC performance. This was thought to be due to the effect of the low gas inlet pressure which limited the amine modified adsorbent performance at post-combustion temperatures. Yu et al. (2012) reported the CO_2 capacity of several commonly used materials, showing that only one material exhibited higher capacity than the adsorbents used in this work, as shown in Table 4.4.

Table 4.4. Comparison of CO_2 capacity in TGA studies. Adapted from Yu et al. (2012) and Pongstabodee et al. (2016)

		Carbon dioxide capacity (mmol/g)	References
Adsorbents	AC	1.66	(Plaza et al., 2008)
	MCM-41	0.14	(Xu et al., 2002)
	SBA-15	0.11	(Ma et al., 2009)
	KIT-6	0.02	(Son et al., 2008)
	HMS	0.22	(Chen et al., 2010)
	Meso-Al2O3	0.84	(Plaza et al., 2008)
	Activated Carbon unmodified	0.018	(Khalil et al., 2012)
	Activated Carbon impregnated with MEA	0.049	
	Activated Carbon impregnated with AMP	0.034	
	Activated Carbon unmodified	0.045	(Bezerra et al., 2014)
	Activated Carbon Impregnated with MEA+Methanol (10%)	0.082	
	Activated Carbon Impregnated with MEA+Methanol (20%)	0.004	

As confirmed by the BET results, the samples modified by amines had a lower surface area when compared with the unmodified material, due to the insertion of chemical groups into the pores and the AC surface which promotes the creation of active sites. The most effective

treatment was due to the modification promoted with TEPA solvent, which presented high performance when tested under TGA post-combustion adsorption conditions. Studies concentrating on amine insertion onto different adsorbent surfaces via several techniques have been investigated by many researchers. The impregnation of polyethylenimine (PEI) in mesoporous silica was investigated (Dowson et al., 2016), aiming to improve the material adsorption capacity. However, the impact of this solvent impregnation reduced surface area, pore volume and pore size. In parallel, the adsorption capacity was improved with the solvent loading saturation in the impregnation procedure.

Sayari et al. (2011) modified MCM-41 using the same solvent for impregnation, improving the CO_2 adsorption capacity to 3.02 mmol/g by the addition of a 75% amine solution in post-combustion conditions. The excess of amine solution did not impact directly on increasing the CO_2 adsorption. Formation of the aggregated amine on supports might decrease the amine molecules accessibility to CO_2, with some supports being more prone to this effect. The same adsorbent was impregnated with a loading of 50% and tested at a different temperature (25^{o}C), whereupon their adsorption capacity also drastically reduced. This might be explained by the high diffusion rate of CO_2 and improvements dedicated to the adsorption rate of CO_2 under post-combustion temperatures. The application of TEPA solvent onto mesopore materials was investigated by Yue et al., (2006). They impregnated TEPA into SBA-15 and MCM-41, improving the CO_2 capacity to 3.93 mmol/g and 5.39 mmol/g onto SBA-15 (70% amine loading for impregnation) and MCM-41 (60% amine loading for impregnation), respectively. Plaza et al. (2008) also investigated the utilisation of amine solvents on AC and alumina. Solvents, such as primary and secondary alkylamines, are listed below:

- Diethylenetriamine (DETA): 40% concentrated; analysed at 100ºC; CO_2 capacity: 1.75 mmol/g;
- Pentaethylenehexamine (PEHA): 31% concentrated; analysed at 97ºC; CO_2 capacity: 1.03 mmol/g;
- Alkanolamines (DIPA): diisopropanolamine; 40% concentrated; analysed at 25ºC; CO_2 capacity: 0.93 mmol/g;
- Sterically hindered 2-amino-2-methyl-1,3-propanediol (AMPD): 40% concentrated; analysed at 25ºC; CO_2 capacity: 0.57 mmol/g;
- Triethanolamine (TEA): 40% concentrated; analysed at 25ºC; CO_2 capacity: 0.39 mmol/g.

However, DETA modified adsorbent was considered as the most efficient material due to its high CO_2 adsorption capacity. This result correlated with the surface area reduction promoted by the amine impregnated solution on the AC, where the microporous dimensions which are responsible for the physical adsorption of CO_2 were reduced after the chemical treatment. The insertion of MEA onto the AC surface was also investigated by Khalil et al., (2012) and Bezerra et al., (2014). These studies provided amine loading onto the AC surface with pure AMP solvent and TGA was performed at 80ºC under pure CO_2 flow (10 ml/min) for adsorption, as shown in Table 4.4. The modified adsorbents exhibited a substantial improvement after impregnation compared to their unmodified AC, providing an increase in the amine adsorbents of 55%. Compared to the MEA (20%) modified RB1 AC and others amines with different loadings (for instance, MEA 30–60% modified RB1 ACs), these samples presented a lower adsorption capacity of 90%, as shown in Table 4.3, which may be attributed to their smaller surface area, as shown in Table 4.2.

4.2.5. Chemical composition investigation via FTIR

The application of the IR methodology is considered as a powerful analytical technique to characterise and identify the AC constituents. This technique was applied to investigate the variation in the functional groups on the AC surface, allowing a comparison between the modified and unmodified samples. FTIR analysis enables identification of the chemical composition and organic functional groups, which might work as adsorption sites. Spectral peaks were in concordance with the literature for AC samples. Knowledge of the presence of functional groups in adsorbents is essential to reveal the adsorption mechanisms. FTIR analysis allows identification of components with covalent bonds, being organic or inorganic (Pavia, Lampman & Kriz, 2001). The region most used in the characterisation is the mid infrared, situated in the wavenumber interval of 4000–400 cm^{-1}. Changes in the energy of the vibrational and rotational motions of the molecule occur in the referred band, generating spectra (Silverstein, Webster & Kiemle, 2005). The Norit® R2030 and RB1 unmodified adsorbents exhibited strong and light intensity and the spectra as represented in Figure 4.16.a and 4.16.b, respectively.

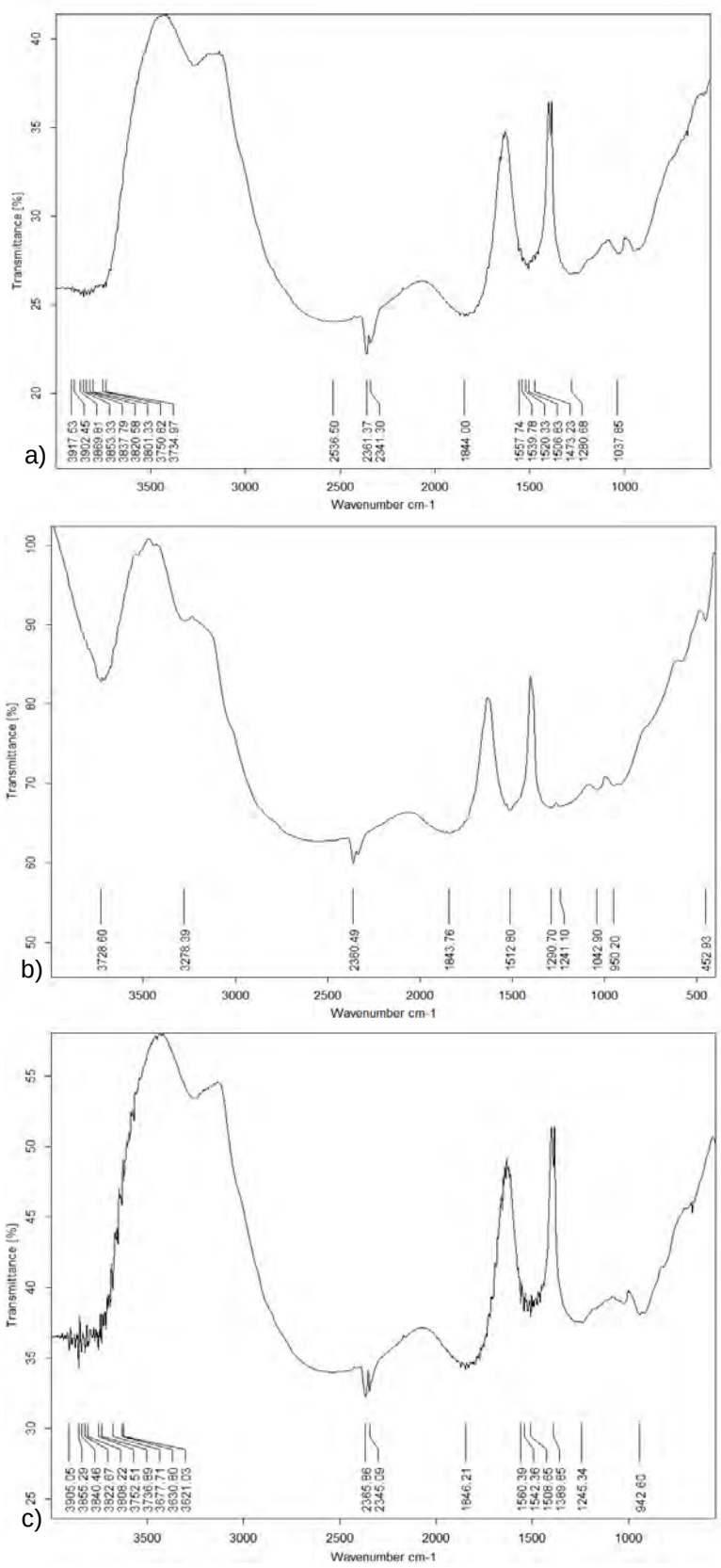

Figure 4.16. FTIR spectra for: a) unmodified AC Norit® R2030 Cabot; b) Unmodified AC Norit® RB1 AC; c) MEA (50%) modified AC Norit® R2030 Cabot

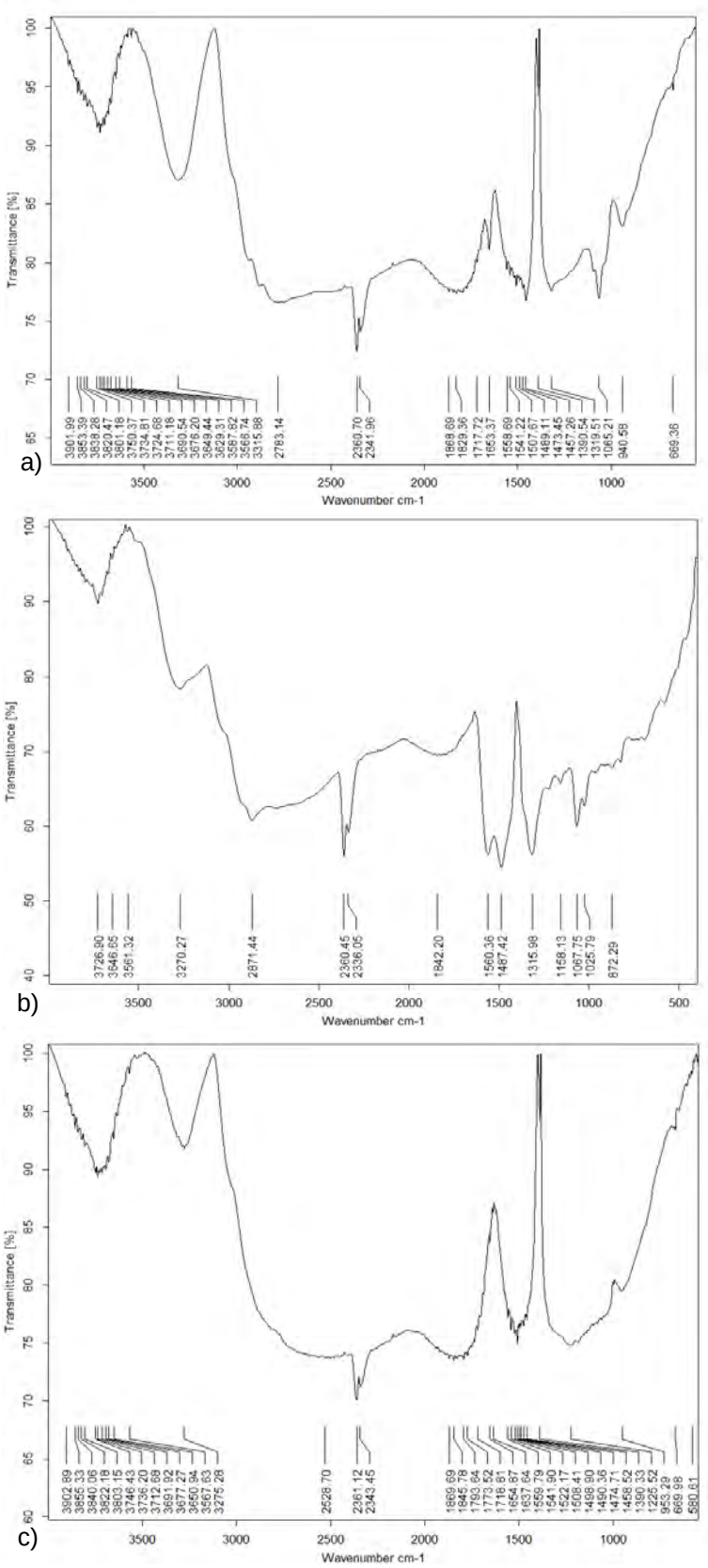

Figure 4.17. FTIR spectra for: a) DEA+AMP blend modified Norit® RB1 AC; b) MEA+AMP blend modified Norit® RB1 AC; c) MEA+MDEA+AMP blend modified Norit® RB1 AC

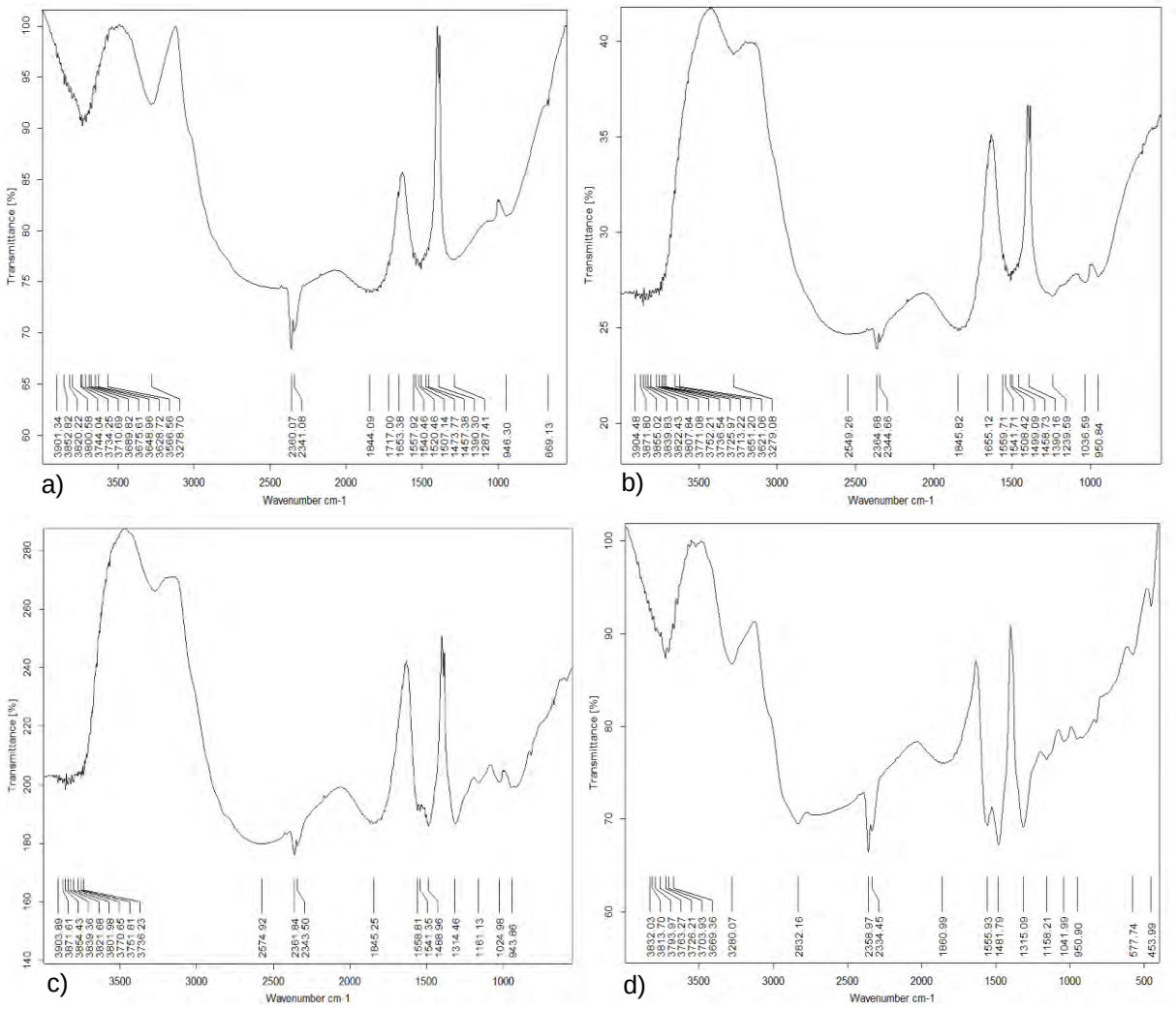

Figure 4.18. FTIR spectra for: a) TEA+AMP blend modified Norit® RB1 AC; b) TEA+MDEA+AMP blend modified Norit® RB1 AC; c) TEPA (20%) modified Norit® RB1 AC; and d) TEPA (30%) modified Norit® RB1 AC

The unmodified R2030 provided a spectrum very similar to the unmodified RB1 (Figure 4.16.b), and their structural difference was concentrated in the intensity of O-H stretching, which is more visible in the RB1 sample.

The amine modified R2030 adsorbent spectra presented in Figure 4.16.c shows an intense band in the region of 3700–3800 cm^{-1} in the spectra obtained for the amine modified and original RB1 ACs. These peaks correspond to an O–H stretching mode of hydroxyl groups, due to the

adsorption of water molecules by the adsorbent when in contact with the ambient environment (Daifullah, Girgis & Gad, 2003; Ibrahim, El-Hemaly & Abdel-Kerim, 1980; Yang & Lua, 2003; Puziy et al., 2003). Stretching bands resulting from the C=O bonds were found between 3,000–2,000 cm^{-1} for the amine treated samples (Figures 4.16, 4.17 & 4.18) (Ji et al., 2007; Biniak et al., 1997; Ishizaki & Martí, 1981; Shin et al., 1997; Yu et al., 2008). Additionally, the stretching found between 2800–2900 cm^{-1} corresponds to the C-H group (Hesas et al., 2013; Nascimento et al., 2014).

Two bands were found in a range from 2500–2000 cm^{-1}, relative to an asymmetric stretching vibration of CO_2 (Hesas et al., 2013). This occurs due to environmental CO_2 in the sample chamber, as the instrument was not purged. Relative to the amine samples, three strong bands were found at 1555.93, 1481.79 and 1315.00 cm^{-1}, which represent the N–H vibration from amine solutions after the treatment was applied, confirming the presence of amine groups on the AC surface (Wang & Guo, 2016). Additionally, the presence of amine groups on the AC surface can effectively improve the AC hydrophilia, reinforcing the motivation for amine modified ACs utilisation (Marsh & Rodríguez-Reinoso, 2006).

The weak bands presented in the spectra for all samples in the range of 700 to 400 cm^{-1} correspond to the C=C stretching. Indeed, the presence of these bands confirmed the success of the amine impregnation treatment on the AC surface and their overall structure. The impregnation success improves the adsorbent capacity, shown in PSA and HPVA studies.

4.2.6. Adsorption in HPVA studies

Adsorption isotherms represent one of the most relevant methods for describing the adsorption capacity of an adsorbent and the mechanism of the adsorption system. The primary purpose of

the isotherm is to analyse the amount of CO_2 adsorbed by the ACs at the solid interface at constant temperature over a range of applied pressures. Langmuir adsorption isotherms (Figures 4.19 and 4.20) and linearisation methodology (Figures 4.21 and 4.22) were used to process the data obtained from HPVA at ambient temperature, tested under a range of pressure (0–40 bar), and calculated by Eq. 3.2 and 3.3. Figures 4.18 and 4.19 display the experimental CO_2 adsorption isotherms for the ACs evaluated under higher pressure conditions. These data were obtained under pure CO_2 flow, and the adsorption isotherm was compared with the Langmuir isotherm model to determine the saturation capacities at a constant temperature, as shown in Table 4.5.

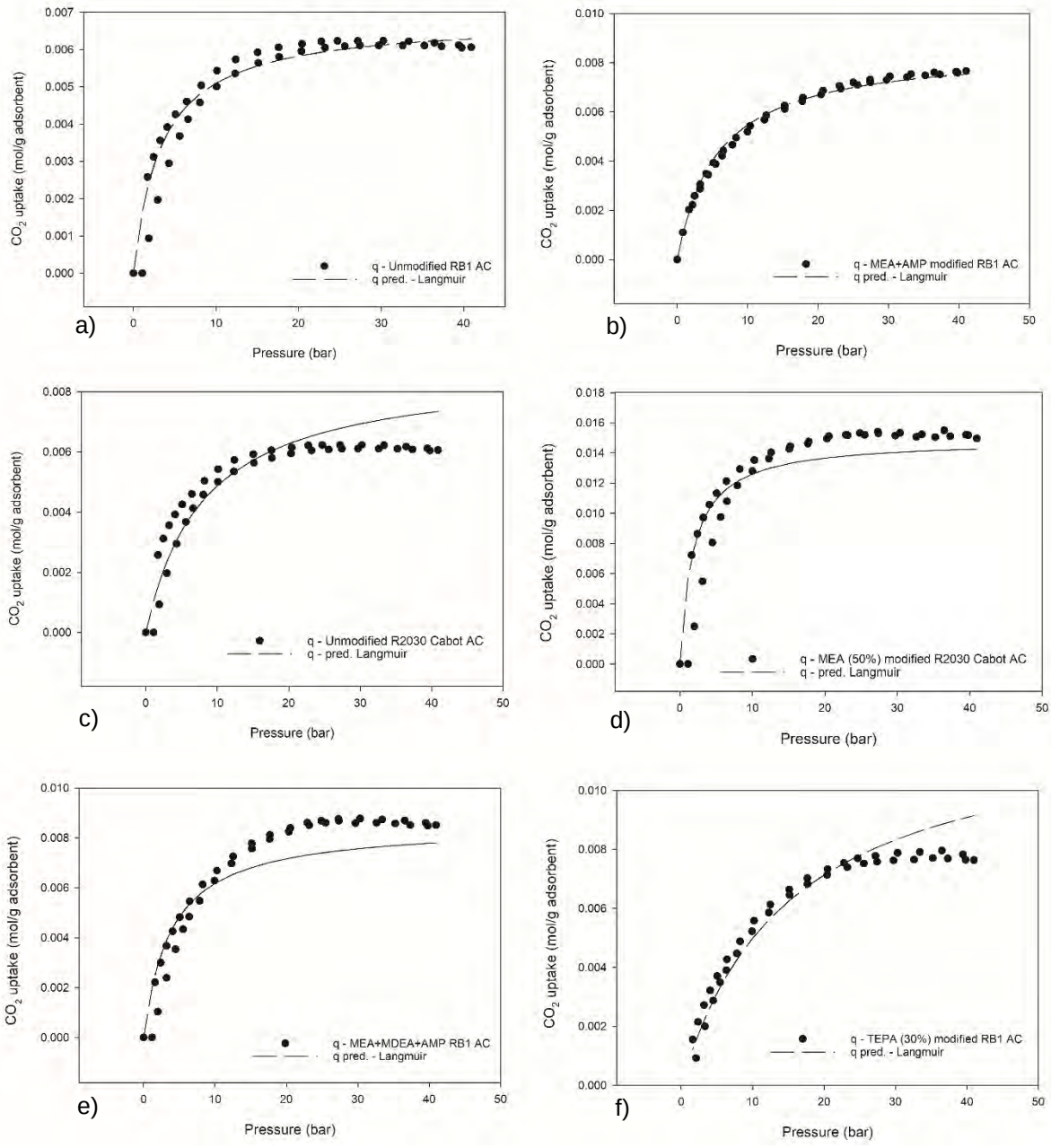

Figure 4.19. Adsorption-desorption isotherms generated by HPVA under pure CO_2 flow in a range of 0–40 bar for: a) Unmodified RB1 AC; b) MEA+AMP modified RB1 AC; c) Unmodified R2030 AC; d) MEA 50% modified RB1 AC; e) MEA+MDEA+AMP modified RB1 AC; and f) TEPA 30% modified RB1 AC

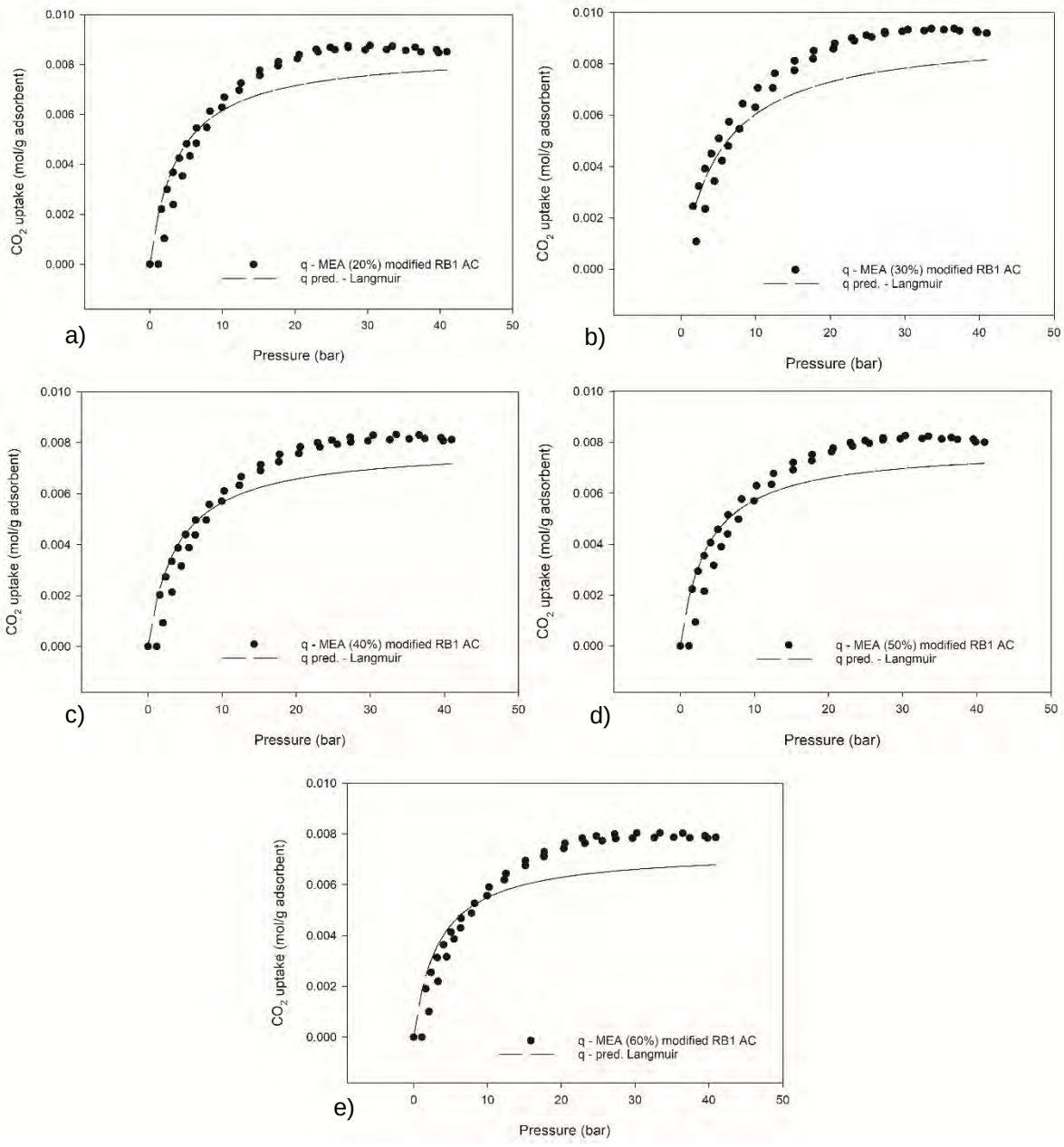

Figure 4.20. Adsorption-desorption isotherms generated via HPVA under pure CO_2 flow in a range of 0–40 bar for: a) MEA 20% modified RB1 AC; b) MEA 30% modified RB1 AC; c) MEA 40% modified RB1 AC; d) MEA 50% modified RB1 AC; and e) MEA (60%) modified RB1 AC

The linearisation method was used to fit the data to calculate the monolayer coverage of the CO_2 on the AC surface. From the slope and intercept obtained from the plot, a parameter estimation for the number of gas molecules occupying the active site of the AC was performed (Yu et al., 2008; Chiang & Juang, 2016). The fit of the linearised Langmuir model (Eq. 3.3) to the data is shown in Figures 4.20 and 4.21.

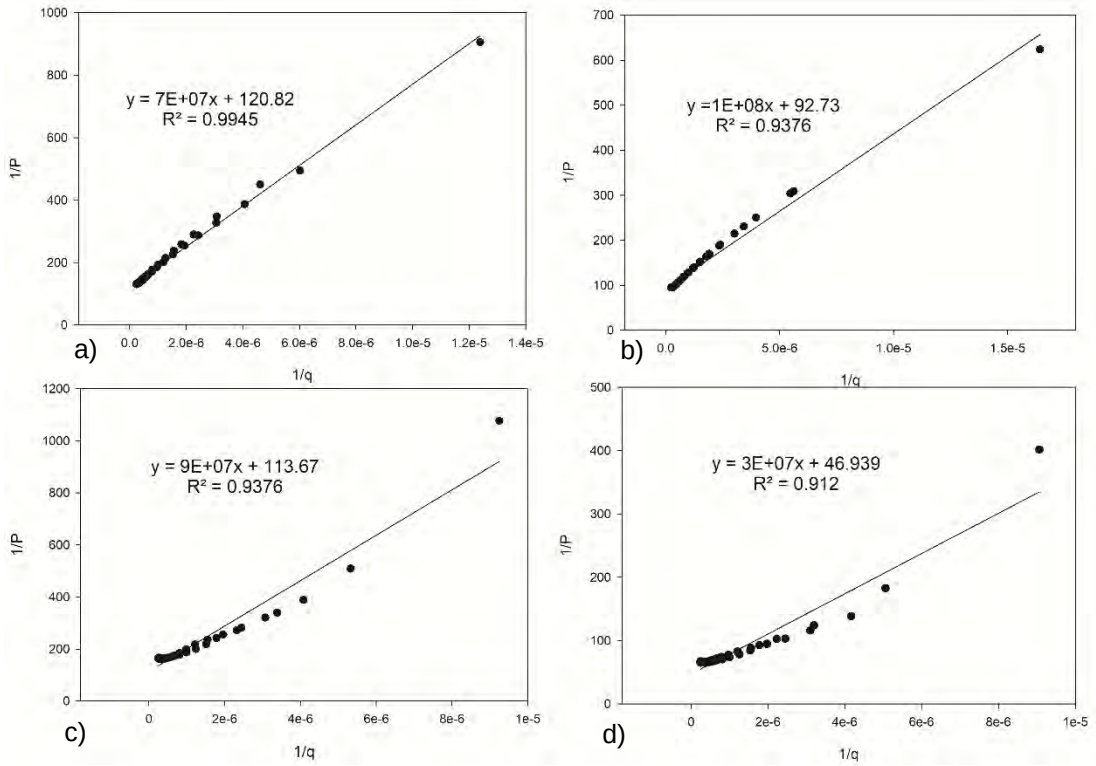

Figure 4.21. Langmuir linearisation methodology applied to the ACs: A) MEA+AMP blend modified Norit® RB1 AC; B) Unmodified AC Norit® RB1 AC; C) Unmodified AC Norit® R2030 Cabot; and D) MEA (50%) modified Norit® R2030 Cabot AC

As predicted in TGA studies, the adsorbent capacity could be improved at post-combustion owing to the temperature difference effect applied to the material structure impacting on the strengthening of the chemisorption phenomenon (Alhassan et al., 2016).

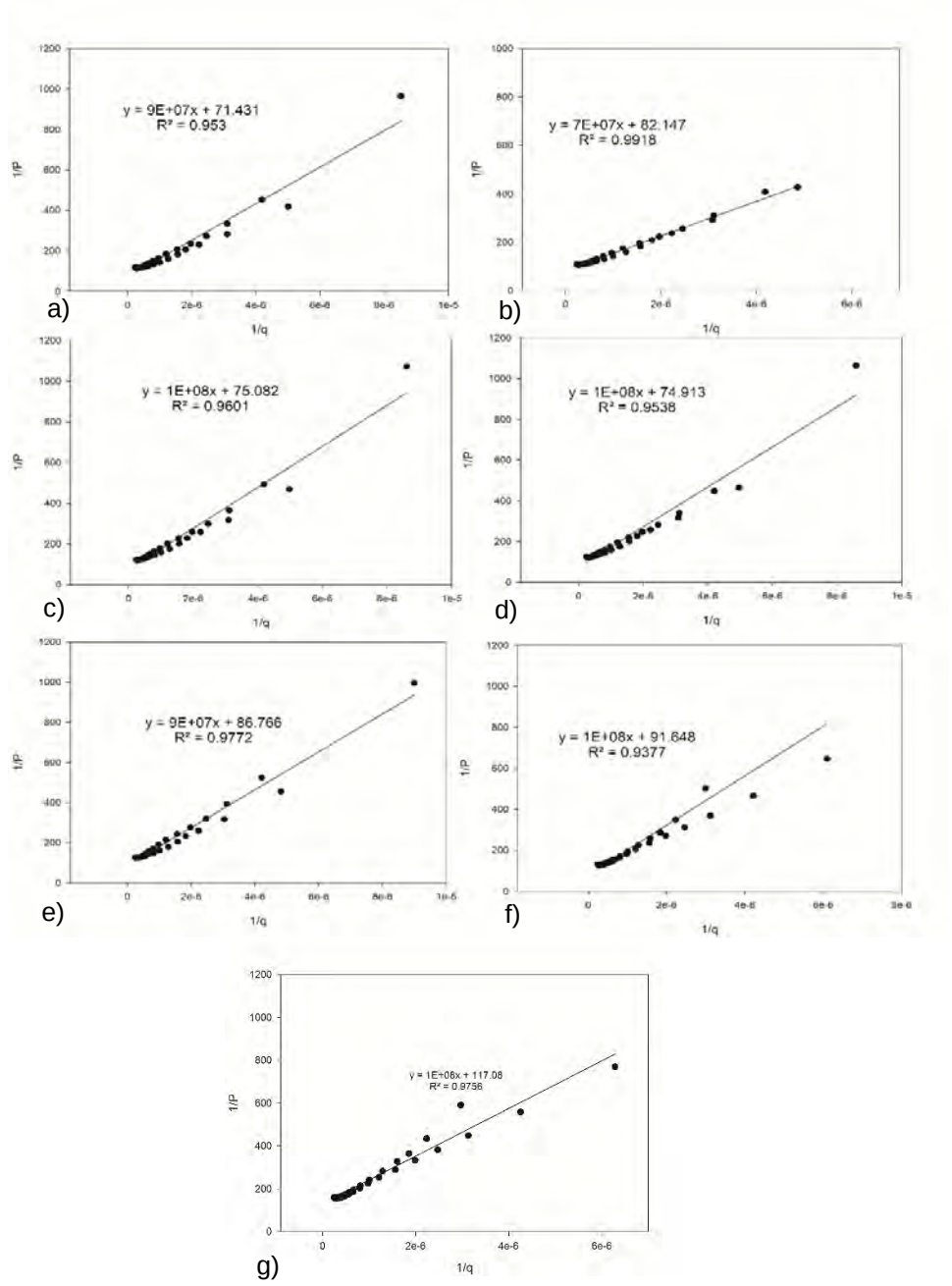

Figure 4.22. Amine ACs Langmuir linearisation: a) MEA (20%) modified Norit® RB1 AC; b) MEA (30%) modified Norit® RB1 AC; c) MEA (40%) modified Norit® RB1 AC; d) MEA (50%) modified Norit® RB1 AC; e) MEA (60%) modified Norit® RB1 AC; f) TEPA (30%) modified Norit® RB1 AC; and g) MEA+MDEA+AMP blend modified Norit® RB1 AC

The ACs maximum adsorption capacity (q_m), the equilibrium constant (k_l) and the goodness of fit of the line (R^2) extracted from the isotherm generated by linear regression method relative to CO_2 uptake experiments and under a high-pressure system were presented in Table 4.5. The slope and intercept values were extracted from Figures 4.20 and 4.21 and converted via Langmuir linearisation equation (Eq. 3.3) to obtain the q_m and k_l values. Additionally, the maximum adsorption capacity was used to estimate the AC selectivity, where the values predicted are presented in Table 4.5. As an alternative solution for the data that did not fit well in the Langmuir linearisation method (for instance, Figures 4.20.c-d and 4.21), were also fitted in the Freundlich isotherm (Eq. 16). However, this alternative did not fit better the data than via Langmuir linearisation.

Table 4.5. Adsorption capacity properties obtained from the Langmuir linearisation results calculated from HPVA experiments

Samples	q_m (mol/kg)	k_l	R^2
Unmodified Norit® R2030 Cabot AC	6.2	113.67	0.94
MEA (50%) modified Norit® R2030 Cabot AC	15.5	46.94	0.91
Unmodified AC Norit® RB1 AC	6.3	92.73	0.94
MEA (20%) modified Norit® RB1 AC	8.8	71.43	0.95
MEA (30%) modified Norit® RB1 AC	9.4	68.95	0.98
MEA (40%) modified Norit® RB1 AC	8.3	75.1	0.96
MEA (50%) modified Norit® RB1 AC	8.3	74.9	0.95
MEA (60%) modified Norit® RB1 AC	8.0	87.76	0.98
MEA+AMP blend modified Norit® RB1 AC	7.6	120.8	0.99
MEA+MDEA+AMP blend modified Norit® RB1 AC	9.2	117.1	0.98
TEPA (30%) modified Norit® RB1 AC	8.0	91.7	0.94

According to Table 4.5, the capacity of the unmodified RB1 AC was 3.4 mol/kg. In contrast, the amine modified ACs showed a superior capacity for CO_2 capture. The MEA (30%) modified RB1 AC provided a capacity (7.4 mol/kg) two times superior than the original AC. In general, the amine samples offered a range of improvements in their CO_2 capacity 1.0–4.0 mol/kg higher than the unmodified RB1 AC. The most significant reduction in the adsorption capacity was observed for the MEA on R2030 Cabot AC, which provided 2.1 mol/kg compared to 4.5 mol/kg for the original R2030 AC. This effect could be due to the blockage of the pores with amines, reducing 50% of the original adsorbent potential selectivity as predicted in BET studies relative to the adsorbent pore volume and surface area measurements. In contrast, the constant related

to the energy of adsorption (k_l) indicates that the amine modified AC improved their interaction with CO_2 by 52%. However, the modified adsorbent did not provide a good working capacity, as confirmed in BET linear isotherm plots.

According to Table 4.5, the amine modified RB1 ACs provided higher adsorption capacity compared with the unmodified RB1 adsorbent in high-pressure conditions. Among these adsorbents, for instance, MEA (30%) modified AC presented 7.4 mol/kg compared to 3.4 mol/kg relative to the unmodified AC, exhibiting an improvement >50% in the maximum adsorption capacities. Consequently, the maximum adsorption capacity was ranked by the MEA (20%) AC (7.1 mol/kg), MEA (50%) AC (6.8 mol/kg), MEA (40%) AC (6.8 mol/kg), TEPA (30%) AC (6.3 mol/kg), MEA (60%) AC (5.9 mol/kg), MEA+AMP AC (4.6 mol/kg), MEA+MDEA+AMP AC (4.4 mol/kg), ordered by the most to the least effective adsorption capacity potential. Additionally, these adsorbents exhibited lower values for the equilibrium constant, conferring weak interaction with CO_2. This problem results in the reduction in the heat of adsorption and impact in the adsorbent working capacity, generating higher operational time during the adsorption stage for these adsorbents (Samanta et al., 2012). Tables 4.6 and A.3 from the PSA studies also confirmed this behaviour, where the amines samples showed higher adsorption capacity for CO_2 in post-combustion conditions.

4.2.7. Dynamic CO_2 adsorption studies via PSA methodology using a FBR process

PSA methodology was applied using the FBR rig under post-combustion conditions at a single adsorption stage, owing to the limitation of having only one bed in the system. This problem tends to limit the duration of the adsorption time, given an early breakthrough curve corresponding to the fast adsorbent saturation. The AC saturation is faster because the

unmodified adsorbent is submitted to high adsorption temperatures, where adsorption on the surface and in the pores were activated, promoting a high kinetic rate and high affinity for CO_2 molecules. The transport of adsorbed CO_2 molecules to the AC pores and surface also decreases the bed pressure. The amine modified AC effectiveness for CO_2 adsorption was evaluated via post-combustion adsorption conditions at 70ºC and 10 bar. To test the potential and performance of the amine modified ACs, these adsorbents were submitted to three adsorption-desorption cycles in sequence.

The amine-tethered groups cover the AC surface and increase the adsorbent chemical interaction towards CO_2 molecules during the adsorption stage. The improvement occurs with the chemical bonds strengthening to attract more CO_2 molecules to the AC pores and surface, increasing the layers of CO_2 adsorbed.

In the PSA technique, the adsorption stage occurs at elevated pressure (studied over a range of –25 bar) and desorption is conducted at ambient pressure. From this process, the adsorbent can be pressurised and depressurised speedily, and be applied to different adsorption/desorption cycle times. The bed adsorption and desorption cycle times impact directly on the product purity of the flow, showing how the adsorption process behaves in a dynamic process environment.

Characterisation studies used in this work (such as BET, TGA and HPVA) offered vital support to the PSA studies, contributing to understanding the dynamic effect on the adsorbent capacity under different pressures and conditions. Moreover, this methodology presents the main advantage to be applied in power plants with no necessity to modify the combustion process. A total of fifteen modified ACs were tested under post-combustion conditions to evaluate the regenerable adsorbents utilisation towards CO_2 capture at elevated temperatures. The application of high temperatures for this condition has the potential to reduce efficiency

penalties concerning wet-absorption methods. Experiments were carried out under a binary mixture of N_2 and CO_2, in a gas concentration range from 10 to 50% (from 20 to 100 Nml.min^{-1} for CO_2 gas inlet flow) for the acidic gas for the adsorption studies. The breakthrough curve for the unmodified AC is shown in Figure 4.23.a. The overall flow rate applied was 200 Nml/min.

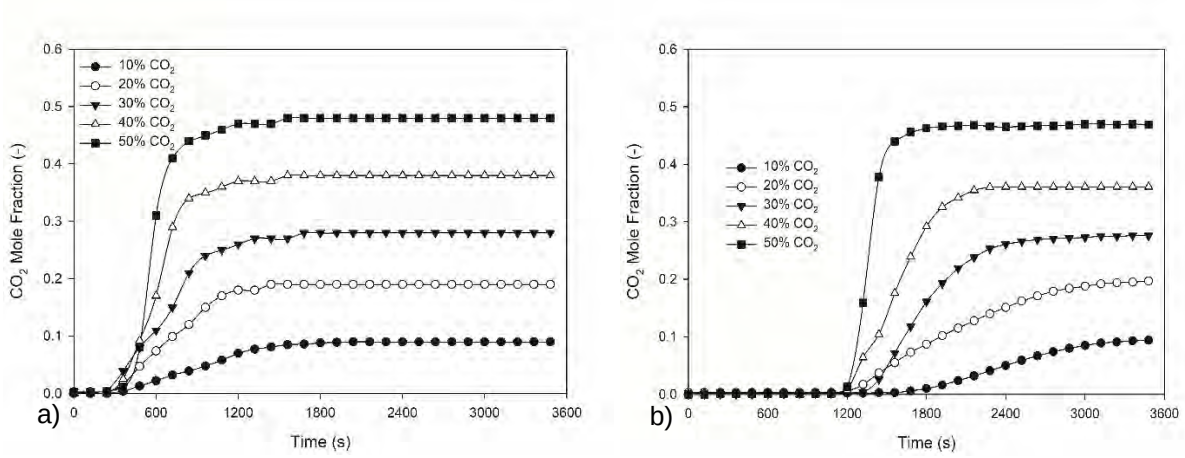

Figure 4.23. Dynamic CO_2 adsorption (in a range from 10 to 50% of the overall flowrate) for PSA experiments at 10 bar and 70ºC using: a) original RB1 AC; and b) Monoethanolamine (MEA) 20% modified RB1 AC

From Figure 4.23.a, it was possible to conclude that the unmodified RB1 adsorbent provided an unexpected early breakpoint, starting from 245 until 347 seconds under different gas inlet conditions. Additionally, the unmodified adsorbent provided faster saturation, due to the weak strength of chemisorption forces during the adsorption stage and low thermal resistance. The success of the insertion of chemical groups onto the surface and pores were reflected in seven modified samples. One of the most effective modified adsorbents was the MEA (20%) modified AC, as displayed in Figure 4.23.b. The amine groups tethered to the AC surface boosted the unmodified thermal resistance and capacity three-fold. It was confirmed by the late breakpoint

(1200–1800 seconds) as demonstrated in Figure 4.23.b, conferring high potential for this AC as a novel adsorbent for post-combustion conditions.

Relative to the seven novel modified ACs, high adsorption capacity was provided compared to the original RB1 AC, owing to the high reactivity of the amine groups at 70ºC and 10 bar, as shown in Table 4.6.

The axial dispersion cannot be ignored in a FBR experiment, because it reduces the adsorption process efficiency (Knox et al., 2016). The breakthrough curves showed a considerable difference in comparison to the unmodified adsorbent, as represented in Figure 4.23. Farooq and Ruthven, (1990a, 1990c) studied the thermal effect on adsorption studies in FBRs and explained the heat effects in adsorption, which may promote dispersion in the system. The post-combustion temperature applied to the adsorbents tested, impacted in the unmodified sample for CO_2 capture capacity, lowering its resistance to the saturation time. The solid/gas interaction improvement could be proved by the results extracted from Figures 4.24–4.26.

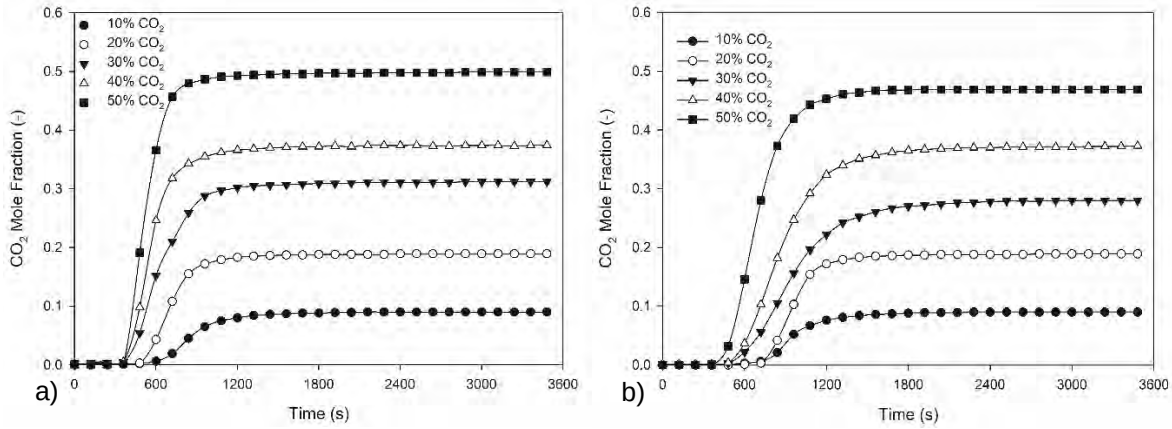

Figure 4.24. Dynamic CO_2 adsorption (in a range from 10 to 50% of the overall flow rate) for PSA experiments at 10 bar and 70ºC using: a) Unmodified R2030 AC; and b) MEA (50%) modified R2030 AC

The second original AC (R2030 AC) was tested to compare the influence of the chemical treatment. Figure 4.24 displays a breakthrough curve comparison between the original R2030 and the amine modified R2030 AC. The original R2030 adsorption capacity is provided in Figure 4.24.a, and the breakpoint was limited to the range 400–600 s for the CO_2 feed concentrations tested. The original adsorbent demonstrated a low thermal and adsorption capacity under post-combustion conditions. In contrast, the modified R2030 AC received a loading of 50% amine solution (number 10, according to Table 3.1), attaching amine groups for the creation of chemical bonds with CO_2 after amine impregnation. Consequently, the amine modified R2030 AC had slightly improved thermal resistance and adsorption capacity of CO_2 as shown in Figure 4.24.b. When the CO_2 gas composition from 0.2–0.5, the potential for acid gas adsorption was unexpectedly high (for instance, from 2.4 to 5.3 mmol/g at 0.3 CO_2 mole fraction inlet concentration for the unmodified R2030 and amine modified R2030 adsorbent, respectively) than without treatment.

The MEA modified R2030 AC tested at 0.4 CO_2 mole fraction feed concentration was 2 mmol/g, more than the unmodified AC tested under the same conditions. However, when both ACs were exposed submitted to a higher CO_2 concentration (0.5), the unmodified sample provided lower adsorption capacity compared to the 0.4 concentration. Moreover, after amine treatment, this limitation was reduced by the AC gas adsorption potential comparison (from 4.3 to 7.5 mmol/g at 0.5 CO_2 fed concentration for the unmodified and amine modified sample, respectively), confirming the strengthening of the chemisorption effect over the physisorption forces, increasing by more than 70% of its adsorption capacity in post-combustion conditions (Maroto-Valer et al., 2005).

Figure 4.25 exhibits two amine modified ACs composed of a group of seven novel modified adsorbents developed for post-combustion conditions. The TEA+AMP and TEA+MDEA+AMP demonstrated substantial improvements for CO_2 adsorption when compared to the original RB1 AC. The TEA+MDEA+AMP modified RB1 AC showed higher CO_2 capacity when compared to that without the co-amine (TEA+AMP blend). The insertion of the co-amine boosted the AC adsorption capacity by 20% compared to the unmodified, capturing more than 0.5–1.4 mmol/g CO_2 than the original AC. In contrast, TEA+AMP modified RB1 adsorbent did not provide improvements compared to the original RB1 AC, wherein a reduction of 6% was observed in CO_2 adsorption capacity, as shown in Table 4.6.

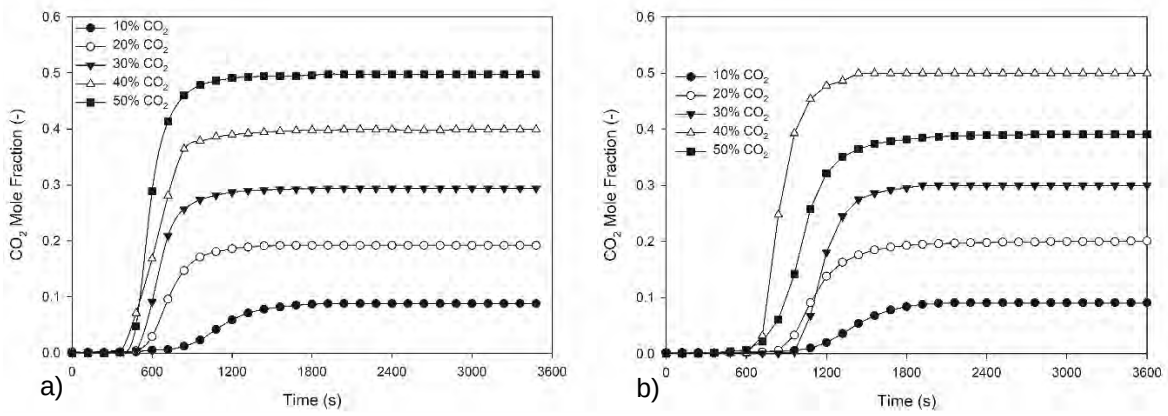

Figure 4.25. Dynamic CO_2 adsorption (in a range from 10 to 50% of the overall flowrate) for PSA experiments at 10 bar and 70°C using: a) TEA+AMP modified RB1 AC; and b) TEA+MDEA+AMP modified RB1 AC

According to Figure 4.26, the modified adsorbent with TEPA (20%) and MEA (20%) solution improved CO_2 adsorption to 9.0 and 10.5 mmol/g, followed by 7.8 mmol/g for MEA-MDEA and 5.0 mmol/g for the unmodified adsorbent (CO_2 inlet flow base comparison: 0.4).

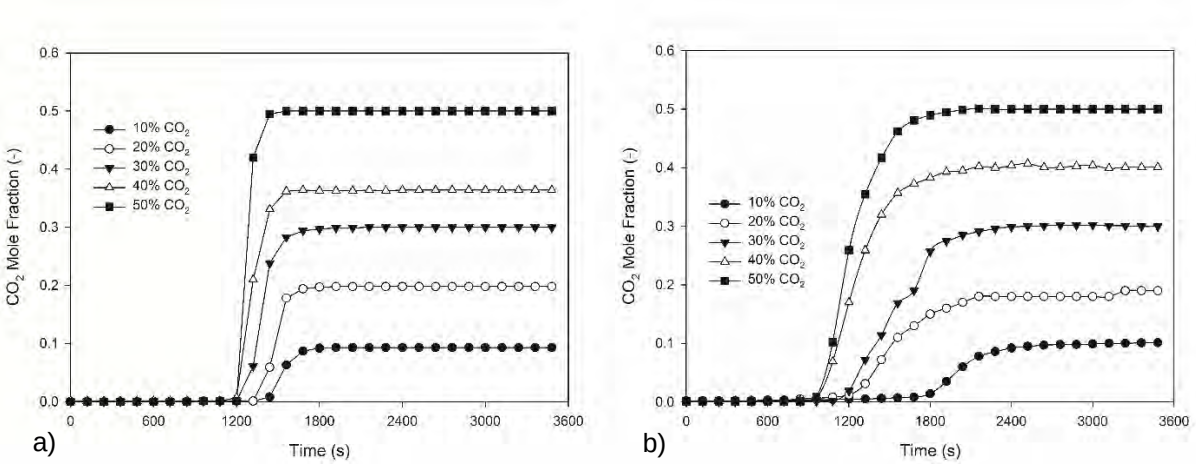

Figure 4.26. Dynamic CO_2 adsorption (in a range from 10 to 50% of the overall flow rate) for PSA experiments at 10 bar and 70ºC using: a) TEPA 20% modified RB1 AC; and b) TEPA 30% modified RB1 AC

From Table 4.1 of BET results (section 4.2.1), it was possible to observe a pore size reduction for the sample modified by TEPA solution. The adsorbent capacity can be explained by the changes in pore size, due to the pore filling after chemical impregnation. For this reason, the TEPA with 20 and 30% solvent loaded onto the AC surface boosted the adsorbent capacity three-fold when compared with the unmodified material, as shown in Figure 4.26.a-b, being highly recommended for application in post-combustion processes. Relative to the improvement promoted by TEPA impregnation, the adsorption capacity was boosted by conducting the analysis at elevated temperatures (Wang & Guo, 2016). The reactivity of the amine groups present in the porous medium increased with the adsorption occurring at 70ºC, wherein the modified adsorbent captured 4.0 mmol/g CO_2 more than the unmodified version (5.0 mmol/g) at a CO_2 feed concentration of 40% (both analysed in the same conditions). With the adsorption temperature variation, the activity for TEPA and MEA increased, due to the well-dispersed solvent molecules in the pores and cracks affecting the kinetic energy and the collision probability for CO_2 with the active sites.

The excess of amine loaded over the AC surface promoted faster adsorbent saturation during the adsorption stage, as demonstrated in Table 4.6. This is supported by the fact that two amine molecules (N molecules) captured one CO_2 molecule in the absence of water, generating a surface-bound ammonium carbamate (Chaffee et al., 2007). Furthermore, the amine modified adsorbent provides higher working capacity in post-combustion adsorption conditions, due to the formation of reactive aminosilane during gas synthesis (Hedin et al., 2013). Moreover, another limitation favours the application of amine adsorbents at post-combustion adsorption conditions, where the diffusion limitation is reduced by the access to the pores generated by the adsorbent submitted to temperatures higher than the pre-combustion conditions (Chaffee et al., 2007).

The shape of the curves shown for post-combustion studies can be explained by the influence of dispersion. The mass transfer coefficient presented a strong influence when the breakthrough curve is steeper, exhibiting a straight vertical behaviour during adsorption. For lower dispersion, the gas is more concentrated, and the solid/gas phase gradient is higher. Therefore, as reported by Knox et al. (2016), the dispersion increases the mass transfer coefficient. A parameter estimation study in breakthrough curves has been conducted by Knox et al. (2016), using the dispersion coefficient as a variable to affect the shape of the breakthrough curves, generating more details for mass transfer and dispersion information from breakthrough curves using a 1-D axial dispersed plug flow model.

The creation of mesopores on amine modified adsorbents, as reported in the PSD studies in section 4.2.2 and predicted by Chaffe et al. (2007), improved gas diffusion for the adsorbed gas molecules over the AC surface and pores. In the mentioned studies, chemical modification via amines group insertion was applied to Zeolite 13X. The modified adsorbent was tested under

two different conditions (25 and 75ºC during the adsorption stage) in a VSA CO_2 capture process from flue gas and compared with two other adsorbents, namely HMS and SBA-15 as well as the three modified forms. The insertion of nitrogen atoms onto the adsorbent surface improved the capacity for CO_2 capture. A comparison between the adsorbent pore size and amount of CO_2 uptake was established to observe the influence of the micro- and mesopores over different adsorption temperatures. The adsorbents with lower pore volumes presented higher adsorption capacity when submitted to conditions similar to post-combustion (70ºC) requirements compared to tests conducted in pre-combustion (25ºC) conditions (Zhang, Li & Lu, 2015a; Zhang et al., 2013). Since the nitrogen molecules are tethered to the adsorbent surface, they can only be accessed by diffusion of CO_2 into the pores where they are located.

Of the fifteen post-combustion AC samples, seven presented excellent adsorption capacity, for instance: (1) MEA (50%) modified AC Norit® R2030 Cabot (Figure 4.24.b); (2) MEA+MDEA+AMP blend modified Norit® RB1 AC (Figure A.2.d); (3) MEA (20%) modified Norit® RB1 AC (Figure 4.23.b); (4) MEA (30%) modified Norit® RB1 AC (Figure A.2.f); (5) TEA+MDEA+AMP blend modified Norit® RB1 AC (Figure 4.25.b); (6) TEPA (20%) modified Norit® RB1 AC (Figure 4.26.a); (7) TEPA (30%) modified Norit® RB1 AC (Figure 4.26.b). Advanced treatment improvements were observed for three AC samples ((1) MEA (40%), (2) DEA+MDEA+AMP and (3) TEA+AMP blend modified Norit® RB1 AC), due to the medium improvement presented during the adsorption stage. These results are reported in Table 4.6, containing the overall adsorbent capacity at different CO_2 compositions in post-combustion studies.

Table 4.6. Overall AC CO_2 adsorption capacity tested in a range of inlet flow

		CO_2 total inlet (-)				
		0.1	0.2	0.3	0.4	0.5
Samples	**AC number**	**Amount of CO_2 uptake (mmol/g)**				
Unmodified AC Norit® R2030 Cabot	1	1.6	2.6	2.4	5.1	4.3
MEA (50%) modified AC Norit® R2030 Cabot	2	1.7	3.2	5.3	7	7.5
Unmodified AC Norit® RB1 AC	3	1.7	2.7	4.3	5.0	6.2
MEA+MDEA+AMP blend modified Norit® RB1 AC	4	3.1	5.9	7.8	8.2	10.4
MEA (20%) modified Norit® RB1 AC	5	3.4	5.7	8.3	10.5	11.3
MEA (30%) modified Norit® RB1 AC	6	3.1	5.9	8.2	9.8	12.1
MEA (40%) modified Norit® RB1 AC	7	1.2	2.0	3.2	6.6	8.4
MEA (50%) modified Norit® RB1 AC	8	1.5	2.1	3.1	4	4.8
MEA (60%) modified Norit® RB1 AC	9	1.6	2.6	3.5	4.5	5.3
DEA+AMP blend modified Norit® RB1 AC	10	1.3	1.9	3.7	2.6	2.4
DEA+MDEA+AMP blend modified Norit® RB1 AC	11	1.9	3.0	3.4	4.6	4.2
TEA+AMP blend modified Norit® RB1 AC	12	2.0	2.6	3.4	3.9	4.7
TEA+MDEA+AMP blend modified Norit® RB1 AC	13	2.2	3.3	5.0	6.4	6.6
TEPA (20%) modified Norit® RB1 AC	14	2.3	4.1	5.7	9.0	8.7
TEPA (30%) modified Norit® RB1 AC	15	2.9	4.7	7.6	9.4	10.8

The unmodified Norit RB1 AC experiments in post-combustion conditions demonstrated higher adsorption capacity under 0.3 and 0.5 CO_2 mole fraction feed concentrations (85 and 45%, respectively) compared with the unmodified Cabot R2030 AC. However, the fast adsorbent saturation was considered as a limitation of the unmodified ACs and resolved after

impregnation. The impact of amine treatment on the AC properties is reported in Table 4.6, showing 90% more CO_2 adsorbed for the primary amine (20 and 30%) modified AC, when compared to the unmodified R2030 and RB1 adsorption capacity. The MEA+MDEA+AMP blend modified AC also provided great affinity towards CO_2 under chemisorption influence in post-combustion studies when compared with the unmodified adsorbent. The performance of this AC was higher than 45% for each gas feed composition, confirming the benefit of amine treatment when analysed at 0.5 CO_2 mole feed fraction, capturing 4 mmol/g more than the unmodified tests. The amine treatment from 0.4 to 0.6 loading did not impact the adsorption capacity as expected, and may be explained by the solvent saturation on the AC surface. This hypothesis is sustained by the amine pore blockage predicted by BET pore volume tests (Table 4.1), confirming a reduction in the gas volume adsorbed and impacting on the adsorption capacity. Additionally, the modification promoted with the secondary and tertiary amines [DEA+AMP and TEA+AMP (Figure 4.26.a), respectively] did not strengthen the chemisorption forces for CO_2 adsorption, due to their lower reactivity and interaction resulting in a reduction of 40% when exposed to acid gas high concentration. However, the tertiary amine blended with the methyldiethanolamine (TEA+MDEA+AMP, Figure 4.26.b) generated stronger chemisorption bonds and improved the lower unmodified AC interaction towards CO_2. The TEA+MDEA+AMP adsorbent confers higher adsorption capacity due to the improved reactivity provided by the combination with MDEA, as predicted in the BET studies.

The treatment using TEPA with two different loadings also promoted the strengthening of the chemisorption effect, as shown in Table 4.6. The amount of adsorbed CO_2 by TEPA (0.2 and 0.3) modified AC contributed to improving the adsorption capacity by approximately 75%, especially for experiments with high CO_2 concentrations, as a limitation presented in the unmodified experiments. The amine molecules covered the sample surface and pores,

generating active sites when submitted to heat, boosting the adsorbent capacity for CO_2 adsorption (Khalil et al., 2012; Bezerra et al., 2014; Farooq & Ruthven, 1990b, 1990a). Additionally, as observed in the TGA experiments (section 4.2.4), TEPA modified AC was better than the unmodified carbon in processes when under atmospheric pressure due to the pressure effect. This suggests that the process can promote an introduction of active sites into the porous structure of AC improving the CO_2 adsorption capacity of the adsorbent.

The amine modified adsorbents provided a higher thermal resistance capacity when compared to the unmodified RB1 and R2030 ACs in PSA studies, as evidenced by the improved CO_2 capture demonstrated by these ACs in the experiemental breakthrough curves obtained. The activated carbon capacity can be extended according to the type of chemical temperature activation conditions and the type of solvent applied. For instance, the effect of activation temperature on porous carbon material surface was tested in Zhang et al. (2018), showing material activation with other chemicals occurred at lower temperatures, the performance of carbonaceous material improved for more than a thousand adsorption cycles.

Table A.5 provides the amount of CO_2 and N_2 that left the bed during the overall adsorption in the PSA experiments, which represent the affinity and selectivity of the ACs towards the molecules inserted in the bed. The most abundant element in the outlet gas stream means low selectivity or preference to a determined molecule by the adsorbent tested. It was concluded that the amine treatment substantially reduced the AC selectivity towards N_2, due to the 40% increase in N_2 in outlet bed stream for the MEA (20%) modified RB1 AC compared to the original adsorbent. The amine samples presented similar behaviour, except TEA+AMP modified RB1 AC, which exhibited reduced selectivity for CO_2 due to the low reactivity potential. The insertion of MDEA in the TEA+AMP solution, which generates

TEA+MDEA+AMP solution, contributed to improving the AC selectivity for CO_2 molecules, as demonstrated in Table A.5. The selectivity and the adsorption capacity data justify the novelty of this work, wherein the modified adsorbents showed considerably more efficiency for CO_2 adsorption in post-combustion conditions. The issue related to the low thermal resistance presented by the unmodified AC was also solved after amine impregnation due to the late breakpoint time demonstrated by the amine modified adsorbents in post-combustion adsorption conditions.

4.3. Conclusions

Two different types of commercial AC were tested as CO_2 adsorbents in post-combustion conditions. Parameters, such as working capacity, selectivity, solid/gas interaction for CO_2/N_2 binary mixtures were also evaluated by HPVA, TGA, BET and PSA studies. The impact of the treatments applied to the adsorbents in most samples was considered satisfactory and recommended for adsorbent capacity improvements. A variety of AC samples were modified and tested for their ability to capture CO_2 in post-combustion conditions. After sample modification, it was possible to improve the performance and interaction with CO_2 during the adsorption process for both conditions studied, highlighted as novel adsorbents.

Thermogravimetric studies represent an essential stage for understanding adsorption. These studies simulated the amine modified adsorbent performance when submitted to post-combustion temperature conditions, allowing to observe their dynamic interaction and affinity for CO_2 capture. This analysis also contributed to predict the TEPA (20%) modified AC improvement for CO_2 due to the high adsorption capacity (0.9 mmol/g) in comparison to unmodified RB1 (0.7 mmol/g). PSA and HPVA experiments allowed the investigation of the

consequence of the thermal influence on the adsorbent capacity for TEPA (20% and 30%) and other amine modified ACs which compose the group that provided higher CO_2 adsorption compared to their respective unmodified conditions.

The FTIR technique contributed to the group investigation of the AC samples, also reinforcing the efficiency of the chemical impregnation of the modified adsorbents and confirming the success of the solvent attachment to the AC properties, through the presence of amine groups as shown by the amine modified ACs spectra compared to the unmodified adsorbent.

From HPVA studies, the ACs isotherms and Langmuir linearisation showed that the amine samples have a large potential for CO_2 capture. The chemical amine impregnation of the RB1 AC samples promoted an increase of 55% compared with the unmodified adsorbent adsorption capacity. The reactivity of the impregnated chemical groups on the AC dimensions were considered responsible for the improvement generated for the amine samples. The amine reactivity contributed to the strengthening of chemical for CO_2 adsorption, as also demonstrated in PSA studies. In parallel, the Freundlich linearisation method was also used as an alternative to fit the data better. However, the Langmuir linearisation method prevailed as the best fitting methodology for the AC HPVA data, due to the lower data fitting potential provided by Freundlich linearisation method. From the BET results, it can be concluded that the most effective treatment was the modification by TEPA solvent, which presented a higher performance for post-combustion adsorption conditions when compared with the unmodified material.

PSA experiments demonstrated the high potential for CO_2 adsorption provided by the amine samples. The modified ACs showed higher CO_2 adsorbed capacity in experiments conducted under a different inlet concentration (10–50%, CO_2 inlet percentage) in post-combustion

conditions. The unmodified AC provided fast saturation compared to the amine samples, wherein their adsorption capacity was three times higher than the original adsorbent.

Lastly, it was possible to conclude that the adsorption technology has a variety of advantages when compared with chemical absorption (for instance, processes based on the cost of MEA solvent utilisation/regeneration as well as tube corrosion), which uses more than 60% of the plant energy for solvent regeneration and gas compressing. However, amine modified adsorbents extended the opportunity to apply this technology for post-combustion conditions, due to the massive CO_2 adsorption capacity, elevated adsorption/desorption performance, in addition to the high thermal resistance and CO_2 selectivity over other gases in the mixture.

CHAPTER 5: CARBON DIOXIDE ADSORPTION IN PRE-COMBUSTION STUDIES

5.1. Introduction

Pre-combustion processes have been used in research studies and some industrial applications for CO_2 capture, as described in section 2.2 (Nwaoha et al., 2017). IGCC utilises fossil fuel gasification with air and/steam to produce syngas (Lee et al., 2014a, 2014b; Chen, Yong & Ghoniem, 2012; Wood, Nwaoha & Towler, 2012). It is possible to separate the CO_2 from the inlet gas and produce H_2 from the syngas for energy generation as an alternative fuel (Theo et al., 2016). Additionally, it is possible to obtain liquid products from part of the stream via gas-liquid conversion via the Fisher-Tropsch reaction, such as methanol, diesel and naphtha. The amount of CO_2 in the syngas stream depends on the chemical fuel source composition (Nwaoha et al., 2017; Wang et al., 2009; DOE/NETL, 2009, 2013). Relative to the flue gas composition, the CO_2 concentration in the inlet gas represents 15–60% of the overall CO_2/H_2 gas composition, including a typical pressure of 20–70 bar (Thambimuthu et al., 2005; Songolzadeh et al., 2014).

From pre-combustion capture, the products can be used in different applications. The first is concentrated in the production of hydrogen, which is a clean and powerful fuel entirely carbon-free. The hydrogen, obtained as the final product, is not pure with traces of CH_4, CO and CO_2 if the separation stage is not completely efficient (Thambimuthu et al., 2005; Kenarsari et al., 2013). However, a fuel with a very low level of CO_2 could provide a high impact in reducing greenhouse gas emissions. The hydrogen produced can be used as the primary fuel for boilers, heaters, fuel cells, vehicles and gas turbines (Thambimuthu et al., 2005; Nwaoha et al., 2017; Caldwell et al., 2015).

Secondly, the reduction of CO_2 emissions can also be attributed to pre-combustion processes, due to the capture of a massive amount from the fuels. The H_2 and CO_2 conversion usually

occurs in a water-gas shift reactor (Nwaoha et al., 2017), with the adsorbed CO_2 captured and transferred for storage or energy conversion (Sayari et al., 2011; Thambimuthu et al., 2005; Abanades et al., 2015). In conclusion, the pre-combustion process combined with an integrated CO_2 separation can generate the production of H_2 and mitigate CO_2 emissions (Aiken et al., 2004; Siefert & Litster, 2013; Siefert, Chang & Litster, 2014).

5.2. Results and discussion

The original and modified ACs were submitted to characterisation analyses under pre-combustion conditions via seven different characterisation techniques, as provided in the following sections. The results included contain the thermal, morphological, and CO_2 adsorption capacity studies.

5.2.1. Morphological investigation of the AC surfaces by SEM

Regarding the amine AC morphological evaluation described in section 4.2.1, the chemically modified and original ACs were also submitted to morphological analyses via SEM to investigate the impact of the chemical treatment. The sample preparation method was described in section 3.1.3. An overall view of the original, KOH (20%), and $ZnCl_2$ (20%) modified RB1 AC external surfaces are demonstrated in Figure 5.1.

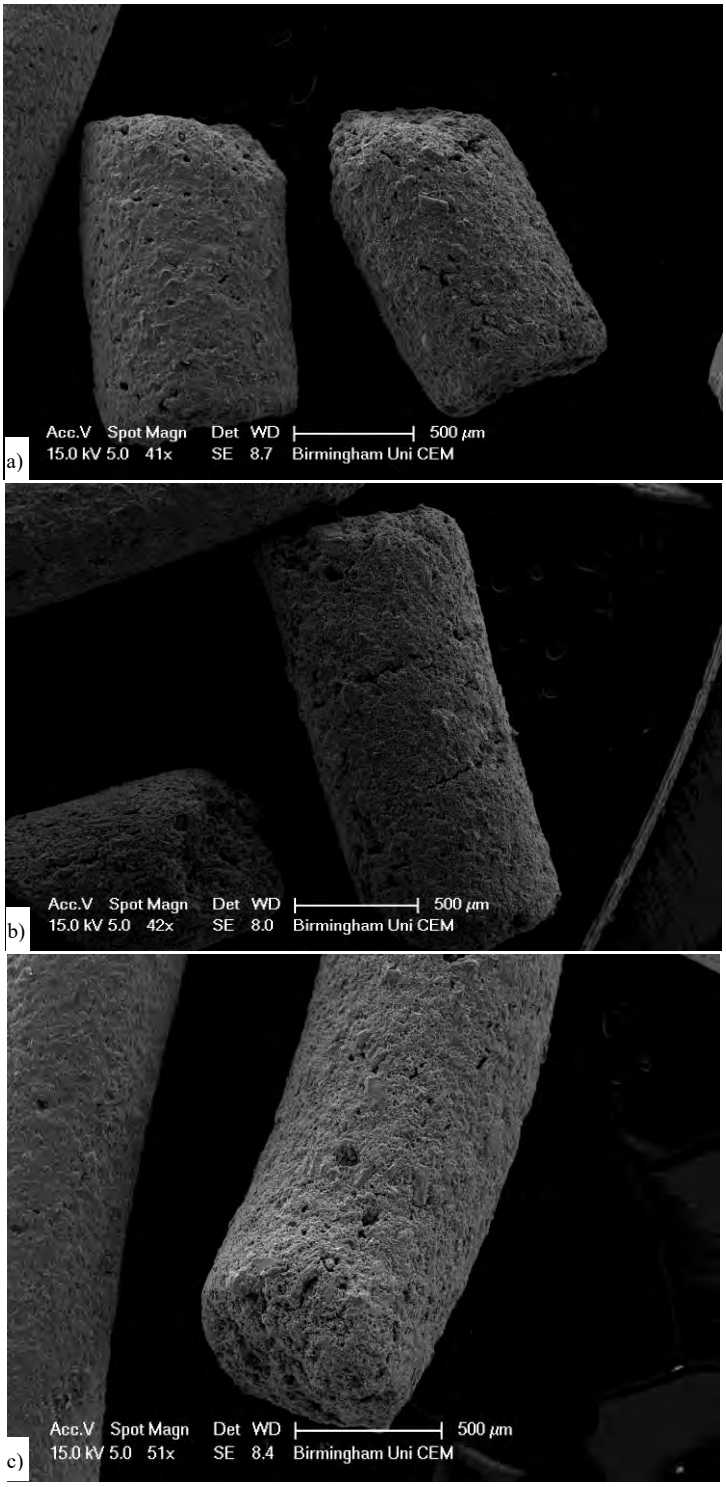

Figure 5.1. SEM images of AC samples: a) unmodified RB1 AC; b) KOH (20%) modified RB1 AC; and c) $ZnCl_2$ modified RB1 AC; scale bar = 500 µm

From Figure 5.1.a, it was possible to observe a limited number of cracks and crevices over the original AC external surface, whereas as shown in Figures 5.1.b, the KOH (20%) modified AC

suffered an expansion in the mouth of the pore and presented crevices along the external adsorbent surface. The formation of the crevices can be related to the chemical impregnation and the exposure to high temperatures (700°C) during the activation stage. In contrast, the $ZnCl_2$ (20%) modified RB1 AC exhibited a reduced number of cracks and crevices on the external adsorbent surface, even when submitted to chemical impregnation temperatures similar to the KOH (20%) modified AC. However, that was not significant in comparison with the KOH (20%) modified RB1 AC, as shown in Figures 5.1.b and c, respectively.

The modified AC also presented a smooth external area compared to the original material. Additionally, the high-temperature exposure (700°C) during chemical impregnation contributed to the pore-mouth expansion (Puziy et al., 2003; Saeidi & Lotfollahi, 2015; Bai et al., 2015; Zhao et al., 2015). The impregnation also removed a substantial quantity of volatiles in the original ACs (Shamsuddin et al., 2016).

Based on the literature, it is likely that the AC chemical activation improved the reaction between the chemical group tethered on the adsorbent surface towards CO_2 molecules, increasing the diffusion of chemical groups into the AC pores, supported by, for instance, KOH-CO_2 molecule reaction (Cansado et al., 2010). The chemically modified AC structures were intercalated with the chemical groups into the layers of graphene (Omri & Benzina, 2012). Additionally, the quantity of micropores and mesopores generated after chemical impregnation is hidden inside the ACs (Heidari et al., 2014). Figure 5.2 exhibits the H_3PO_4 modified RB1 AC in three different scales. In Figure 5.2.a, a red circle was inserted and numbered to indicate the zoomed area, as demonstrated by the number 2 in Figure 5.2.b.

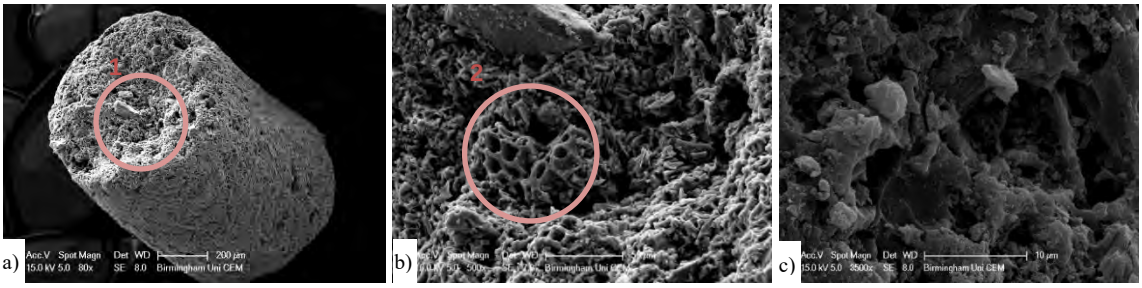

Figure 5.2. SEM photograph of two modified ACs: H_3PO_4 (20%) modified RB1 AC. a) scale: 200 µm, 80x magnification; b) 50 µm, 500x magnification; and c) KOH (20%) modified RB1 AC at10 µm, 3500x magnification

From Figure 5.2.a, which provides an overall image for the phosphoric acid modified AC, it was possible to observe that the phosphoric acid modified AC external surface exhibits a larger pore size compared to the original AC (Figure 5.1.a). The chemical impregnation with H_3PO_4 increased the roughness of the surface when compared to the unmodified AC. From Figures 5.2.a and b, it was observed that the phosphoric acid solvent impregnation generated cracks and cavities on the external surfaces. Additionally, these cavities might be produced within the evaporation of phosphoric acid during the chemical activation, followed by AC carbonisation promoting free-space previously occupied by H_3PO_4 molecules, as shown in Figure 5.3.b (Yakout & Sharaf El-Deen, 2016; Heidari et al., 2014). An additional zoomed SEM image for the KOH (20%) modified RB1 AC is shown in Figure 5.2.c. Based on similar results available in the literature, the presence of crystals of various sizes were observed on the AC surface from the analysis conducted at 10 µm and 3500x magnification, which correspond to potassium compounds. This was confirmed by EDX analysis reported in the literature for an identical material which presented similar characteristics (Sahira & Bhadra, 2014).

5.2.2. XRD application for AC physicochemical and structural analysis

The arrangement of chemical groups on the AC samples was investigated via XRD analysis. Additionally, the degree of crystallinity and the structural order in the chemically modified adsorbents was obtained according to the methodology described in section 3.1.7. A total of five samples were exposed to the X-rays, as represented in Figures 5.3–5.4.

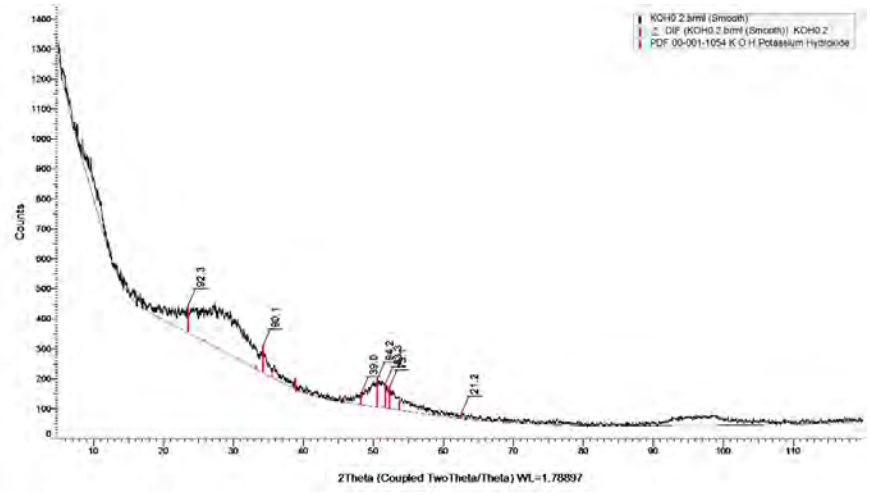

Figure 5.3. KOH (20%) modified RB1 AC XRD pattern

As reported in section 4.2.3, the AC typically presents amourphous behaviour due to their very broad diffraction peaks and absence of sharp peaks (Bamdad, Hawboldt & MacQuarrie, 2018; Omri & Benzina, 2012; Story, 2017). From Figure 5.3 of the investigation of the KOH (20%) modified RB1 AC XRD pattern, the KOH distribution was observed in two intensive peaks found at $2\theta = 30^{o}$ and $2\theta = 51^{o}$. Another factor that needs to be considered is that the chemical impregnation tends to increase the degree of crystallinity in comparison to the unmodified XRD pattern (Figure 4.9), due to the layer alignment provided by the impregnated chemical molecules (Morais, 2014; Omri & Benzina, 2012). However, the KOH (20%) pattern did not exhibit a significant difference in the spectra when compared to the other loadings, such as 60 and 70% (as shown in Figures 5.4.a and b, respectively), as proven by the intensity level

[represented by counts (y axis) in the graph] variation provided in their diffraction patterns. The KOH low loading was not enough to observe microcrystals along the modified AC XRD pattern, wherein an amorphous spectra was observed similar to the unmodified RB1 AC.

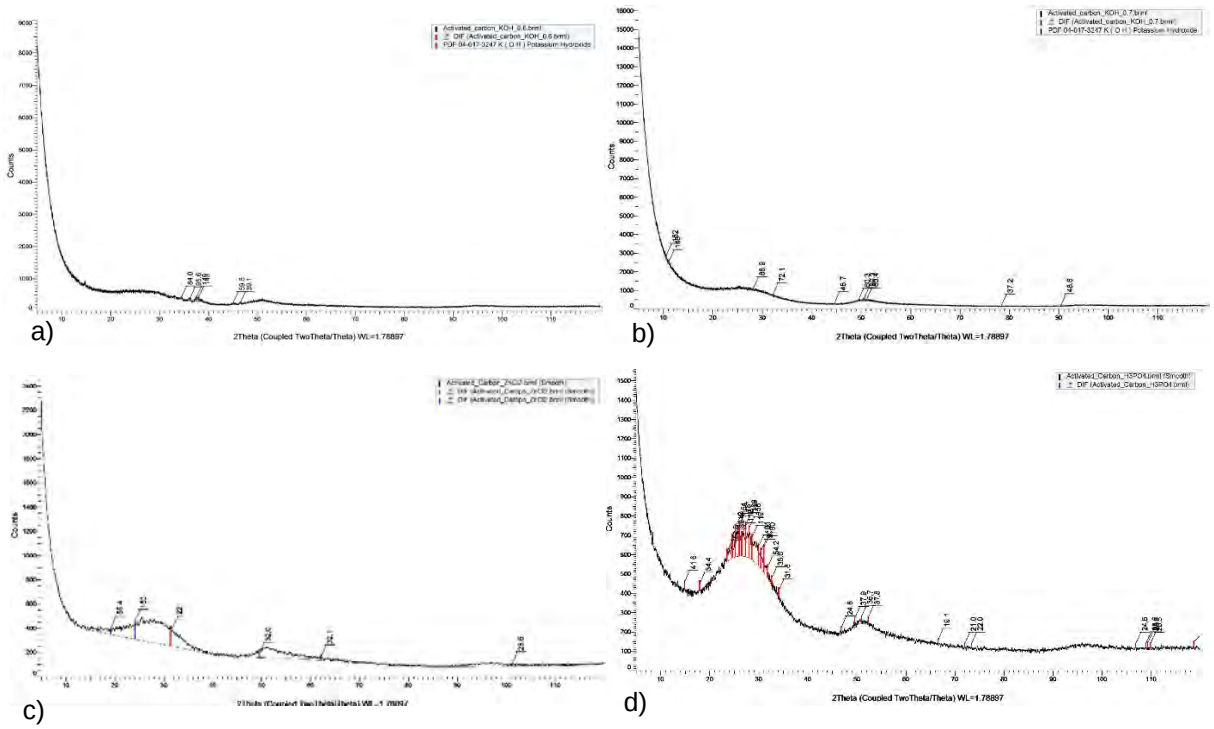

Figure 5.4. XRD pattern analysed from 5 to 120º 2θ for: a) KOH (60%) modified RB1 AC; b) KOH (70%) modified RB1 AC; c) $ZnCl_2$ (20%) modified RB1 AC; and d) H_3PO_4 (20%) modified RB1 AC

In contrast, Figure 5.4.a displays the KOH (60%) modified AC XRD pattern demonstrating an increase in the KOH molecules along the surface, as evidenced by the three peaks at 2θ = 34º, 2θ = 36º and 2θ = 38º. The chemical impregnation with higher KOH loading slightly improved the crystallinity of the AC, due to the high presence of KOH molecules along the AC structure identified by the XRD analysis. This was confirmed by the KOH (70%) modified RB1 AC diffraction pattern (Figure 5.4.b), in which the peak intensities are two times higher compared to the original RB1 diffraction pattern (Figure 4.9). In contrast to Figure 5.4.a, the higher KOH loading was broadly detected along the pattern generated, due to the better distribution of KOH

molecules along the AC surface, as demonstrated in Figure 5.4.b. Figure 5.4.c and d exhibit the $ZnCl_2$ and H_3PO_4 modified RB1 chemical diffraction patterns, respectively. From Figure 5.4.c, the modified material demonstrated the presence of the $ZnCl_2$ molecules impregnated on the AC structure. However, the amorphous behaviour of the AC was not impacted when compared to the unmodified material (Figure 4.9). By contrast, the diffraction pattern for the KOH modified RB1 AC (Figure 5.4.b) demonstrated improved crystallinity due to the intensity of peaks provided. Two broad diffraction peaks, as shown in Figure 5.4.b, proves that the chemical group reaction on the AC surface created microcrystals on the amorphous material (Shamsuddin et al., 2016).

5.2.3. Study of the influence of the adsorption temperature on ACs by TGA

Thermal adsorption studies were conducted to investigate the CO_2 capacity of the original and chemically modified ACs at ambient temperatures (25ºC). Additionally, the amine modified ACs were included in the thermal adsorption capacity tests to evaluate the potential of application in pre-combustion processes. In pre-combustion CO_2 capture processes, a gaseous mixture of CO_2 and H_2 is obtained from the combustion stage at high pressure and the gaseous separation process occurs at 25ºC, according to the methodology described in section 3.1.2. However, due to safety concerns, N_2 was used instead of H_2, due to the highly flammable potential of the latter. Additionally, the TGA did not support high pressures. For this reason, the maximum pressure for the gases inserted was limited to 0.5 bar. The CO_2 adsorption curves generated are demonstrated in Figures 5.6–5.8. The AC CO_2 uptake capacities were calculated by the conversion of the mass loss to mmol of CO_2/g of the sample per time (s), only considering the adsorption time in this calculation, as described in section 3.1.2.

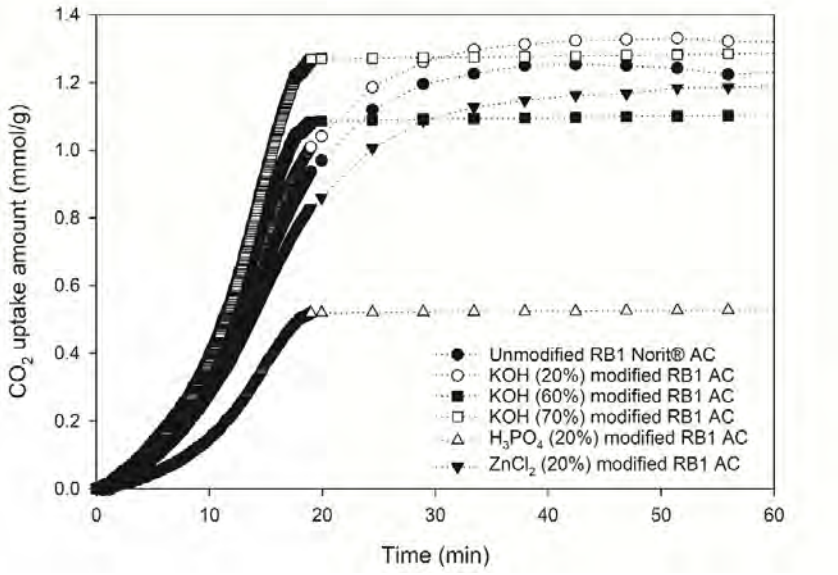

Figure 5.5. CO_2 thermo-adsorption of the chemically modified adsorbents in comparison with the original RB1 AC

From Figure 5.5, the three KOH modified ACs provided a higher potential for CO_2 adsorption compared to the original AC. The KOH ACs were a target as an advanced adsorbent, owing to their performance at pre-combustion adsorption temperatures. According to Table 5.1, the KOH (70, 60 and 20%) modified AC provided a competitive and higher CO_2 adsorption capacity (1.7, 1.4 and 1.3 mmol of CO_2/g of catalyst, respectively), when compared to the unmodified adsorbent (1.19 mmol of CO_2/ g of catalyst) in the thermal experiment, which can be explained by the action of the KOH solution over the adsorbent surface area.

The pre-treatment temperature increased the pore activity, influencing the chemical bond energy due to exposure to elevated temperatures before the adsorption stage. In contrast, the H_3PO_4 and $ZnCl_2$ modified ACs did not provide a substantial improvement in the adsorbent CO_2 capacity compared to the original AC, which can be explained by the creation of weak interactions by the solvents applied for CO_2 at low gas inlet pressures and the gross

morphological change (such as impact on adsorbent surface area and pore volume) promoted during the chemical impregnation.

The amine ACs were also tested under pre-combustion temperatures, aiming to investigate their performance at the proposed conditions. The CO_2 adsorption capacity for the amine modified ACs are demonstrated in Figures 5.6 and 5.7. From Figure 5.6, the CO_2 adsorption capacity for the original RB1 and R2030 AC is shown compared with their respective amine modifications. However, the original ACs showed higher adsorption capacity when compared to the modified versions, which may be due to the limited reactivity of the molecules at low temperatures. For higher interactions with CO_2, the amine ACs need to be investigated at temperatures above 35ºC and below 80ºC (Kongnoo et al., 2016).

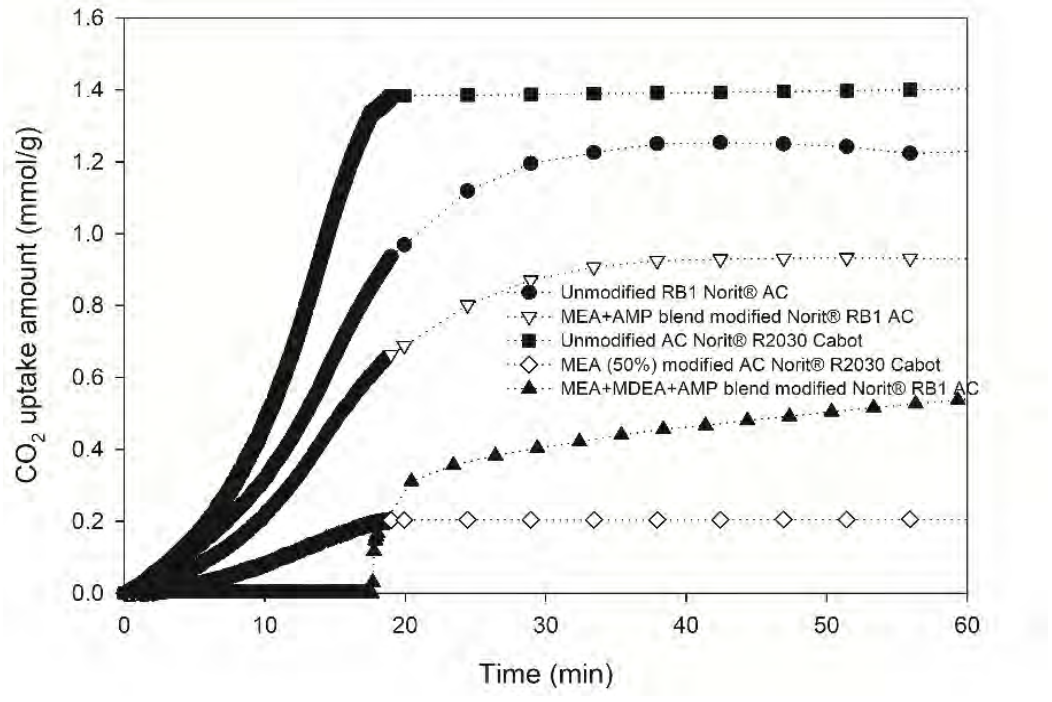

Figure 5.6. Unmodified AC (RB1 and R2030) thermo-adsorption capacities compared with their respective monoethanolamine modified versions at pre-combustion temperatures (25ºC) under pure CO_2 (50 ml.min^{-1}) flow

From Figure 5.6, it was also possible to observe the elevated CO_2 capacity offered by the original R2030 AC compared to the original RB1 AC. In parallel, the amine modified version for the R2030 AC suffered the impact of CO_2 adsorption at pre-combustion temperature (25ºC), reducing its capacity 1.4 mmol/g when compared with the original R2030 AC (1.7 mmol/g). This can be related with the amine pore blockage effect, as demonstrated in BET studies (section 4.2.2), wherein the volume of gas adsorbed by the MEA (50%) modified R2030 AC (0.07 m^2/g) was reduced by 45% compared to the original version (0.13 m^2/g). It was concluded that the modified AC was affected by the pore filling phenomenon. The absence of thermal energy for site activation to improve the amine chemical bonds with CO_2 molecules also impacted in the low performance presented by the amine modified R2030 AC, as compared to their unmodified version, as shown in Table 5.1. The AMP solvent insertion into the MEA solution boosted the CO_2 adsorption capacity of the amine modified AC, as demonstrated in the thermo-adsorption curve for MEA+AMP adsorbent in Figure 5.6. The MEA+AMP modified AC provided a higher CO_2 capacity (0.9 mmol/g) in comparison to all amine samples, including those with higher amine loading on the AC surface, for instance, MEA (60%) modified AC. In contrast, the MEA+MDEA+AMP blend did not perform as well as expected and compared to the unmodified AC, due to the high reactivity of the co-amine (MDEA).

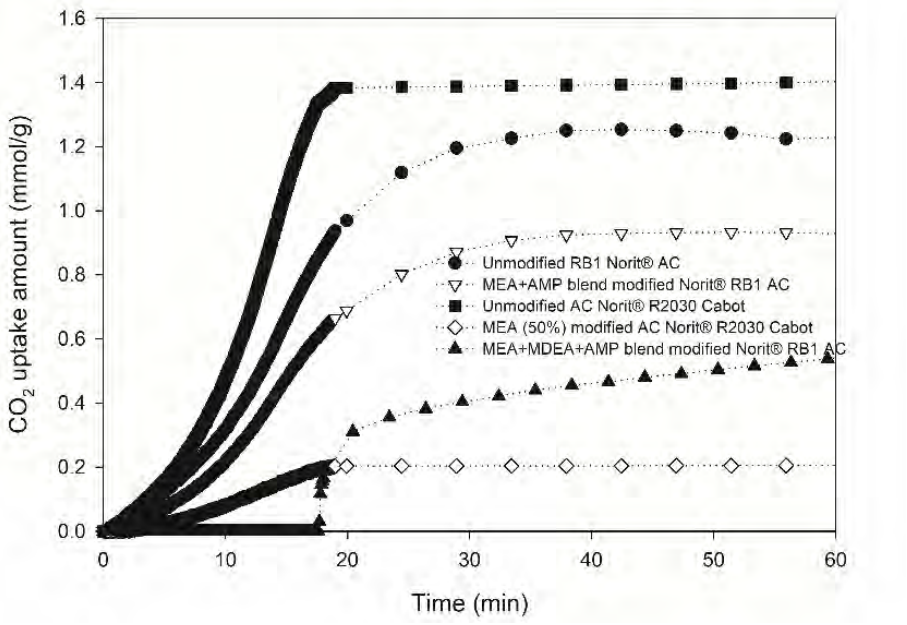

Figure 5.7. CO_2 adsorption for different amine loadings (20–60%) on the RB1 AC compared with the original adsorbent at pre-combustion temperatures (25ºC) under pure CO_2 (50 ml.min^{-1}) flow

From Figure 5.7, following similar behaviour as demonstrated in Figure 5.6, the different amine loadings applied to the modified RB1 AC did not provide a significant impact. The principal reason for this result was due to the lower pre-combustion adsorption temperature (25ºC), which considerably reduced the amine molecule reactivity, limiting their potential for adsorption of CO_2 molecules. Additionally, another limiting factor that needs to be considered is the low pressure used during the adsorption stage (0.5 bar). The pore blockage effect also was a limiting factor, as demonstrated in pore volume tests in BET studies in section 4.2.2., due to the absence of energy to activate the amine groups.

Table 5.1. Comparison of CO_2 uptake under pre-combustion temperatures for the AC samples in thermogravimetric studies at 25ºC/0.5 bar and pure CO_2 (50 ml.min^{-1}) flow

Samples	CO_2 uptake (mmol/g)
Unmodified RB1 Norit® AC	1.3
KOH (20%) modified RB1 AC	1.3
KOH (60%) modified RB1 AC	1.4
KOH (70%) modified RB1 AC	1.7
H_3PO_4 (20%) modified RB1 AC	0.7
$ZnCl_2$ (20%) modified RB1 AC	1.2
MEA+AMP blend modified Norit® RB1 AC	0.9
MEA+MDEA+AMP blend modified Norit® RB1 AC	0.6
DEA+AMP blend modified Norit® RB1 AC	No BT generation
DEA+MDEA+AMP blend modified Norit® RB1 AC	
TEA+AMP blend modified Norit® RB1 AC	
TEA+MDEA+AMP blend modified Norit® RB1 AC	
TEPA (20%) modified Norit® RB1 AC	
TEPA (30%) modified Norit® RB1 AC	
MEA (20%) modified Norit® RB1 AC	0.4
MEA (30%) modified Norit® RB1 AC	0.5
MEA (40%) modified Norit® RB1 AC	0.5
MEA (50%) modified Norit® RB1 AC	0.4
MEA (60%) modified Norit® RB1 AC	0.4
Unmodified AC Norit® R2030 Cabot	1.7
MEA (50%) modified Norit® R2030 Cabot AC	0.3

Table 5.1 shows the overall CO_2 uptake for the ACs tested. From the results presented, it was possible to observe the effect of the chemical and amine treatment on the AC surface. The KOH modified ACs demonstrated a higher potential for CO_2 adsorption, due to the increase of 0.4 mmol/g recorded with the KOH (70%) modified AC compared to the original adsorbent. This justifies the potential of KOH modified adsorbents in the application of pre-combustion adsorption for CO_2 capture. In contrast, it was observed that the RB1 and R2030 modified adsorbents with amine solutions provided a reduction in their CO_2 capacity. The modification

by MEA significantly reduced the AC CO_2 adsorption, owing to the pore blockage effect at low adsorption temperatures. The most affected adsorbent by the pore blockage effect was the MEA (50%) modified R2030 AC, due to their drastically reduced CO_2 adsorption capacity (83% less compared to the unmodified material). Activated carbon application for CO_2 capture has also been investigated by many researchers, who reported the effect of higher temperature on ACs led to increased chemisorption bonds during adsorption. As compared to the unmodified RB1 AC adsorption capacity (1.3 mmol/g at 25°C and 0.5 bar; Table 5.1), the unmodified AC beads provided an adsorption capacity in the range 2.3–3.3 mmol/g at typical pre-combustion temperatures. The higher CO_2 diffusion into the pores can be attributed to the higher pressure during the adsorption stage, as mentioned by Sun et al. (2015). The chemical treatment enhanced the AC beads adsorption capacity for CO_2.

5.2.4. Activated carbon textural property BET studies

The ACs textural properties were evaluated using the BET method. Adsorption-desorption isotherms under pure N_2 at 77 K were obtained from BET analysis conducted as described in section 3.1.6. From the BET analysis, parameters such as surface area, total micropore volume and area were determined by the adsorption-desorption isotherms. The pore area and size distribution were calculated by the DFT method, and the volume of the pores was obtained by the Horvath-Kawazoe method. As described in section 2.3.3 and 4.2.2, according to the IUPAC isotherms classification, the AC presents a type I isotherm (Sing & Williams, 2004; Gregg & Sing, 1982). Figure 5.8 shows the adsorption-desorption isotherms for the chemically modified ACs, plotted as the adsorbed volume of N_2 by the ACs versus the logarithmic pressure. From Figure 5.8, it was possible to investigate the volume of gas adsorbed and the type of hysteresis (H4, according to Figure 2.5) provided by the KOH (20 and 70%) modified ACs. The modified adsorbents provided an unexpected reduction in the amount of N_2 adsorbed compared to the

unmodified, as demonstrated in Figure 5.8.b-c and Table 5.2. The amount of adsorbed N_2 predicted for the KOH modified adsorbents was 25–45% higher than the other amine modified ACs adsorption-desorption (Figures 4.4-4.5), due to the higher solvent loading during impregnation. However, the KOH modified ACs hysteresis displayed an increase when compared to the unmodified adsorption-desorption isotherm, due to the creation of large pores in the modified ACs by the different loadings of KOH solutions, as clearly observed in Figure 5.8.c which corresponds to the KOH (70%) modified AC adsorption-desorption isotherm (Yakout & Sharaf El-Deen, 2016). The $ZnCl_2$ (20%) modified RB1 AC provided the highest hysteresis, as shown in Figure 5.8, suggesting that it was promoted by the textural changes in the $ZnCl_2$ and H_3PO_4 modified RB1 adsorbents (Lowell et al., 2006). The effect of chemicals on the AC surface are reported in Table 5.2, including the modified adsorbent surface area, individual and total pore volumes.

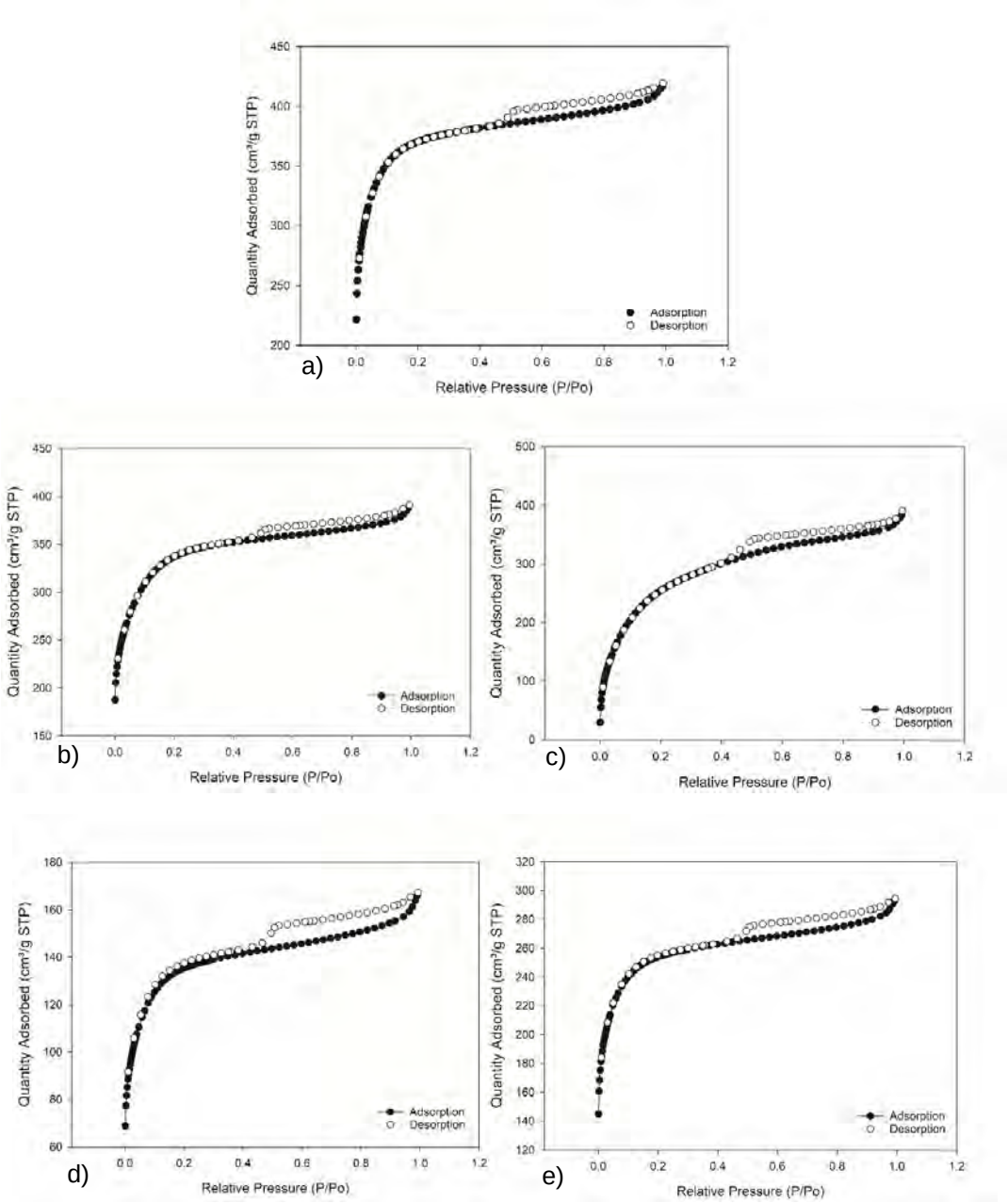

Figure 5.8. Adsorption-desorption isotherms generated at 77 K for: a) unmodified RB1 AC; b) KOH (20%) modified RB1 AC; c) KOH (70%) modified RB1 AC; d) $ZnCl_2$ (20%) modified RB1 AC; and e) H_3PO_4 (20%) modified RB1 AC

Table 5.2. Summary of the original and modified adsorbent textural properties

Samples	Surface Area (m^2/g)		DFT Pore Size (nm)		Horvath-Kawazoe	
	S_A (m^2/g)	S_{BET} (cm^3/g)	V_{total} (m^2/g)	A_{Total} (nm)	V_{Max} (cm^3/g)	W_{median} (nm)
Unmodified Norit® RB1 Cabot AC	1,378.76	1,437.31	0.58	42.45	0.65	1.05
H_3PO_4 (20%) modified Norit® RB1 AC	491.24	522.51	0.23	29.15	0.26	1.34
$ZnCl_2$ (20%) modified Norit® RB1 AC	940.27	982.99	0.41	34.03	0.46	1.07
KOH (20%) modified Norit® RB1 AC	1,207.22	1,272.81	0.55	77.60	0.61	1.12
KOH (70%) modified Norit® RB1 AC	795.34	1,027.88	0.55	215.21	0.61	2.52

The impregnation treatment (section 3.1.1) can be applied for chemical or physical AC improvements. Chemical impregnation treatment has two effects, AC carbonisation and the activation of the carbonised sample (Abechi et al., 2013b). In this work, the ACs were activated and submitted to a re-activation step, wherein the adsorbent was subjected to high temperatures to improve the attachment of chemical groups on the surface (Song et al., 2013; Hunsom & Autthanit, 2013; Muniandy et al., 2014; Abechi et al., 2013b, 2013a). The physical activation includes high temperatures (>900°C) to create the material properties (Yang, 1987); however, chemical activation occurs at lower temperatures (400–700°C), as carried out by KOH, $ZnCl_2$ and H_3PO_4 solutions (Katesa, Junpiromand & Tangsathitkulchai, 2013). The impregnation treatment includes two crucial factors for surface area modifications, the activation temperature and amount of solvent loading. If the AC is submitted to an activation temperature lower than their primary activation temperatures, the adsorbent surface area might present a high reduction in their surface area. In contrast, the treatment of the AC surface with chemical solutions, such as KOH, improved the absorbent capacity for CO_2 capture and expanded the volume of pores.

SA = Single point surface area at P/Po = 0.099458015; SBET = BET Surface Area; Vtotal = Volume in Pores (<1.857 nm); ATotal = Total Area in Pores (>= 1.857 nm); VMax = Maximum pore volume (cm3/g) at P/Po = 0.994989778; Wmedian = Median pore width (nm).

Table 5.2 shows that the application of a high KOH concentration (70%) promoted an increase of 125% AC pore size compared to the original sample. Additionally, the chemical treatment increased the degree of micro- and mesopores created after the solvent/adsorbent reaction (Hui & Zaini, 2015).

The adsorbent pore structure is considered as a fundamental concept for selective gas separation (Presser et al., 2011; Chmiola et al., 2010). The PSD characterises the structural heterogeneity of the AC samples (Yakout & Sharaf El-Deen, 2016) and can significantly influence the adsorbent kinetic and equilibrium properties, representing the most useful alternative method to characterise AC heterogeneity for industrial scale application (Ustinov & Do, 2002).

The adsorbents need to provide a substantial number of micropores with an appropriate size for CO_2 molecules to pass through and adsorb. Additionally, well-dispersed surface chemical functional groups are also required from the carbon materials to polarise the CO_2 molecules (Zhang et al., 2015a). Other factors that need to be considered are pore volume, pore size, and degree of connectivity between the different pore types (such as micropores, mesopores and macropores). The pore connectivity and tortuosity determine the diffusion coefficient of CO_2 into the adsorbent (Zhang et al., 2015a). The solid/gas interaction origin is also considered an important factor for CO_2 adsorption. Considering the weak polarisation strength of CO_2, the insertion of chemical functional groups into the AC framework increases their adsorption capacity for CO_2 (Zhang, Lin & Chen, 2015b; Qian, Hao & Li, 2013; Thote et al., 2010; Zhong et al., 2012).

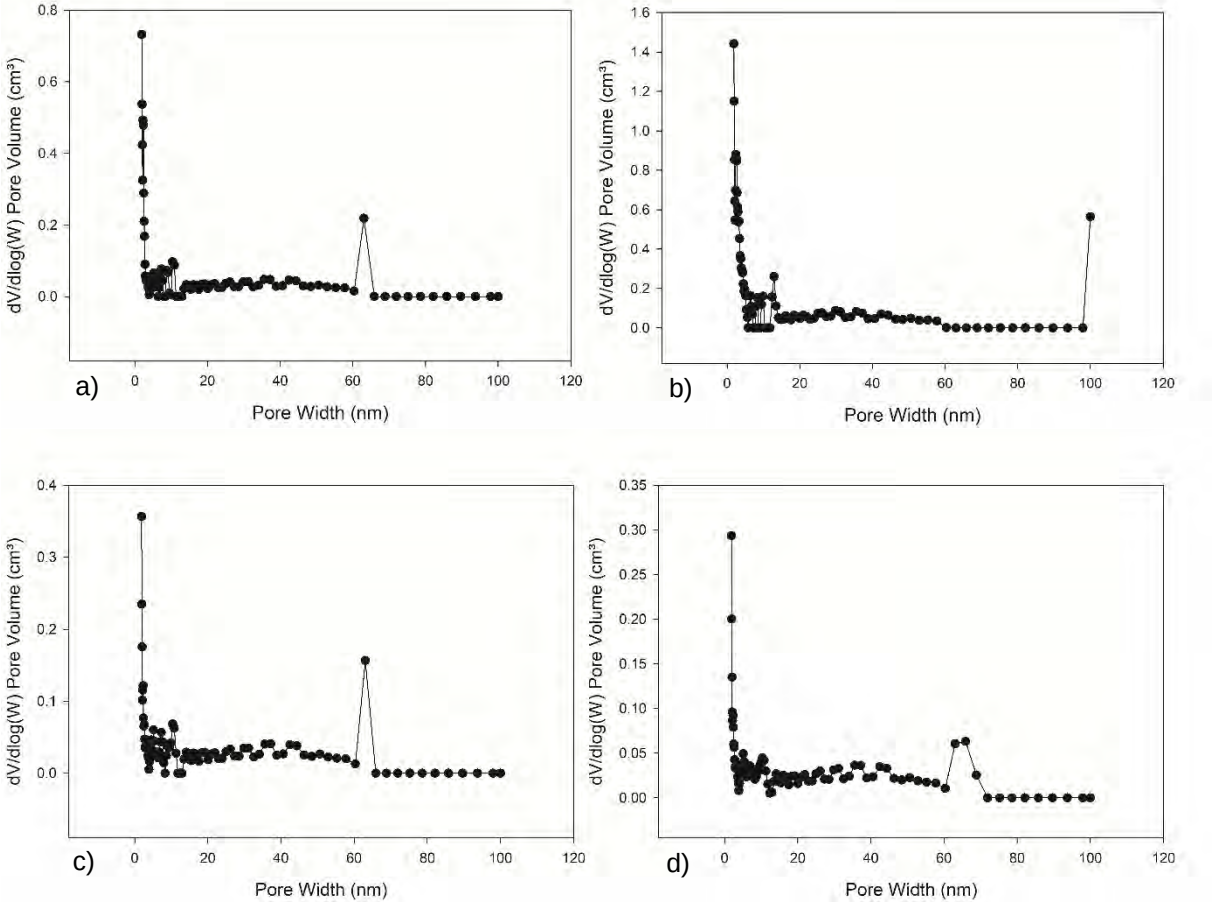

Figure 5.9. Adsorbent PSD comparison: a) KOH (20%) modified RB1 AC; b) KOH (70%) modified RB1 AC; c) $ZnCl_2$ (20%) modified RB1 AC; and d) H_3PO_4 (20%) modified RB1 AC

Figure 5.9 exhibits the PSD for the chemically modified adsorbents. Compared to the unmodified RB1 AC (Figure 4.7.a), the number of micropores was considerably higher for the KOH modified ACs, particularly for the KOH (70%) modified AC (as shown in Figure 5.9.b). In parallel, the volume of macropores (region between 60–70 nm) was better developed by the $ZnCl_2$ (20%) and H_3PO_4 (20%) modified RB1 ACs, according to Figures 5.9.c and d, respectively. It was also observed in KOH modified ACs PSD graphs, where the increase of the KOH loading during impregnation generated a higher volume of the pores. The KOH (70%) modified AC pore area provided was five times higher than the original RB1 according to Table 5.2 and attributed to the effect of thermal treatment on the modified adsorbent surface and the

high concentration of KOH solution during impregnation. The impact of the high impregnation temperatures enlarged the pore width in the micropore range, as demonstrated in Figure 5.9.b (Przepiórski, Skrodzewicz & Morawski, 2004). Liu et al. (2012) also investigated the micropore surface area and pore area improvements of carbon materials for CO_2 adsorption, reporting a micropore size in the range of 0.6–1.3 nm, and the adsorbent surface area was limited to 528–936 m^2/g. The modified adsorbents provided good performance for CO_2 capture due to the large number of micropores created (in the range of 1 nm) after chemical treatment with KOH solution. The $ZnCl_2$ and H_3PO_4 (20%) modified RB1 ACs pore size distributions are provided in Figures 5.11.c and d, respectively. It was observed that the mesopore and macropore range were better distributed by the chemical impregnation compared to the original PSD AC (Figure 4.7.a). Yakout and Sharaf El-Deen (2016) studied the effect of different loadings of H_3PO_4 (60–80%), showing that exposure to highly concentrated solutions confers a higher pore volume to the maximum concentration applied. As reported in their study, the contact with these highly concentrated solutions released the presence of tars from the cross-linked framework after treatment (Hsu & Teng, 2000). The main conclusion from these results is that the volume of pores suffered a considerable expansion when the AC was impregnated with highly concentrated solutions. This was supported by other researchers (Molina-Sabio et al., 1995) who elevated the volume of micro- and mesopores as the amount of H_3PO_4 is increased. A similar effect compared to the result reported in Table 5.2 was described by Heidari et al., (2014), where the surface area of the $ZnCl_2$ modified AC decreased after treatment with a highly concentrated solution. However, it increased the occurrence of mesoporosity in the modified AC. In conclusion, the AC origin, the type of solvent and the activation conditions applied strongly influence the adsorbent porosity (Timur et al., 2010). As observed in the RB1 chemically modified adsorbents in this work, chemical activation with KOH tends to generate

large mesopores, while $ZnCl_2$ activation increases the microporosity and low mesopore occurrence (El-Hendawy et al., 2008).

5.2.5. HPVA adsorption studies .

Experimental tests for CO_2 adsorption capacity on two chemically modified ACs were carried out, investigating the amount of gas adsorbed when exposed to high-pressure inlet streams in pre-combustion conditions. Figure 5.10 shows the CO_2 uptake for the KOH (20 and 70%, respectively) modified RB1 ACs. As shown in Figure 5.10.a, the KOH (20%) modified AC demonstrated higher capacity for CO_2 capture when compared to their unmodified version (Figure 4.20.a).

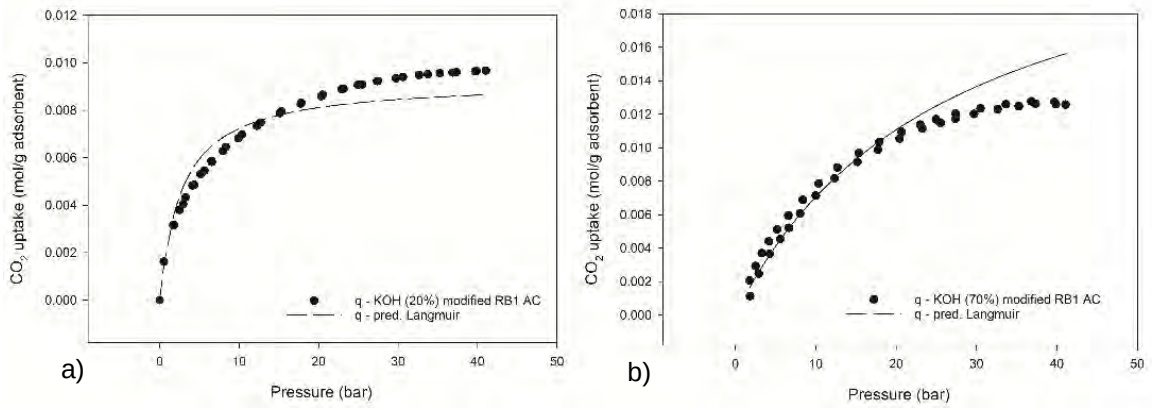

Figure 5.10. Adsorbent capacity prediction for: a) KOH (20%) modified RB1 AC; and b) KOH (70%) modified RB1 AC

The KOH (20%) modified AC provided an increase in the adsorption capacity of 75% in flowing pure CO_2, based on the original AC performance. In parallel, Figure 5.10.b exhibits the CO_2 uptake for the KOH (70%) modified AC. The use of the KOH (70%) solution on the AC surface more than doubled (105%) the modified AC capacity for CO_2 capture when compared to the original adsorbent. Consequently, it was assumed that the large amount of hydroxyl

groups on the AC surface were responsible for the enhanced adsorption of CO_2. The hydroxyl molecules were also responsible for the AC mesopore structure development, as demonstrated in Figure 5.9.a and b (Zhang et al., 2015a). The linear isotherms plots are a useful tool for best fitting the adsorption data (Kumar, 2006; Boulinguiez, Le Cloirec and Wolbert, 2008). To define the amount of gas adsorbed during the HPVA studies, the Langmuir linearisation method applied is demonstrated in Figure 5.11.

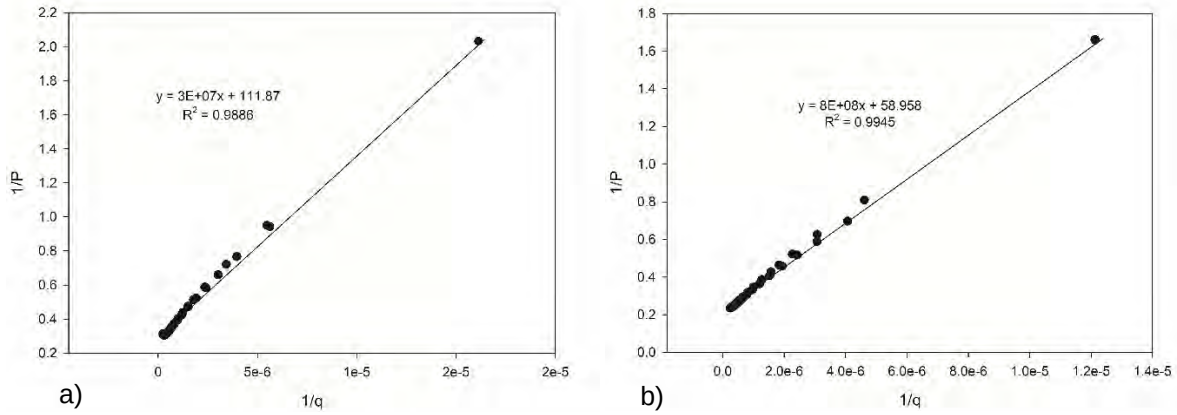

Figure 5.11. Langmuir linearisation for: a) KOH (20%) modified RB1 AC; and b) KOH (70%) modified RB1 AC

The adsorption efficiency depends on a number of factors including AC CO_2 adsorption capacity, mechanical strength, adsorption rate, the limits of adsorption cycles and the possibility of AC reuse (Adelodun et al., 2016). However, among the details previously provided, the most important parameter is the AC adsorption capacity (Brdar et al., 2012). The parameters obtained from the experimental HPVA tests are presented in Table 5.3.

Table 5.3. Langmuir linearisation results for the original and chemically modified adsorbents

Samples	*Temperature (°C)*	q_m (mol/kg)	k_l	R^2	*References*
Unmodified AC Norit® RB1 AC	25	6.3	92.73	0.94	
KOH (20%) modified Norit® RB1 AC		9.7	111.87	0.99	
KOH (70%) modified Norit® RB1 AC		12.8	58.96	0.99	

The maximum adsorption capacity and the equilibrium constant were obtained by conversion of the slope and intercept provided in Figure 5.11, according to the methodology described in section 3.1.5. As supported by TGA studies (section 5.2.3) and Table 5.3, the most reactive ACs provided an adsorption capacity two times higher than the original adsorbent, as predicted by Langmuir linearisation. The KOH (70%) modified AC captured 2.7 mol/kg CO_2 more than the original adsorbent, due to the reactivity of impregnated hydroxyl groups on the AC surface and their potential for attracting CO_2 molecules. The lower KOH loading also enhanced the adsorbent capacity, as shown in Table 5.3, however, the equilibrium constant (k_l) and the goodness of fit of the line (R^2) demonstrated that the chemical modification reduced the adsorption equilibrium. Therefore, it was concluded that even though the adsorbent presents higher capacities, the adsorption equilibrium can be easily affected due to the low energy of the chemical bonds. The Freundlich linearisation methodology applied was demonstrated in Figure A.2.f-g. The KOH modified ACs did not fit better via the Freundlich linearisation method, due to the adsorption equilibrium provided compared to the Langmuir linearisation methodology, as demonstrated in full in Appendix A (Zhang, Xie & Ho, 2009). Heidari et al.,(2014) reported the three experimental adsorption-desorption tests for the KOH modified samples (impregnation ratio of 3.5 g/g) conducted under different adsorption temperatures (30, 40 and 75ºC, respectively) under a high-pressure system. The temperature variance in the adsorption experiments considerably reduced (30%) the adsorbent capacity for CO_2. The adsorption equilibrium also was affected by the temperature, providing lower equilibrium at high adsorption temperatures. Compared to the adsorbents developed in this work, this justifies the restriction of the application of chemically modified ACs at higher temperatures than pre-

combustion CO_2 adsorption systems. The KOH modified adsorbent presents lower capacity due to its low thermal resistance at post-combustion conditions.

5.2.6. Investigation of the chemical composition by FTIR

Investigations of the AC chemical structures and their respective functional groups were conducted by FTIR. The chemically modified ACs were analysed, and similar spectra were found to these adsorbents. As reported by Yakout and Sharaf El-Deen (2016), the activated carbon matrix is not only composed of carbon atoms, also containing hydrogen, nitrogen, oxygen, halogen and phosphorous atoms. The type of AC chemical composition is closely related to the adsorbent origin. Figure 5.12 presents the spectra relative to the chemically modified RB1 ACs, generated in a range from 4000 to 400 cm^{-1}.

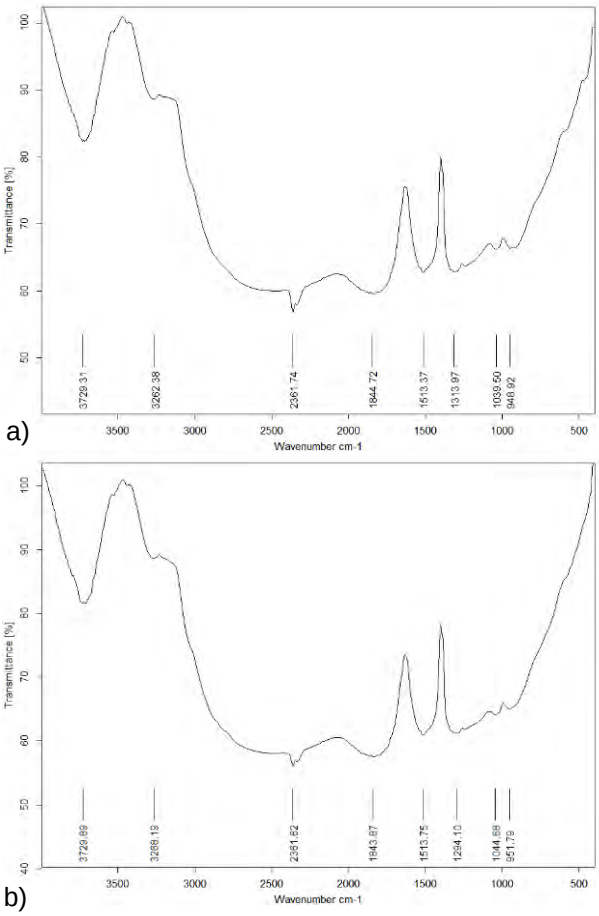

Figure 5.12. FTIR spectra for: a) H_3PO_4 (20%) modified RB1 AC; and b) KOH (20%) modified RB1 AC

In Figure 5.12, it was observed that three different scans generated similar spectra and two exhibited a strong peak at 3729 cm^{-1}, which is attributed to the O-H stretching mode, assigned with hydroxyl groups or adsorbed water molecules (Nascimento et al., 2014). These peaks demonstrate the presence of strong hydrogen bonds, originating from the carbon matrix and the chemical solutions used in the impregnation treatment (Solum et al., 1995).

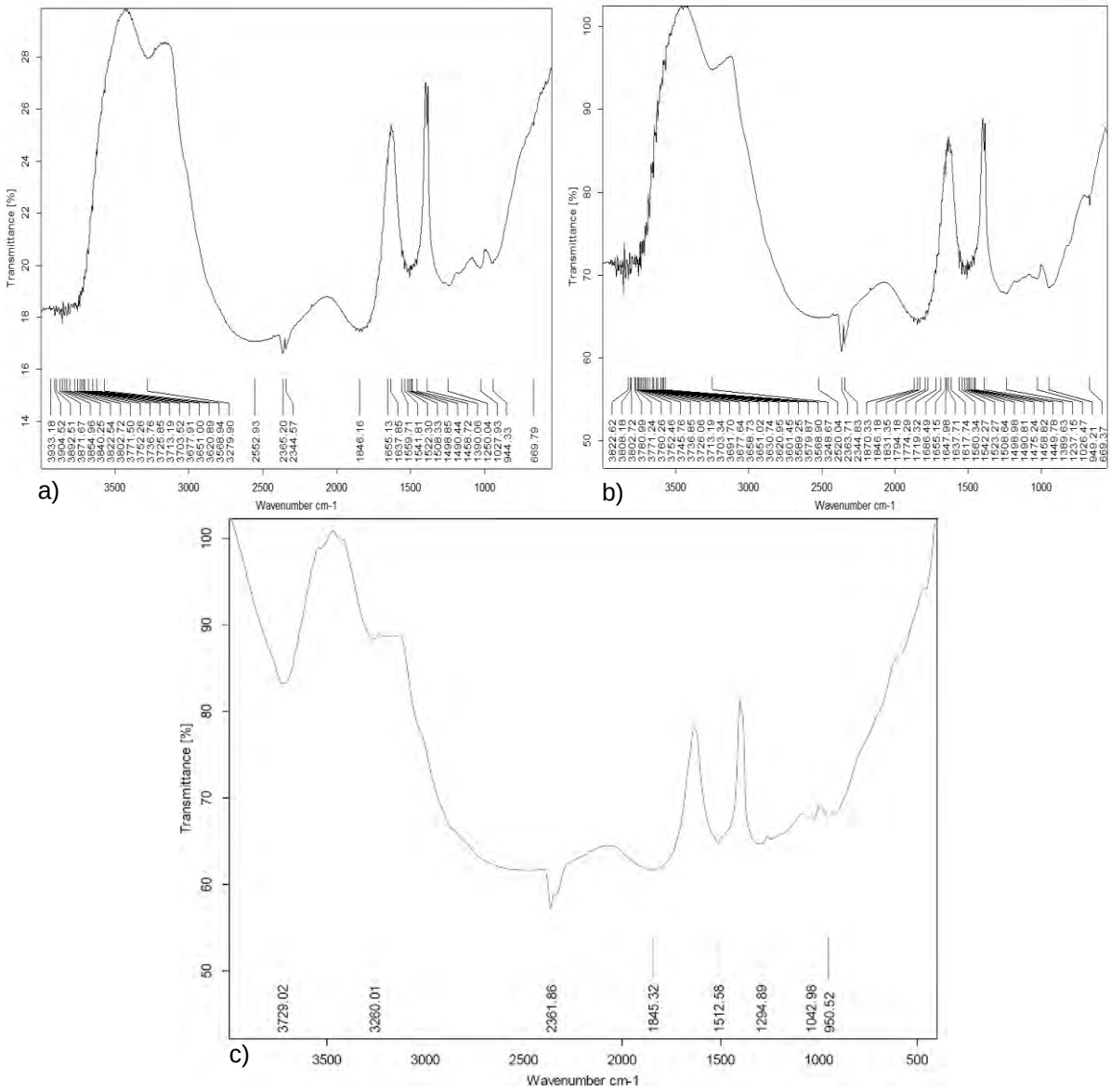

Figure 5.13. FTIR spectra for: a) KOH (60%) modified RB1 AC; b) KOH (70%) modified RB1 AC; and, c) $ZnCl_2$ (20%) modified RB1 AC

As demonstrated in Figures 5.13.a and b, it could be observed that the increase in the KOH loading on the AC for impregnation conferred higher intensity to the O-H (among the region of 4000–3200 cm^{-1}) and C-H (1500 cm^{-1}) bonds. The increase in the intensity can be attributed to two different factors, the first is related to the amount of the solvent loading on the AC surface, which increases the reactive group molecules present for highly concentrated solutions. Secondly, the chemical impregnation temperature influences the formation of new structures on the AC surface, due to the reaction promoted by the chemical solution application. For instance, the peaks in the region of 1800 cm^{-1} represent the C=C stretching of the aromatic rings (Chen et al., 2011), which can be formed during impregnation at high temperatures (700ºC), due to the C-H bonds decomposition to generate a more stable aromatic C=C bond (Muniandy et al., 2014). The C=O and C-O stretching in the region of 1400–1600 cm^{-1} can be attributed to carboxyl-carbonate structures (Ji et al., 2007) or vibration of O-H of the carboxylic group (Gao et al., 2013). Lastly, the C-H bonds found between 1000-500 cm^{-1} correspond to the AC matrix (Lendzion-Bieluń et al., 2018). From Figure 5.12, it was concluded that the chemical impregnation treatment applied on the Norit® RB1 AC surface was satisfactorily completed, due to the insertion of the chemically reactive groups proven by the IR spectra.

5.2.7. Dynamic CO_2 adsorption studies via PSA methodology using a FBR process

Dynamic CO_2 adsorption was carried out in a FBR (stainless steel; mass: 552.14 g; diameter: 2.5 cm; length: 6.9 cm; height: 2 cm) via PSA under a binary gas mixture. The system was fed with N_2 and CO_2 (20, 40, 60, 80 and 100 $Nml.min^{-1}$; 10-50% volume) streams given by different fractions at an overall flowrate of 200 $Nml.min^{-1}$. The data generated were evaluated by dynamic adsorption equations following the description given in section 4.2.8. The breakthrough curves generated from the experimental studies are reported in Figures 5.14–5.18.

The results were classified according to the two different impregnation groups, such as amine (solutions 4–11) and chemically (KOH, $ZnCl_2$ and H_3PO_4) modified ACs, as described in section 3.1.1

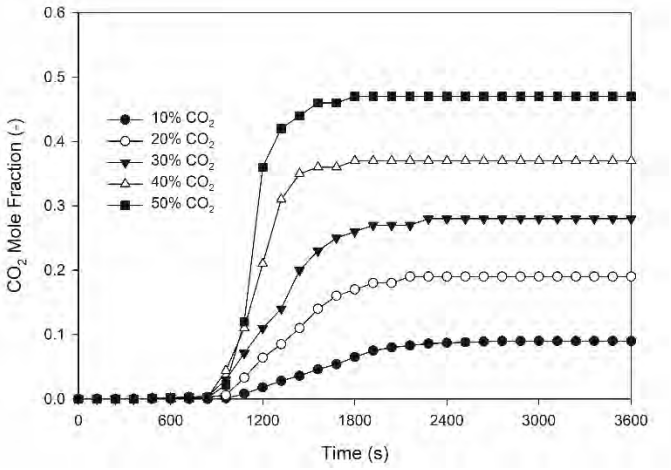

Figure 5.14. Unmodified RB1 AC breakthrough curve obtained at different CO_2 fractions using a CO_2/N_2 binary mixture (200 $Nml.min^{-1}$) in pre-combustion conditions (25°C and 25 bar)

Figure 5.14 shows the adsorption capacity for the unmodified RB1 AC in pre-combustion conditions. The original RB1 AC breakthrough time was in the range 850 to 1100 seconds under the different CO_2 compositions. The original AC presented high mass transfer until the maximum saturation stage was reached for 40 and 50% CO_2 concentrations. In contrast, the dispersion effect was noted under low CO_2 concentration, as observed in the breakthrough curves generated for the 10–30% CO_2/N_2 binary gas mixture. Relative to the modified adsorbent adsorption capacities, the KOH modified ACs demonstrated a higher adsorption capacity compared to 90% of the amine modified ACs, as demonstrated in section 5.2.3. This was justified by their higher affinity for CO_2 molecules at low pressure (0.5 bar) and pre-combustion adsorption temperature (25°C). The absence of an ideal pre-combustion condition system (for instance, at 25 bar and 25°C) reduced the capacity to demonstrate and exploit the amine modified adsorbents potential for CO_2 adsorption. In contrast, a different scenario was observed

for the amine modified adsorbents in PSA studies. Figure 5.15 displays the breakthrough curves for MEA+MDEA+AMP and MEA (20%) modified RB1 ACs.

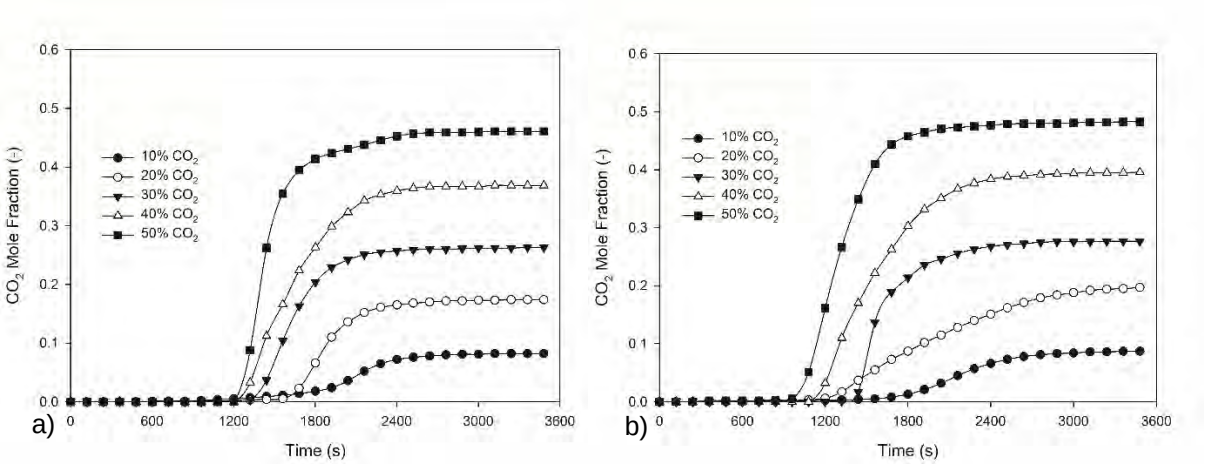

Figure 5.15. Dynamic CO2 adsorption using a CO_2/N_2 binary mixture (200 Nml.min^{-1}) in pre-combustion conditions (25ºC and 25 bar) for: a) MEA+MDEA+AMP modified RB1 AC; b) MEA (20%) modified RB1 AC

The MEA+MDEA+AMP modified RB1 AC was the most effective adsorbent among the amine modified ACs applied at pre-combustion conditions, due to their high adsorption capacity and affinity towards CO_2 molecules in the high-pressure environment. As demonstrated in Figure 5.15.a, the most effective amine impregnated adsorbent provided a much later breakpoint (1200–1800 s) compared to the unmodified AC (Figure 5.14). The MEA+MDEA+AMP modified AC overall adsorption capacity demonstrated an improvement of 35% for the amount of CO_2 captured, as reported in Table 5.4.

Table 5.4. Amount of CO_2 captured in pre-combustion PSA experiments, including different CO_2 inlet concentrations

		CO_2 total inlet (%)				
		10	20	30	40	50
Samples	**AC number**	**CO_2 adsorbed (mmol/g)**				
Unmodified AC Norit® R2030 Cabot	1	3.6	5.6	6.6	8.8	10.8
MEA (50%) modified AC Norit® R2030 Cabot	2	1.9	3.3	5.3	7	7.5
Unmodified AC Norit® RB1 AC	3	2.4	4.2	6.4	8.1	9.9
MEA+MDEA+AMP blend modified Norit® RB1 AC	4	3.1	5.9	8.2	10.6	12.6
MEA (20%) modified Norit® RB1 AC	5	3.2	5.5	7.7	9.2	10.6
MEA (30%) modified Norit® RB1 AC	6	2.7	5.5	9.1	11.4	12
MEA (40%) modified Norit® RB1 AC	7	2.4	5.5	7.4	10.5	12.9
MEA (50%) modified Norit® RB1 AC	8	3.2	5.6	7.1	7.9	8
MEA (60%) modified Norit® RB1 AC	9	3.2	5.5	7.6	9.3	10.7
TEPA (20%) modified Norit® RB1 AC	10	1.9	3.4	4.9	7.2	7.6
TEPA (30%) modified Norit® RB1 AC	11	2.7	4.9	6.5	7.2	9
KOH (20%) modified Norit® RB1 AC	12	2.2	4.2	6.4	8.7	10.4
KOH (60%) modified Norit® RB1 AC	13	2.8	5.1	7.2	9.1	11.7
KOH (70%) modified Norit® RB1 AC	14	2.9	5.1	7.5	8.6	10.2
H_3PO_4 (20%) modified Norit® RB1 AC	15	2.3	4.3	5.5	6.9	8.7
$ZnCl_2$ (20%) modified Norit® RB1 AC	16	2.2	3.6	5	7.3	7.4

The maximum loading for CO_2 was found by the integration of the breakthrough curve, following Eq. 2.11. The novel amine modified AC showed an adsorption capacity of 10.6 mmol/g, whereas the capacity for the unmodified AC was 9.6 mmol/g using 80 $Nml.min^{-1}$ CO_2 inlet flow. The higher adsorption capacity justifies the improvement of the AC performance and has been proved for amine modified adsorbents under pre-combustion conditions (Hao, Li & Lu, 2011; Shafeeyan et al., 2015b), which is also promising for binary mixtures of CO_2 in large-scale pre-combustion processes.

The adsorption capacity improvement shows an increase of the mass transfer between the gas and the solid surface for the MEA+MDEA+AMP modified AC. It can be explained by the inclusion of active amine sites into the porous surface of the carbons (Bai et al., 2015; Campbell, 1988; Sun et al., 2015). Additionally, the MEA+MDEA+AMP modified RB1 AC showed improved selectivity for CO_2 compared to the unmodified activated carbons. This was analysed by measuring the amount of N_2 leaving the FBR during the experiments, as reported in Appendix A. The amount of N_2 that left the adsorption experiment was 15% higher for the MEA+MDEA+AMP modified RB1 AC compared to the unmodified AC. According to Table A.5, eight modified adsorbents exhibited higher selectivity towards CO_2, due to more N_2 in the outlet bed stream: MEA+MDEA+AMP, MEA (20–60%) and KOH (60–70%) modified RB1 ACs.

Figure 5.15.b shows the performance of the MEA (20%) modified RB1 AC for CO_2 adsorption. The MEA (20%) modified AC breakthrough curves presented a similar affinity for CO_2 compared to the MEA+MDEA+AMP modified adsorbent. However, it was concluded that the MDEA working as an additional amine improved the reactivity towards CO_2, due to the higher captured amount compared to the MEA (20%) modified AC. Table 5.4 presents the ACs capacities obtained from different CO_2 fractions in the high-pressure process. Seven modified ACs demonstrated higher adsorption capacity for CO_2 when compared to the unmodified adsorbent. Additionally, according to Table 5.4, the MEA (20–40%) modified adsorbents also offered higher capacity as provided by the novel amine modified AC (for instance, MEA+MDEA+AMP modified adsorbent).

According to Table 5.4, the amine modified adsorbents provided higher adsorption capacity in higher CO_2 inlet flow, such as 40 and 50% total volume. The MEA (40%) modified AC, for

instance, adsorbed 3.0 mmol/g CO_2 more than the original adsorbent at 50% total CO_2/N_2 inlet flow. In contrast, as demonstrated in Table 5.4 (also in Appendix A), the adsorbents modified with 50 and 60% MEA solutions showed a reduction in their adsorption capacity, due to the rapid saturation provided during the CO_2 adsorption stages.

Potassium hydroxide modifications were integrated into the list of effective adsorbents (solutions 1–3, according to section 3.1.1). Figure 5.16 displays, the three KOH modified AC breakthrough curves demonstrating their potential improvement of CO_2 absorbance in different binary gas mixture concentrations.

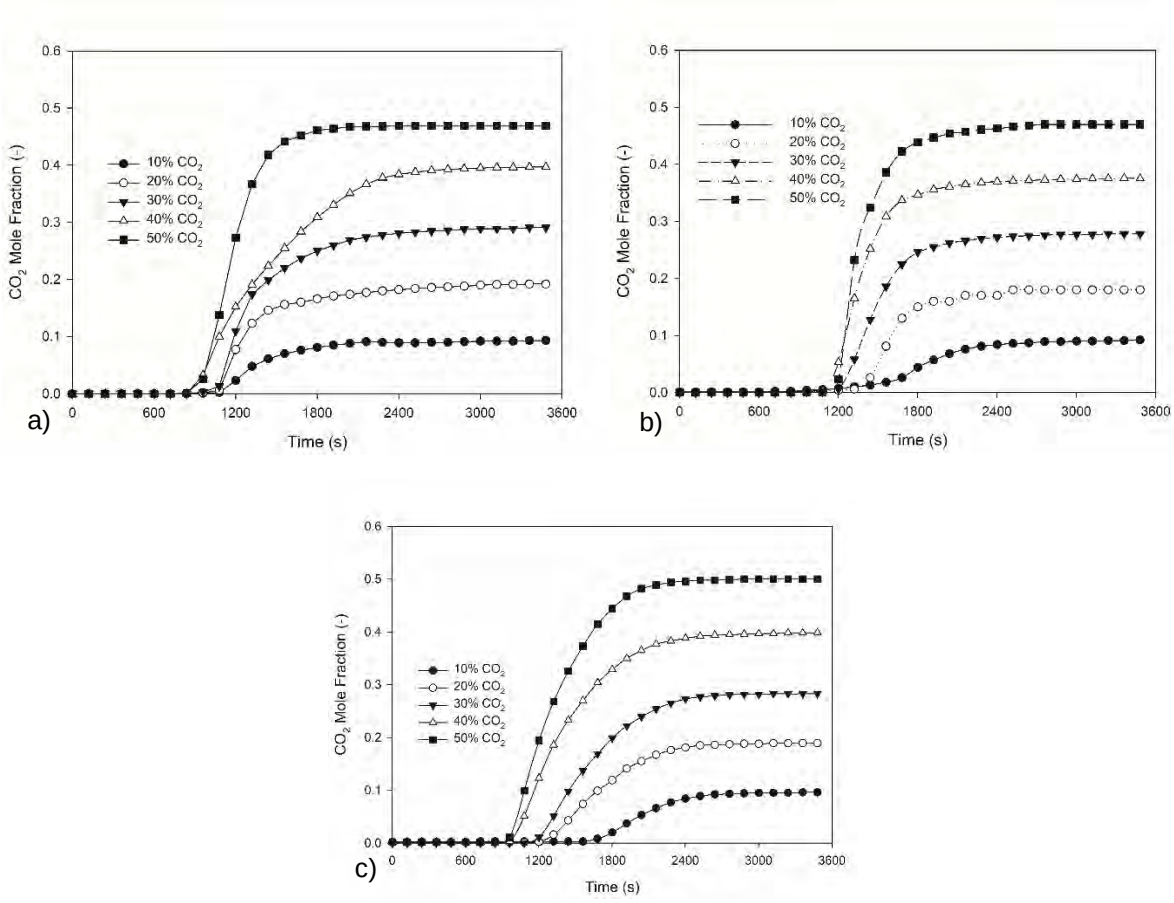

Figure 5.16. Breakthrough curves generated using a CO_2/N_2 binary mixture (200 Nml.min^{-1}) in pre-combustion adsorption conditions (25ºC and 25 bar) for: a) KOH (20%) modified RB1 AC; b) KOH (60%) modified RB1 AC; and c) KOH (70%) modified RB1 AC

The most effective adsorbent was the KOH modified AC compared to $ZnCl_2$ and H_3PO_4 modified ACs for dynamic CO_2 adsorption. Additionally, the most promising was the KOH (60 and 70%) modified RB1 AC, due to the improvement of 18% in the overall CO_2 adsorption capacity, as reported in Table 5.4. In general, the maximum adsorption time reached by these samples was in the range 900–1800 seconds in high and low CO_2 inlet concentrations, respectively. Romanos et al. (2012) also investigated the effect of the chemical treatment on the AC surface chemistry via low concentration KOH solutions. High specific surface area and porosities were obtained after treatment, and the AC adsorption capacity was enhanced using KOH impregnation solutions. The AC surface chemistry modification improved the AC capacity at high concentration impregnation solutions and activation temperatures (>700ºC). In studies by Heidari et al. (2014), the KOH modified AC adsorption capacity for CO_2 was investigated at different adsorption temperatures (from 15 to 75ºC). They concluded that the KOH modified AC maximum adsorption capacity (37.9 mmol/g at 15ºC) decreased with increasing adsorption temperature, wherein the maxiumum adsorption capacity was 15.8 mmol/g at 75ºC, demonstrating physical bonds for CO_2 adsorption, eliminating any possibility of chemisorption for the KOH modified AC at high adsorption temperatures (Heidari et al., 2014; Romanos et al., 2012).

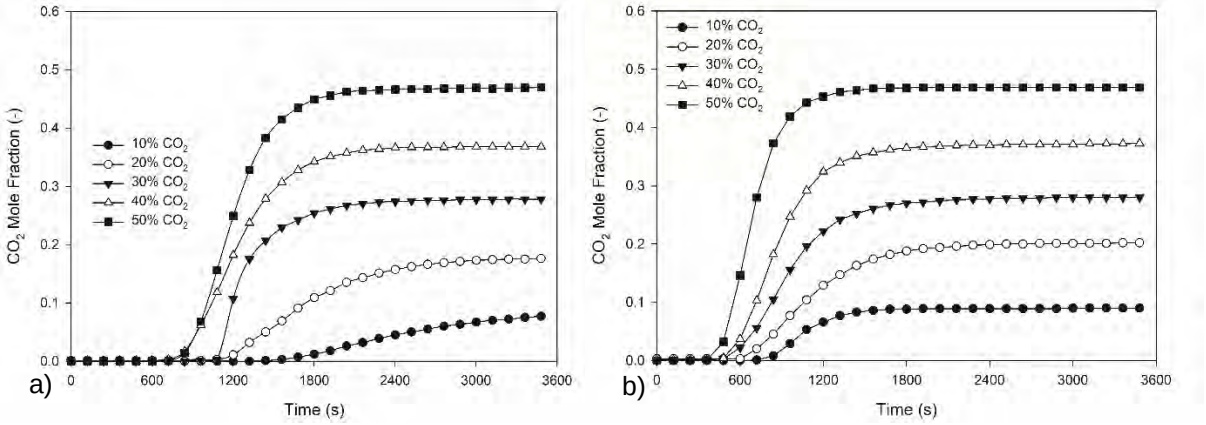

Figure 5.17. Dynamic CO_2 adsorption using a CO_2/N_2 binary mixture (200 Nml.min^{-1}) in pre-combustion conditions (25^{o}C and 25 bar) for: a) Unmodified R2030 Cabot AC; and b) MEA (50%) modified R2030 Cabot AC

Figure 5.17 provides a comparison of the original R2030 AC and the amine modified version. As demonstrated in Figure 5.16.a, the original R2030 AC provided a breakpoint 900–1300 s from 50–10% CO_2 inlet flow. An opposite dynamic behaviour was observed for the original and amine modified R2030 versions when tested under high-pressure. The amine modified R2030 AC demonstrated lower capacity for CO_2 as shown in Figure 5.17.b. The breakpoint provided by the amine modified R2030 was limited to the range of 450–800 s for 50–10% CO_2 inlet flow. As predicted in the thermo-adsorption experiments (section 5.2.3), the amine modified R2030 AC reduced the CO_2 capacity after impregnation. Indeed, even though the test for the amine modified R2030 AC was conducted under high pressure, the absence of high adsorption temperatures limited the modified sample to achieve a great performance.

The high-pressure system was not appropriate to improve the adsorbent capacity for CO_2 molecules. In contrast, as proven by the post-combustion results in section 4.2.8, the high temperature boosted the amine modified R2030 AC CO_2 capacity, due to the pore thermal-activation effect. However, in pre-combustion conditions, the adsorbent was entirely affected

by pore blockage, due to the low reactivity of the amine molecules on the surface and pores. Additionally, the amine impregnation treatment applied to the R2030 AC reduced the chemical bond forces during adsorption.

A similar pore blockage behaviour was found for another type of amine, as demonstrated in Table 5.4. From TEPA (20 and 30%) modified RB1 AC breakthrough curves (Figures A.3.a and b), it was possible to observe the impact on the adsorption capacity in comparison to the original adsorbent. As mentioned in section 2.3.2 and 4.2.8, TEPA molecules are the most reactive when compared to the other amines selected in this work. However, their high affinity for CO_2 did not promote great results in high-pressure experiments. From the breakthrough curves and the data shown in Tables 5.4, it was concluded that the TEPA (20%) modified RB1 AC exhibited a slight reduction compared to the unmodified adsorbent. According to Table 5.4, the amount of CO_2 adsorbed by this amine modified AC was 15% lower in comparison to the original AC. In this case, the lower amine concentration on the AC surface was not sufficient to increase the adsorbent performance, even considering the TEPA high reactivity potential for CO_2 adsorption. The low temperature and high-pressure conditions did not favour the TEPA affinity for CO_2, as demonstrated in the TGA (section 5.2.3).

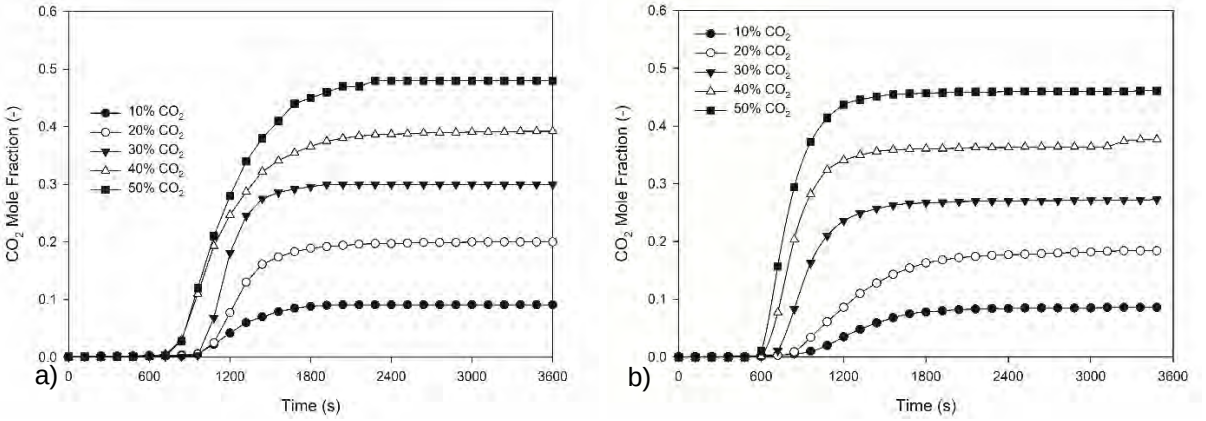

Figure 5.18. Dynamic CO_2 adsorption using a CO_2/N_2 binary mixture (200 Nml.min^{-1}) in pre-combustion conditions (25ºC and 25 bar) for two chemically modified ACs: a) $ZnCl_2$ (20%) modified RB1 AC; and b) H_3PO_4 (20%) modified RB1 AC

Zinc chloride and phosphoric acid modified ACs breakthrough curves are shown for different CO_2 mole fraction inlet concentrations in Figure 5.18. The two chemically modified adsorbents provided faster saturation, between 700–900 seconds and 600–850 seconds for $ZnCl_2$ (20%) and H_3PO_4 (20%) modified RB1 AC, respectively compared to the unmodified adsorbent. From Figures 5.18.a-b, it was concluded that the $ZnCl_2$ and H_3PO_4 impregnated adsorbents demonstrated weak interaction for CO_2 adsorption due to the morphological changes on the AC surface. Owing to the low success of these two impregnation treatments for AC application, more solvent loading needs to be applied to the adsorbent surface. Additionally, the activation temperature could contribute to the low adsorption capacity, as compared with Yang and Qiu (2013). In their study, the AC was activated using a $ZnCl_2$ solution with a ratio of 1.225 for impregnation. Additionally, the activation was 437ºC, lower than the 700ºC applied in this work. The elevated activation temperature may contribute to reducing the CO_2 adsorption capacity, due to the formation of more mesopores and reduction of micropores.

Heidari et al., (2014) also investigated $ZnCl_2$ impregnation at different solvent loadings (0.75, 1.5 and 2.5 g/g) in quantities higher than used in this work. They observed that the amount of CO_2 captured increased proportionally to the $ZnCl_2$ loading during impregnation. However, the high solution concentration had a higher impact on the surface area and the AC porosity, with increased CO_2 adsorbed when the AC mesoporosity increases. The most effective $ZnCl_2$ modified AC was treated with an impregnation ratio of 0.75, due to the high percentage of micropores (up to 100%) presented by the modified AC. Restricted for $ZnCl_2$ modified ACs, the insertion of highly concentrated solutions and the creation of mesopores reduces their adsorption capacity for CO_2 (Arami-Niya et al., 2010). In contrast, the KOH modified AC provided higher adsorption capacity when modified with highly concentrated solutions. In studies of Heidari et al., (2014), three different H_3PO_4 concentrations were applied to modify the adsorbent, such as 1.5, 2 and 2.5 g/g for impregnation ratio. According to the adsorption data provided, the H_3PO_4 modified adsorbent substantially improved their adsorption capacity when modified with 2 g/g impregnated solution compared to the 1.5 g/g. However, their adsorption capacity decreased when impregnated with the highest solution loading (2.5 g/g), due to the creation of more mesopores and low microporosity.

5.3. Conclusions

The two groups of modified adsorbents were investigated in this chapter. Five chemically modified RB1 AC samples were produced via KOH (20, 60 and 70%), $ZnCl_2$ and H_3PO_4 solutions, aiming to enhance the activated CO_2 capacity for CO_2 molecules. The amine modified adsorbents evaluated in this chapter were composed of MEA, DEA, TEA (including blends with AMP and MDEA), and TEPA (20 and 30%), which generated fourteen amine

modified adsorbents from RB1 and R2030 original ACs. Experimental tests were conducted using a variety of techniques for AC characterisation, testing the dynamic, thermal and maximum adsorbent resistance and potential for carbon capture application.

SEM analysis allowed the observation of the textural changes promoted by chemical impregnation. A smooth surface area was developed after impregnation compared to the original AC properties demonstrated during the analysis. The modified ACs also presented crevices and wide open mouths to the original adsorbent, promoted by erosion during exposure to high temperatures in the impregnation drying stage. The identification of chemical groups was performed by FTIR analysis, allowing the investigation of the presence of functional groups on the AC surface. The success of the chemical impregnation treatment was highlighted by the appearance of -OH, C=O, C-H, defined as the functional groups on the AC impregnated surface.

Studies of the volumetric amount of CO_2 in high-pressure conditions were performed by HPVA. The adsorbents submitted to ambient temperature and high-pressure conditions revealed the maximum adsorption capacity for the KOH modified adsorbents based on the original AC result. The KOH modified AC provided a higher capacity of 75 and 105% CO_2 capture (KOH 20 and 70% samples, respectively) compared to the original AC adsorption capacity.

BET studies demonstrated that the chemically modified ACs had considerably more micropores, particularly for the KOH (70%) modified AC. However, the $ZnCl_2$ (20%) and H_3PO_4 (20%) modified RB1 ACs provided a better developed volume of macropores (region between 60–70 nm). Additionally, it was concluded that the KOH modified ACs PSD graphs demonstrated an increase in the volume of the pores according to the increased KOH loading on the surface.

Thermal CO_2 adsorption studies were conducted in the TGA, aiming to investigate the AC behaviour at pre-combustion temperatures, demonstrating that the KOH modified ACs had higher CO_2 adsorption capacities than the unmodified adsorbent. However, the limitation of this technique was in the low pressure of the stream inlet in the adsorption stage, so high adsorption capacity could not be achieved due to their low reactivity. Nonetheless, this technique predicted the potential for high CO_2 adsorption for the three modified adsorbents with KOH solutions, as reflected in PSA and HPVA studies.

Dynamic CO_2 adsorption experiments were performed in the FBR process using PSA technology. The chemically modified ACs and their CO_2 adsorption capacity were evaluated at pre-combustion conditions. A total of sixteen samples were submitted to high-pressure adsorption experiments. The novelty of this work was concentrated in the high potential of MEA+MDEA+AMP modified AC as the main adsorbent for pre-combustion conditions, due to the MEA+MDEA+AMP high capacity compared to the original adsorbent, wherein, for instance, the modified adsorbent captured 2.5 mmol/g CO_2 at 80 $Nml.min^{-1}$. KOH modified RB1 ACs were also shown to be potential materials for dynamic pre-combustion CO_2 adsorption, due to the relevant improvements (18%) in the AC overall adsorption capacity compared to the unmodified AC performance.

Furthermore, the novel adsorbent provided increased adsorption capacity compared to the unmodified AC for all CO_2 inlet streams. As reported in Table 5.4, among the list of modified adsorbents, six adsorbents [MEA+MDEA+AMP modified AC (Nº 4), MEA (20%) modified AC (Nº 5), MEA (30%) modified AC (Nº 6), MEA (40%) modified AC (Nº 7), KOH (60%) modified AC (Nº 13), and KOH (70%) modified AC (Nº 14)] presented a significant potential for application on a large scale, due to the effective success of the chemical treatment on the

AC surface and ranked as the novel for pre-combustion application. Substantial improvements of the impregnation treatment are recommended for $ZnCl_2$ and KOH impregnated samples, as the solution residence time was not enough to promote higher adsorption capacities owing to the limited success of chemically modified ACs and their satisfactory adsorption capacity for CO_2. In parallel, the drying temperature during the activation stage for adsorbents focused in pre-combustion process could be reduced to enhance the adsorption capacity for these modified adsorbents.

Relative to the amine samples, DEA and TEA modified ACs (including their blends with MDEA) were not included in the PSA experiments due to the low reactivity at low adsorption temperatures. The decision was taken after the sequence tests carried out in the TGA and PSA process and the absence of a suitable CO_2 adsorption capacity in pre-combustion conditions. Lastly, as cited in section 5.2.8, the chemical impregnation treatment based on $ZnCl_2$ and KOH solutions may present enhanced adsorption capacity for CO_2 capture when high solution concentrations are applied.

CHAPTER 6: PRESSURE SWING ADSORPTION MODEL VALIDATION VIA PARAMETER ESTIMATION OF BREAKTHROUGH CURVES FOR MODIFIED ACTIVATED CARBONS

6.1. Introduction

Process simulation has been developed by many researchers to represent carbon capture processes to optimise and reduce as much as possible the energy penalty for adsorption processes in power plant stations (Ko, Siriwardane & Biegler, 2003; Agarwal, Biegler & Zitney, 2010; Dowling, Vetukuri & Biegler, 2012; Wang et al., 2015; Casas et al., 2012; Siqueira et al., 2017; Gaeini, Zondag & Rindt, 2016). Models have been developed for pre-combustion CO_2 adsorption from flue gas using carbon-based materials, such as AC (Riboldi & Bolland, 2017; Casas et al., 2012; Siqueira et al., 2017). PSA has been considered as the most promising process for CO_2 capture from flue gas, due to the high purity and low energy consumption required (Samanta et al., 2012; Nikolaidis et al., 2014). Moreover, studies of PSA technology have confirmed the low capital investment costs compared to liquid MEA based capture systems, which confers higher potential for broad scale process implementation (Shafeeyan et al., 2014; Agarwal et al., 2010; Cen & Yang, 1985; Delgado et al., 2007; Gomes & Yee, 2002; Dowson et al., 2016). Studies on the dynamic behaviour of the PSA process have contributed to the process optimisation and design (Rutherford & Do, 2000). The nature of the solid-gas interaction and equilibrium defines the dynamic behaviour that occurs in an adsorption column (Shafeeyan et al., 2014). The gPROMS® ModelBuilder software (version 4.1) was introduced as a powerful tool for process simulations, due to the capacity to develop a robust dynamic model and determination of kinetic parameters for CO_2 adsorption. It encompasses a feature called 'parameter estimation' which allows the user to fit the developed model to a set of experimental data to calculate the values of the fitted parameters. In the estimated process, it was possible to study the impact of conditions, such as mass transfer, diffusivity, adsorbent particle size and axial dispersion, on adsorption breakthrough curves from a binary gas mixture (for instance, CO_2/N_2). Adsorption modelling can be applied to simulate and fit the

breakthrough curves under thermodynamic conditions and to optimise the power plant energy consumption. Models also contribute to process integration, such as retrofitted chemical absorption processes, and simulations have been used to investigate the potential of alternative technologies (PSA and membrane permeation), reducing the amount of energy dedicated to the solvent regeneration and for CO_2 separation from the product stream.

6.2. Mathematical modelling for laboratory scaled process via parameter estimation validation

In this work, a PSA model using a FBR was developed for CO_2 capture in pre-combustion conditions (25ºC and 25 bar). A parameter estimation was executed using similar conditions to those applied in the FBR rig on the laboratory scale. Nitrogen and carbon dioxide were applied to this model taking into account the physical behaviour of the PSA unit. The overall inlet flowrate used was concentrated in a binary N_2/CO_2 (0.6/0.4, N_2 and CO_2 inlet fraction, respectively) gas mixture, according to Table 6.1.

Table 6.1. List of variables pre-defined in the PSA-FBR model

Parameters	Values	Minimum value	Maximum value
Area (m^2)	1.0	1.0E-10	100
Diffusivity (m^2/s)	1.0	-10000.0	1.0E20
Dimensionless	0.5	-1.0E20	1.0E20
Length (m)	0.5	1.0E-10	100.0
MassCoefficient (1/s)	1.0	-1000.0	1000.0
MoleFraction	0.5	-100000.0	1000000.0
NoType	0.5	-1.0E10	1.0E9
Pressure (Pa)	100000.0	100.0	1.0E10
Solid concentration (mol/m^3)	1.0	-1000.0	1000000.0
Temperature (K)	295.0	1.0E-10	10000.0
Velocity (m/s)	1.0	-1000000.0	1.0E10
Volumetric flowrate (m^3/s)	1.0	-1.0E10	1.0E10

The model was developed by Rebeca Azpiri Solares (D Eng student) in gPROMS®, and the data to construct the model originated from the experiments reported in this work (section 5.2.7). gPROMS® language environment contains different subtasks, such as the insertion of operational parameters, variables, boundary conditions and equations. The structure of the model was provided in the section, 'Model'. Details relative to the process variables and the equations for each phenomenon involved were inserted in the model section. The parameters and type of process variables were entered in this section (entitled as 'Variable Types' in gPROMS simulation environment), including the boundary conditions as listed in Table 6.1. In the section named as 'Tasks', commands for PSA process were set, such as adsorption and desorption stage.

The model was then fitted to experimental breakthrough data for two modified samples [TEPA (20%) and MEA+MDEA+AMP modified RB1 ACs] to study the effect on fitting parameters of chemical modifications of the adsorbent tested under pre-combustion conditions. The dynamic model developed in gPROMS® (ModelBuilder v4.3.1) describes the simulated adsorption process based on the experimental laboratory conditions to predict the breakthrough curves. Parameter estimations were conducted to fit the laboratory data to the model, controlled by mass transfer and dispersion coefficient, which were adjusted as the fitting parameters. The thermodynamic properties were calculated using the Multiflash® package (version: gSW-0861) developed by PSE. The Soave-Redlich-Kwong equation was used to calculate the compressibility factor of the gas mixture, which was over 0.95. Therefore, the feed gas was considered ideal, wherein this approach has been recognised by most authors in the field (Agarwal et al., 2010; Khalil et al., 2012; Casas et al., 2012; Riboldi et al., 2014; Riboldi & Bolland, 2015; Dowling et al., 2012; Ribeiro et al., 2008; Wang et al., 2015).

The development of a FBR column modelling contributes to improving the understanding of the adsorbent performance when submitted to CO_2 adsorption/desorption cycles. In the developed model, a list of assumptions was considered to establish a laboratory scale FBR process comparison, as described below:

- The gases used in the model were regarded as ideal (Agarwal et al., 2010; Khalil et al., 2012; Casas et al., 2012; Riboldi et al., 2014; Riboldi & Bolland, 2015; Dowling et al., 2012; Ribeiro et al., 2008; Wang et al., 2015).
- The components in the gas and solid phase did not have radial variations in the parameters, for instance, pressure and temperature.
- The diffusion through micropores promotes mass transfer resistance, considered as a limiting step (Agarwal et al., 2010; Casas et al., 2012; Riboldi et al., 2014; Riboldi & Bolland, 2015; Wang et al., 2015). It was described using the LDF equation for the adsorption kinetics (Ribeiro et al., 2008). The LDF is considered as the most used kinetics model for adsorption modelling, due to its simplicity and physical consistency (Gaeini et al., 2016; Sircar, 1983). This assumption is mainly supported by Ribeiro et al. (2008), owing to a complete PSA model and a model that considered this assumption were compared, providing an identical result for both purposes.
- A stable thermal equilibrium was provided to the solid and gas phases, and there were no modifications in the solid initial density (Ribeiro et al., 2008).

The following equations were used to compose the model. Equations 6.1 and 6.2 correspond to the overall and component mass balances. The main equations used in the PSA model are described using the partial algebraic differential equations (PADEs) as listed below (Agarwal

et al., 2010; Riboldi & Bolland, 2015; Dowling et al., 2012; Ribeiro et al., 2008; Wang et al., 2015; García et al., 2013; Bai et al., 2015):

$$\varepsilon_t \frac{\partial C(z)}{\partial t} = -\varepsilon_b \frac{\partial\big(C(z)v(z)\big)}{\partial z} + \varepsilon_b D_x \frac{\partial^2 C(z)}{\partial z^2} + (1-\varepsilon_b)\frac{\partial Q(i,z)}{\partial t} \qquad \text{Eq. (6.1)}$$

$$\varepsilon_t \frac{\partial Y(i,z)}{\partial t} = -\varepsilon_b v(z)\frac{\partial Y(i,z)}{\partial z} + \varepsilon_b D_x \frac{\partial^2 Y(i,z)}{\partial z^2} + \frac{2}{C(z)}\frac{\partial Y(i,z)}{\partial z}\frac{\partial C(z)}{\partial z} - (1-\varepsilon_b)\Big(\frac{\partial Q(i,z)}{\partial t} - \frac{\partial Y(i,z)}{\partial z}\sum_{i=1}^{n}\frac{\partial Q(i,z)}{\partial t}\Big) \qquad \text{Eq. (6.2)}$$

Equation 6.3 describes the material balance for the glass beads in the FBR as nonporous and non-adsorbing particles. This experiment was performed to determine the level of dispersion in the absence of the diffusion of gas into the particles or adsorption on their surface. The dispersion model created for the system is described by Equation 6.3, where a constant temperature in the reactor was assumed due to the absence of reaction.

$$\frac{\partial Y(z)}{\partial t} = -v\frac{\partial\big(Y(i,z)\big)}{\partial z} + D_x \frac{\partial^2 Y(i,z)}{\partial z^2} \qquad \text{Eq. (6.3)}$$

Equation 6.4 is the thermal energy balance in the FBR, wherein the heat accumulation in the solid-gas phase, heat transfer in the gas phase, the heat produced from adsorption stage and the heat transfer from the gas phase to the reactor wall are taken into account.

$$ec_{p,g(z)}\frac{\partial(T(z)v)}{\partial z} + \varepsilon_t ec_{p,g(z)}\frac{\partial T(z)}{\partial t} + \varepsilon_t e_s c_{p,s}\frac{\partial T(z)}{\partial t} - (1-\varepsilon_b)e_s\sum_{i=1}^{N_{comp}}\Delta H_{ads(i)}\frac{\partial Q(_i,z)}{\partial t} + \frac{3h_{amb}}{R_{bed}}(T(z)-T_{wall)} = \lambda\frac{\partial^2 T(z)}{\partial z^2} \qquad \text{Eq. (6.4)}$$

The parameters, such as the maximum adsorption capacity (q_m) and the equilibrium constant (k_l) obtained from the HPVA analysis (section 5.2.5), were also included in the model based on the equilibrium of adsorption obtained from the modified ACs tested in this technique. The data was used to select the most suitable isotherm which could be applied in this work, the Langmuir isotherm (Eq. 6.5). The Ergun equation (6.6) for pressure drop and momentum losses calculations (Agarwal et al., 2010; Casas et al., 2012; Dowling et al., 2012; Ribeiro et al., 2008). Equation 6.7 refers to the Linear driving force (LDF) model, which has been used for small- and large-scale PSA models (Riboldi & Bolland, 2015; Dowling et al., 2012; Ribeiro et al., 2008; Agarwal et al., 2010; Wang et al., 2015).

$$Q^*_{(i,z)} = \frac{q_{m,} bP(z)RT(z)}{1+bP(z)RT(z)} \quad \text{Eq. (6.5)}$$

$$\frac{\partial P(z)}{\partial Z} = 150u_{g(z)} \frac{(1-\varepsilon_b)^2}{D_p^2 \varepsilon_t^3} + \frac{1.75}{D_p} \frac{(1-\varepsilon_t)}{\varepsilon_t^3} \; v(z)e/v(z)/ \quad \text{Eq. (6.6)}$$

$$\frac{\partial Q_{(i,z)}}{\partial t} = K_{\,(i)}(Q^*_{\,(i,z)} - Q_{(i,z)}) \quad \text{Eq. (6.7)}$$

The finite difference method (FDM) contributed to solving PADEs. In this case, the forward FDM (FFDM) and backward FDM (BFDM) were applied in accordance with the flow direction (Moon et al., 2018). The overall component concentrations, velocity, and temperature variables were defined by the BFDM. In contrast, for the system pressure, the FFDM was applied because the pressure was defined in the outlet of the bed. The boundary conditions of the model are described by equations 6.8–6.14:

$$-\varepsilon_b D_x \frac{\partial C_i}{\partial z}_{z=0} = v_{z=0}(C_{i,feed} - C_{i,z=0}) \quad \text{Eq. (6.8)}$$

$$-\varepsilon_b \lambda \frac{\partial T}{\partial z}_{z=0} = v_{z=0} e c_{p,g,z=0}(T_{feed} - T_{z=0}) \quad \text{Eq. (6.9)}$$

$$v_{z=0} = v_{feed} \quad \text{Eq. (6.10)}$$

$$\frac{\partial C_i}{\partial z}_{z=L} = 0 \quad \text{Eq. (6.11)}$$

$$\frac{\partial T}{\partial z}_{z=L} = 0 \quad \text{Eq. (6.12)}$$

$$\frac{\partial v}{\partial z}_{z=L} = 0 \quad \text{Eq. (6.13)}$$

$$P_{z=L} = P_{ads} \quad \text{Eq. (6.14)}$$

Equations 6.15 and 6.16 correspond to the transition equations which describe the depressurisation and equalisation stages. These equations show the inlet boundary conditions for those steps. The pressure changes with time during those steps. The pressure change was simulated using a linear valve model, controlled by a linear equation:

$$\frac{\partial P_{Depress}}{\partial t}_{z=0} = \left(-\frac{P_{eq}-P_{atm}}{t_{Blowdown}}\right) \quad \text{Eq. (6.15)}$$

$$\frac{\partial P_{equal}}{\partial t}_{z=0} = \left(-\frac{P_{feed}-P_{eq}}{t_{equalization}}\right) \quad \text{Eq. (6.16)}$$

The adsorbent and the FBR process parameters used in the model were guided by the physical laboratory rig dimensions and the adsorbent property measurements obtained by the characterisation studies described in the previous chapters. The optimisation and modelling of FBRs have been developed by many researchers to improve the performance of the experimental process (Shafeeyan et al., 2014). In this work, the PSA model included the adsorption-desorption stage of one FBR process. The primary purpose was to test the impact of the mass transfer on the selected modified AC breakthrough curves. The impregnation treatment changed the structure of the adsorbent pores, as described in chapters 4 and 5 in BET, HPVA, TGA and PSA studies. For this reason, the amount of CO_2 adsorbed and the adsorbent

selectivity were evaluated under the mass transfer coefficient influence via a Maximum Likelihood Parameter Estimation algorithm, which is integrated in the gPROMS® software (PSE). The experiments were compared to the model during the adsorption step, as this step mainly determines the purity of the nitrogen product and the amount of CO_2 adsorbed. The model considered the following four steps:

- Pressurisation (P): a binary gas mixture (CO_2 and N_2) at 25 bar enters the FBR;
- Adsorption (ADS): CO_2 adsorption occurs on the adsorbent surface at 25 bar, and the N_2 is obtained in the reactor outlet;
- Depressurisation: the pressure in the bed decreases to 1 bar;
- Purge: pure N_2 inlet flow is inserted in the FBR at 1 bar and CO_2 is obtained as a product.

In the literature, some authors added additional steps to the model to improve the purity and recovery rate of CO_2, as well as the energy efficiency of the process (Agarwal et al., 2010; Moon et al., 2018). These additional steps were reported as rinse and pressure equalisation. However, in pressure equalisation, the bed pressure is decreased to 12.5 bar (the middle point between the adsorption and the purge pressure) when connected to a pressurising bed. In the rinse step, the CO_2 enters the bed at 1 bar, and CO_2 is obtained as a product. This step was introduced to achieve higher purity of the CO_2 product. Moreover, the rinse and pressure equalisation steps are considered fundamentals when the model includes multiple beds of cyclic operation for CO_2 adsorption (Chahbani & Tondeur, 2010; Ahn et al., 2012).

The four steps described previously respected the experimental PSA process, wherein the model followed the order and conditions used for the FBR process for pre-combustion CO_2 adsorption. The adsorption step of the PSA model was compared with the experiments using TEPA (20%)

and MEA+MDEA+AMP modified Norit® RB1 AC breakthrough curves obtained from the experimental PSA process, one at a time. These four breakthrough curves were experimentally obtained using a binary gas mixture of 30 and 40% CO_2 in the feed stream in pre-combustion conditions, as demonstrated in section 5.2.8 and Appendix A. PSA process simulation was initially estimated with the glass beads laboratory experimental data, testing the accuracy and performance of the developed model. The dispersion coefficient was obtained from the parameter estimation with the glass beads' breakthrough curves, to use later in the PSA model for the modified adsorbent simulations. It was supported by the fact that the glass beads do not present pores for gas diffusion, where the adsorption phenomenon occurs in the pores of the AC samples. Figure 6.1 shows the breakthrough curves of the dispersion model and the experiment using glass beads.

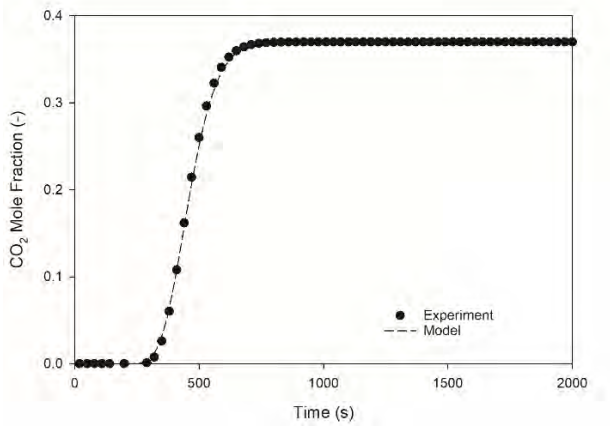

Figure 6.1. Comparison of the dispersed plug flow model against experimental data using glass beads under PSA conditions

The level of dispersion in the outlet of the FBR process was estimated as 5 x 10^{-6} m^2s^{-1}. The simulated results provided a good visual match between the experimental and the dispersion

model. In contrast, the four modified AC breakthrough curves estimated in gPROMS® demonstrated satisfactory agreement to the simulated data, as shown in Figure 6.2.

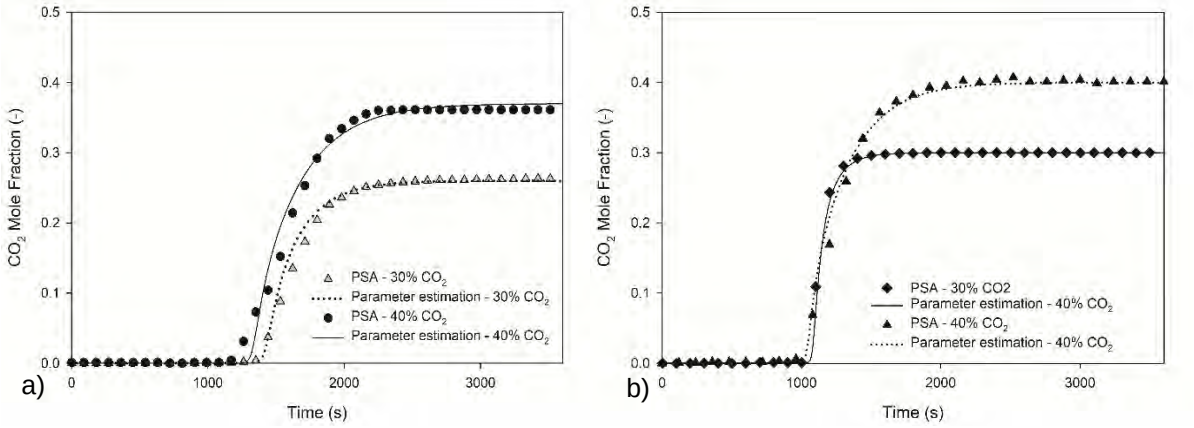

Figure 6.2. Comparison of the experimental and simulated data obtained from the parameter estimation by mass transfer coefficient variation for: a) MEA+MDEA+AMP modified RB1 AC (0.3 and 0.4 CO_2 inlet fraction); b) TEPA (20%) modified RB1 AC (0.3 and 0.4 CO_2 inlet fraction)

The four breakthrough curves obtained from the experimental PSA studies using the modified adsorbents are shown in Figure 6.2. They were estimated based on 0.3 and 0.4 CO_2 inlet mole fraction. The parameter estimation showed a good fit for MEA+MDEA+AMP and TEPA (20%) modified RB1 ACs experimental data tested under 0.3 and 0.4 CO_2 inlet fraction, as shown in Figures 6.2.a and b, respectively. These estimations demonstrated an excellent approximation to the experimental breakthrough curve for both adsorbents, which validates the model also supported by the SSR values. The mass transfer coefficient for TEPA (20%) and MEA+MEA+AMP modified RB1 ACs (analysed at 0.4 CO_2 inlet fraction) which best fitted the experimental breakthrough through the simulated data were 0.07 and 0.04 s^{-1}, respectively. The SSR from Figure 6.2 was 0.4% for the MEA+MDEA+AMP modified RB1 AC and 0.1% for TEPA (20%) modified RB1 AC. These values are in accordance with the acceptable percentage (≤10%) for engineering purposes using parameter estimation (Agarwal et al., 2010).

Highly pure levels of CO_2 adsorbed were obtained in the developed PSA model, wherein the purity was 98% in the outlet stream.

The great result predicted by the developed model demonstrated concise agreement with the experimental data suggesting that the LDF equation correctly represents the mass transfer of gas into the particle in the model structure (Shafeeyan et al., 2014). The later breakpoint provided by MEA+MDEA+AMP modified RB1 AC compared to their unmodified adsorbent performance reinforces the novelty of the modified material in pre-combustion conditions, as represented in Figure 6.2.b. The attachment of reactive amine groups onto the AC surface generated a high selectivity and adsorption capacity for CO_2 molecules. Additional information regarding the adsorbent selectivity is included in Appendix A (Table A.5), which supports the novelty of the MEA+MDEA+AMP modified RB1 AC over the original adsorbent. Additionally, TEPA (20%) modified AC provided the highest mass transfer compared to the MEA+MDEA+AMP modified AC, as evidenced by the steeper breakthrough curve. Indeed, the enrichment of the AC surface by nitrogen functional groups increased their selectivity for CO_2 and impacted in mass transfer to the reactive sites found in the mesopores region (Hao et al., 2011).

In this work, only one bed with four steps was modelled to represent the adsorption stage. However, researchers have provided more advanced simulations which include the use of two or more beds (up to eight) and up to six steps, aiming to increase the purity of CO_2 adsorbed and reduce the energy penalty (Ben-Mansour et al., 2016; Casas et al., 2012; Mulgundmath et al., 2012; Nikolaidis, Kikkinides & Georgiadis, 2017; Nikolaidis et al., 2014; Maring & Webley, 2013; Lei et al., 2013; Omell et al., 2016; Shafeeyan et al., 2014, 2015a). Many researchers have investigated the influence and impact of different effects, such as diffusion

into micro- and macropore CO_2 adsorption. The models have been structured by the application of PADEs to obtain a numerical model. Good levels of predictive accuracy have been achieved in adsorption models, such as Ahn and Brandani (2005), wherein an excellent match to the experimental CO_2 breakthrough curves data was obtained from a carbon monolith column at different gas concentrations.

6.3. Conclusions

Studies on PSA FBR process via mathematical modelling have been considered as a powerful tool for understanding the effects that contribute to adsorbent performance and their adsorption capacity. The mathematical model also investigates the applicability of different conditions to improve PSA operations and optimise the process, increasing PSA efficiency through the new adsorption cycles suggested. The PSA experimental laboratory scale process was simulated in gPROMS® ModelBuilder 4.1 to investigate the kinetics that affect the breakthrough curves and the ACs adsorption capacity, for instance, the mass transfer coefficient. The two most promising modified adsorbents (e.g., TEPA (20%) and MEA+MDEA+AMP modified RB1 AC) analysed in the laboratory scale adsorption process under pre-combustion PSA conditions were estimated at two different CO_2 inlet fractions and compared with the PSA model developed. The experimental adsorption data were fitted to the simulation via a Maximum Likelihood Parameter Estimation algorithm, an integrated tool in gPROMS® software.

From the simulations proposed, it was evident that the application of PADEs to define the thermal energy and mass balances contributed to the design and simulation of the FBR adsorption process. Initially, a glass beads experiment was used to estimate the dispersion coefficient ($5x10^{-6}$ m^2s^{-1}) that represented the amount of dispersion in the system. The value

reported was set in the model to provide higher accuracy to the parameter estimation for the mass transfer coefficient for the two modified ACs. The experimental data for the two modified adsorbents were fitted, and it was possible to observe that the highest mass transfer coefficient was provided by TEPA (20%) modified RB1 AC (0.07 s^{-1}), followed by the MEA+MDEA+AMP modified AC (0.04 s^{-1}). The simulated breakthrough curves accuracy and approximation to the experimental data demonstrated the high potential to validate the model. It was justified due to the excellent match, and the small number of errors presented by the simulation, which provided a SSR lower than 10% [0.1 and 0.4% for TEPA (20%) and MEA+MDEA+AMP modified RB1 AC, respectively]. Additionally, a similar performance was found by the estimation of these two amine modified adsorbents via different CO_2 inlet fractions, attributing higher accuracy and relevance to the model validation.

These PSA pre-combustion simulations were essential to estimate how mass transfer affects the breakthrough curve, concluding that the mass transfer did not impact the overall AC capacity, wherein this parameter remains constant with mass transfer changes in the model. The mass transfer modification affected only the breakpoint and the slope of the breakthrough curve during the adsorption stage. From a small variation in the mass transfer coefficient in the parameter estimation, it was observed that the breakthrough curve presented a later breakpoint (2 minutes longer when compared to the experimental laboratory data). Due to the mass transfer values obtained, it was concluded that these adsorbents have high potential to capture CO_2 at high purity levels in the final product. In conclusion, the parameter estimation confirmed the potential of the two amine modified adsorbents for pre-combustion CO_2 adsorption, as evidenced by their ability to capture the desired gas in a binary mixture in the PSA FBR process.

CHAPTER 7: CONCLUSION AND PERSPECTIVES

7.1. Conclusions

Diverse technologies and alternatives for CCS have been developed for GHG mitigation and clean energy production. However, among these technologies, adsorption has been considered as the most promising technology due to the low energy consumption (compared to chemical absorption via amine aqueous solutions) and final products (such as CO_2 captured) at high purity levels. Chemical and amine impregnation treatments of the two ACs surfaces (RB1 and R2030) were performed, aiming to improve their adsorption capacity and selectivity for CO_2 molecules. These adsorbents (both modified and unmodified versions) were submitted to experimental pre- and post-combustion adsorption conditions. The AC adsorption capacity and selectivity potential for CO_2 molecules were measured at conditions representative of a PSA FBR process. Additionally, the modified and original ACs were evaluated by six characterisation techniques, HPVA, FTIR, TGA, XRD, BET and SEM. The modified adsorbents developed in this work demonstrated their high potential to compete with the liquid amines used in chemical absorption process, due to their considerable improvement in adsorption capacities and selectivity for CO_2 molecules.

7.1.1. Post-combustion results

Due to the limited number of suitable adsorbents applied to processes in post-combustion adsorption conditions, the attachment of functional amine groups onto the AC surface generated novel and promising adsorbents, as discussed in chapters 2 and 4. A variety of adsorbents, such as MOFs, have been considered as potential materials for post-combustion adsorption conditions in the literature. However, AC demonstrates lower adsorption capacity caused by its absence of chemical and thermal stability in post-combustion adsorption conditions, ranked as

the most problematic issue associated with this material utilisation. It was found that unmodified AC demonstrated very limited CO_2 adsorption capacity when exposed to high adsorption temperatures, displaying low thermal resistance and capacity in post-combustion conditions. In contrast, these limitations were resolved by amine impregnation, as demonstrated below:

- AC selectivity and adsorption capacity improvements for CO_2 were confirmed by HPVA studies, wherein the attached amine groups increased (55%) overall adsorption capacity for the modified adsorbent (e.g., MEA+MDEA+AMP modified RB1 AC).
- The high reactivity of the attached amine molecules on the AC surface were responsible for the elevated CO_2 adsorption capacity of the novel adsorbents, such as MEA+MDEA+AMP modified RB1 AC.
- The attached amine molecules contributed to the strengthening of chemisorption forces for CO_2 adsorption, as demonstrated in PSA, HPVA and TGA studies.

Furthermore, the impact of the amine impregnation treatment was observed via SEM, where the surface became smooth when compared to the rough surface area of the original adsorbent analysis. The creation of crevices over the AC surface was observed in most of the amine modified adsorbents analysed by SEM, which increased the number of actives sites, owing to the wider opening of the mouth of the crevices. The attachment of amine groups onto the AC surface was confirmed by IR analysis, demonstrating the presence of amine molecules in the region of 1555.9–1315.0 cm^{-1}, which correspond to the N-H vibration and confirms the attachment of amine groups on the AC surface. Additionally, it was also observed that the attachment of amine molecules reduced the AC surface area compared to their original conditions in BET studies, due to the pore filling effect which blocks off part of the

microporosity of the AC in a limited number of samples, for instance, DEA+AMP modified RB1 AC. In contrast, the MEA+MDEA+AMP, TEPA (30%) and TEA+MDEA+AMP modified RB1 ACs (highlighted as novel adsorbents) had larger pore sizes due to the absence of the amine pore blockage effect. From the PSD tests conducted in BET studies, it was observed that the unmodified AC provided a microporosity behaviour, while the microporosity level was reduced by the amine modified ACs due to the rise in mesoporosity.

As described in the PSA post-combustion experimental section, seven amine modified adsorbents exhibited substantial improvements in their CO_2 adsorption potential. These amine modified adsorbents considered as novel post-combustion ACs are as follows: (1) MEA (20%), (2) MEA (30%), (3) MEA+MDEA+AMP, (4) TEPA (30%), (5) TEPA (20%), (6) TEA+MDEA+AMP modified RB1 ACs and (7) MEA (50%) modified R2030 AC. Three modified ACs demonstrated fair potential for CO_2 capture, for instance, (1) MEA (40%), (2) DEA+MDEA+AMP and (3) TEA+AMP modified RB1 ACs compared to the unmodified version. Five adsorbents demonstrated a reduced adsorption capacity, including the unmodified (1) RB1 and (2) R2030 ACs, for instance: (3) MEA (50%), (4) MEA (60%), (5) DEA+AMP modified RB1 ACs. However, these five modified adsorbents did not compete with the seven novel adsorbents and their CO_2 adsorption capacity. Additional adjustment in the impregnation ratio may promote substantial improvements in their adsorption capacity and selectivity for CO_2. From gas selectivity studies, it was concluded that the modified adsorbent became more selective for CO_2 molecules than for N_2, as the amount of N_2 that left the bed was 20% higher compared to the unmodified adsorbent from the binary gas stream outlet.

7.1.2. Pre-combustion results

Experimental adsorption studies under pre-combustion conditions were carried out for the two groups of impregnated adsorbents. The main objectives were concentrated in tests for the thermal resistance for amine modified groups and the maximum adsorption capacity performed via dynamic characterisation techniques.

SEM was used to investigate the morphological changes promoted by the treatment on the chemically modified ACs surface. The chemical treatment resulted in a smooth surface area on the ACs compared to the original adsorbent analysis. It was also concluded that the impregnation treatment expanded the pores on the AC surface, due to the observation of crevices and wide open mouths compared to the original adsorbent pictures and BET studies. The occurrence of these changes was attributed to the high temperature (700ºC) during the drying stage for chemical impregnation treatment, wherein the solvent (for instance, KOH solutions) developed erosions on the AC surface. Furthermore, the attachment of chemically impregnated molecules on the AC surface was confirmed by FTIR analysis, as evidenced by the appearance of -OH, C=O, C-H, defined as the functional groups on the AC impregnated surface.

HPVA confirmed that the KOH modified AC demonstrated higher interaction with CO_2 in the high-pressure system compared to the unmodified adsorbents. The KOH modified ACs (for instance, 20 and 70%) exhibited a CO_2 adsorption capacity 75 and 105% higher than the original RB1 AC. The maximum adsorption capacity (q_m) and the equilibrium constant (k_l) proved that the impregnation treatment improved the modified adsorbent due to the KOH molecules attached to the AC surface. The Langmuir and Freundlich linearisation methods were applied to the isotherms obtained from HPVA analysis, to define the amount of gas adsorbed during

the adsorption-desorption stage under high-pressure conditions. The Langmuir linearisation method was considered as the most suitable methodology to determine the amount of gas adsorbed for best fitting the adsorption data. The KOH modified adsorbents provided a CO_2 capacity two times higher than the unmodified materials, due to the impregnated hydroxyl groups which interacted more with CO_2 than N_2.

Thermo-adsorption studies were carried out in the TGA using pure CO_2 for the adsorption stage, comparing the amine and chemicalyl modified ACs performance in pre-combustion temperatures. KOH demonstrated a high potential for CO_2 capture in this technique, compared to the other adsorbents evaluated, due to the great adsorption capacity provided (1.7 mmol/g) compared to the unmodified RB1 AC performance (1.3 mmol/g). The amine modified ACs did not offer a high adsorption capacity due to the low temperatures (compared to post-combustion adsorption temperatures for molecules and sites activation) and very low pressure (0.5 bar) destinated to the gas feed in the system. The amine modified adsorbents demonstrated limited adsorption capacity at the pre-combustion temperatures and the maximum conditions (such as the volume of the gas fed in the system) required by the equipment.

The impact of chemical treatment was also observed in BET studies. The KOH modified ACs, especially KOH (70%) modified RB1 AC, developed microporosity, as observed in PSD analysis. Otherwise, the adsorbents modified using $ZnCl_2$ and H_3PO_4 solutions developed macroporosity (most evident in the region 60–70 nm). Furthermore, it was observed that the rise of KOH loading for the impregnation procedure increased the volume of the pores, as demonstrated in the PSD graphs.

In contrast to the thermo-adsorption studies, the chemical adsorbents behaved differently when tested under dynamic techniques, such as PSA and HPVA. The amine modified RB1 ACs

showed higher adsorption capacity compared to the chemically modified and original ACs, due to the effect of the inlet pressure and the higher volume of gas inserted. The dynamic conditions favoured the amine modified AC performance, owing to the action of the reactive groups for CO_2 capture. The MEA+MDEA+AMP modified AC was selected as a novel adsorbent for the pre-combustion process, due to the higher adsorption capacity (e.g., 2.5 mmol/g CO_2 captured at 0.4 inlet fraction) and later breakpoint provided as demonstrated in the breakthrough curves in section 5.2.7. Furthermore, CO_2/N_2 selectivity tests showed that the amine impregnation became more selective for CO_2 than for N_2, due to the amount of N_2 presented in the outlet gas stream from PSA-FBR process. These overall CO_2/N_2 selectivity data are included in Appendix A. These modified adsorbents considered as novel pre-combustion ACs are as follows: (1) MEA+MDEA+AMP, (2) MEA (20%), (3) MEA (30%), (4) MEA (40%), (5) KOH (60%) and (6) KOH (70%) modified RB1 ACs. Four modified ACs demonstrated fair potential for CO_2 capture, (1) MEA (50%), (2) MEA (60%), (3) TEPA (30%) and KOH (20%) modified RB1 ACs compared to the unmodified version. In contrast, four samples demonstrated a reduced adsorption capacity when compared to the original adsorbent performance, (1) TEPA (20%), H_3PO_4 (20%), $ZnCl_2$ (20%) modified RB1 ACs and MEA (50%) modified R2030 AC.

In conclusion, based on the facts presented, the amine impregnation treatment impproved the AC adsorption capacity and selectivity towards CO_2 molecules when applied to pre- and post-combustion adsorption conditions, as evidenced by the HPVA and PSA studies. The amine impregnation method was the most eficient treatment, due to the increase of the amount of CO_2 captured during the adsorption stage offered by the amine modified ACs (R2030 and RB1 samples) compared to their unmodified versions. In parallel, the high quantity of N_2 in the FBR outlet stream during adsorption was also considered indictative of the potential of the amine impregnated adsorbents as novel materials for pre- and post-combustion adsorption

technologies. Improvements in the selectivity of the modified adsorbent increased their adsorption capacity potential for CO_2 molecules compared to the unmodified adsorption results provided in this work.

7.1.3. PSA pre-combustion model validation

A mathematical model was developed in gPROMS® software for pre-combustion process optimisation. The model was composed of four main stages (Pressurisation, Adsorption, Depressurisation and Purge), promoting a complete representation of the laboratory scale FBR used in this work. The PADEs applied for thermal energy and mass balance calculations demonstrated relevant importance to the design and simulation of the FBR adsorption process. The LDF equation inserted in the model provided excellent consistency to the simulation, considered as the most used equation for kinetics in adsorption modelling. The LDF equation was used to include the mass transfer resistance in the amount of CO_2 captured.

The CO_2 adsorption stage was estimated in the Maximum Likelihood Parameter Estimation problem, provided as an integrated tool in the gPROMS® ModelBuilder software. This tool allows evaluating only the adsorption stage of the process. The experimental data obtained from HPVA analysis was also included in the model parameters, where the maximum adsorption capacity and equilibrium constant obtained were used to determine the equilibrium of adsorption of the modified adsorbents. The glass beads experiment was essential to determine the amount of dispersion produced in the FBR during the adsorption stage. The amount of dispersion measured (5×10^{-6} m^2s^{-1}) was set in the model, improving the accuracy of the parameter estimation based on the mass transfer coefficient.

In the proposed model, the mass transfer effect was evaluated during the adsorption stage based on the FBR process experimental data. The MEA+MDEA+AMP modified RB1 AC provided the lowest mass transfer value (0.04 s^{-1}) compared to the TEPA (20%) modified RB1 AC (0.07 s^{-1}) for all CO_2 inlet fractions evaluated in the estimated adsorption stage. The SSR was also in accordance with the acceptable percentage (≤10%), wherein 0.4 and 0.1% were obtained for TEPA (20%) and MEA+MDEA+AMP modified RB1 AC samples, respectively. The later breakpoint provided by the MEA+MDEA+AMP modified RB1 AC confirmed the novelty of this adsorbent, as also demonstrated in the proposed modelling.

7.2. Future work

This study has contributed to the development of novel adsorbents for pre- and post-combustion adsorption systems for CO_2 capture at different feed fractions. Due to the PSA scale still not achieving a mature stage, several improvements and developments should be considered to further develop this technology as a robust and broad application in the future.

7.2.1. Considerations for the impregnation treatment and modified ACs

The impregnation treatment includes two essential factors for surface area modifications, as described section 3.1.1. They are summarised in AC activation temperature and amount of solvent loading onto the AC. Regarding the solvent loading, it would be important to dedicate more residence time for the soaking step in the impregnation method, thereby improving the adsorbent interaction with CO_2 and strengthening the chemisorption bonds. Furthermore, a longer residence time for the chemical impregnation by $ZnCl_2$ and H_3PO_4 could help to increase

their CO_2 adsorption capacity. Additionally, the drying temperature applied in the activation stage could be reduced to investigate possible enhancement in the adsorption capacity for both modified ACs. It is also recommended that the fixed bed PSA reactor process needs to be submitted to an upgrade in scale, where the amine modified ACs adsorption capacity and lifespan could be evaluated under a number of reactors in sequence at various adsorption-desorption stages. Additionally, the presence of H_2 in the process (instead of N_2 for pre-combustion conditions used in inlet flow mixture at laboratory scale) and real operational temperatures could confer a more realistic situation compared to the adsorption conditions used in this work.

7.2.2. Economic Evaluation and large-scale application

Economic studies of a PSA system focused in pre- and post-combustion system has demonstrated fundamental importance to achieve a mature stage. PSA has been considered as the most suitable technology compared to chemical absorption, owing to the versatile application at a range of pressures and temperatures, low energy demand and low CAPEX (based on chemical absorption costs). Among the essential premises for PSA application on a large scale, the adsorbent needs to be cost-effective, due to material selection to compose the process design. Post-combustion adsorption processes provide a lower energy penalty compared to pre-combustion processes, due to the lower energy requirements for adsorbent regeneration, gas compression and storage. Furthermore, post-combustion carbon capture demonstrates a feasible integration into existing plants, wherein no substantial combustion technology changes are necessary in the plant. The process itself is flexible in terms of maintenance, owing to the absence of stopping the power plant for potential repairs. The

gaseous separations in the pre-combustion capture system demand the utilisation of a sequence of beds to improve the purity of the product, which justifies the significant investment in CAPEX and OPEX. A robust economic analysis will contribute to the design of a feasible PSA system. In parallel, this could allow the comparison of a variety of CO_2 capture system investments and operational costs, demonstrating the most viable technology for gas processing and CCUS application.

7.2.3. Model improvements to achieve mature scales

The adsorption model developed in this work was based on an experimental scale. Improvements need to be carried out to develop and simulate the adsorption model on a large scale, investigating possible issues associated with the operational conditions. Several adsorption-desorption cycles need to be designed to test the potential of regeneration for the amine modified AC (highlighted as novel adsorbent) in pre- and post-combustion adsorption conditions. From these adaptations, it would then be possible to develop a model for integration to an IGCC power plant model, wherein the process efficiency and purity of CO_2 can be evaluated and optimised.

References

Abanades, J.C., Wiley, D.E., Mangano, E., Li, H., Ho, M.T., Mattisson, T., Brandani, S., Lyngfelt, A. and Arias, B. (2015) Emerging CO_2 capture systems. *International Journal of Greenhouse Gas Control*, 40: 126–166. doi:10.1016/j.ijggc.2015.04.018.

Abdelmoaty, Y.H., Tessema, T.-D., Norouzi, N., El-Kadri, O.M., Turner, J.B.M. and El-Kaderi, H.M. (2017) Effective Approach for Increasing the Heteroatom Doping Levels of Porous Carbons for Superior CO_2 Capture and Separation Performance. *ACS applied materials & interfaces*, 9 (41): 35802–35810. doi:10.1021/acsami.7b09989.

Abdullah, M.Z. and Qasim, A. (2016) Parametric Analysis of Carbon Dioxide Adsorption on Nanoporous Activated Carbon Using Computational Approach. *Procedia Engineering*, 148: 1416–1422. doi:10.1016/j.proeng.2016.06.626.

Abechi, S.E., Gimba, C.E., Uzairu, A. and Dallatu, Y.A. (2013a) Preparation and Characterization of Activated Carbon from Rubber-seed Shell by Chemical Activation. *J. Appl. Sci.*, 3 (7): 54–61.

Abechi, S.E., Gimba, C.E., Uzairu, A., Kagbu, J.A. and Ocholi, O.J. (2013b) Equilibrium Adsorption Studies Of Methylene Blue Onto Palm Kernel Shell-Based Activated Carbon. *International Refereed Journal of Engineering and Science (IRJES) ISSN (Online)*, 2 (5): 2319–183. doi:10.1378/chest.97.4.1010.

Adelodun, A.A., Ngila, J.C., Kim, D.G. and Jo, Y.M. (2016) Isotherm, thermodynamic and kinetic studies of selective CO_2 adsorption on chemically modified carbon surfaces. *Aerosol and Air Quality Research*, 16 (12): 3312–3329. doi:10.4209/aaqr.2016.01.0014.

Agarwal, A., Biegler, L.T. and Zitney, S.E. (2010) Superstructure-Based Optimal Synthesis of Pressure Swing Adsorption Cycles for Precombustion CO_2 Capture. *Industrial & Engineering Chemistry Research*, 49 (11): 5066–5079. doi:10.1021/ie900873j.

Ahn, H. and Brandani, S. (2005) Dynamics of Carbon Dioxide Breakthrough in a Carbon Monolith Over a Wide Concentration Range. *Adsorption*, 11 (1): 473–477. doi:10.1007/s10450-005-5970-z.

Ahn, S., You, Y.-W., Lee, D.-G., Kim, K.-H., Oh, M. and Lee, C.-H. (2012) Layered two- and four-bed PSA processes for H_2 recovery from coal gas. *Chemical Engineering Science*, 68 (1): 413–423. doi:https://doi.org/10.1016/j.ces.2011.09.053.

Aiken, R., Ditzel, K.H., Morra, F. and Wilson, D.S. (2004) Coal-Based integrated gasification combined cycle: market penetration strategies and recommendations. *Study prepared for DOE, NETL, GTC by Booz Allen Hamilton*.

Alhassan, M., Auta, M., Sabo, J., Umaru, M. and Kovo, A. (2016) CO_2 Capture Using Amine-impregnated Activated Carbon from Jatropha curcas Shell. *British Journal of Applied Science & Technology*, 14 (4): 1–11. doi:10.9734/BJAST/2016/24253.

Anderson, K. and Peters, G. (2016) The trouble with negative emissions. *Science*, 354 (6309): 182–183. doi:10.1126/science.aah4567.

AquaCache (2018) *Granular Activated Carbon (GAC) Mechanism for Chemical Adsorption*. Available at: http://aqua-cache.com/components/wpu (Accessed: 18 August 2018).

Arami-Niya, A., Daud, W.M.A.W. and Mjalli, F.S. (2010) Using granular activated carbon prepared from oil palm shell by $ZnCl_2$ and physical activation for methane adsorption. *Journal of Analytical and Applied Pyrolysis*, 89 (2): 197–203. doi:https://doi.org/10.1016/j.jaap.2010.08.006.

Bae, Y.S., Hauser, B.G., Farha, O.K., Hupp, J.T. and Snurr, R.Q. (2011) Enhancement of CO_2/CH_4 selectivity in metal-organic frameworks containing lithium cations. *Microporous and Mesoporous Materials*, 141 (1–3): 231–235. doi:10.1016/j.micromeso.2010.10.048.

Bai, B.C., Kim, E.A., Lee, C.W., Lee, Y.-S. and Im, J.S. (2015) Effects of surface chemical properties of activated carbon fibers modified by liquid oxidation for CO_2 adsorption. *Applied Surface Science*, 353: 158–164. doi:10.1016/j.apsusc.2015.06.046.

Bamdad, H., Hawboldt, K. and MacQuarrie, S. (2018) A review on common adsorbents for acid gases removal: Focus on biochar. *Renewable and Sustainable Energy Reviews*, 81 (June 2017): 1705–1720. doi:10.1016/j.rser.2017.05.261.

Bao, Z., Alnemrat, S., Yu, L., Vasiliev, I., Ren, Q., Lu, X. and Deng, S. (2011a) Kinetic separation of carbon dioxide and methane on a copper metal-organic framework. *Journal of colloid and interface science*, 357 (2): 504—509. doi:10.1016/j.jcis.2011.01.103.

Bao, Z., Yu, L., Ren, Q., Lu, X. and Deng, S. (2011b) Adsorption of CO_2 and CH_4 on a magnesium-based metal organic framework. *Journal of Colloid and Interface Science*, 353 (2): 549–556. doi:10.1016/j.jcis.2010.09.065.

Barros, M., Piekarski, C.M., Francisco, A.C. De and Grossa, P. (2018) *Carbon Footprint of Electricity Generation in Brazil : An Analysis of the 2016 – 2026 Period*., (June). doi:10.3390/en11061412.

Bastos-neto, M., Moeller, A., Staudt, R., Böhm, J. and Gläser, R. (2011) Dynamic bed measurements of CO adsorption on microporous adsorbents at high pressures for hydrogen purification processes. *Separation and Purification Technology*, 77 (2): 251–260. doi:10.1016/j.seppur.2010.12.015.

Belmabkhout, Y., Guillerm, V. and Eddaoudi, M. (2016) Low concentration CO_2 capture using physical adsorbents: Are metal–organic frameworks becoming the new benchmark materials? *Chemical Engineering Journal*, 296: 386–397.

Ben-Mansour, R., Habib, M. a., Bamidele, O.E., Basha, M., Qasem, N. a a, Peedikakkal, a., Laoui, T. and Ali, M. (2016) Carbon capture by physical adsorption: Materials, experimental investigations and numerical modeling and simulations - A review. *Applied Energy*, 161: 225–255. doi:10.1016/j.apenergy.2015.10.011.

Bezerra, D.P., Oliveira, R.S., Vieira, R.S., Cavalcante, C.L. and Azevedo, D.C.S. (2011)

Adsorption of CO_2 on nitrogen-enriched activated carbon and zeolite 13X. *Adsorption*, 17 (1): 235–246. doi:10.1007/s10450-011-9320-z.

Bezerra, D.P., Silva, F.W.M., Moura, P.A.S. De, Sapag, K., Vieira, R.S., Rodriguez-castellon, E. and Azevedo, D.C.S. De (2014) Adsorption of CO_2 on Amine-Grafted Activated Carbon. *Adsorption Science & Technology*, 32 (1): 141. doi:10.1260/0263-6174.32.2-3.141.

Biniak, S., Szymański, G., Siedlewski, J. and Świątkowski, A. (1997) The characterization of activated carbons with oxygen and nitrogen surface groups. *Carbon*, 35 (12): 1799–1810. doi:10.1016/S0008-6223(97)00096-1.

Biofuels Digest (2018) *Vivergo to cease production due to delays in E10*. Available at: https://www.biofuelsdigest.com/bdigest/2018/09/06/vivergo-to-cease-production-due-to-delays-in-e10/ (Accessed: 9 September 2018).

Bolster, C.H. and Hornberger, G.M. (2008) On the Use of Linearized Langmuir Equations. *Soil Science Society of America Journal*, 72 (6): 1848. doi:10.2136/sssaj2006.0304er.

Bonalumi, D., Lillia, S., Manzolini, G. and Grande, C. (2017) Innovative Process Cycle with Zeolite (MS13X) for Post Combustion Adsorption. *Energy Procedia*, 114 (November 2016): 2211–2218. doi:10.1016/j.egypro.2017.03.1358.

Bonenfant, D., Mimeault, M. and Hausler, R. (2003) Determination of the Structural Features of Distinct Amines Important for the Absorption of CO_2 and Regeneration in Aqueous Solution. *Industrial & Engineering Chemistry Research*, 42 (14): 3179–3184. doi:10.1021/ie020738k.

Boulinguiez, B., Le Cloirec, P. and Wolbert, D. (2008) Revisiting the Determination of Langmuir Parameters - Application to Tetrahydrothiophene Adsorption onto Activated Carbon. *Langmuir*, 24 (13): 6420–6424. doi:10.1021/la800725s.

Boyjoo, Y., Cheng, Y., Zhong, H., Tian, H., Pan, J., Pareek, V.K., Jiang, S.P., Lamonier, J.-F., Jaroniec, M. and Liu, J. (2017) From waste Coca Cola® to activated carbons with impressive capabilities for CO_2 adsorption and supercapacitors. *Carbon*, 116: 490–499.

Brdar, M., Šćiban, M., Takači, A. and Došenović, T. (2012) Comparison of two and three parameters adsorption isotherm for Cr(VI) onto Kraft lignin. *Chemical Engineering Journal*, 183: 108–111. doi:10.1016/j.cej.2011.12.036.

British Petroleum (2018) *Statistical Review of World Energy*.

Brunauer, S. (1944) *The adsorption of gases and vapours. Vol. 1, Physical adsorption.* London, UK: OUP. doi:https://doi.org/10.1021/ed021p52.1.

Brunauer, S., Emmett, P.H. and Teller, E. (1938) Adsorption of Gases in Multimolecular Layers. *Journal of the American Chemical Society*, 60 (2): 309–319. doi:10.1021/ja01269a023.

Buczek, B. (2016) *Preparation of activated carbon with different shape of particles and characterization of their properties*., 2016: 1–5.

Caldwell, S.J., Al-Duri, B., Sun, N., Sun, C.G., Snape, C.E., Li, K. and Wood, J. (2015) Carbon

dioxide separation from nitrogen/hydrogen mixtures over activated carbon beads: Adsorption isotherms and breakthrough studies. *Energy and Fuels*, 29 (6): 3796–3807. doi:10.1021/acs.energyfuels.5b00164.

Campbell, I.M. (1988) *Catalysis at surfaces*. 1st Ed. London, UK: Chapman and Hall Ltd.

Campbell, J.M. (1998) *Gas conditioning and processing*. 4th ed. Norman, Okla.: Campbell Petroleum Series. (Includes bibliographical references and indexes.v. 1. Phase behavior, physical properties, energy changes, vessel sizing, heat transfer and fluid flow.--v. 2. Absorption and fractionation; pumping, compressing, and expansion; refrigeration; hydrate inhibition, dehydration and process control.). Available at: file://catalog.hathitrust.org/Record/000105453.

Cansado, I.P.P., Mourão, P.A.M., Ribeiro Carrott, M.M.L. and Carrott, P.J.M. (2010) Activated Carbons Prepared from Natural and Synthetic Raw Materials with Potential Applications in Gas Separations. *Advanced Materials Research*, 107: 1–7. doi:10.4028/www.scientific.net/AMR.107.1.

Carberry, J.J. and Bretton, R.H. (1958) Axial dispersion of mass in flow through fixed beds. *AIChE Journal*, 4 (3): 367–375.

Carbon Brief (2015) *Paris 2015: Tracking country climate pledges*. Available at: https://www.carbonbrief.org/paris-2015-tracking-country-climate-pledges (Accessed: 6 September 2018).

Carpenter, S.M. and Long, H.A. (2017) *Integration of carbon capture in IGCC systems*. Elsevier Ltd. doi:10.1016/B978-0-08-100167-7.00036-6.

Casas, N., Schell, J., Pini, R. and Mazzotti, M. (2012) Fixed bed adsorption of CO_2/H_2 mixtures on activated carbon: Experiments and modeling. *Adsorption*, 18 (2): 143–161. doi:10.1007/s10450-012-9389-z.

Cavenati, S., Grande, C.A. and Rodrigues, A.E. (2004) Adsorption Equilibrium of Methane, Carbon Dioxide, and Nitrogen on Zeolite 13X at High Pressures. *Journal of Chemical & Engineering Data*, 49 (4): 1095–1101. doi:10.1021/je0498917.

Cen, P. and Yang, R.T. (1985) Separation of a Five-Component Gas Mixture by Pressure Swing Adsorption. *Separation Science and Technology*, 20 (9–10): 725–747. doi:10.1080/01496398508060701.

Chaffee, A.L., Knowles, G.P., Liang, Z., Zhang, J., Xiao, P. and Webley, P.A. (2007) CO_2 capture by adsorption: Materials and process development. *International Journal of Greenhouse Gas Control*, 1 (1): 11–18. doi:https://doi.org/10.1016/S1750-5836(07)00031-X.

Chahbani, M.H. and Tondeur, D. (2010) Predicting the final pressure in the equalization step of PSA cycles. *Separation and Purification Technology*, 71 (2): 225–232. doi:https://doi.org/10.1016/j.seppur.2009.11.027.

Chatti, R., Bansiwal, A.K., Thote, J.A., Kumar, V., Jadhav, P., Lokhande, S.K., Biniwale, R.B., Labhsetwar, N.K. and Rayalu, S.S. (2009) Amine loaded zeolites for carbon dioxide capture:

Amine loading and adsorption studies. *Microporous and Mesoporous Materials*, 121 (1): 84–89. doi:https://doi.org/10.1016/j.micromeso.2009.01.007.

Chen, C., Son, W.-J., You, K.-S., Ahn, J.-W. and Ahn, W.-S. (2010) Carbon dioxide capture using amine-impregnated HMS having textural mesoporosity. *Chemical Engineering Journal*, 161 (1): 46–52. doi:https://doi.org/10.1016/j.cej.2010.04.019.

Chen, L., Yong, S.Z. and Ghoniem, A.F. (2012) Oxy-fuel combustion of pulverized coal: Characterization, fundamentals, stabilization and CFD modeling. *Progress in Energy and Combustion Science*, 38 (2): 156–214. doi:https://doi.org/10.1016/j.pecs.2011.09.003.

Chen, X. (2015) *Modeling of Experimental Adsorption Isotherm Data*., pp. 14–22. doi:10.3390/info6010014.

Chen, Y., Huang, B., Huang, M. and Cai, B. (2011) On the preparation and characterization of activated carbon from mangosteen shell. *Journal of the Taiwan Institute of Chemical Engineers*, 42 (5): 837–842. doi:https://doi.org/10.1016/j.jtice.2011.01.007.

Chen, Z., Deng, S., Wei, H., Wang, B., Huang, J. and Yu, G. (2013) Activated carbons and amine-modified materials for carbon dioxide capture — a review. *Frontiers of Environmental Science & Engineering*, 7 (3): 326–340.

Chiang, Y.-C. and Juang, R.-S. (2016) Surface modifications of carbonaceous materials for carbon dioxide adsorption: A review. *Journal of the Taiwan Institute of Chemical Engineers*, 71: 214–234. doi:10.1016/j.jtice.2016.12.014.

China National Renewable Energy Centre and Energy Reform Institute (2018) *Energy Transition Trends 2018 - China, Europe, USA*. The Program Partners.

Chmiola, J., Largeot, C., Taberna, P.-L., Simon, P. and Gogotsi, Y. (2010) Monolithic carbide-derived carbon films for micro-supercapacitors. *Science (New York, N.Y.)*, 328 (5977): 480–483. doi:10.1126/science.1184126.

Choi, W., Min, K., Kim, C., Ko, Y.S., Jeon, J.W., Seo, H., Park, Y.-K. and Choi, M. (2016) Epoxide-functionalization of polyethyleneimine for synthesis of stable carbon dioxide adsorbent in temperature swing adsorption. *Nature Communications*, 7: 12640. Available at: http://dx.doi.org/10.1038/ncomms12640.

Climate Action (2019) *Carbon emissions in UK fall for sixth consecutive year*. Available at: http://www.climateaction.org/news/uks-carbon-emissions-fall-for-sixth-consecutive-year?utm_source=ActiveCampaign&utm_medium=email&utm_content=Carbon+emissions+in+UK+fall+for+sixth+consecutive+year+-+Climate+Action+News&utm_campaign=CA+Newsletter+5th+March (Accessed: 14 March 2019).

Climate Action Tracker (2018) *Countries Summary for Greenhouse Gas Mitigation Targets*. Available at: https://climateactiontracker.org/countries/eu/ (Accessed: 6 September 2018).

Coballasi, J., Yokota, J., Schwarz, M., Fullone, C. and Ferreira, V. (2018) *Industry Top Trends 2018 Utilities – Latin America*.

Cooney, D.O. (1999) *Adsorption Design for Wastewater treatment*. Florida, USA: Boca Raton, Fl.: Lewis Publishers.

Cormos, C.C. (2015) Assessment of chemical absorption/adsorption for post-combustion CO_2 capture from Natural Gas Combined Cycle (NGCC) power plants. *Applied Thermal Engineering*, 82: 120–128. doi:10.1016/j.applthermaleng.2015.02.054.

Cota, I. and Fernandez Martinez, F. (2017) Recent advances in the synthesis and applications of metal organic frameworks doped with ionic liquids for CO_2 adsorption. *Coordination Chemistry Reviews*, 351: 189–204.

Daifullah, A.A.M., Girgis, B.S. and Gad, H.M.H. (2003) Utilization of agro-residues (rice husk) in small waste water treatment plans. *Materials Letters*, 57 (11): 1723–1731. doi:10.1016/S0167-577X(02)01058-3.

Dantas, T.L.P., Amorim, S.M., Luna, F.M.T., Jr., I.J.S., de Azevedo, D.C.S., Rodrigues, A.E. and Moreira, R.F.P.M. (2009) Adsorption of Carbon Dioxide onto Activated Carbon and Nitrogen-Enriched Activated Carbon: Surface Changes, Equilibrium, and Modeling of Fixed-Bed Adsorption. *Separation Science and Technology*, 45 (1): 73–84. doi:10.1080/01496390903401762.

Dantas, T.L.P., Rodrigues, A.E. and Moreira, R.F.P.M. (2012) "Separation of Carbon Dioxide from Flue Gas Using Adsorption on Porous Solids." In *Greenhouse Gases – Capturing, Utilization and Reduction*. Rijeka, Croatia: InTech. pp. 57–80. doi:10.13140/2.1.2092.6404.

Darunte, L.A.., Walton, K.S.., Sholl, D.S.. and Jones, C.W. (2016) CO_2 capture via adsorption in amine-functionalized sorbents. *Current Opinion in Chemical Engineering*, 12: 82–90. doi:10.1016/j.coche.2016.03.002.

Das, D. and Meikap, B.C. (2018) Comparison of adsorption capacity of mono-ethanolamine and di-ethanolamine impregnated activated carbon in a multi-staged fluidized bed reactor for carbon-dioxide capture. *Fuel*, 224 (March): 47–56. doi:10.1016/j.fuel.2018.03.090.

Das, D., Samal, D.P. and BC, M. (2015) Preparation of Activated Carbon from Green Coconut Shell and its Characterization. *Journal of Chemical Engineering & Process Technology*, 06 (05). doi:10.4172/2157-7048.1000248.

Delgado, J.A., Uguina, M.A., Gómez, J.M. and Ortega, L. (2006) Adsorption equilibrium of carbon dioxide, methane and nitrogen onto Na- and H-mordenite at high pressures. *Separation and Purification Technology*, 48 (3): 223–228. doi:https://doi.org/10.1016/j.seppur.2005.07.027.

Delgado, J.A., Uguina, M.A., Sotelo, J.L., Ruíz, B. and Rosário, M. (2007) Carbon Dioxide/Methane Separation by Adsorption on Sepiolite. *Journal of Natural Gas Chemistry*, 16 (3): 235–243. doi:https://doi.org/10.1016/S1003-9953(07)60054-1.

Delgado, J.M.P.Q. (2006) A critical review of dispersion in packed beds. *Heat and Mass Transfer/Waerme- und Stoffuebertragung*, 42 (4): 279–310. doi:10.1007/s00231-005-0019-0.

Delle Site, A. (2001) Factors Affecting Sorption of Organic Compounds in Natural

Sorbent/Water Systems and Sorption Coefficients for Selected Pollutants. A Review. *Journal of Physical and Chemical Reference Data*, 30 (1): 187–439. doi:10.1063/1.1347984.

Deng, S., Hu, B., Chen, T., Wang, B., Huang, J., Wang, Y. and Yu, G. (2015) Activated carbons prepared from peanut shell and sunflower seed shell for high CO_2 adsorption. *Adsorption*, 21: 125–133.

DOE/NETL (2009) *Carbon Capture R&D Program for Existing Coal-Fired Power Plants*.

DOE/NETL (2013) *Advanced Carbon Dioxide Capture R&D Program: Technology Update*. Pittsburgh, PA. Available at: http://www.netl.doe.gov/File Library/Research/Coal/carbon capture/handbook/CO2-Capture-Tech-Update-2013.pdf.

Dortmundt, D. and Doshi, K. (1999) *Recent Developments in CO_2 Removal Membrane Technology*. Des Plaines, Illinois, USA.

Dowling, A.W., Vetukuri, S.R.R. and Biegler, L.T. (2012) Large-Scale Optimization Strategies for Pressure Swing Adsorption Cycle Synthesis. *AIChE Journal*, 58 (12): 3777–3791. doi:10.1002/aic.13928.

Dowson, G.R.M., Reed, D.G., Bellas, J.M., Charalambous, C. and Styring, P. (2016) Fast and selective separation of carbon dioxide from dilute streams by pressure swing adsorption using solid ionic liquids. *Faraday Discussions*, 192: 511–527. doi:10.1039/c6fd00035e.

Dreisbach, F., Staudt, R. and Keller, J.U. (1999) High Pressure Adsorption Data of Methane, Nitrogen, Carbon Dioxide and their Binary and Ternary Mixtures on Activated Carbon. *Adsorption*, 5 (3): 215–227. doi:10.1023/A:1008914703884.

Drese, J.H., Choi, S., Lively, R.P., Koros, W.J., Fauth, D.J., Gray, M.L. and Jones, C.W. (2009) Synthesis–Structure–Property Relationships for Hyperbranched Aminosilica CO_2 Adsorbents. *Advanced Functional Materials*, 19 (23): 3821–3832.

Dutcher, B., Fan, M. and Russell, A.G. (2015) Amine-Based CO_2 Capture Technology Development from the Beginning of 2013—A Review. *ACS Applied Materials & Interfaces*, 7 (4): 2137–2148. doi:10.1021/am507465f.

El-Hendawy, A.-N.A., Alexander, A.J., Andrews, R.J. and Forrest, G. (2008) Effects of activation schemes on porous, surface and thermal properties of activated carbons prepared from cotton stalks. *Journal of Analytical and Applied Pyrolysis*, 82 (2): 272–278. doi:https://doi.org/10.1016/j.jaap.2008.04.006.

Esteves, I.A.A.C., Lopes, M.S.S., Nunes, P.M.C. and Mota, J.P.B. (2008) Adsorption of natural gas and biogas components on activated carbon. *Separation and Purification Technology*, 62 (2): 281–296. doi:10.1016/j.seppur.2008.01.027.

European Commission (2016) *Report from the commission to the European Parliament and the Council*. Sweden: European Commission.

European Commission (2018) *Share of renewables in energy consumption in the EU reached 17% in 2016*. Luxembourg, Belgium.

Eurostat (2018) *Smarter, greener, more inclusive? Indicators to support the Europe 2020 strategy*. 2017 ed. Union, E. (ed.). Luxembourg: Publications Office of the European Union. doi:10.2785/092296.

Eze, J. and Agbo, K. (2010) *Maximizing the potentials of biogas through upgrading*. doi:10.5251/ajsir.2010.1.3.604.609.

Fan, X., Zhang, L., Zhang, G., Shu, Z. and Shi, J. (2013) Chitosan derived nitrogen-doped microporous carbons for high performance CO_2 capture. *Carbon*, 61: 423–430. Available at: http://search.proquest.com/docview/1671406886/.

Farooq, S. and Ruthven, D.M. (1990a) Heat effects in adsorption column dynamics. 1. Comparison of one- and two-dimensional models. *Industrial & Engineering Chemistry Research*, 29 (6): 1076–1084. doi:10.1021/ie00102a019.

Farooq, S. and Ruthven, D.M. (1990b) Heat effects in adsorption column dynamics. 2. Experimental validation of the one-dimensional model. *Industrial & Engineering Chemistry Research*, 29 (6): 1084–1090. doi:10.1021/ie00102a020.

Fauth, D.J., Filburn, T.P., Gray, M.L., Hedges, S.W., Hoffman, J.S. and Pennline, H.W. (2007) Development of novel CO_2 adsorbents for capture of CO_2 from flue gas. *100th Annual Conference and Exhibition of the Air and Waste Management Association 2007, ACE 2007*, 5: 3552–3564. doi:10.1016/j.lithos.2009.06.037.

Febrianto, J., Kosasih, A.N., Sunarso, J., Ju, Y.-H., Indraswati, N. and Ismadji, S. (2009) Equilibrium and kinetic studies in adsorption of heavy metals using biosorbent: A summary of recent studies. *Journal of Hazardous Materials*, 162 (2): 616–645. doi:https://doi.org/10.1016/j.jhazmat.2008.06.042.

Figueroa, J.D., Fout, T., Plasynski, S., McIlvried, H. and Srivastava, R.D. (2008) Advances in CO_2 capture technology-The U.S. Department of Energy's Carbon Sequestration Program. *International Journal of Greenhouse Gas Control*, 2 (1): 9–20. doi:10.1016/S1750-5836(07)00094-1.

Financial Times (2015) *UK bioethanol sector struggles to fuel growth*. Available at: https://www.ft.com/content/5ac7eaf4-1da9-11e5-ab0f-6bb9974f25d0 (Accessed: 9 September 2018).

Franchi, R.S., Harlick, P.J.E. and Sayari, A. (2005) Applications of Pore-Expanded Mesoporous Silica. 2. Development of a High-Capacity, Water-Tolerant Adsorbent for CO_2. *Industrial & Engineering Chemistry Research*, 44 (21): 8007–8013. doi:10.1021/ie0504194.

Furukawa, H., Cordova, K.E., O'Keeffe, M. and Yaghi, O.M. (2013) The Chemistry and Applications of Metal-Organic Frameworks. *Science (AAAS)*, 341 (6149): 1230444. doi:10.1126/science.1230444.

Gabrielsen, J., Michelsen, M.L., Stenby, E.H. and Kontogeorgis, G.M. (2005) A Model for Estimating CO_2 Solubility in Aqueous Alkanolamines. *Industrial & Engineering Chemistry Research*, 44 (9): 3348–3354. doi:10.1021/ie048857i.

Gaeini, M., Zondag, H.A. and Rindt, C.C.M. (2016) Effect of kinetics on the thermal performance of a sorption heat storage reactor. *Applied Thermal Engineering*, 102: 520–531. doi:10.1016/j.applthermaleng.2016.03.055.

Gangupomu, R.H., Sattler, M.L. and Ramirez, D. (2016) Comparative study of carbon nanotubes and granular activated carbon: Physicochemical properties and adsorption capacities. *Journal of Hazardous Materials*, 302: 362–374. doi:10.1016/j.jhazmat.2015.09.002.

Gao, Y., Yue, Q., Gao, B., Sun, Y., Wang, W., Li, Q. and Wang, Y. (2013) Comparisons of porous, surface chemistry and adsorption properties of carbon derived from Enteromorpha prolifera activated by $H_4P_2O_7$ and KOH. *Chemical Engineering Journal*, 232: 582–590. doi:https://doi.org/10.1016/j.cej.2013.08.011.

García, S., Pis, J.J., Rubiera, F. and Pevida, C. (2013) Predicting mixed-gas adsorption equilibria on activated carbon for precombustion CO_2 capture. *Langmuir*, 29 (20): 6042–6052. doi:10.1021/la4004998.

Gholidoust, A., Atkinson, J.D. and Hashisho, Z. (2017) *Enhancing CO_2 Adsorption via Amine-Impregnated Activated Carbon from Oil Sands Coke*. doi:10.1021/acs.energyfuels.6b02800.

Girgis, B.S., Temerk, Y.M., Gadelrab, M.M. and Abdullah, I.D. (2007) X-ray Diffraction Patterns of Activated Carbons Prepared under Various Conditions. *Carbon Letters*, 8 (2): 95–100. doi:10.5714/CL.2007.8.2.095.

Global CCS Institute (2017) *Paris climate change targets cannot be met without CCS: COP23*. Bonn, Germany. Available at: https://www.globalccsinstitute.com/sites/www.globalccsinstitute.com/files/content/mediarelease/123543/files/global-status-ccs-2017.pdf.

Global CCS Institute (2018) *CO_2 Capture and Separation*. Available at: https://hub.globalccsinstitute.com/publications/brazilian-atlas-co2-capture-and-geological-storage/co2-capture-and-separation (Accessed: 24 August 2018).

Goeppert, A., Zhang, H., Sen, R., Dang, H. and Prakash, G.K.S. (2019) Oxidation-Resistant, Cost-Effective Epoxide-Modified Polyamine Adsorbents for CO_2 Capture from Various Sources Including Air. *ChemSusChem*, 12 (8): 1712–1723. doi:10.1002/cssc.201802978.

Gomes, V.G. and Yee, K.W.K. (2002) Pressure swing adsorption for carbon dioxide sequestration from exhaust gases. *Separation and Purification Technology*, 28 (2): 161–171. doi:https://doi.org/10.1016/S1383-5866(02)00064-3.

Grande, C.A. (2012) Advances in Pressure Swing Adsorption for Gas Separation. *ISRN Chemical Engineering*, 2012: 1–13. doi:10.5402/2012/982934.

Grande, C.A., Roussanaly, S., Anantharaman, R., Lindqvist, K., Singh, P. and Kemper, J. (2017) CO_2 Capture in Natural Gas Production by Adsorption Processes. *Energy Procedia*, 114 (November 2016): 2259–2264. doi:10.1016/j.egypro.2017.03.1363.

Gray, M.L., Champagne, K.J., Fauth, D., Baltrus, J.P. and Pennline, H. (2008) Performance of immobilized tertiary amine solid sorbents for the capture of carbon dioxide. *International*

Journal of Greenhouse Gas Control, 2 (1): 3–8. doi:10.1016/S1750-5836(07)00088-6.

Gregg, S.J. and Sing, K.S.. (1982) *Adsorption, surface area and porosity.* London - UK: Academic Press Inc. (London) Ltd.

Gunn, D.J. (1987) Axial and radial dispersion in fixed beds. *Chemical Engineering Science*, 42 (2): 363–373.

Guo, L., Yang, J., Hu, G., Hu, X., Wang, L., Dong, Y., Dacosta, H. and Fan, M. (2016) Role of Hydrogen Peroxide Preoxidizing on CO_2 Adsorption of Nitrogen-Doped Carbons Produced from Coconut Shell. *ACS Sustainable Chemistry & Engineering*, 4 (5): 2806–2813.

Hahn, M.W., Jelic, J., Berger, E., Reuter, K., Jentys, A. and Lercher, J.A. (2016) Role of Amine Functionality for CO_2 Chemisorption on Silica. *The Journal of Physical Chemistry B*, 120 (8): 1988–1995. doi:10.1021/acs.jpcb.5b10012.

Hahn, M.W., Steib, M., Jentys, A. and Lercher, J.A. (2015) Mechanism and Kinetics of CO_2 Adsorption on Surface Bonded Amines. *The Journal of Physical Chemistry C*, 119 (8): 4126–4135. doi:10.1021/jp512001t.

Hammond, G.P. and Spargo, J. (2014) The prospects for coal-fired power plants with carbon capture and storage: A UK perspective. *Energy Conversion and Management*, 86: 476–489. doi:10.1016/j.enconman.2014.05.030.

Hao, G.-P., Li, W.-C. and Lu, A.-H. (2011) Novel porous solids for carbon dioxide capture. *Journal of Materials Chemistry*, 21 (18): 6447. doi:10.1039/c0jm03564e.

Hao, P., Shi, Y., Li, S., Zhu, X. and Cai, N. (2018) Correlations between adsorbent characteristics and the performance of pressure swing adsorption separation process. *Fuel*, 230 (April): 9–17. doi:10.1016/j.fuel.2018.05.030.

Hao, W., Björnerbäck, F., Trushkina, Y., Bengoechea, M.O., Salazar-Alvarez, G., Barth, T. and Hedin, N. (2017) High-performance Magnetic Activated Carbon from Solid Waste from Lignin Conversion Processes. Part I: Their Use as Adsorbents for CO_2. *Energy Procedia*, 114: 6272–6296.

Hasib-ur-Rahman, M., Siaj, M. and Larachi, F. (2012) CO_2 capture in alkanolamine/room-temperature ionic liquid emulsions: A viable approach with carbamate crystallization and curbed corrosion behavior. *International Journal of Greenhouse Gas Control*, 6: 246–252. doi:10.1016/j.ijggc.2011.10.014.

Hedberg, A. (2017) *Germany's energy transition: making it deliver. EPC Discussion Paper*. Brussels, Belgium.

Hedin, N., Andersson, L., Bergström, L. and Yan, J. (2013) Adsorbents for the post-combustion capture of CO_2 using rapid temperature swing or vacuum swing adsorption. *Applied Energy*, 104: 418–433. doi:10.1016/j.apenergy.2012.11.034.

Heidari, A., Younesi, H., Rashidi, A. and Ghoreyshi, A.A. (2014) Adsorptive removal of CO_2 on highly microporous activated carbons prepared from Eucalyptus camaldulensis wood: Effect

of chemical activation. *Journal of the Taiwan Institute of Chemical Engineers*, 45 (2): 579–588. doi:10.1016/j.jtice.2013.06.007.

Henley, E.J. (2011) *Separation Process Principles*. 3rd ed. Roper, D.K. and Seader, J.D. (eds.). Hoboken, N.J. : Wiley, c2011.

Hesas, R.H., Arami-Niya, A., Daud, W.M.A.W. and Sahu, J.N. (2013) Preparation and Characterization of Activated Carbon from Apple Waste by Microwave-Assisted Phosphoric Acid Activation: Application in Methylene Blue Adsorption. *BioResouces.com*, 8 (2): 2950–2966. doi:10.1016/j.jct.2012.11.031.

Hicks, J.C., Drese, J.H., Fauth, D.J., Gray, M.L., Qi, G.G. and Jones, C.W. (2008) Designing adsorbents for CO_2 capture from flue gas-hyperbranched aminosilicas capable of capturing CO_2 reversibly. *Journal of the American Chemical Society*, 130 (10).

Himeno, S., Komatsu, T. and Fujita, S. (2005) High-Pressure Adsorption Equilibria of Methane and Carbon Dioxide on Several Activated Carbons. *Journal of Chemical & Engineering Data*, 50 (2): 369–376. doi:10.1021/je049786x.

Hiyoshi, N., Yogo, K. and Yashima, T. (2005) Adsorption characteristics of carbon dioxide on organically functionalized SBA-15. *Microporous and Mesoporous Materials*, 84 (1–3): 357–365. doi:10.1016/j.micromeso.2005.06.010.

Hsu, L.-Y. and Teng, H. (2000) Influence of different chemical reagents on the preparation of activated carbons from bituminous coal. *Fuel processing technology*, 64 (1): 155–166. doi:10.1016/S0378-3820(00)00071-0.

Huang, H.Y., Yang, R.T., Chinn, D. and Munson, C.L. (2003) Amine-Grafted MCM-48 and Silica Xerogel as Superior Sorbents for Acidic Gas Removal from Natural Gas. *Industrial & Engineering Chemistry Research*, 42 (12): 2427–2433. doi:10.1021/ie020440u.

Huang, I.-S., Li, J.-J. and Tsai, M.-K. (2017) Solvation Dynamics of $CO_{2(g)}$ by Monoethanolamine at the Gas–Liquid Interface: A Molecular Mechanics Approach. *Molecules*, 22 (1). doi:10.3390/molecules22010008.

Huang, Y. and Shih, M. (2016) Effect of linearized expressions of Langmuir equations on the prediction of the adsorption of methylene blue on rice husk. *International Journal of Scientific and Research Publications*, 6 (4): 549–554.

Hui, T.S. and Zaini, M.A.A. (2015) Potassium hydroxide activation of activated carbon: a commentary. *Carbon letters*, 16 (4): 275–280. doi:10.5714/CL.2015.16.4.275.

Hunsom, M. and Autthanit, C. (2013) Adsorptive purification of crude glycerol by sewage sludge-derived activated carbon prepared by chemical activation with H_3PO_4, K_2CO_3 and KOH. *Chemical Engineering Journal*, 229: 334–343. doi:https://doi.org/10.1016/j.cej.2013.05.120.

Ibrahim, D.M., El-Hemaly, S.A. and Abdel-Kerim, F.M. (1980) Study of rice-husk ash silica by infrared spectroscopy. *Thermochimica Acta*, 37 (3): 307–314. doi:10.1016/0040-6031(80)87160-7.

International Hydropower Association (2017) *Hydropower Status Report*. London - UK.

IPCC (2018) *Summary for Policymarkers. Global Warming of 1.5ºC.* Paris, France.

Ishizaki, C. and Martí, I. (1981) Surface oxide structures on a commercial activated carbon. *Carbon*, 19 (6): 409–412. doi:10.1016/0008-6223(81)90023-3.

Jansen, D., Gazzani, M., Manzolini, G., Dijk, E. Van and Carbo, M. (2015) Pre-combustion CO_2 capture. *International Journal of Greenhouse Gas Control*, 40: 167–187. doi:10.1016/j.ijggc.2015.05.028.

Ji, Y., Li, T., Zhu, L., Wang, X. and Lin, Q. (2007) Preparation of activated carbons by microwave heating KOH activation. *Applied Surface Science*, 254 (2): 506–512. doi:https://doi.org/10.1016/j.apsusc.2007.06.034.

Jung, H., Jeon, S., Jo, D.H., Huh, J. and Kim, S.H. (2017) Effect of crosslinking on the CO_2 adsorption of polyethyleneimine-impregnated sorbents. *Chemical Engineering Journal*, 307: 836–844. doi:https://doi.org/10.1016/j.cej.2016.09.005.

Jung, W., Park, J. and Lee, K.S. (2018) Kinetic modeling of CO_2 adsorption on an amine-functionalized solid sorbent. *Chemical Engineering Science*, 177: 122–131.

Kalderis, D., Bethanis, S., Paraskeva, P. and Diamadopoulos, E. (2008) Production of activated carbon from bagasse and rice husk by a single-stage chemical activation method at low retention times. *Bioresource Technology*, 99 (15): 6809–6816.

Kapdi, S., Vijay, V.K., S Kempegowda, R. and Prasad, R. (2005) *Biogas Scrubbing, Compression and Storage: Perspective and Prospectus in Indian Context*. doi:10.1016/j.renene.2004.09.012.

Katesa, J., Junpiromand, S. and Tangsathitkulchai, C. (2013) Effect of Carbonization Temperature On Properties of Char And Activated Carbon From Coconut Shell. *Suranaree Journal of Science and Technology*, 20 (4): 269–278.

Kenarsari, S.D., Yang, D., Jiang, G., Zhang, S., Wang, J., Russell, A.G., Wei, Q. and Fan, M. (2013) Review of recent advances in carbon dioxide separation and capture. *RSC Advances*, 3 (45): 22739. doi:10.1039/c3ra43965h.

Kennedy, L.J., Vijaya, J.J., Kayalvizhi, K. and Sekaran, G. (2007) Adsorption of phenol from aqueous solutions using mesoporous carbon prepared by two-stage process. *Chemical Engineering Journal*, 132 (1): 279–287. doi:https://doi.org/10.1016/j.cej.2007.01.009.

Ketzer, J.M.M., Machado, C.X., Rockett, G.C. and Iglesias, R.S. (2014) *Brazilian Atlas of CO_2 Capture and Geological Storage*. Porto Alegre, RS. Brazil.

Khalil, S.H., Aroua, M.K. and Daud, W.M.A.W. (2012) Study on the improvement of the capacity of amine-impregnated commercial activated carbon beds for CO_2 adsorbing. *Chemical Engineering Journal*, 183: 15–20. doi:10.1016/j.cej.2011.12.011.

Kitagawa, S. (2017) Future Porous Materials. *Accounts of Chemical Research*, 50 (3): 514–

516. doi:10.1021/acs.accounts.6b00500.

Knox, J.C., Ebner, A.D., Levan, M.D., Coker, R.F. and Ritter, J.A. (2016) Limitations of Breakthrough Curve Analysis in Fixed-Bed Adsorption. *Industrial and Engineering Chemistry Research*. doi:10.1021/acs.iecr.6b00516.

Ko, D., Siriwardane, R. and Biegler, L.T. (2003) Optimization of a pressure-swing adsorption process using zeolite 13X for CO_2 sequestration. *Industrial & Engineering Chemistry Research*, 42 (2): 339–348. doi:Doi 10.1021/Ie0204540.

Kohl, A.L. and Nielsen, R.B. (1997) *Gas Purification*. 5th ed. Houston, TX. USA: Gulf Professional Publishing. doi:10.1016/B978-088415220-0/50009-4.

Kongnoo, A., Intharapat, P., Worathanakul, P. and Phalakornkule, C. (2016) Diethanolamine impregnated palm shell activated carbon for CO_2 adsorption at elevated temperatures. *Journal of Environmental Chemical Engineering*, 4 (1): 73–81. doi:10.1016/j.jece.2015.11.015.

Kumar, K.V. (2006) Comparative analysis of linear and non-linear method of estimating the sorption isotherm parameters for malachite green onto activated carbon. *Journal of Hazardous Materials*, 136 (2): 197–202. doi:https://doi.org/10.1016/j.jhazmat.2005.09.018.

Kumar, M. and Gupta, R.C. (1994) Influence of carbonization conditions on the gasification of acacia and eucalyptus wood chars by carbon dioxide. *Fuel*, 73 (12): 1922–1925. doi:https://doi.org/10.1016/0016-2361(94)90223-2.

Langmuir, I. (1916) The Constitution and Fundamental Properties of Solids and Liquids. Part I. Solids. *Journal of the American Chemical Society*, 38 (11): 2221–2295. doi:10.1021/ja02268a002.

Langmuir, I. (1917) American Society. *Journal of the American Chemical Society*, XXXVIII (1916): 1916–1918.

Lee, C.S., Ong, Y.L., Aroua, M.K. and Daud, W.M.A.W. (2013) Impregnation of palm shell-based activated carbon with sterically hindered amines for CO_2 adsorption. *Chemical Engineering Journal*, 219: 558–564. doi:10.1016/j.cej.2012.10.064.

Lee, H.-H., Lee, J.-C., Joo, Y.-J., Oh, M. and Lee, C.-H. (2014a) Dynamic modeling of Shell entrained flow gasifier in an integrated gasification combined cycle process. *Applied Energy*, 131: 425–440. doi:https://doi.org/10.1016/j.apenergy.2014.06.044.

Lee, J.C., Lee, H.H., Joo, Y.J., Lee, C.H. and Oh, M. (2014b) Process simulation and thermodynamic analysis of an IGCC (integrated gasification combined cycle) plant with an entrained coal gasifier. *Energy*, 64: 58–68. doi:https://doi.org/10.1016/j.energy.2013.11.069.

Lei, M., Vallieres, C., Grevillot, G. and Latifi, M. a. (2013) Thermal swing adsorption process for carbon dioxide capture and recovery: Modeling, simulation, parameters estimability, and identification. *Industrial and Engineering Chemistry Research*, 52 (22): 7526–7533. doi:10.1021/ie3029152.

Lendzion-Bieluń, Z., Czekajło, Sibera, D., Moszyński, D., Sreńscek-Nazzal, J., Morawski,

A.W., Wrobel, R.J., Michalkiewicz, B., Arabczyk, W. and Narkiewicz, U. (2018) Surface characteristics of KOH-treated commercial carbons applied for CO_2 adsorption. *Adsorption Science and Technology*, 36 (1–2): 478–492. doi:10.1177/0263617417704527.

Leung, D.Y.C., Caramanna, G. and Maroto-Valer, M.M. (2014) An overview of current status of carbon dioxide capture and storage technologies. *Renewable and Sustainable Energy Reviews*, 39: 426–443. doi:https://doi.org/10.1016/j.rser.2014.07.093.

Li, J. and Hitch, M. (2015) Carbon Dioxide Sorption Isotherm Study on Pristine and Acid-Treated Olivine and Its Application in the Vacuum Swing Adsorption Process. *Minerals*, 5 (2): 259–275. doi:10.3390/min5020259.

Lin, K.-Y.A. and Park, A.-H.A. (2011) Effects of Bonding Types and Functional Groups on CO_2 Capture using Novel Multiphase Systems of Liquid-like Nanoparticle Organic Hybrid Materials. *Environmental Science & Technology*, 45 (15): 6633–6639. doi:10.1021/es200146g.

Ling, J., Ntiamoah, A., Xiao, P., Webley, P. a. and Zhai, Y. (2015) Effects of feed gas concentration, temperature and process parameters on vacuum swing adsorption performance for CO_2 capture. *Chemical Engineering Journal*, 265: 47–57. doi:10.1016/j.cej.2014.11.121.

Liu, H., Liu, B., Lin, L.C., Chen, G., Wu, Y., Wang, J., Gao, X., Lv, Y., Pan, Y., Zhang, X., et al. (2014) A hybrid absorption-adsorption method to efficiently capture carbon. *Nature Communications*, 5: 1–7. doi:10.1038/ncomms6147.

Liu, L., Deng, Q.-F., Hou, X.-X. and Yuan, Z.-Y. (2012) User-friendly synthesis of nitrogen-containing polymer and microporous carbon spheres for efficient CO_2 capture. *Journal of Materials Chemistry*, 22 (31): 15540–15548. doi:10.1039/C2JM31441J.

Lockwood, T. (2017) A compararitive review of next-generation carbon capture technologies for coal-fired power plant. *Energy Procedia*, 114 (November 2016): 2658–2670. doi:10.1016/j.egypro.2017.03.1850.

Lowell, S.S., Shields, J.E., Thomas, M. and Thommes, M. (2006) *Characterization of Porous Solids and Powders: Surface Area, Pore Size and Density*., 1. doi:10.1007/978-1-4020-2303-3.

Ma, X., Wang, X. and Song, C. (2009) "Molecular Basket" Sorbents for Separation of CO_2 and H_2S from Various Gas Streams. *Journal of the American Chemical Society*, 131 (16): 5777–5783. doi:10.1021/ja8074105.

Maring, B.J. and Webley, P.A. (2013) A new simplified pressure/vacuum swing adsorption model for rapid adsorbent screening for CO_2 capture applications. *International Journal of Greenhouse Gas Control*, 15: 16–31. doi:10.1016/j.ijggc.2013.01.009.

Maroto-Valer, M.M., Tang, Z. and Zhang, Y. (2005) CO_2 capture by activated and impregnated anthracites. *Fuel Processing Technology*, 86 (14): 1487–1502.

Marsh, H. and Rodríguez-Reinoso, F. (2006) *Characterization of Activated Carbon*. Elsevier Science & Technology Books (Augst 2006). doi:10.1016/B978-008044463-5/50018-2.

Masel, R.I. (1996) Principles of adsorption and reaction on solid surfaces. *Wiley series in chemical engineering*, pp. xiv, 804 p. Available at: http://cds.cern.ch/record/643993/files/0471303925_TOC.pdf.

Mason, J. a., McDonald, T.M., Bae, T.H., Bachman, J.E., Sumida, K., Dutton, J.J., Kaye, S.S. and Long, J.R. (2015) Application of a High-Throughput Analyzer in Evaluating Solid Adsorbents for Post-Combustion Carbon Capture via Multicomponent Adsorption of CO_2, N_2, and H_2O. *Journal of the American Chemical Society*, 137 (14): 4787–4803. doi:10.1021/jacs.5b00838.

McKay, G. (1995) *Use of Adsorbents for the Removal of Pollutants from Wastewater*. 1st ed. Boca Raton, Florida. USA: CRC Press.

Ministry of Mines and Energy of Brazil (2017) *Decennial Energy Expansion Plan*. Brasilia - Federal District.

Molina-Sabio, M., RodRíguez-Reinoso, F., Caturla, F. and Sellés, M.J. (1995) Porosity in granular carbons activated with phosphoric acid. *Carbon*, 33 (8): 1105–1113. doi:https://doi.org/10.1016/0008-6223(95)00059-M.

Möller, A., Eschrich, R., Reichenbach, C., Guderian, J., Lange, M. and Möllmer, J. (2017) Dynamic and equilibrium-based investigations of CO_2-removal from CH_4-rich gas mixtures on microporous adsorbents. *Adsorption*, 23 (2): 197–209. doi:10.1007/s10450-016-9821-x.

Montagnaro, F., Silvestre-Albero, A., Silvestre-Albero, J., Rodríguez-Reinoso, F., Erto, A., Lancia, A. and Balsamo, M. (2015) Post-combustion CO_2 adsorption on activated carbons with different textural properties. *Microporous and Mesoporous Materials*, 209: 157–164. doi:10.1016/j.micromeso.2014.09.037.

Moon, D., Park, Y., Oh, H., Kim, S., Oh, M. and Lee, C. (2018) Performance analysis of an eight-layered bed PSA process for H_2 recovery from IGCC with pre-combustion carbon capture. *Energy Conversion and Management*, 156 (July 2017): 202–214. doi:10.1016/j.enconman.2017.11.013.

Morais, E.D. de (2014) Produção do carvão ativado a partirdo mesocarpo do coco - da - baía(cocos nucifera linn) utilizando H_3PO_4, CH_3COONa e KOH como ativantes. *Biblioteca Setorial "Professor Horácio Nícolás Sólimo"*., p. 70. doi:661.183(043.3).

Moreira, J.R., Romeiro, V., Fuss, S., Kraxner, F. and Pacca, S.A. (2016) BECCS potential in Brazil: Achieving negative emissions in ethanol and electricity production based on sugar cane bagasse and other residues. *Applied Energy*, 179: 55–63. doi:https://doi.org/10.1016/j.apenergy.2016.06.044.

Mulgundmath, V.P., Tezel, F.H., Jones, R.A. and Thibault, J. (2012) Fixed bed adsorption for the removal of carbon dioxide from nitrogen: Breakthrough behaviour and modelling for heat and mass transfer. *Separation and Purification Technology*, 85: 17–27. doi:10.1016/j.seppur.2011.07.038.

Muniandy, L., Adam, F., Mohamed, A.R. and Ng, E.-P. (2014) The synthesis and characterization of high purity mixed microporous/mesoporous activated carbon from rice husk

using chemical activation with NaOH and KOH. *Microporous and Mesoporous Materials*, 197: 316–323. doi:https://doi.org/10.1016/j.micromeso.2014.06.020.

NASA (2019) *Carbon Dioxide Measurement*. Available at: https://climate.nasa.gov/vital-signs/carbon-dioxide/ (Accessed: 13 June 2019).

Nascimento, R.F., Lima, A.C.A. de, Vidal, C.B., Melo, D. de Q. and Raulino, G.S.C. (2014) *Adsorção: aspectos teóricos e aplicações ambientais.* 1st ed. Fortaleza, CE: Impresa Universitária da Universidade Federal do Ceará (UFC).

NETZSCH (2019) *Thermogravimetric Analysis*. Available at: https://www.netzsch-thermal-analysis.com/en/products-solutions/thermogravimetric-analysis/tg-209-f1-libra/ (Accessed: 25 June 2019).

Nik, O.G., Nohair, B. and Kaliaguine, S. (2011) Aminosilanes grafting on FAU/EMT zeolite: Effect on CO_2 adsorptive properties. *Microporous and Mesoporous Materials*, 143 (1): 221–229. doi:10.1016/j.micromeso.2011.03.002.

Nikolaidis, G.N., Georgiadis, M.C., Kikkinides, E.S. and Konstantinidis, D. (2014) *Modelling of Pressure Swing Adsorption (PSA) Processes for post-combustion Carbon Dioxide (CO_2) capture from flue gas*. Elsevier. doi:10.1016/B978-0-444-63578-5.50043-8.

Nikolaidis, G.N., Kikkinides, E.S. and Georgiadis, M.C. (2017) Modelling, Simulation and Optimisation of an Integrated Two-Stage P/VSA Process for Post-Combustion CO_2 Capture Using Combinations of Adsorbents. *Computer Aided Chemical Engineering*, 40 (2015): 2647–2652. doi:10.1016/B978-0-444-63965-3.50443-8.

Nwaoha, C., Supap, T., Idem, R., Saiwan, C., Tontiwachwuthikul, P., Al-marri, M.J. and Benamor, A. (2017) Advancement and new perspectives of using formulated reactive amine blends for post-combustion carbon dioxide (CO_2) capture technologies. *Petroleum*, 3 (1): 10–36. doi:10.1016/j.petlm.2016.11.002.

Ohs, B., Krödel, M. and Wessling, M. (2018) Adsorption of carbon dioxide on solid amine-functionalized sorbents: A dual kinetic model. *Separation and Purification Technology*, 204 (April): 13–20. doi:10.1016/j.seppur.2018.04.009.

Olivares-Marín, M. and Maroto-Valer, M.M. (2012) Development of adsorbents for CO_2 capture from waste materials: a review. *Greenhouse Gases: Science and Technology*, 2 (1): 20–35. doi:10.1002/ghg.45.

Omell, B.P., Ma, J., Mahapatra, P., Yu, M., Lee, A., Bhattacharyya, D., Zitney, S.E., Biegler, L.T. and Miller, D.C. (2016) Advanced Modeling and Control of a Solid Sorbent-Based CO_2 Capture Process. *IFAC-PapersOnLine*, 49 (7): 633–638. doi:10.1016/j.ifacol.2016.07.240.

Omri, A. and Benzina, M. (2012) Characterization of Activated Carbon Prepared from a New Raw Lignocellulosic Material : Ziziphus Spina-Christi Seeds. *Journal de la Soci t Chimique de Tunisie*, 14: 175–183.

Park, J.H. and Yang, R.T. (2005) Simple criterion for adsorbent selection for gas purification by pressure swing adsorption processes. *Industrial and Engineering Chemistry Research*, 44

(6): 1914–1921. doi:10.1021/ie049105r.

Pavia, D.L., Lampman, G.M. and Kriz, G.S. (2001) *Introduction to Spectroscopy third edition*. 3rd Editio. Bellingham, Washington: Thomson Learning, Inc.

Plaza, M.G., Durán, I., Rubiera, F. and Pevida, C. (2017) Adsorption-based Process Modelling for Post-combustion CO_2 Capture. *Energy Procedia*, 114 (November 2016): 2353–2361. doi:10.1016/j.egypro.2017.03.1365.

Plaza, M.G., García, S., Rubiera, F., Pis, J.J. and Pevida, C. (2010) Post-combustion CO_2 capture with a commercial activated carbon: Comparison of different regeneration strategies. *Chemical Engineering Journal*, 163 (1–2): 41–47. doi:10.1016/j.cej.2010.07.030.

Plaza, M.G., Pevida, C., Arias, B., Fermoso, J., Arenillas, A., Rubiera, F. and Pis, J.J. (2008) Application of thermogravimetric analysis to the evaluation of aminated solid sorbents for CO_2 capture. *Journal of Thermal Analysis and Calorimetry*, 92 (2): 601–606. doi:10.1007/s10973-007-8493-x.

Plaza, M.G., Pevida, C., Arias, B., Fermoso, J., Casal, M.D., Martín, C.F., Rubiera, F. and Pis, J.J. (2009) Development of low-cost biomass-based adsorbents for postcombustion CO_2 capture. *Fuel*, 88 (12): 2442–2447.

Pongstabodee, S., Pornaroontham, P., Pintuyothin, N., Pootrakulchote, N. and Thouchprasitchai, N. (2016) CO_2 capture performance of bi-functional activated bleaching earth modified with basic-alcoholic solution and functionalization with monoethanolamine: isotherms, kinetics and thermodynamics. *Journal of Environmental Sciences (China)*, 48: 126–137. doi:10.1016/j.jes.2015.09.028.

Presser, V., Mcdonough, J., Yeon, S.-H. and Gogotsi, Y. (2011) Effect of pore size on carbon dioxide sorption by carbide derived carbon. *Energy Environ. Sci.*, 4: 3059–3066. doi:10.1039/C1EE01176F.

Przepiórski, J., Skrodzewicz, M. and Morawski, A. (2004) High Temperature Ammonia Treatment of Activated Carbon for Enhancement of CO_2 Adsorption. *Applied Surface Science*, 225: 235–242. doi:10.1016/j.apsusc.2003.10.006.

Puziy, A.M., Poddubnaya, O.I., Martínez-Alonso, A., Suárez-García, F. and Tascón, J.M.D. (2003) Synthetic carbons activated with phosphoric acid III. Carbons prepared in air. *Carbon*, 41 (6): 1181–1191. doi:10.1016/S0008-6223(03)00031-9.

Qian, D., Hao, G.-P. and Li, W.-C. (2013) Synthesis of a nitrogen-doped porous carbon monolith and its use for CO_2 capture. *Carbon*, 64: 557–558. doi:10.1016/j.carbon.2013.07.073.

Quang, D.V., Hatton, T.A. and Abu-Zahra, M.R.M. (2016) Thermally Stable Amine-Grafted Adsorbent Prepared by Impregnating 3-Aminopropyltriethoxysilane on Mesoporous Silica for CO_2 Capture. *Industrial & Engineering Chemistry Research*, 55 (29): 7842–7852. doi:10.1021/acs.iecr.5b04096.

Radosz, M., Hu, X., Krutkramelis, K. and Shen, Y. (2008) Flue-Gas Carbon Capture on Carbonaceous Sorbents: Toward a Low-Cost Multifunctional Carbon Filter for "Green"

Energy Producers. *Industrial & Engineering Chemistry Research*, 47 (10): 3783–3794. doi:10.1021/ie0707974.

Raganati, F., Ammendola, P. and Chirone, R. (2016) On improving the CO_2 recovery efficiency of a conventional TSA process in a sound assisted fluidized bed by separating heating and purging. *Separation and Purification Technology*, 167: 24–31. doi:10.1016/j.seppur.2016.05.001.

Rampe, M.J. and Tiwow, V.A. (2018) Fabrication and Characterization of Activated Carbon from Charcoal Coconut Shell Minahasa, Indonesia. *Journal of Physics: Conference Series*, 1028 (1). doi:10.1088/1742-6596/1028/1/012033.

Rao, A.B. and Rubin, E.S. (2002) A technical, economic, and environmental assessment of amine-based CO_2 capture technology for power plant greenhouse gas control. *Environmental Science and Technology*, 36 (20): 4467–4475. doi:10.1021/es0158861.

Rashidi, N.A. and Yusup, S. (2016) An overview of activated carbons utilization for the post-combustion carbon dioxide capture. *Journal of CO_2 Utilization*, 13: 1–16. doi:10.1016/j.jcou.2015.11.002.

Rashidi, N.A., Yusup, S. and Borhan, A. (2016) Isotherm and Thermodynamic Analysis of Carbon Dioxide on Activated Carbon. *Procedia Engineering*, 148: 630–637. doi:10.1016/j.proeng.2016.06.527.

Ribeiro, A.M., Grande, C.A., Lopes, F.V.S., Loureiro, J.M. and Rodrigues, A.E. (2008) A parametric study of layered bed PSA for hydrogen purification. *Chemical Engineering Science*, 63 (21): 5258–5273. doi:10.1016/j.ces.2008.07.017.

Riboldi, L. and Bolland, O. (2015) Evaluating Pressure Swing Adsorption as a CO_2 separation technique in coal-fired power plants. *International Journal of Greenhouse Gas Control*, 39: 1–16. doi:10.1016/j.ijggc.2015.02.001.

Riboldi, L. and Bolland, O. (2017) Overview on Pressure Swing Adsorption (PSA) as CO_2 Capture Technology: State-of-the-Art, Limits and Potentials. *Energy Procedia*, 114 (1876): 2390–2400. doi:10.1016/j.egypro.2017.03.1385.

Riboldi, L., Bolland, O., Ngoy, J.M. and Wagner, N. (2014) Full-plant analysis of a PSA CO_2 capture unit integrated in coalfired power plants: Post- And pre-combustion scenarios. *Energy Procedia*, 63 (1876): 2289–2304. doi:10.1016/j.egypro.2014.11.248.

Ritter, J.A. and Yang, R.T. (1987) Equilibrium adsorption of multicomponent gas mixtures at elevated pressures. *Industrial & Engineering Chemistry Research*, 26 (8): 1679–1686. doi:10.1021/ie00068a032.

Rochelle, G.T. (2009) Amine Scrubbing for CO_2 Capture. *Science*, 325 (5948): 1652–1654. doi:10.1126/science.1176731.

Rockett, G.C., Ketzer, J.M.M., Ramírez, A. and Broek, M. Van Den (2013) CO_2 Storage Capacity of Campos Basin's Oil Fields, Brazil. *Elsevier*, 37: 5124–5133. doi:10.1016/j.egypro.2013.06.427.

Román, M. (2014) *Energy Policy in Brazil: Perspectives for the medium and long term.* Östersund, Sweden.

Romanos, J., Beckner, M., Rash, T., Firlej, L., Kuchta, B., Yu, P., Suppes, G., Wexler, C. and Pfeifer, P. (2012) Nanospace engineering of KOH activated carbon. *Nanotechnology*, 23 (1): 15401. Available at: http://stacks.iop.org/0957-4484/23/i=1/a=015401.

Rufford, T.E., Smart, S., Watson, G.C.Y., Graham, B.F., Boxall, J., Diniz da Costa, J.C. and May, E.F. (2012) The removal of CO_2 and N_2 from natural gas: A review of conventional and emerging process technologies. *Journal of Petroleum Science and Engineering*, 94–95: 123–154. doi:10.1016/j.petrol.2012.06.016.

Rutherford, S.W. and Do, D.D. (2000) Adsorption dynamics measured by permeation and batch adsorption methods. *Chemical Engineering Journal*, 76 (1): 23–31. doi:https://doi.org/10.1016/S1385-8947(99)00111-4.

Ruthven, D.M. (1984) *Principles of adsorption and adsorption processes*. New York ; Chichester: Wiley.

Saeidi, N. and Lotfollahi, M.N. (2015) Effects of powder activated carbon particle size on adsorption capacity and mechanical properties of the semi activated carbon fiber. *Fibers and Polymers*, 16 (3): 543–549. doi:10.1007/s12221-015-0543-6.

Saha, D., Bao, Z., Jia, F. and Deng, S. (2010) Adsorption of CO_2, CH_4, N_2O, and N_2 on MOF-5, MOF-177, and Zeolite 5A. *Environmental Science & Technology*, 44 (5): 1820–1826. doi:10.1021/es9032309.

Saha, D., Van Bramer, S.E., Orkoulas, G., Ho, H.-C., Chen, J. and Henley, D.K. (2017) CO_2 capture in lignin-derived and nitrogen-doped hierarchical porous carbons. *Carbon*, 121: 257–266.

Sahira, J. and Bhadra, P.P. (2014) Preparation and Characterization of Activated Carbon from Lapsi (Choerospondias axillaris) Seed Stone by Chemical Activation with Potassium Hydroxide Preparation of Adsorbent Characterization of Activated Carbons Thermal Behavior of Lapsi seed stone par. *Journal of the Institute of Engineering*, 9 (1): 79–88. doi:http://dx.doi.org.idpproxy.reading.ac.uk/10.1016/S0140-6701(98)96563-8.

Samanta, A., Zhao, A., Shimizu, G.K.H., Sarkar, P. and Gupta, R. (2012) Post-Combustion CO_2 Capture Using Solid Sorbents: A Review. *Industrial & Engineering Chemistry Research*, 51 (4): 1438–1463. doi:10.1021/ie200686q.

Satyapal, S., Filburn, T., Trela, J. and Strange, J. (2001) Performance and Properties of a Solid Amine Sorbent for Carbon Dioxide Removal in Space Life Support Applications. *Energy & Fuels*, 15 (2): 250–255. doi:10.1021/ef0002391.

Von Saussure, T. (1814) Beobachtungen über die Absorption der Gasarten durch verschiedene Körper. *Annalen der Physik*, 47 (6): 113–183.

Sayari, A. and Belmabkhout, Y. (2010) Stabilization of Amine-Containing CO_2 Adsorbents: Dramatic Effect of Water Vapor. *Journal of the American Chemical Society (JACS)*, 132 (18):

6312–6314. doi:10.1021/ja1013773.

Sayari, A., Belmabkhout, Y. and Serna-Guerrero, R. (2011) Flue gas treatment via CO_2 adsorption. *Chemical Engineering Journal*, 171 (3): 760–774. doi:10.1016/j.cej.2011.02.007.

Schettino Jr, M.A., Freitas, J.C.C., Cunha, A.G., Emmerich, F.G., Soares, A.B. and Silva, P.R.N. (2007) Preparation and Characterization of Chemically activated carbon from rice hulls. *Química Nova*, 30 (7): 1663–1668. doi:10.1016/j.biortech.2006.08.001.

Serna-Guerrero, R., Belmabkhout, Y. and Sayari, A. (2010) Further investigations of CO_2 capture using triamine-grafted pore-expanded mesoporous silica. *Chemical Engineering Journal*, 158 (3): 513–519. doi:10.1016/j.cej.2010.01.041.

Shafeeyan, M.S., Daud, W.M.A.W., Shamiri, A. and Aghamohammadi, N. (2015a) Modeling of Carbon Dioxide Adsorption onto Ammonia-Modified Activated Carbon: Kinetic Analysis and Breakthrough Behavior. *Energy and Fuels*, 29 (10): 6565–6577. doi:10.1021/acs.energyfuels.5b00653.

Shafeeyan, M.S., Houshmand, A., Arami-Niya, A., Razaghizadeh, H. and Daud, W.M.A.W. (2015b) Modification of Activated Carbon Using Nitration Followed by Reduction for Carbon Dioxide Capture. *Bulletin of the Korean Chemical Society*, 36 (2): 533–538. doi:10.1002/bkcs.10100.

Shafeeyan, M.S., Wan Daud, W.M.A., Shamiri, A., Mohd, W., Wan, A. and Shamiri, A. (2014) A review of mathematical modeling of fixed-bed columns for carbon dioxide adsorption. *Chemical Engineering Research and Design*, 92 (5): 961–988. doi:10.1016/j.cherd.2013.08.018.

Shamsuddin, M.S., Yusoff, N.R.N. and Sulaiman, M.A. (2016) Synthesis and Characterization of Activated Carbon Produced from Kenaf Core Fiber Using H_3PO_4 Activation. *Procedia Chemistry*, 19: 558–565. doi:10.1016/j.proche.2016.03.053.

Shin, S., Jang, J., Yoon, S.-H. and Mochida, I. (1997) A study on the effect of heat treatment on functional groups of pitch based activated carbon fiber using FTIR. *Carbon*, 35 (12): 1739–1743. doi:10.1016/S0008-6223(97)00132-2.

Siefert, N.S., Chang, B.Y. and Litster, S. (2014) Exergy and economic analysis of a CaO-looping gasifier for IGFC–CCS and IGCC–CCS. *Applied Energy*, 128: 230–245. doi:https://doi.org/10.1016/j.apenergy.2014.04.065.

Siefert, N.S. and Litster, S. (2013) Exergy and economic analyses of advanced IGCC–CCS and IGFC–CCS power plants. *Applied Energy*, 107: 315–328. doi:https://doi.org/10.1016/j.apenergy.2013.02.006.

da Silva, E.F. and Svendsen, H.F. (2004) Ab Initio Study of the Reaction of Carbamate Formation from CO_2 and Alkanolamines. *Industrial & Engineering Chemistry Research*, 43 (13): 3413–3418. doi:10.1021/ie030619k.

Silverstein, R.M., Webster, F.X. and Kiemle, D.J. (2005) Spectrometric identification of organic compounds. *Journal of Molecular Structure*. p. 512. doi:10.1016/0022-

2860(76)87024-X.

Sing, K.S.W. (1985) Reporting physisorption data for gas/solid systems with special reference to the determination of surface area and porosity (Recommendations 1984). *Pure and Applied Chemistry*, 57 (4): 603–619. doi:10.1351/pac198557040603.

Sing, K.S.W. and Williams, R.T. (2004) *Review Physisorption Hysteresis Loops and the Characterization of Nanoporous Materials*., (1): 773–782. doi:10.1260/0263617053499032.

Singh, V.K., Anil Kumar, E. and Kumar, E.A. (2015) Measurement and analysis of adsorption isotherms of CO_2 on activated carbon. *Applied Thermal Engineering*. doi:10.1016/j.applthermaleng.2015.10.052.

Siqueira, R.M., Freitas, G.R., Peixoto, H.R., Nascimento, J.F. do, Musse, A.P.S., Torres, A.E.B., Azevedo, D.C.S. and Bastos-Neto, M. (2017) Carbon Dioxide Capture by Pressure Swing Adsorption. *Energy Procedia*, 114 (November 2016): 2182–2192. doi:10.1016/j.egypro.2017.03.1355.

Sircar, S. (1983) Linear-driving-force model for non-isothermal gas adsorption kinetics. *Journal of the Chemical Society, Faraday Transactions 1: Physical Chemistry in Condensed Phases*, 79 (4): 785–796. doi:10.1039/F19837900785.

Siriwardane, R. V, Shen, M.-S., Fisher, E.P. and Poston, J.A. (2001) Adsorption of CO_2 on Molecular Sieves and Activated Carbon. *Energy & Fuels*, 15 (2): 279–284. doi:10.1021/ef000241s.

Solum, M.S., Pugmire, R.J., Jagtoyen, M. and Derbyshire, F. (1995) Evolution of carbon structure in chemically activated wood. *Carbon*, 33 (9): 1247–1254. doi:https://doi.org/10.1016/0008-6223(95)00067-N.

Son, W.-J., Choi, J.-S. and Ahn, W.-S. (2008) Adsorptive removal of carbon dioxide using polyethyleneimine-loaded mesoporous silica materials. *Microporous and Mesoporous Materials*, 113 (1): 31–40. doi:https://doi.org/10.1016/j.micromeso.2007.10.049.

Song, M., Jin, B., Xiao, R., Yang, L., Wu, Y., Zhong, Z. and Huang, Y. (2013) The comparison of two activation techniques to prepare activated carbon from corn cob. *Biomass and Bioenergy*, 48: 250–256. doi:https://doi.org/10.1016/j.biombioe.2012.11.007.

Songolzadeh, M., Soleimani, M., Takht Ravanchi, M. and Songolzadeh, R. (2014) Carbon dioxide separation from flue gases: a technological review emphasizing reduction in greenhouse gas emissions. *TheScientificWorldJournal*, 2014: 828131. doi:10.1155/2014/828131.

Spigarelli, B.P. and Kawatra, S.K. (2013) Opportunities and challenges in carbon dioxide capture. *Journal of CO_2 Utilization*, 1: 69–87. doi:10.1016/j.jcou.2013.03.002.

Stern, N. (2006) The Economics of Climate Change. *Stern Review*, p. 662. doi:10.1257/aer.98.2.1.

Story, C. (2017) *Activated Carbon : Fundamentals and New Applications for which it is being*

employed., (July).

Su, F., Lu, C. and Chen, H.S. (2011) Adsorption, desorption, and thermodynamic studies of CO_2 with high-amine-loaded multiwalled carbon nanotubes. *Langmuir*, 27 (13): 8090–8098. doi:10.1021/la201745y.

Sumida, K., Rogow, D.L., Mason, J.A., McDonald, T.M., Bloch, E.D., Herm, Z.R., Bae, T.-H. and Long, J.R. (2012) Carbon Dioxide Capture in Metal–Organic Frameworks. *Chemical Reviews*, 112 (2): 724–781. doi:10.1021/cr2003272.

Sun, J., Hippo, E.J., Marsh, H., O&Amp;Apos, Brien, W.S. and Crelling, J.C. (1997) Activated carbon produced from an Illinois Basin coal. *Carbon*, 35 (3): 341–352.

Sun, N., Sun, C., Liu, J., Liu, H., Snape, C.E., Li, K., Wei, W. and Sun, Y. (2015) Surface-modified spherical activated carbon materials for pre-combustion carbon dioxide capture. *RSC Adv.*, 5 (42): 33681–33690. doi:10.1039/C5RA02665B.

Sutar, P.N., Jha, A., Vaidya, P.D. and Kenig, E.Y. (2012) Secondary amines for CO_2 capture: A kinetic investigation using N-ethylmonoethanolamine. *Chemical Engineering Journal*, 207–208 (C): 718–724. doi:10.1016/j.cej.2012.07.042.

Tchobanoglous, G. (2014) *Wastewater engineering : Treatment and Reuse.* 5th ed. Burton, F.L., Stensel, H.D. and Metcalf & Eddy (eds.). New York: McGraw-Hilll, 2014. doi:10.1016/0191-2615(91)90038-K.

Thambimuthu, K. (Kailai), Soltanieh, M., Abanades, J.C., Allam, R., Bolland, O., Davison, J., Feron, P., Goede, F., Herrera, A., Iijima, M., et al. (2005) Capture of CO_2. *IPCC Special Report on Carbon dioxide Capture and Storage*, pp. 105–178.

The UN Environment (2017) *The Adaptation Gap Report 2017*. Nairobi, Kenya: United Nations Environment Programme (UNEP). Available at: papers3://publication/uuid/931E5A77-EB53-4B4E-96D2-AAFC7F45DA11.

Theo, W.L., Lim, J.S., Hashim, H., Mustaffa, A.A. and Ho, W.S. (2016) Review of pre-combustion capture and ionic liquid in carbon capture and storage. *Applied Energy*, 183: 1633–1663. doi:10.1016/j.apenergy.2016.09.103.

Thommes, M., Kaneko, K., Neimark, A. V, Olivier, J.P., Rodriguez-reinoso, F., Rouquerol, J. and Sing, K.S.W. (2015) *Physisorption of gases , with special reference to the evaluation of surface area and pore size distribution (IUPAC Technical Report)*., 87: 1051–1069. doi:10.1515/pac-2014-1117.

Thote, J., Iyer, K., Chatti, R., Labhsetwar, N., Biniwale, R. and Rayalu, S. (2010) In situ nitrogen enriched carbon for carbon dioxide capture. *Carbon*, 48: 396–402. doi:10.1016/j.carbon.2009.09.042.

Timur, S., Kantarli, I.C., Onenc, S. and Yanik, J. (2010) Characterization and application of activated carbon produced from oak cups pulp. *Journal of Analytical and Applied Pyrolysis*, 89 (1): 129–136. doi:https://doi.org/10.1016/j.jaap.2010.07.002.

Tiwari, D., Goel, C., Bhunia, H. and Bajpai, P.K. (2016) Novel nanostructured carbons derived from epoxy resin and their adsorption characteristics for CO_2 capture. *RSC Advances*, 6 (100): 97728–97738.

Treese, S.A., Pujadó, P.R. and Jones, D.S.J. (2015) *Handbook of Petroleum Processing*. Second Ed. Dordrecht: Springer International Publishing Switzerland. doi:10.1007/978-3-319-14529-7.

U.S. Energy Information Administration (EIA) (2016) *International Energy Outlook 2016*. Washington, DC: Office of Energy Analysis.

UNFCC (2011) *Report of the Conference of the Parties serving as the meeting of the Parties to the Kyoto Protocol on its sixth session, held in Cancun from 29 November to 10 December 2010*. Cancun, Mexico.

UNFCC (2018) *New Era of Global Climate Action To Begin Under Paris Climate Change Agreement*. Available at: https://unfccc.int/news/new-era-of-global-climate-action-to-begin-under-paris-climate-change-agreement-0 (Accessed: 26 December 2018).

Ustinov, E.A. and Do, D.D. (2002) Adsorption in Slit-Like Pores of Activated Carbons: Improvement of the Horvath and Kawazoe Method. *Langmuir*, 18 (12): 4637–4647. doi:10.1021/la0105351.

Valencia, C.A.V. (2007) *Application of activated carbon and other carbonaceous material in the treatment of agricultural wastewater.* Pontifical Catholic University of Rio de Janeiro, Brazil.

Veneman, R., Kamphuis, H. and Brilman, D.W.F. (2013) Post-Combustion CO_2 capture using supported amine sorbents: A process integration study. *Energy Procedia*, 37: 2100–2108. doi:https://doi.org/10.1016/j.egypro.2013.06.089.

Viswanathan, B., Kannan, S. and Deka, R.C. (2010) *Catalysts and surfaces: characterization techniques*. Oxford: Alpha Science International. Available at: www.alphasci.com.

Wahby, A., Ramos-Fernández, J.M., Martínez-Escandell, M., Sepúlveda-Escribano, A., Silvestre-Albero, J. and Rodríguez-Reinoso, F. (2010) High-Surface-Area Carbon Molecular Sieves for Selective CO_2 Adsorption. *ChemSusChem*, 3 (8): 974–981. doi:10.1002/cssc.201000083.

Walther, H.-J. (1980) *Carbon Adsorption Handbook. Edited by Second Printing. USA, Michigan, Collingwood. Ann Arbor Science Publishers, 1980, 1054 S., 393 Abb. ISBN 0-250-40236-X*. Cheremisinoff, P.N. Ellerbusch, F.. (ed.). doi:10.1002/aheh.19830110106.

Wang, X. and Guo, Q. (2016) CO_2 Adsorption Behavior of Activated Coal Char Modified with Tetraethylenepentamine. *Energy & Fuels*, 30 (4): 3281–3288. doi:10.1021/acs.energyfuels.5b02882.

Wang, Y., Dowling, A.W., Krieft, C., Walther, A. and Biegler, L.T. (2015) Pressure Swing Adsorption Optimization Strategies for CO_2 Capture. *Computer Aided Chemical Engineering*, 36: 197–223. doi:10.1016/B978-0-444-63472-6.00008-2.

Wang, Z., Yang, J., Li, Z. and Xiang, Y. (2009) Syngas composition study. *Frontiers of Energy and Power Engineering in China*, 3 (3): 369–372. doi:10.1007/s11708-009-0044-7.

Watson, G., May, E.F., Graham, B.F., Trebble, M.A., Trengove, R.D. and Chan, K.I. (2009) Equilibrium Adsorption Measurements of Pure Nitrogen, Carbon Dioxide, and Methane on a Carbon Molecular Sieve at Cryogenic Temperatures and High Pressures. *Journal of Chemical & Engineering Data*, 54 (9): 2701–2707. doi:10.1021/je900224w.

Wiheeb, A.D., Helwani, Z., Kim, J. and Othman, M.R. (2016a) Pressure swing adsorption technologies for carbon dioxide capture. *Separation & Purification Reviews*, 45 (2): 108–121. doi:10.1080/15422119.2015.1047958.

Wiheeb, A.D., Helwani, Z., Kim, J. and Othman, M.R. (2016b) Pressure Swing Adsorption Technologies for Carbon Dioxide Capture. *Separation and Purification Reviews*, 45 (2): 108–121. doi:10.1080/15422119.2015.1047958.

Wood, D.A., Nwaoha, C. and Towler, B.F. (2012) Gas-to-liquids (GTL): A review of an industry offering several routes for monetizing natural gas. *Journal of Natural Gas Science and Engineering*, 9: 196–208. doi:https://doi.org/10.1016/j.jngse.2012.07.001.

Xiao, J., Peng, Y., Benard, P. and Chahine, R. (2016) Thermal effects on breakthrough curves of pressure swing adsorption for hydrogen purification. *International Journal of Hydrogen Energy*, 41 (19): 8236–8245. doi:10.1016/j.ijhydene.2015.11.126.

Xu, X., Song, C., Andresen, J.M., Miller, B.G. and Scaroni, A.W. (2002) Novel Polyethylenimine-Modified Mesoporous Molecular Sieve of MCM-41 Type as High-Capacity Adsorbent for CO_2 Capture. *Energy & Fuels*, 16 (6): 1463–1469. doi:10.1021/ef020058u.

Yakout, S.M. and Sharaf El-Deen, G. (2016) Characterization of activated carbon prepared by phosphoric acid activation of olive stones. *Arabian Journal of Chemistry*, 9: S1155–S1162. doi:10.1016/j.arabjc.2011.12.002.

Yang, J., Li, J., Wang, W., Li, L. and Jinping, L. (2013) Adsorption of CO_2, CH_4, and N_2 on 8-, 10-, and 12-Membered Ring Hydrophobic Microporous High-Silica Zeolites: DDR, Silicalite-1, and Beta. *Industrial & Engineering Chemistry Research*, 52 (50): 17856–17864. doi:10.1021/ie403217n.

Yang, J. and Qiu, K. (2013) Preparation of activated carbons by $ZnCl_2$ activation from herb residues under vacuum. *Carbon*, 51: 437. doi:https://doi.org/10.1016/j.carbon.2012.08.039.

Yang, R.T. (1987) *Gas separation by adsorption processes*. Boston ; London: Butterworths.

Yang, S.-T., Kim, J. and Ahn, W.-S. (2010) CO_2 adsorption over ion-exchanged zeolite beta with alkali and alkaline earth metal ions. *Microporous and Mesoporous Materials*, 135 (1): 90–94.

Yang, T. and Lua, A.C. (2003) Characteristics of activated carbons prepared from pistachio-nut shells by physical activation. *Journal of Colloid and Interface Science*, 267 (2): 408–417. doi:10.1016/S0021-9797(03)00689-1.

Yaumi, a. L., Abu Bakar, M.Z. and Hameed, B.H. (2017) Recent advances in functionalized composite solid materials for carbon dioxide capture. *Energy*, 124. doi:10.1016/j.energy.2017.02.053.

You, H.-S., Jin, H., Mo, Y.-H. and Park, S.-E. (2013) CO_2 adsorption behavior of microwave synthesized zeolite beta. *Materials Letters*, 108: 106–109. doi:10.1016/j.matlet.2013.06.088.

Yu, C., Qiu, J.S., Sun, Y.F., Li, X.H., Chen, G. and Zhao, Z. Bin (2008) Adsorption removal of thiophene and dibenzothiophene from oils with activated carbon as adsorbent: Effect of surface chemistry. *Journal of Porous Materials*, 15 (2): 151–157. doi:10.1007/s10934-007-9116-4.

Yu, C.H., Huang, C.H. and Tan, C.S. (2012) A review of CO_2 capture by absorption and adsorption. *Aerosol and Air Quality Research*, 12 (5): 745–769. doi:10.4209/aaqr.2012.05.0132.

Yu, J. and Chuang, S.S.C. (2016) The Structure of Adsorbed Species on Immobilized Amines in CO_2 Capture: An in Situ IR Study. *Energy & Fuels*, 30 (9): 7579–7587. doi:10.1021/acs.energyfuels.6b01423.

Yu, J., Xie, L.-H., Li, J.-R., Ma, Y., Seminario, J.M. and Balbuena, P.B. (2017) CO_2 Capture and Separations Using MOFs: Computational and Experimental Studies. *Chemical reviews*, 117 (14).

Yue, M.B., Chun, Y., Cao, Y., Dong, X. and Zhu, J.H. (2006) CO_2 Capture by As-Prepared SBA-15 with an Occluded Organic Template. *Advanced Functional Materials*, 16 (13): 1717–1722. doi:10.1002/adfm.200600427.

Zeleňák, V., Badaničová, M., Halamová, D., Čejka, J., Zukal, a., Murafa, N. and Goerigk, G. (2008) Amine-modified ordered mesoporous silica: Effect of pore size on carbon dioxide capture. *Chemical Engineering Journal*, 144 (2): 336–342. doi:10.1016/j.cej.2008.07.025.

Zeng, D., Zhang, Q., Chen, S., Liu, S. and Wang, G. (2016) Synthesis porous carbon-based solid acid from rice husk for esterification of fatty acids. *Microporous and Mesoporous Materials*, 219: 54–58.

Zhang, D., Cao, J., Wu, G. and Cui, L. (2018a) Dynamic Adsorption Model Fitting Studies of Typical VOCs Using Commercial Activated Carbon in a Fixed Bed. *Water, Air, and Soil Pollution*, 229 (6). doi:10.1007/s11270-018-3763-8.

Zhang, J., Xie, S. and Ho, Y.-S. (2009) Removal of fluoride ions from aqueous solution using modified attapulgite as adsorbent. *Journal of Hazardous Materials*, 165 (1): 218–222.

Zhang, X., Li, W. and Lu, A. (2015a) Designed porous carbon materials for efficient CO_2 adsorption and separation. *New Carbon Materials*, 30 (6): 481–501. doi:10.1016/S1872-5805(15)60203-7.

Zhang, X., Lin, D. and Chen, W. (2015b) Nitrogen-doped porous carbon prepared from a liquid carbon precursor for CO_2 adsorption. *RSC Advances*, 5 (56): 45136–45143. doi:10.1039/C5RA08014B.

Zhang, X., Zhang, S., Yang, H., Feng, Y., Chen, Y., Wang, X. and Chen, H. (2014) Nitrogen enriched biochar modified by high temperature CO_2–ammonia treatment: Characterization and adsorption of CO_2. *Chemical Engineering Journal*, 257 (C): 20–27.

Zhang, Y., Cong, Y., Zhang, J., Li, X., Li, Y., Dong, Z., Yuan, G., Zhang, J. and Cui, Z. (2018b) Effects of activation temperatures on the surface structures and supercapacitive performances of porous carbon fibers. *Surface and Coatings Technology*, 349 (March): 384–391. doi:10.1016/j.surfcoat.2018.06.012.

Zhang, Z., Zhou, J., Xing, W., Xue, Q., Yan, Z., Zhuo, S. and Qiao, S. (2013) Critical role of small micropores in high CO_2 uptake. *Physical chemistry chemical physics : PCCP*, 15. doi:10.1039/c2cp44436d.

Zhao, C., Guo, Y. and Yan, J. (2019) Enhanced CO_2 sorption capacity of amine-tethered fly ash residues derived from co-firing of coal and biomass blends. *Applied energy*, v. 242: 453-461–2019 v.242. doi:10.1016/j.apenergy.2019.03.143.

Zhao, H., Luo, X., Zhang, H., Sun, N., Wei, W. and Sun, Y. (2018) Carbon-based adsorbents for post-combustion capture: a review. *Greenhouse Gases: Science and Technology*, 8 (1): 11–36. doi:10.1002/ghg.1758.

Zhao, Y., Liu, X. and Han, Y. (2015) Microporous carbonaceous adsorbents for CO_2 separation via selective adsorption. *RSC Adv.*, 5 (38): 30310–30330. doi:10.1039/C5RA00569H.

Zhong, M., Natesakhawat, S., P Baltrus, J., Luebke, D., Nulwala, H., Matyjaszewski, K. and Kowalewski, T. (2012) Copolymer-templated nitrogen-enriched porous nanocarbons for CO_2 capture. *Chemical communications (Cambridge, England)*, 48. doi:10.1039/c2cc36652e.

Zhu, B., Shang, C. and Guo, Z. (2016) Naturally Nitrogen and Calcium-Doped Nanoporous Carbon from Pine Cone with Superior CO_2 Capture Capacities. *ACS Sustainable Chemistry & Engineering*, 4 (3): 1050–1057.

APPENDIX A: POST- AND PRE-COMBUSTION SUPPLEMENTARY DATA

Appendix A provides the supplementary data corresponding to the post- and pre-combustion experimental studies, as described in chapters 4 and 5, respectively. The tables contained in this section show the complete PSA process details, as well as providing additional results obtained from the characterisation techniques used in this work, such as HPVA Freundlich linearisation method data.

A.1. HPVA studies

The adsorption-desorption isotherms produced in the high-pressure system were also linearised by the Freundlich isotherm (Figures A.1-A.3) to establish a comparison with the Langmuir linearisation method. However, as outlined in sections 4.2.6 and 5.2.5, the Freundlich linearisation method did not demonstrate higher interaction to the modified adsorbents compared to the Langmuir linearisation method (see Table A.1).

Table A.1. HPVA Freundlich linearisation data

	Freundlich linearisation			
Samples	1/n	n	Ln K	K
Unmodified AC Norit® R2030 Cabot	0.400	2.503	-4.7375	0.009
MEA (50%) modified AC Norit® R2030 Cabot	0.309	3.234	-4.1421	0.016
Unmodified AC Norit® RB1 AC	0.382	2.619	-4.4715	0.011
MEA (20%) modified Norit® RB1 AC	0.467	2.142	-5.424	0.004
MEA (30%) modified Norit® RB1 AC	0.144	6.969	-0.8029	0.448
MEA (40%) modified Norit® RB1 AC	0.485	2.064	-5.7545	0.003
MEA (50%) modified Norit® RB1 AC	0.465	2.151	-5.4662	0.004
MEA (60%) modified Norit® RB1 AC	0.484	2.068	-5.7676	0.003
MEA+AMP blend modified Norit® RB1 AC	0.433	2.312	-5.0019	0.007
MEA+MDEA+AMP blend modified Norit® RB1 AC	0.591	1.693	-7.5718	0.001
TEPA (30%) modified Norit® RB1 AC	1.072	0.933	-13.531	0.000
KOH (20%) modified Norit® RB1 AC	0.3721	2.69	-3.8883	0.020
KOH (70%) modified Norit® RB1 AC	1.0246	0.98	-15.211	2.48E-07

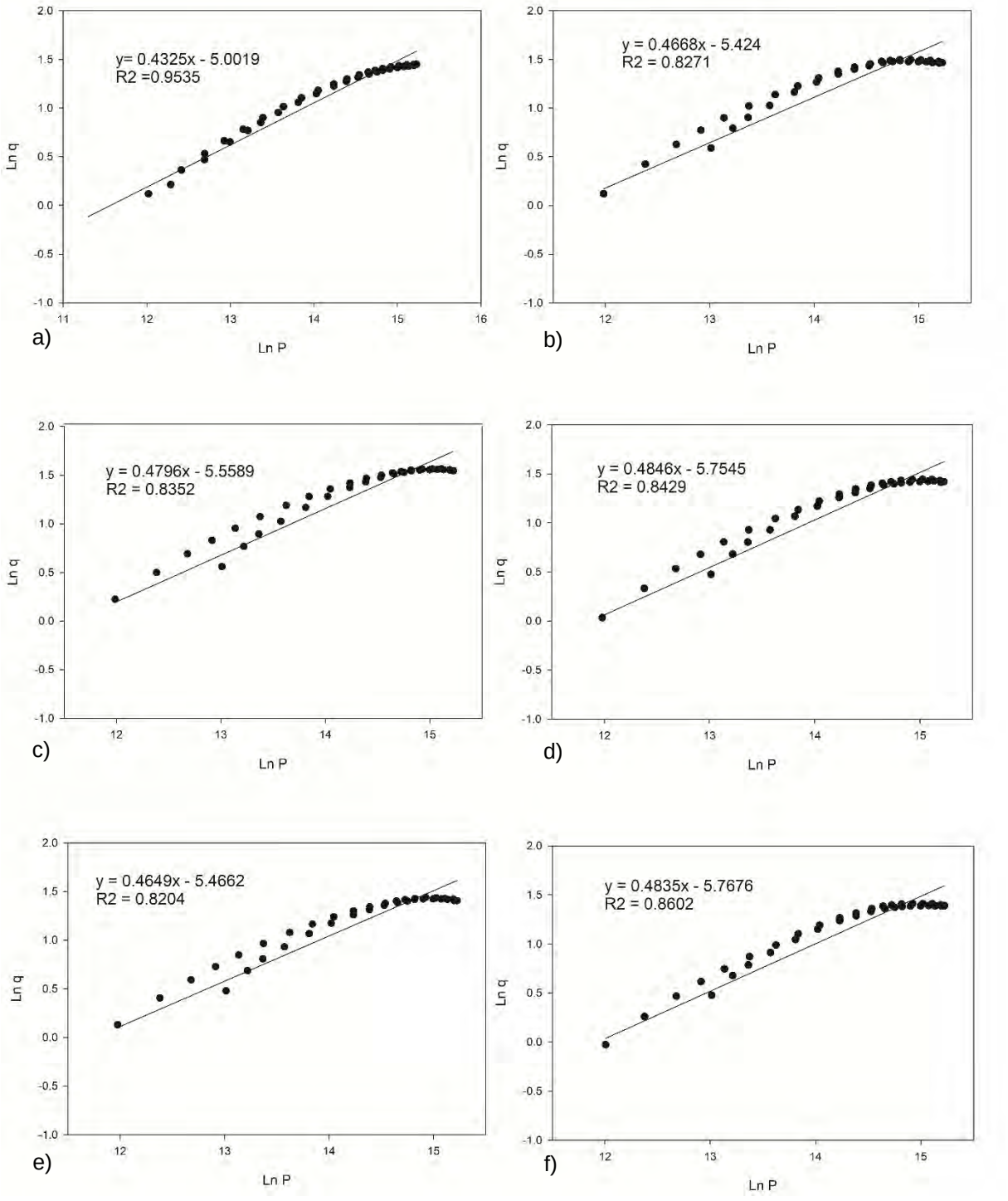

Figure A.1. Freundlich linearisation methodology applied to the ACs: A) MEA+AMP modified RB1 AC; B) MEA (20%) modified RB1 AC; C) MEA (30%) modified RB1 AC; D) MEA (40%) modified RB1 AC; E) MEA (50%) modified RB1 AC; and F) MEA (60%) modified RB1 AC

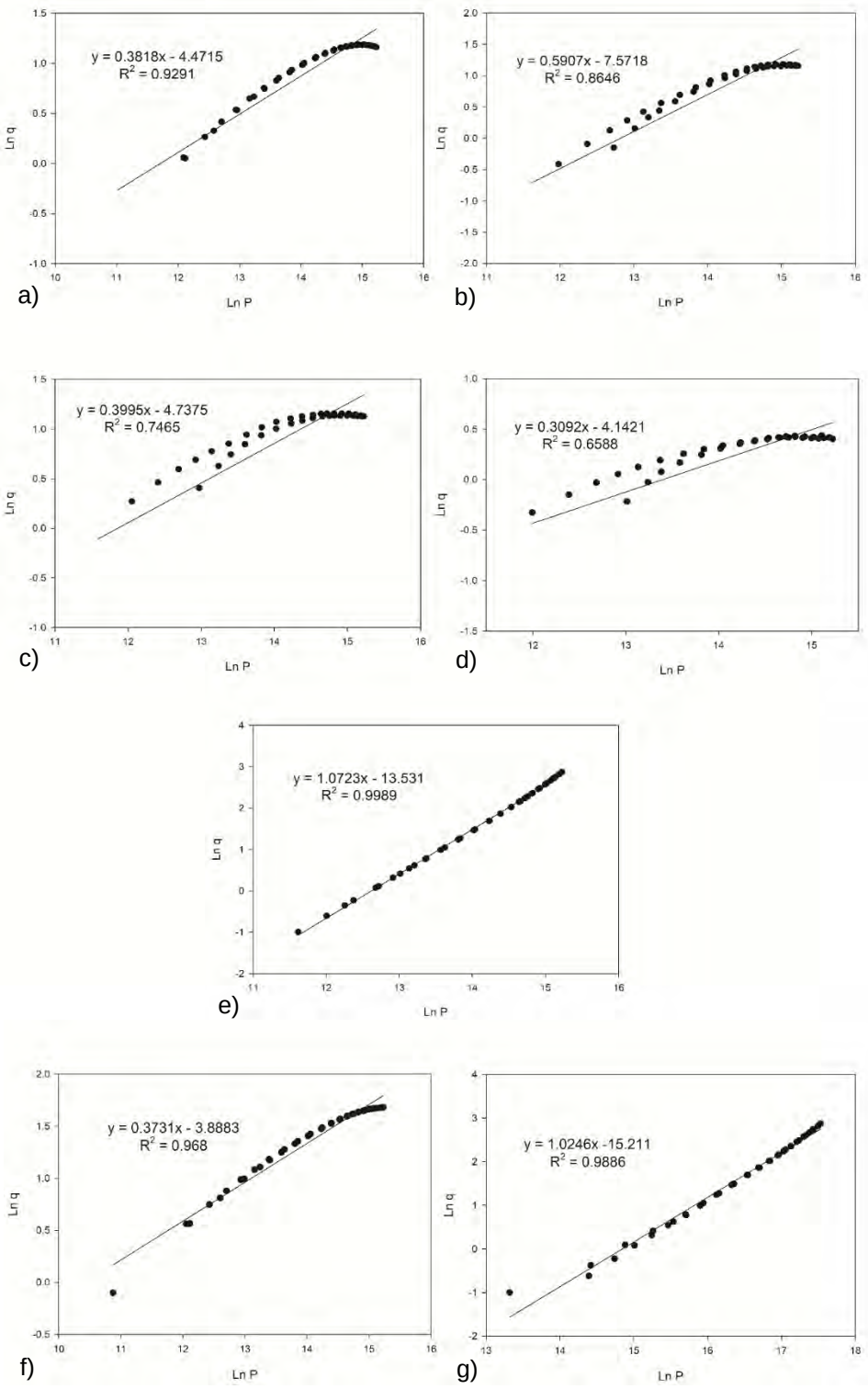

Figure A.2. Freundlich linearisation methodology applied to the ACs: A) Unmodified RB1 AC; B) MEA+MDEA+AMP modified RB1 AC; C) Unmodified R2030 Cabot AC; D) MEA (50%) modified R2030 Cabot AC; E) TEPA (30%) modified RB1 AC; F) KOH (20%) modified RB1 AC; and G) KOH (70%) modified RB1 AC

A.2. FTIR studies

Six amine FTIR graphs are demonstrated in Figure A.1, which correspond to the MEA (20-60%) and DEA+MDEA+AMP modified RB1 ACs and were obtained according to the methodology reported in section 3.1.4.

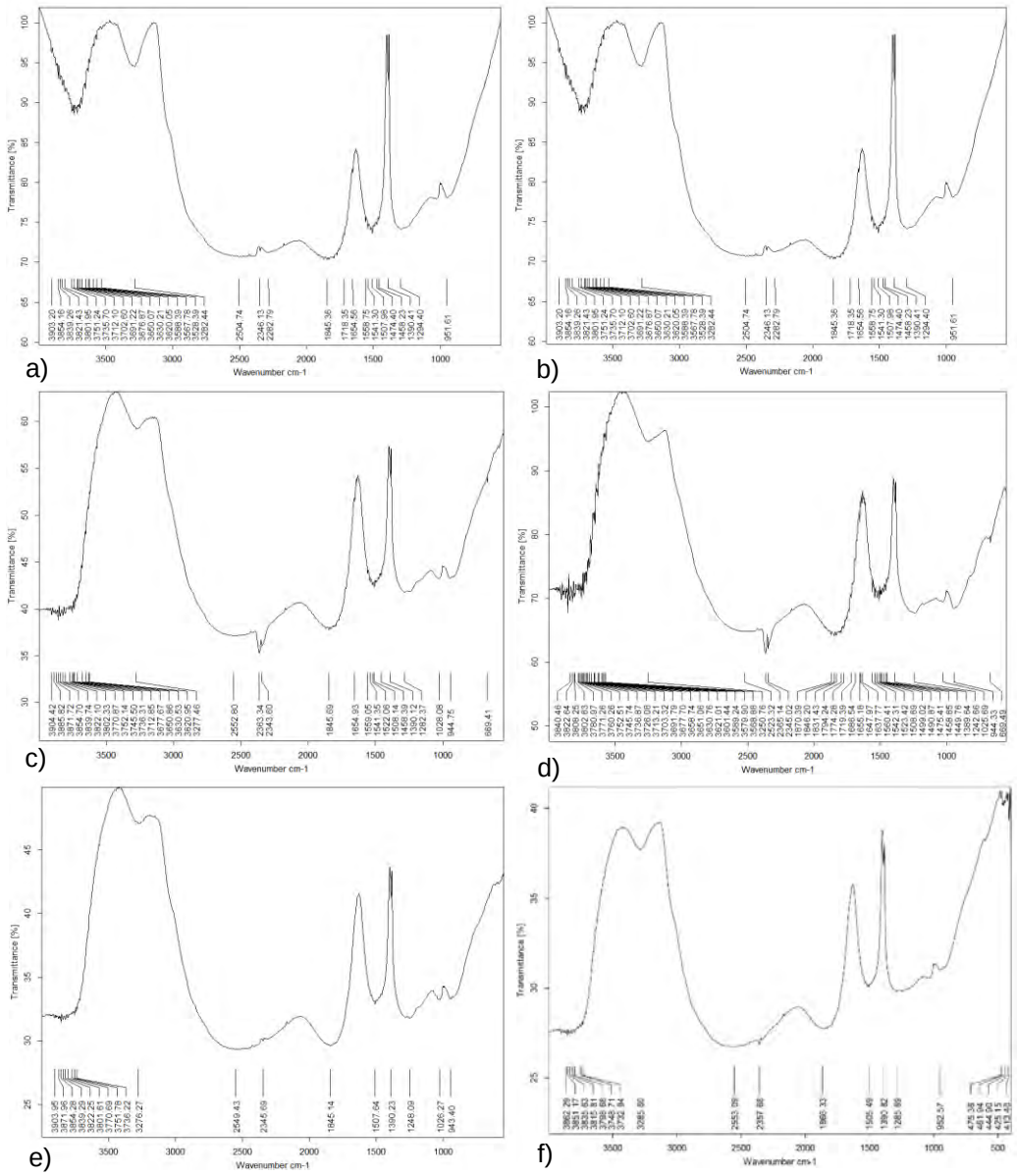

Figure A. 3. FTIR spectra for: a) MEA (20%) modified Norit® RB1 AC; b) MEA (30%) modified Norit® RB1 AC; c) MEA (40%) modified Norit® RB1 AC; d) MEA (50%) modified Norit® RB1 AC; e) MEA (60%) modified Norit® RB1 AC; and f) DEA+MDEA+AMP blend modified Norit® RB1 AC

A.3. Adsorption studies via PSA in pre- and post-combustion conditions

The breakthrough curves for a limited number of amine modified ACs are included in this section. Figure A.4 displays two different amine loadings (20 and 30%) for TEPA modified RB1 AC. In contrast, these two adsorbents were analysed in pre-combustion adsorption conditions (25ºC/ 25 bar), as well as in a range of CO_2 inlet concentrations. Figure A.5 exhibits the MEA (30-60%), MEA+MDEA+AMP and DEA+MDEA+AMP modified RB1 ACs breakthrough curves obtained from the FBR process in post-combustion adsorption conditions. The overall flowrate used in these experiments respected the maximum bed capacity (200 $Nml.min^{-1}$), as applied in sections 4.2.7 and 5.2.7. Supplementary information for the adsorbents tested under the FBR-PSA process, including the bed capacity during the complete adsorption stage, the overall inlet and outlet streams (mg) for a binary gas mixture and the amount of CO_2 adsorbed are described in Table A.2 and A.3.

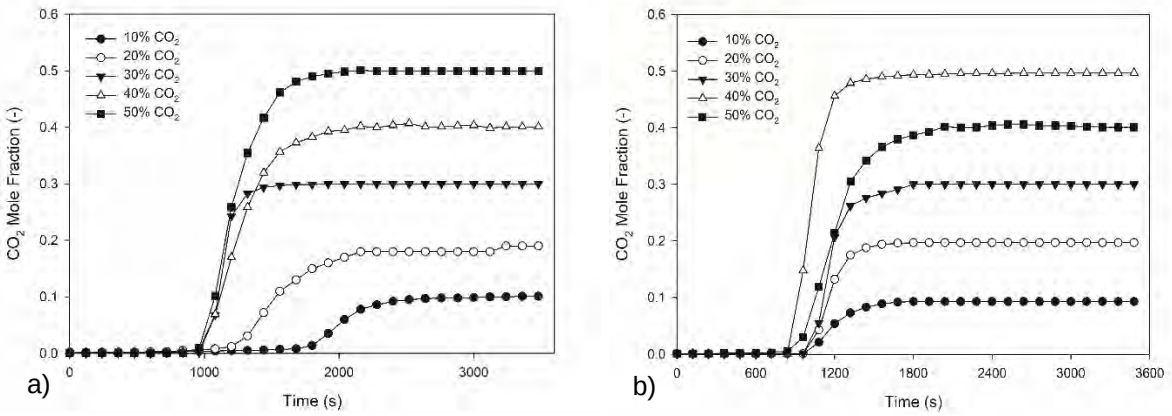

Figure A.4. Dynamic CO_2 adsorption (from 10 to 50% of the overall flow rate) for PSA experiments in pre-combustion conditions (25 bar/25ºC) using: a) TEPA (20%) modified RB1 AC; and b) TEPA (30%) modified RB1 AC

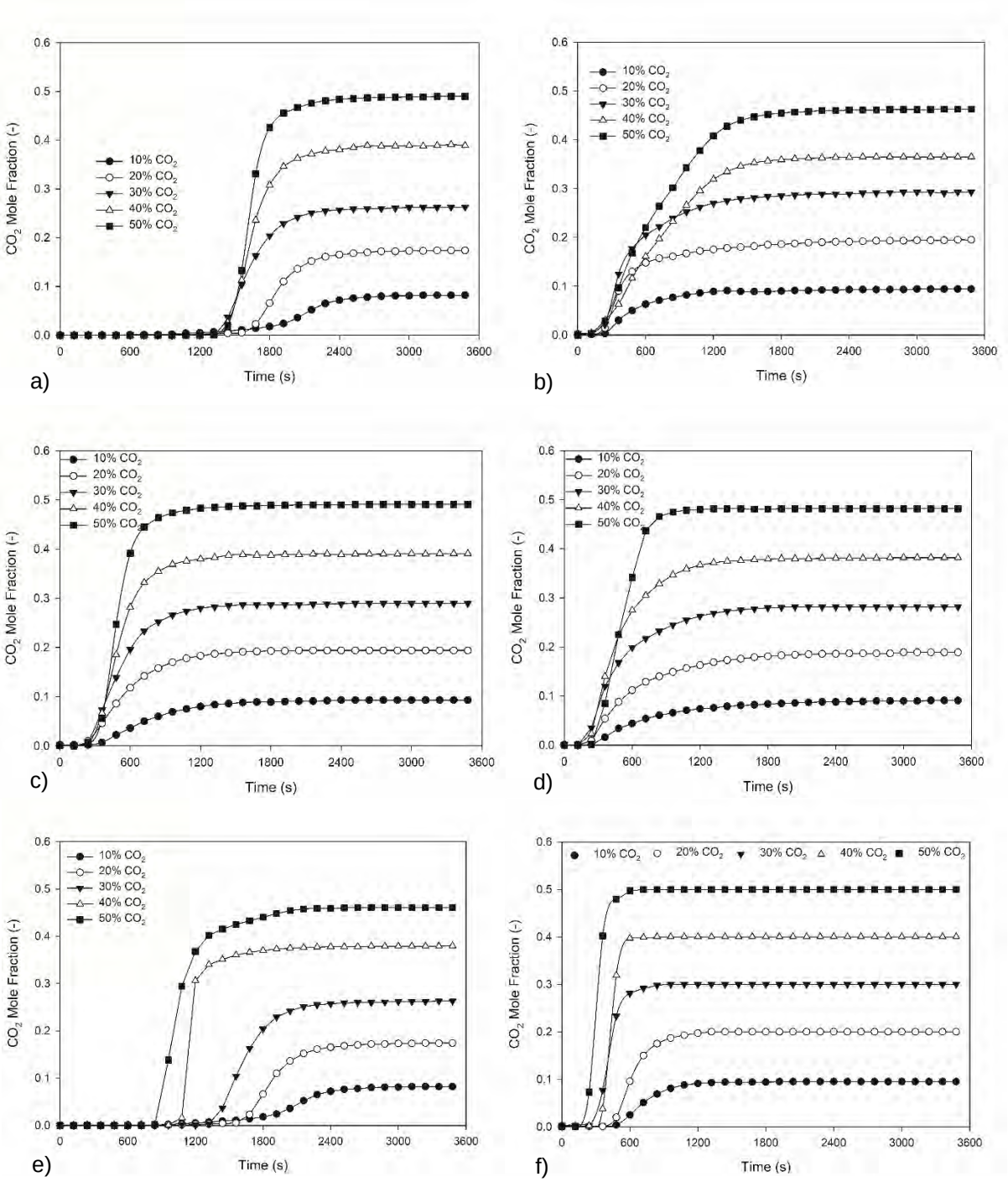

Figure A.5. Dynamic CO_2 adsorption (from 10 to 50% of the overall flow rate) for PSA experiments at post-combustion conditions (10 bar/70ºC) using: a) MEA (30%) modified RB1 AC; b) MEA (40%) modified RB1 AC; c) MEA (50%) modified RB1 AC; d) MEA (60%) modified RB1 AC; e) MEA+MDEA+AMP modified RB1 AC; and f) DEA+MDEA+AMP modified RB1 AC

Table A.2 and A.3 details the amount of CO_2 adsorbed in the PSA process during the overall adsorption stage in pre- as post-combustion conditions, respectively. This report allowed comparison of the modified and original adsorbent CO_2 adsorption capacities demonstrated during in PSA studies.

Firstly, three parameters [pressure (Pa), temperature (ºC), and the flowrate (200 $Nml.min^{-1}$)] were considered to obtain the total inlet flow per second (0.14 mmol/s) of the binary gas mixture. Using the total inlet flow value, the amount of CO_2 and N_2 fed in the system were obtained considering their fractions in the overall flowrate. Based on the CO_2/N_2 inlet flowrate (for instance, 40/60% for the unmodified RB1 AC experiment at pre-combustion conditions), the amount of 0.06 and 0.08 mmol/s for CO_2 and N_2 was fed in the system, respectively. Then, during the overall adsorption stage, the total amount of CO_2 fed in the system was 8524.47 mg. The amount calculated in the bed outlet stream for adsorption was 4967.97 mg. The quantity of CO_2 adsorbed (3556.5 mg) was subtracted from these two parameters. The bed capacity (355.6 mg/g) was obtained from the amount of CO_2 found divided by the mass (10 g) of the adsorbent in the FBR. The adsorbent capacity was obtained from the bed capacity value. This parameter was derived from the bed capacity divided by the mass of one mol of CO_2 (44 g), resulting in 8.1 mmol/g adsorbed CO_2 by the unmodified RB1 AC in pre-combustion adsorption conditions. Additionally, these data were used to calculate the AC selectivity potential for CO_2 and N_2 molecules during the overall PSA adsorption stage in pre- (Table A.4) and post-combustion (Table A.5).

Table A.2. Amount of adsorbed CO_2 in different gas mixture concentrations in PSA pre-combustion conditions

		CO_2 total inlet (%)				
		10	20	30	40	50
	Total CO_2 in the inlet stream (mg)	2131.7	4263.4	6395.1	8526.8	10658.6
Unmodified AC Norit® RB1 AC	Total CO_2 in the outlet stream (mg)	1055.6	2425.3	3583.9	4968.0	6286.5
	Amount of CO_2 adsorbed (mg)	1075.5	1837.0	2809.4	3556.5	4369.1
	Bed capacity (mg/g)	107.5	183.7	280.9	355.7	436.9
Unmodified Norit® R2030 Cabot AC	Total CO_2 in the outlet stream (mg)	534.1	1788.8	3499.8	4635.0	5924.5
	Amount of CO_2 adsorbed (mg)	1597.1	2473.4	2893.6	3889.5	4731.1
	Bed capacity (mg/g)	159.7	247.3	289.4	388.9	473.1
MEA (50%) modified Norit® R2030 Cabot AC	Total CO_2 in the outlet stream (mg)	1309.6	2813.9	4078.6	5464.1	7349.6
	Amount of CO_2 adsorbed (mg)	821.5	1448.3	2314.7	3060.4	3306.0
	Bed capacity (mg/g)	82.2	144.8	231.5	306.0	330.6
MEA+MDEA+AMP blend modified Norit® RB1 AC	Total CO_2 in the outlet stream (mg)	748.2	1670.5	2793.3	3859.9	5098.4
	Amount of CO_2 adsorbed (mg)	1382.9	2591.7	3600.0	4664.6	5557.2
	Bed capacity (mg/g)	138.3	259.2	360.0	466.5	555.7
MEA (20%) modified Norit® RB1 AC	Total CO_2 in the outlet stream (mg)	725.6	1817.1	2981.1	4448.2	5959.4
	Amount of CO_2 adsorbed (mg)	1405.5	2445.2	3412.3	4076.3	4696.2
	Bed capacity (mg/g)	140.5	244.5	341.2	407.6	469.6
MEA (30%) modified Norit® RB1 AC	Total CO_2 in the outlet stream (mg)	940.7	1839.2	2376.7	3514.8	5360.8
	Amount of CO_2 adsorbed (mg)	1190.5	2423.0	4016.6	5009.7	5294.8
	Bed capacity (mg/g)	119.0	242.3	401.7	501.0	529.5
MEA (40%) modified Norit® RB1 AC	Total CO_2 in the outlet stream (mg)	1096.2	1836.2	3130.1	3919.2	4989.3
	Amount of CO_2 adsorbed (mg)	1034.9	2426.0	3263.3	4605.3	5666.3
	Bed capacity (mg/g)	103.5	242.6	326.3	460.5	566.6
MEA (50%) modified Norit® RB1 AC	Total CO_2 in the outlet stream (mg)	714.9	1791.5	3263.3	5038.6	7129.2
	Amount of CO_2 adsorbed (mg)	1416.8	2471.9	3131.8	3488.2	3529.3
	Bed capacity (mg/g)	141.7	247.2	313.2	348.8	352.9
MEA (60%) modified Norit® RB1 AC	Total CO_2 in the outlet stream (mg)	714.9	1838.4	3044.8	4426.0	5935.4
	Amount of CO_2 adsorbed (mg)	1416.8	2425.0	3350.3	4100.9	4723.2
	Bed capacity (mg/g)	141.7	242.5	335.0	410.1	472.3
TEPA (20%) modified Norit® RB1 AC	Total CO_2 in the outlet stream (mg)	1282.6	2780.6	4233.0	5353.1	7292.4
	Amount of CO_2 adsorbed (mg)	848.5	1481.6	2160.4	3171.4	3363.2
	Bed capacity (mg/g)	84.9	148.2	216.0	317.1	336.3
TEPA (30%) modified Norit® RB1 AC	Total CO_2 in the outlet stream (mg)	930.0	2121.0	3553.3	5335.1	6700.6
	Amount of CO_2 adsorbed (mg)	1201.1	2141.3	2840.1	3189.4	3954.9
	Bed capacity (mg/g)	120.1	214.1	284.0	318.9	395.5
$ZnCl_2$ (20%) modified Norit® RB1 AC	Total CO_2 in the outlet stream (mg)	1149.7	2657.2	4181.9	5300.9	7411.3
	Amount of CO_2 adsorbed (mg)	981.4	1605.0	2211.4	3223.5	3244.3
	Bed capacity (mg/g)	98.1	160.5	221.1	322.4	324.4
H_3PO_4 (20%) modified Norit® RB1 AC	Total CO_2 in the outlet stream (mg)	1149.7	2657.2	4181.9	5300.9	7411.3
	Amount of CO_2 adsorbed (mg)	981.4	1605.0	2211.4	3223.5	3244.3
	Bed capacity (mg/g)	102.4	190.0	240.3	302.9	384.6
KOH (20%) modified Norit® RB1 AC	Total CO_2 in the outlet stream (mg)	1171.7	2428.0	3597.4	4716.7	6072.5
	Amount of CO_2 adsorbed (mg)	959.4	1834.2	2796.0	3807.8	4583.1
	Bed capacity (mg/g)	95.9	183.4	279.6	380.8	458.3
KOH (60%) modified Norit® RB1 AC	Total CO_2 in the outlet stream (mg)	917.1	2004.7	3231.7	4522.8	5522.4
	Amount of CO_2 adsorbed (mg)	1214.0	2257.5	3161.7	4001.7	5133.2
	Bed capacity (mg/g)	121.4	225.7	316.2	400.2	513.3
KOH (70%) modified Norit® RB1 AC	Total CO_2 in the outlet stream (mg)	849.4	2010.1	3075.6	4747.3	6169.3
	Amount of CO_2 adsorbed (mg)	1282.3	2253.3	3319.5	3779.5	4489.3
	Bed capacity (mg/g)	128.2	225.3	331.9	377.9	448.9

Table A.3. Amount of absorbed CO_2 in different gas mixture concentrations in PSA studies in post-combustion conditions

		CO_2 **total inlet (-)**				
		0.1	0.2	0.3	0.4	0.5
	Total CO_2 in the inlet stream (mg)	2131.7	4263.4	6395.1	8526.8	10658.6
Unmodified AC Norit® RB1 AC	Total CO_2 in the outlet stream (mg)	714.9	1838.4	3044.8	4426	5935.4
	Amount of CO_2 adsorbed (mg)	732	1186.4	1874.2	2218.2	2732.6
	Bed capacity (mg/g)	73.2	118.6	187.4	221.8	273.3
Unmodified Norit® R2030 Cabot AC	Total CO_2 in the outlet stream (mg)	1419	3136.3	5359.3	6271	8761.3
	Amount of CO_2 adsorbed (mg)	712.1	1125.9	1034	2253.5	1894.3
	Bed capacity (mg/g)	71.2	112.6	103.4	225.3	189.4
MEA (50%) modified Norit® R2030 Cabot AC	Total CO_2 in the outlet stream (mg)	1365.8	2868.1	4078.6	5464.1	7349.6
	Amount of CO_2 adsorbed (mg)	765.4	1394.1	2314.7	3060.4	3306
	Bed capacity (mg/g)	76.5	139.4	231.5	306	330.6
MEA+MDEA+AMP blend modified Norit® RB1 AC	Total CO_2 in the outlet stream (mg)	748.2	1670.5	2793.3	5110	6088.3
	Amount of CO_2 adsorbed (mg)	1382.9	2591.7	3600	3414.5	4567.3
	Bed capacity (mg/g)	138.3	259.2	360	341.4	456.7
MEA (20%) modified Norit® RB1 AC	Total CO_2 in the outlet stream (mg)	640.4	1764.6	2748.6	4341.7	3893.6
	Amount of CO_2 adsorbed (mg)	1490.7	2497.6	3644.8	4182.8	4630.8
	Bed capacity (mg/g)	149.1	249.8	364.5	418.3	463.1
MEA (30%) modified Norit® RB1 AC	Total CO_2 in the outlet stream (mg)	748.2	1670.5	2793.3	4205.8	5317.3
	Amount of CO_2 adsorbed (mg)	1382.9	2591.7	3600	4318.7	5338.2
	Bed capacity (mg/g)	138.3	259.2	360	431.9	533.8
MEA (40%) modified Norit® RB1 AC	Total CO_2 in the outlet stream (mg)	1625	3363.4	4997.8	5636.6	6972.4
	Amount of CO_2 adsorbed (mg)	506.1	898.9	1395.5	2887.8	3683.2
	Bed capacity (mg/g)	50.6	89.9	139.6	288.8	368.3
MEA (40%) modified Norit® RB1 AC	Total CO_2 in the outlet stream (mg)	1478.4	3358.7	5032	6778	8547.9
	Amount of CO_2 adsorbed (mg)	652.7	903.5	1361.3	1746.5	2107.7
	Bed capacity (mg/g)	65.3	90.4	136.1	174.6	210.8
MEA (60%) modified Norit® RB1 AC	Total CO_2 in the outlet stream (mg)	1446.2	3129.9	4855.1	6535.4	8320.9
	Amount of CO_2 adsorbed (mg)	684.9	1132.4	1538.2	1989.1	2334.7
	Bed capacity (mg/g)	68.5	113.2	153.8	198.9	233.5
DEA+AMP blend modified Norit® RB1 AC	Total CO_2 in the outlet stream (mg)	1546.5	3424.1	4750.2	7397.5	9605.7
	Amount of CO_2 adsorbed (mg)	584.6	838.1	1643.2	1127	1049.9
	Bed capacity (mg/g)	58.5	83.8	164.3	112.7	105
DEA+MDEA+AMP blend modified Norit® RB1 AC	Total CO_2 in the outlet stream (mg)	1290	2940.4	4899.8	6504	8820.2
	Amount of CO_2 adsorbed (mg)	841.1	1321.8	1493.6	2020.4	1835.4
	Bed capacity (mg/g)	84.1	132.2	149.4	202	183.5
TEA+AMP blend modified Norit® RB1 AC	Total CO_2 in the outlet stream (mg)	1254.1	3131.7	4912.9	6822.9	8566.7
	Amount of CO_2 adsorbed (mg)	877	1130.5	1480.5	1701.5	2088.9
	Bed capacity (mg/g)	87.7	113.1	148	170.2	208.9
TEA+MDEA+AMP blend modified Norit® RB1 AC	Total CO_2 in the outlet stream (mg)	1158.1	2806.3	4181.9	5635.4	7847.7
	Amount of CO_2 adsorbed (mg)	973	1455.9	2211.4	2889	2807.9
	Bed capacity (mg/g)	97.3	145.6	221.1	288.9	280.8
TEPA (20%) modified Norit® RB1 AC	Total CO_2 in the outlet stream (mg)	1128	2471.3	3893.4	4570.3	6810.6
	Amount of CO_2 adsorbed (mg)	1003.1	1791	2500	3954.2	3845
	Bed capacity (mg/g)	100.3	179.1	250	395.4	384.5
TEPA (30%) modified Norit® RB1 AC	Total CO_2 in the outlet stream (mg)	851.5	2208	3044.8	4391.8	5924.5
	Amount of CO_2 adsorbed (mg)	1279.6	2054.2	3348.5	4132.7	4731.1
	Bed capacity (mg/g)	128	205.4	334.9	413.3	473.1

Table A.4. Amount of CO_2 and N_2 obtained outside the FBR during adsorption for CO_2/N_2 mixtures in post-combustion conditions for AC selectivity studies

		CO_2 total inlet (%)				
		10	20	30	40	50
Unmodified AC Norit® RB1 AC	1*	8644.9	8190.6	7502.7	7158.8	6644.3
	2*	6834.8	6611.0	6620.8	6286.7	6123.0
Unmodified Norit® R2030 Cabot AC	1*	8664.8	8251.0	8342.9	7123.5	7482.7
	2*	6814.9	6550.6	5780.6	6322.0	5284.7
MEA (50%) modified Norit® R2030 Cabot AC	1*	8611.6	7982.8	7062.2	6316.5	6070.9
	2*	6868.1	6818.8	7061.3	7128.9	6696.4
MEA+MDEA+AMP blend modified Norit® RB1 AC	1*	7994.0	6785.2	5776.9	5962.4	4809.6
	2*	7485.7	8016.4	8346.6	7483.0	7957.7
MEA (20%) modified Norit® RB1 AC	1*	7886.2	6879.3	5732.1	4746.1	4417.13
	2*	7593.4	7922.3	8391.4	8699.3	8350.2
MEA (30%) modified Norit® RB1 AC	1*	7994.0	6785.2	5776.9	5058.2	4038.7
	2*	7485.7	8016.4	8346.6	8387.2	8728.7
MEA (40%) modified Norit® RB1 AC	1*	8870.8	8478.0	7981.4	6489.1	5693.8
	2*	6608.9	6323.5	6142.1	6956.3	7073.6
MEA (50%) modified Norit® RB1 AC	1*	8724.2	8473.4	8015.6	7630.4	7269.2
	2*	6755.4	6328.2	6107.9	5815.0	5498.1
MEA (60%) modified Norit® RB1 AC	1*	8692.0	8244.6	7838.7	7387.8	7042.2
	2*	6787.6	6557.0	6284.8	6057.6	5725.1
DEA+AMP blend modified Norit® RB1 AC	1*	8792.3	8538.8	9376.9	8249.9	9376.8
	2*	6687.4	6262.8	4746.6	5195.5	3390.5
DEA+MDEA+AMP blend modified Norit® RB1 AC	1*	8535.8	8055.1	7883.3	7541.5	7356.5
	2*	6943.9	6746.5	6240.2	5903.9	5410.9
TEA+AMP blend modified Norit® RB1 AC	1*	8499.9	8246.4	7896.5	7675.4	7288.0
	2*	6979.8	6555.2	6227.1	5770.0	5479.3
TEA+MDEA+AMP blend modified Norit® RB1 AC	1*	8403.9	7921.0	7165.5	6487.9	6569.1
	2*	7075.8	6880.6	6958.0	6957.5	6198.3
TEPA (20%) modified Norit® RB1 AC	1*	8373.8	7586.0	6876.9	5422.8	5532.0
	2*	7105.8	7215.6	7246.6	8022.7	7235.4
TEPA (30%) modified Norit® RB1 AC	1*	8097.3	7322.7	6028.4	5244.2	4645.8
	2*	7382.4	7478.9	8095.1	8201.2	8121.5

Table A.5. Amount of CO_2 and N_2 obtained outside the FBR during adsorption for CO_2/N_2 mixtures in pre-combustion conditions for AC selectivity studies

		CO_2 total inlet (%)				
		10	20	30	40	50
Unmodified AC Norit® RB1 AC	1*	8301.4	7540.0	6567.5	5820.4	5007.8
	2*	7178.2	7261.6	7556.0	7625.0	7759.5
Unmodified Norit® R2030 Cabot AC	1*	7779.9	6903.5	6483.4	5487.5	4645.8
	2*	7699.8	7898.1	7640.1	7958.0	8121.5
MEA (50%) modified Norit® R2030 Cabot AC	1*	8555.4	7928.6	7062.2	6316.5	6070.9
	2*	6924.3	6873.0	7061.3	7128.9	6696.4
MEA+MDEA+AMP blend modified Norit® RB1 AC	1*	7994.0	6785.2	5776.9	4712.3	3819.8
	2*	7485.7	8016.4	8346.6	8733.1	8947.6
MEA (20%) modified Norit® RB1 AC	1*	7971.4	6931.7	5964.6	5300.7	4680.7
	2*	7508.3	7869.8	8158.9	8144.8	8086.6
MEA (30%) modified Norit® RB1 AC	1*	8186.5	6953.9	5360.3	4367.2	4082.1
	2*	7293.2	7847.7	8763.2	9078.2	8685.2
MEA (40%) modified Norit® RB1 AC	1*	8342.0	6950.9	6113.6	4771.7	3710.6
	2*	7137.7	7850.7	8009.9	8673.8	9056.7
MEA (50%) modified Norit® RB1 AC	1*	7960.1	6905.0	6245.1	5888.7	5847.6
	2*	7519.5	7896.6	7878.4	7556.7	6919.8
MEA (60%) modified Norit® RB1 AC	1*	7960.1	6951.9	6026.6	5276.0	4653.8
	2*	7519.5	7849.7	8096.9	8169.4	8113.6
TEPA (20%) modified Norit® RB1 AC	1*	8528.4	7895.3	7216.6	6205.5	6013.7
	2*	6951.3	6906.3	6907.0	7239.9	6753.6
TEPA (30%) modified Norit® RB1 AC	1*	8175.8	7235.7	6536.9	6187.6	5422.0
	2*	7303.8	7565.9	7586.6	7257.9	7345.4
ZnCl2(20%) modified Norit® RB1 AC	1*	8395.5	7771.9	7165.5	6153.4	6132.6
	2*	7084.2	7029.7	6958.0	7292.0	6634.7
H_3PO_4(20%) modified Norit® RB1 AC	1*	8353.2	7476.5	6973.7	6347.7	5530.6
	2*	7126.4	7325.1	7149.8	7097.7	7236.7
KOH (20%) modified Norit® RB1 AC	1*	8417.5	7542.7	6580.9	5569.2	4793.8
	2*	7062.2	7258.9	7542.6	7876.3	7973.5
KOH (60%) modified Norit® RB1 AC	1*	8162.9	7119.4	6215.2	5375.3	4243.7
	2*	7316.7	7682.2	7908.3	8070.2	8523.7
KOH (70%) modified Norit® RB1 AC	1*	8094.6	7123.6	6057.4	5597.4	4887.7
	2*	7385.0	7677.9	8066.1	7848.0	7879.7